MASTERARBEIT / MASTER'S THESIS

Titel der Masterarbeit / Title of the Master's Thesis

Computer control and data acquisition for the Kapitza-Dirac-Talbot-Lau interferometer

verfasst von / submitted by

Johannes Bischoff, BSc

angestrebter akademischer Grad / in partial fulfilment of the requirements for the degree of

Master of Science (MSc)

Wien, 2018 / Vienna 2018

Studienkennzahl lt. Studienblatt / degree programme code as it appears on the student record sheet:	A 066 876
Studienrichtung lt. Studienblatt / degree programme as it appears on the student record sheet:	Physics
Betreut von / Supervisor:	Prof. Markus Arndt
Mitbetreut von / Co-Supervisor:	Dr. Sandra Eibenberger

Acknowledgements

I would like to take this opportunity to express my gratitude to Prof. Markus Arndt, Dr. Joseph Cotter, Dr. Lukas Mairhofer, and all people from the quantum nanophysics group in Vienna. Their kind participation in my explorative study added great value to my thesis and also inspired me to continue focusing on fundamental research in the future. In addition, I would like to thank Dr. Sandra Eibenberger for all the feedback and help during the process of writing the thesis. Lastly, I would like to express my eternal appreciation for the emotional support provided by my family and friends helping me to see 'the light at the end of the tunnel'. Thank You!

Vienna 2018, Johannes Bischoff

Abstract

The discrepancy between the classical and the quantum world of physics is interesting without doubt. One promising way to tackle the enigma is matter wave interferometry with large molecules to see quantum phenomena with particles as macroscopic as possible. This thesis describes the development and implementation of a new integrated computer software controlling the Kapitza-Dirac-Talbot-Lau interferometer (KDTLI) [1]. The KDTLI accomplished to show interference with molecules weighing up to 10 000 atomic masses, which entails the current mass record [2]. In essence, it is built of a thermal oven as a source, a three grating interferometer, and a quadrupole mass spectrometer (QMS) as a detector. The second grating is not a material grating like the other two, but made of a standing laser light wave. The measured fringe visibility depends therefore apart from others on the laser's parameters. The new control software continuously reads and saves several parameters of devices linked to the experiment. As a consequence, an increasing database is created and built up while running the experiment. In conclusion, a better understanding and control of the experiment is achieved. Additionally, the automation of repetitive measurements is integrated into the control software leading to a number of new advantages and it saves time operating the experiment.

Kurzzusammenfassung

Der Übergang von der klassischen Physik unserer Alltagswelt zur Quantenmechanik wirft bisher noch mehr Fragen auf, als es Antworten gibt. Ein vielversprechender Weg, um dem Mysterium ein Stück näher zu kommen, ist die Materiewelleninterferometrie mit Molekülen, da sich Quantenphänome anhand makroskopischer, komplexer Teilchen aufzeigen lassen.

In dieser Masterarbeit wird eine neue Software zur Steuerung des Kapitza-Dirac-Talbot-Lau-Interferometers (KDTLI) entwickelt und vorgestellt [1]. Mit dem KDTLI konnte bereits Interferenz mit Molekülen mit bis zu 10 000 atomaren Massen gemessen werden, was bisher den Massenrekord setzt [2].

Das KDTLI besteht aus einem thermischen Ofen als Molekülquelle, einem Drei-Gitter-Interferometer und einem Quadrupol-Massenspektrometer (QMS) als Detektor. Das erste und letzte Gitter sind absorbierende Materialgitter. Das zweite Gitter besteht aus einer stehenden Laser-Lichtwelle. Der gemessene Interferenzkontrast hängt daher auch entscheidend von den Laserparametern ab. Die neue Steuerungssoftware liest erstmalig sämtliche Parameter der Geräte ein, die mit dem Experiment verbundenen sind. Diese werden automatisch und kontinuierlich abgespeichert. Folglich wird mit der Nutzung der Software eine Datenbank der Messergebnisse mit sämtlichen Messparametern fortlaufend aufgebaut, deren Analyse ein besseres Verständnis des Experiments mit sich bringt und die Reproduzierbarkeit erhöht. Des Weiteren wurden sich wiederholende Messdurchführungen automatisiert und in die Steuerungssoftware integriert. Dadurch können auch fragile Biomoleküle vermessen werden, deren Signal vergleichsweise kurzlebig ist.

Contents

List of Figures

List of Tables

Chapter 1

Motivation and introduction to the KDTLI

In this thesis, a measurement and control software is developed for the control of the Kapitza-Dirac-Talbot-Lau interferometer (KDTLI). The KDTLI is a near-field matter-wave interferometer, which has been successfully used to perform quantum interference and quantum-assisted metrology experiments with a variety of molecules [1, 3].

The new and improved LabVIEW [1] control software has been developed, tested, and implemented. There are three main aspects in this software development. First, all existing features and control programmes are united in a single application. Stability and adjustability of the programme are very important to produce reliable and reproducible data. Secondly, future development of the experiment will call for new tasks form the software or new hardware needs to be controlled and included into the programme. Therefore, the software is built in a modular way, where the software modules are combined in one main application. The focus is on continuously reading and saving the experiment's parameters to create a searchable database. Being able to compare previous measurements will lead to a better understanding of the experiment and will help to plan and develop new ideas. For example, an analysis of the database over a longer time could discover unknown correlations or the cause of drifts. Last but not least, different measurement processes are automated. Previously,

[1] Laboratory Virtual Instrument Engineering Workbench (LabVIEW) a visual programming language from National Instruments.

the measurement of interference patterns with the KDTLI varying one parameter at a time was a repetitive and time consuming work. Also, manually adjusting things on the optical table risks the introduction of system instabilities, since the experiment is very sensitive to any external perturbations. Especially when working with biomolecules on the KDTLI, the signal lasts only a short time compared with C_{60}, which is used routinely and produces a long-lasting stable signal in the KDTLI. Therefore, an efficient and automated KDTLI can facilitate new metrology with biomolecules.

The scheme of the experimental setup is shown in figure 1.1. An oven heats the molecules to their vaporization temperature and prepares a molecular beam in high vacuum. Three delimiters define a parabolic flight path in the gravitational field. The heart of the experiment is the three grating setup using the Kapitza-Dirac and Talbot-Lau effects. Here, all three gratings have the same periodicity. The first and third gratings are made of SiN_x [4]. The 3rd grating is shifted transversely across the molecular beam to measure the interference pattern as illustrated in figure 1.1. A standing laser light wave forms the second grating, which introduces a phase shift according to the optical dipole force. At the end of the experimental setup, the molecules are detected with a quadrupole mass spectrometer (QMS). A more detailed description of the experiment is found in section 2.2.

The overall purpose of the KDTLI is to investigate the discrepancy between the classical and the quantum world of physics. Measuring interference patterns with increasingly larger molecules is a promising way to study that incongruity. The KDTLI operates in the near field to make very tiny de Broglie wavelengths of heavy particles detectable, which are in the regime of picometers. As a result, it contributes important limits to the development of decoherence theories. Also, the KDTLI is an instrument for metrology of biomolecules, because it is exceptionally sensitive to external forces. Deflection instruments of molecules have a high relevance for determining their electric properties. Hence, an electrostatic deflector is placed in the beam path between the first and second grating to generate an electric field, where the electric force is constant [5]. Then, the molecules susceptibility is interacting with the electric field and a shift of the interference pattern is measured.

This thesis first describes the working principle of the KDTLI in chapter 2. The focus is on explaining the dependency of the fringe visibility from various criteria, such as the laser parameters e.g. power, waist, position, and wavelength, the velocity of the molecules, their beam path and alignment to the gratings, and external vibrations. This leads to the next chapter, which covers the description of the new control software including these parameters. Finally, some measurements and analysing strategies are presented as a result of the new control software and newly generated database.

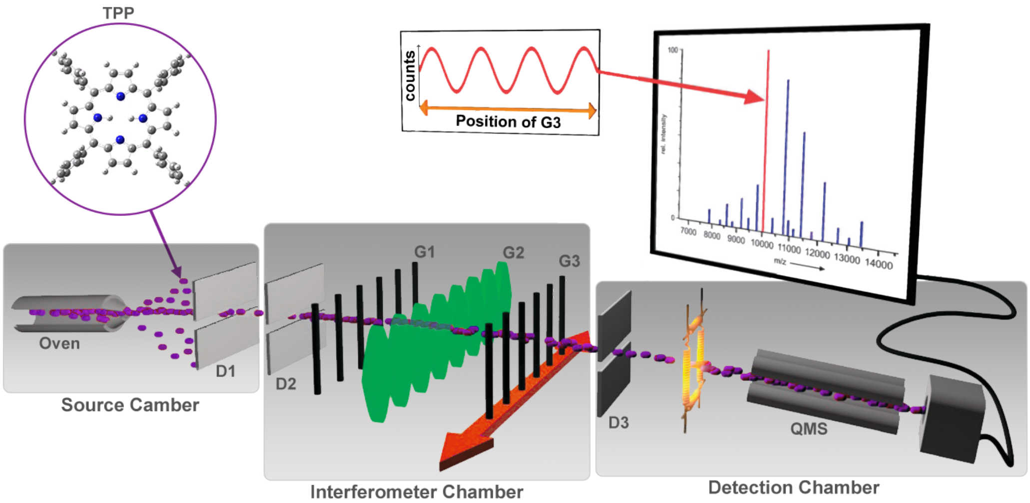

Figure 1.1: The figure shows the experimental setup of the Kapitza-Dirac-Talbot-Lau interferometer (KDTLI), which is separated into three chambers: The source chamber containing the oven, which heats molecules like tetraphenylporphyrin (TPP) until they evaporate into the chamber. The interferometer chamber holds the three gratings (G1-3). The first and last are SiN material gratings and the other one is made of a standing laser light wave. In the last chamber, the molecules are ionized and detected by a quadrupole mass spectrometer (QMS). A mass range is selected for the QMS as displayed above the detection chamber. Last, the molecules within the mass range are converted into a logic TTL signal. The counts are displayed versus the third grating's position to build an interferogram. Additionally, a velocity class of the molecules, thermally emitted from the oven, is selected by three delimiters (D1-D3). The positions of the delimiters define a parabola in the gravitational field for the molecule's free-flight through the chambers. The complete length of the molecular beam path is approximately 2.3 m long from the source to the detection (Adapted from [2]).

Chapter 2

Matter wave interferometry

Matter wave physics is a promising field of physics to bring light into the still unexplained transition from unintuitive quantum phenomena to the classical world as we know it. The explanations to a unified framework to the quantum-to-classical transition are still a matter of debate [6]. Superposing particles such as electrons is well established in interferometers [7]. Interferometry with neutrons [8] and atoms [9, 10] have taken on the quest for probing the potential limits of the quantum superposition principle as well as probing the internal properties of the specimen. From this point on, it seems only natural to strive for the development of an interferometer for molecules [11]. Technical challenges arise using molecules such as the establishment of a coherent source, effective manipulations in the free flight, or a general low detection efficiency. Despite these difficulties, complex molecules were spatially superposed in the Kapitza-Dirac-Talbot-Lau interferometer, which operates in the near-field [12].

This chapter explains first the underlying physical concepts of matter wave interferometry leading to an understanding of the KDTLI. The second section of this chapter describes the experimental setup and the main components of the KDTLI.

2.1 The physics of matter wave interferometry with molecules

The physical concepts of matter wave interferometry are based on methods established for light, which were already used by Thomas Young to demonstrate the wave nature of light in 1807 [13]. Even though Estermann und Stern showed first diffraction experiments with a molecular beam in 1930 [14], the first interferometer for molecules was not established before 1994 using I_2 molecules [11]. Around the same time, the helium dimer and trimer showed interference after passing through a diffraction grating made of silicon nitride [15]. Similarly, a beam of sodium molecules (Na_2) was diffracted and additionally the index of refraction for the Na_2 de Broglie waves was measured [16]. Only four years later in 1999, the first diffraction of large molecules was demonstrated in the far-field with the fullerene C_{60} [17], which paved the way to the development of the KDTLI.

This section 2.1 presents first the idea from Louis de Broglie of the wave-particle duality and how to apply optical phenomena to particles. Next, the findings of Talbot and Lau are explained, which led to the first Talbot-Lau interferometry (TLI) for complex molecules [3]. The next major development step was the assembling of the Kapitza-Dirac-Talbot-Lau interferometer, which is based on the TLI and combined with the Kapitza-Dirac effect. That effect is described in the following subsection. Last, some theoretical concepts about decoherence are discussed, which are relevant for the KDTLI.

2.1.1 Wave-particle duality

A revolutionary idea and the origin of matter wave interferometry came from Louis de Broglie in 1923 [18]. He assigned a frequency to every particle with a mass m. The matter wavelength λ_{dB}, named after him, is calculated from the momentum $p = mv$ of the particle using the molecule's velocity v and the Planck constant h:

$$\lambda_{\mathrm{dB}} = \frac{\mathrm{h}}{mv} \tag{2.1}$$

The possibility of matter waves was derived by combining the energy-frequency equivalence for photons $E = \mathrm{h}\nu$ with the energy-mass equivalence for matter $E = mc^2$ [19]. As an example, a thermal beam of tetraphenylporphyrin molecules (TPP: mass of 614 amu at $T = 665\,\mathrm{K}$) with a most probable velocity of $135\,\mathrm{ms}^{-1}$ (see equation 2.11) has a respective de Broglie wavelength of $\lambda_{\mathrm{dB}} \cong 5\,\mathrm{pm}$, which depends only inversely proportionally on the velocity.

Furthermore, the wave-particle duality is also embedded into the Schrödinger equation itself. The stationary Schrödinger equation can be separated into a product of a spatial and a temporal part by making the ansatz of a general wavefunction $\psi(r,t) = \Phi(r)\exp(\mathrm{i}\omega t)$:

$$\left[\nabla^2 + \frac{2m}{\hbar^2}\left(E - V(r)\right)\right]\Phi(r) = 0 \tag{2.2}$$

On the other hand, the Helmholtz equation of electrodynamics, which represents a time-independent form of the wave equation, describes the propagation of light in classical optics:

$$\left[\nabla^2 + k^2\right]\Phi(r) = 0 \tag{2.3}$$

One can see the form equivalence of both equations 2.2 and 2.3 [20]. Therefore, analogous forms of phenomena from classical wave optics are to be expected in non-relativistic quantum mechanics such as diffraction of matter waves.

Coherence or phase order is mandatory in a particle ensemble to show matter wave interference. "The degree of motional quantum coherence can be defined as the normalized correlation function between probability amplitudes at different points in space and time." [21] This sentence summarized temporal and spatial coherence, which are described in the following paragraphs.

Starting with temporal coherence, two wavetrains frozen in time run out of phase in longitudinal direction, if their wavelengths differ too much, which is related to their spectral purity in the Wiener-Khintchine theorem [22]. The theorem expresses the spectral power density of a stationary random process as the Fourier transform of the corresponding autocorrelation function [23]. The longitudinal coherence length is well measured by $l_{\mathrm{lc}} = \lambda^2/\Delta\lambda$. For massless light, this is also related to temporal coherence, because the coherence time is the length l_{lc} divided by c the speed of light [24]. For instance, the coherence length of TPP results in 48 pm using its previously calculated De Broglie wavelength of $\lambda_{\mathrm{dB}} \cong 5\,\mathrm{pm}$ and a velocity spread of $\Delta v = 10\%$ (see section 2.2.2). This longitudinal coherence is magnitudes smaller than the geometrical size of the molecule itself.

In general, two waveforms show interference at some point in space, if they are at least partially coherent, at that point in space [25]. Spatial or transversal coherence describes the ability of the extended waves to interfere when averaged over time or in other words when averaged over their path length differences from the source. A point source has perfect spatial coherence. The larger the source diameter, the smaller the angle θ at which the phases are correlated [26]. The transversal coherence length l_{tc} is calculated on the distance R between source and observer, the source diameter d_{s}, and the diffracted wavelength λ: $l_{\mathrm{tc}} \cong \lambda \cdot R \cdot d_{\mathrm{s}}^{-1}$ [24, 27]. It can also be expressed in terms of the angle θ. For the example of TPP exiting a thermal source with an opening of 0.2 mm, the transversal coherence length amounts only to $l_{\mathrm{tc}} \cong 2.5\,\mathrm{nm}$ in a distance of 10.5 cm. For that reason, the Talbot-Lau effect, explained in the next section 2.1.2, is used to prepare the spatial coherence. The transverse coherence is summarized in the van Cittert-Zernike theorem; the correlation function of the points under consideration of the wave is form equivalent to the intensity distribution behind the source upon coherent illumination [28].

The Kirchhoff-Fresnel integral generally describes the diffraction of a coherent light field E_0 at an arbitrary aperture A [29, 30]. The integral sums over all wavelets emanating from every surface element $\mathrm{d}x\mathrm{d}y$ of the aperture according to Huygens principle to compute the resulting field $E(x, y)$ in the distance z:

$$E(x_1, y_1) \propto \int_A \frac{1}{r} \mathrm{e}^{-\mathrm{i}kr} E_0(x_0, y_0)\,\mathrm{d}x\mathrm{d}y \tag{2.4}$$

In the paraxial approximation, the distance r between the source point $P_0(x_0, y_0, 0)$ and the observation point $P_1(x_1, y_1, z)$ can be expressed as $r = \sqrt{z^2 + (x_1 - x_0)^2 + (y_1 - y_0)^2}$. This expression for r is expanded to a Taylor series (substituting $\left((x_1 - x_0)^2 + (y_1 - y_0)^2\right) = q$). The resulting expression is then inserted back into the Kirchhoff-Fresnel integral.

If only the linear term of the Taylor series is considered, the integral reduces to a Fourier transform of the wave across the diffraction aperture. This is called

Frauenhofer diffraction and it premises a long distance $r \gg (x^2 + y^2) \cdot \lambda^{-1}$ [30]. Therefore, it is applicable in the far-field of the diffracting aperture.
In contrast to the far-field, the Fresnel approximation takes the wave front curvature into account and considers the quadratic term in the Taylor series as well. This is important for near-field diffraction phenomena such as the Talbot-Lau effect explained in the next section.

2.1.2 Talbot-Lau effect

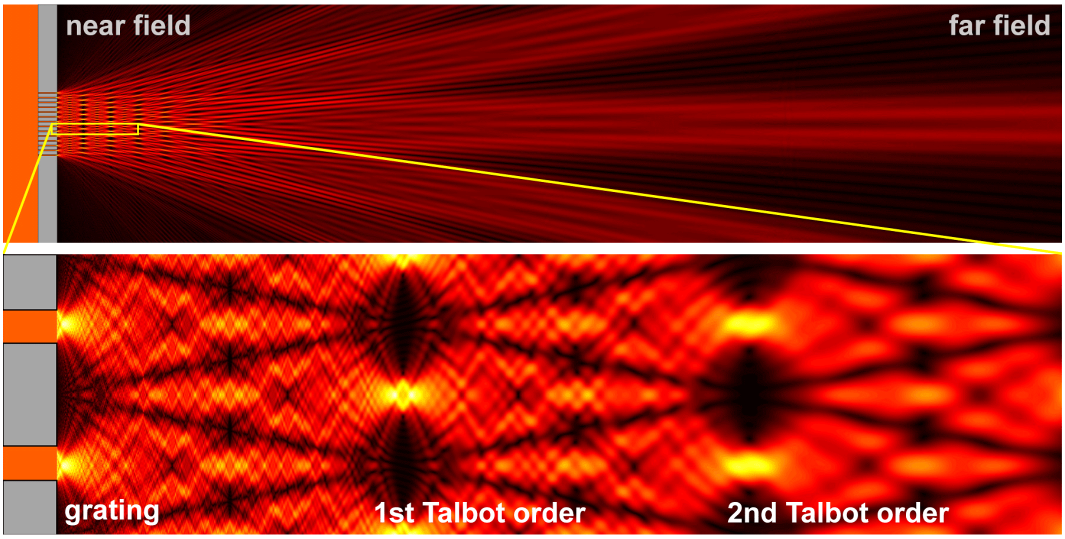

Figure 2.1: The figure shows the diffraction of a plane wave through a grating [31]. On the top, the transition from near-field to far-field effects is visualized. A small section behind the grating is magnified to show the optical carpet as seen on the bottom. The grating is reproduced in certain Talbot lengths creating a so called Talbot carpet. The self-images of the grating in odd orders of Talbot length are shifted by half a period. If the grating were infinite and under illumination of a perfectly coherent laser, the Talbot carpet would not wash out.

In 1836, William Henry Fox Talbot examined light behind prisms and gratings using magnifying lenses. He found numerous regular alternations of lines parallel to the grating, which were changing with the distance to the grating [32]. Today, this is known as the Talbot effect or Talbot carpet, a near-field phenomenon displayed in figure 2.1. Diffraction through a grating can image the grating itself by virtue of the interference at certain distances, first explained by Lord Rayleigh [33]. The self-imaging of the grating at multiples of the Talbot length $L_T = \frac{d^2}{\lambda}$ is calculated on the grating's periodicity d and on the diffracted wavelength λ. In odd orders of the Talbot length the image is shifted by half the period with regard to the grating. Ernst Lau published an extension to the Talbot effect in 1948 [34]. He was able to observe interference using spatially incoherent light by placing two grating structures behind each other. The required transversal coherence is prepared by the first grating, which acts as a periodic spatial mask. Numerous wavelets emerge from the neighbouring slits. Even though there is no phase coherence between neighbouring slits, the wavelets within each slit develop sufficient transverse coherence after the propagation to allow coherent diffraction at the second grating. The ensuing diffraction at the second grating leads to the formation of an intensity pattern with the period equal to the first grating, if the distance between the gratings is close to a multiple of the Talbot length [20].

The effect has also been measured with monochromatic but spatially incoherent light in agreement with the theory [35]. The Talbot-Lau effect can also be used to prepare spatial coherence in large molecules and has been successfully implemented for interference of large molecules in a Talbot-Lau interferometer (TLI) with the fullerenes C_{60} and other molecules [17]. A optical Talbot-Lau configuration was later used to experimentally realize the predicted optical carpet from figure 2.1 with a sodium lamp providing a monochromatic spatially incoherent illumination of the first grating [36].

The Heisenberg uncertainty is the principle underlying the preparation of spatial coherence. This could be experimentally shown for fullerene molecules by observing their momentum spread after passing through a slit with decreasing width. The results are in quantitative agreement with the theoretical prediction of Heisenberg uncertainty principle [37].

The momentum uncertainty for a monochromatic molecular matter wave at a rectangular slit with the width d_{s} is given by: $\Delta d_{\mathrm{s}} \Delta p_{\mathrm{mol}} \geq 0.89\,\mathrm{h}$ [38, 37]. To calculate the spatial uncertainty Δx in the distance L (see section 2.2.3), the momentum uncertainty has to be rewritten using the perpendicular velocity v_{mp}, which is the molecule's velocity passing through the slit:

$$\Delta x \geq \frac{0.89\,\mathrm{h}\,L}{m\,v_{\mathrm{mp}}\,\Delta d_{\mathrm{s}}} \tag{2.5}$$

As a result from the inequation above, the lower boundary for the spatial uncertainty

is $\Delta x = 4.0\,\mu\text{m}$ for TPP at the second grating in the KDTLI. This is in agreement with the transversal coherence length, which results in $l_{\text{tc}} \cong 4.5\,\mu\text{m}$ for TPP with the same set of parameters.
In conclusion, the matter wave is delocalized over several grating periods (266 nm) at the second grating of the KDTLI. As mentioned before, the second grating in the KDTLI is not a material one, but an optical grating relying on the Kapitza-Dirac effect.

2.1.3 Kapitza-Dirac effect

Kapitza and Dirac suggested to reflect an electron beam from a standing light wave in 1933, which is a striking prediction [39], because only the inverted process of diffraction of light by a material grating has been observed before. Remarkably, the realization of the original proposal of the Kapitza-Dirac effect with electrons was not observed before the year 2001 [40]. The optical grating has the advantage of a very accurate periodicity compared to a material grating, but it dependent on the detailed internal character of the diffracted object [41].
Already in 1985, atomic scattering by a standing-wave laser field in agreement with the the Kapitza-Dirac effect was studied [42]. The atomic de Broglie waves diffracts at $2\hbar k_{\text{L}}$ (k_{L} laser light wavevector) intervals by the intensity grating as a result of its periodicity of $\lambda_{\text{Laser}}/2$. Alternatively, the quantization can be interpreted as the absorption and stimulated emission of photon pairs from the counter-propagating laser light causing a momentum transfer of $2\hbar k_{\text{L}}$ [43]. The standing wave was produced by a polarized Gaussian beam from a single-mode laser focused with a cylindrical lens onto a flat mirror. The laser beam waist had to be focused to 50 μm allowing energy conservation for many final momentum states due to the Kapitza-Dirac effect. Otherwise, a waist of the regime of millimetres conserves energy and momentum only for Bragg scattering [43].
After first demonstration of coherent control of the motion of complex molecules in 2001 [41], the Kapitza-Dirac effect was integrated into the Talbot-Lau interferometer. The central material grating of the TLI was replaced by a standing laser light wave [1]. The standing wave must be perpendicular to the molecular beam in order for the molecules to see a light potential that is not averaged out during the transit [41].

The electric field produced by the laser light induces a dipole potential $V(x, z)$ and a dipole moment oscillating at the laser frequency far-off any molecular resonance. The molecule accumulates a phase shift $\phi(x)$ during the transit through the standing laser light wave in x-direction given by the transmission function: $t(x) = \exp(-\mathrm{i}\phi(x))$ [38, 44]. The laser with a power P_L has a Gaussian beam waist w_y along the y-axis (see coordinate system in figure 2.4). The position in z-direction is replaced by the time t times the velocity of the molecule v_z. The maximal phase shift ϕ_0 is then calculated from α_ω, which is the is the real part of the polarizability of the molecule at the laser frequency $\omega_\mathrm{L} = 2\pi\mathrm{c}/\lambda_\mathrm{L}$ [12]:

$$\phi(x) = -\frac{1}{\hbar}\int_{-\infty}^{\infty} V(x, vt)\,\mathrm{d}t = \phi_0 \cdot \cos^2(k_\mathrm{L} x) \tag{2.6}$$

$$\phi_0 = \frac{4\sqrt{2\pi}\,\alpha_\omega\,P_\mathrm{L}}{\mathrm{h}\,\mathrm{c}\,\epsilon_0\,w_\mathrm{y}\,v_\mathrm{z}} \tag{2.7}$$

The maximum phase shift increases linearly with the laser power and it is inversely proportional to the molecule's velocity. Note, that the equation describes the phase shift only for a pure phase grating assuming no absorption of light grating photons. However, for molecules with a non-zero absorption cross section at λ_L, the absorption of photons can occur. This absolute absorption cross sections has been measured in the KDTLI from photon recoil [45]. Remarkably is also a coherent diffraction effect in addition to the phase grating [46], where a momentum of $\Delta p = \pm\hbar k_L$ is added to the molecular momentum for each absorbed photon from either of the two directions of the retro-reflected laser beam.

The experimental details of the KDTLI are explained in section 2.2, but before some general physical concepts involving the quantum mechanical relevance of the KDTLI are discussed.

2.1.4 Decoherence, dephasing, and perturbation

One of the big puzzles of physics is the question, how quantum physics is connected with the classical world. There are many interesting theories and interpretations in this field. This chapter presents only some of these ideas, which are related to matter wave interferometry. Matter wave interference experiments such as the KDTLI could provide a direct test to the limit of the quantum superposition principle [2], which theories like the continuous spontaneous localization (CSL) have to take into account. CSL postulates the spontaneous collapse of the superposition above a certain mass scale. This prediction originates from modifications of the Schrödinger equation using a non-linear, stochastic term [21].

In general, decoherence theory explains the decay of coherence within the framework of quantum physics as a result of objects interacting with their environment. In more detail, decoherence is the irreversible disappearance of certain non-diagonal elements in the density matrix, when the system openly propagates. The irreversible process of phase relations delocalizing seems to be omnipresent in nature itself [47].

Among this, collisional decoherence has also been experimentally proven with fullerenes in a three-material-grating Talbot-Lau interferometer [6]. In these experiments, the background gas pressure was continuously increased causing collisions with the delocalized fullerene molecules. A gradual loss of fringe visibility was detected. The loss is distinctively different from Beer's law of absorption and in good agreement with decoherence theory [48].

Considering hot and sufficient complex molecules, decoherence is also caused by their interaction with the environment via scattering or even emission of thermal photons. Therefore, new visionary proposals are needed to observe interference with truly macroscopic bodies, because they emit far too many photons. These photons can carry the which-path information causing thermal decoherence. In practice, fullerenes in the TLI were laser heated from their evaporating temperature of approximately 1000 K up to 3000 K, where the emitted photon's wavelength is comparable to the maximum path separation holding the which-path information. The interference visibility as a function of the heating is completely declining. In conclusion, the distinction between the quantum and classical mechanics becomes more a smooth transition due to the observation of thermal decoherence in the TLI [49].

When the fullerenes leave the oven at their evaporating temperature, infra-red quanta are radiated at a very low rate [50]. Thus, coupling to the environment is minimal obviating decoherence. However, the interference contrast can still be reduced by several velocity-dependent mechanisms if the detection is not velocity resolving.

Additionally, vibrations of the interferometer lead to a reduction in visibility, as well. Especially, motions horizontal to the grating and perpendicular to the molecular beam, general torsional pendulum motion, and independent grating vibrations have the strongest affect on the measurements [51]. The frequencies of the vibrations in the regime of 50 to 1000 Hz influence the experiment, because they correspond to the molecule's flight time through the three gratings. Furthermore, even little mechanical perturbations can sabotage the overall performance of the experiment. Moreover, the frame of reference of the experiment is not an inertial system giving rise to inertial forces like gravity and the Coriolis acceleration. On the one hand, the Coriolis acceleration is to small to affect the KDTLI's parameter and its visibility [51]. On the other hand however, gravitation is forcing the molecules on a parabola, which will be explained in the section 2.2.2 velocity selection.

Matter wave interferometry in the KDTLI spatially superposes material objects up to a thousand times their own size. It has been proposed to even detect decoherence when scattering dark matter against normal matter [52]. Unfortunately, the current version of the KDTLI is just not sensitive enough [52], but future generations will be. The experimental set up of the KDTLI and its applicability are explained in the next section.

2.2 The Kapitza-Dirac-Talbot-Lau interferometer

The Kapitza-Dirac-Talbot-Lau interferometer (KDTLI) embraces the physical phenomena, explained in the previous sections, to examine matter wave behaviour of large molecules. It combines the advantages of the Talbot-Lau interferometer, operating in the near-field, with the benefits of an optical phase grating [1, 53]. Furthermore, the interferometer is capable of testing the metrology of molecules due to its sensitivity to the absolute polarizability of the molecules [5].

The complete experimental setup is placed on an optical table. Newport and Thorlabs active pneumatic vibration isolators levitate the table. Therefore, the experiment is decouple from external vibrations [54], because they cause a reduction in visibility [51, 53]. In conclusion, the table's and gratings' positions are measured by electrolytic tilt sensors (see section 4.5.2) to recognize perturbations. Further, an acceleration sensors is placed on the optical table. The background gas pressure inside the experimental chambers is reduced by a set of vacuum pumps ensuring a high vacuum pressure of $P = (10^{-7}–10^{-8})$ mbar [55]. The approximate mean free path length Λ of a molecule is calculated assuming its diameter $d_{\mathrm{mol}} = 1$ nm [20] and using its most probable velocity v_{mp} (equation 2.10) [56, 57]:

$$\Lambda = \frac{v_{\mathrm{mp}}^2\, m}{2\sqrt{2}\pi \cdot d_{\mathrm{mol}}^2\, P} > 20\,\mathrm{m} \tag{2.8}$$

As a result, the molecules have a mean free path much greater than the length of the entire setup of approximately $L_{\mathrm{KDTLI}} = 2.3\,\mathrm{m}$ making collisions very unlikely. However, the expression treats the molecules as hard spheres colliding, whereas their dipole moment and electrical interactions are neglected.
In this section, the setup of the KDTLI as illustrated in figure 1.1 and its components are presented starting from the source to the detection. The oven as the source heats the molecules, which determines their velocity distribution. The measurement of that distribution is explained in the next section using a pseudorandom chopper method. Afterwards, the realization of the three-grating setup is described and last the detection scheme of the quadrupole mass spectrometer is briefly introduced.

2.2.1 Thermal molecular source

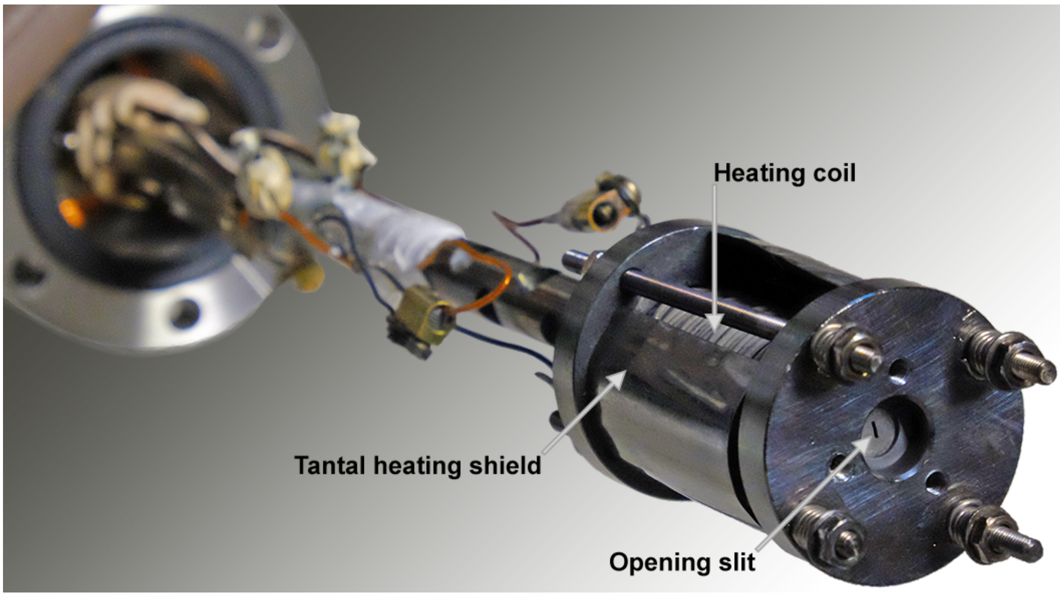

Figure 2.2: The photo shows the oven used inside the KDTLI. On the right side of the picture, one can see the small opening with the dimensions $2\,\mathrm{mm} \times 0.2\,\mathrm{mm}$. It is the slit, through which the molecules can evaporate into the chamber. The heating coils are covered with a tantalum shield to prevent heating the chamber. On the left, the mounting to the vacuum chamber is recognizable (adapted from [58]).

The source of the examined molecules is a thermal oven as shown in figure 2.2.

Molecules are heated until they evaporate and exit the oven. The oven's main component is a cylinder covered in stainless steel and the cap sealing the oven. Both are made out of Shapal. Shapal is a ceramic, which combines a high thermal conductivity as well as a high mechanical strength with an extremely low coefficient of thermal expansion [59]. In conclusion, Shapal is an excellent choice of material for the oven also given its sealing ability to vacuum.

Inside the cap is a slit of the dimensions $2\,\mathrm{mm} \times 0.2\,\mathrm{mm}$, which acts like a nozzle. The molecules enter the high vacuum of the source chamber through that nozzle. The vacuum of the source chamber is important, because collisions between the examined molecules and the background gas radically reduces the signal and manipulates the expected velocity distribution.

The oven's cylinder is wrapped in coils of an approximately two-meter long heating wire with a resistance of $R = 150\,\Omega$, which was measured during the construction [53] and confirmed recently investigating the oven's durability. It can be heated up to 1000 K by supplying an electrical power of 80 W. A thermocouple type K is included into the oven's design to monitor its temperature. For several reasons, the coils are shielded by a tantalum sheet lowering heat radiation. First, it reduces the stress on the wire and the energy needed, which speeds up the heating process. Mainly, it keeps the temperature in the chamber from rising. Conclusively, a higher temperature increases the background gas pressure, because previously condensated molecules or fragments can evaporate again.

The amount of the filling of the oven is a trade-off between a long lasting signal and a minimal risk to clog the opening slit or having a spitting oven. When the oven is refilled, it is detached from the experimental setup and the four screws on the oven's cap are removed (see figure 2.2). The small springs ensure that the cover remains fixed during the heating and cooling, because the used materials have different thermal expansion coefficients. Afterwards the oven is remounted to the X/Y-translation stage to adjust the vertical and horizontal position of the opening slit deciding the beam path. More detailed descriptions of the oven can be found in previous theses [60, 53, 55].

When the oven is heated, the molecules evaporate into a thermodynamical equilibrium. Therefore, the Maxwell-Boltzmann distribution $f(v)$ characterises the molecule's velocities v, where m is the molecule's mass, T is the temperature inside the oven, and k_B the Boltzmann's constant [57]:

$$f(v) = \left(\frac{m}{2\pi k_\mathrm{B}T}\right)^{\frac{3}{2}} 4\pi v^2 \mathrm{e}^{-\frac{mv^2}{2k_\mathrm{B}T}} \tag{2.9}$$

$$v_\mathrm{mp} = \sqrt{\frac{2k_\mathrm{B}T}{m}} \tag{2.10}$$

$$\mathrm{TPP:} \quad v_\mathrm{mp} = \sqrt{\frac{2\cdot 1.38\cdot 10^{-23}\,\mathrm{JK}^{-1}\cdot 665\,\mathrm{K}}{614\cdot 1.66\cdot 10^{-27}\mathrm{kg}}} \approx 135\,\mathrm{ms}^{-1} \tag{2.11}$$

From that distribution, one can deviate the average velocity (v_avg), the most probable velocity (v_mp), and the root-mean-square (v_rms) [57]. The most probable velocity is the maximum of the distribution curve and will be determined from measurements in the analysis in section 5.2.2.

In addition, it has been shown, that the Maxwell distribution can be derived more generally for molecules, which makes it applicable here [61]. However, one defendable assumption remains to use the Maxwell distribution, that no collisions occur between the molecules while flying through the opening slit. On the one hand, the fraction of the particles that can leave the oven through the orifice is negligible and the thermodynamic equilibrium is not disturbed. On the other hand, some molecule species evaporate at high temperatures up to 900 K like C_{60} causing a high vapour-pressure. In conclusion, the mean free path length of the molecules is comparable to the dimension of the orifice. Under those circumstances, the assumption made is slightly violated. Therefore, one expects a more narrower velocity distribution which is also shifted towards faster velocities [60, 53]. Nevertheless, the most probable velocity (v_mp) will be in close agreement to the thermal one [19]. Since the mass of the molecule stays constant, the velocity depends only on the temperature as a variable.

2.2.2 Velocity selection and measurement

The velocity of the molecules is a curial parameter of the experiment. It determines the De Broglie wavelength of the examined molecule (equation 2.1) and its free-flight path through the interferometer (equation 2.8). As indicated in figure 1.1, three delimiters are placed in the beam path. Therefore, a velocity class is selected due to the parabola flight path in the gravitational field. Typically on the KDTLI,

$10\,\% - 20\,\%$ ($\Delta v/v$) of the velocity distribution are selected by the delimiters. In contrast to the first and last, the second delimiter's width is adjustable by a piezo crystal. The widths of the delimiters has to be chosen to optimise the interference patter, where counts are traded for contrast. However, the pure selection of the velocities is lacking a quantitative measurement for an overall understanding of the experiment. Therefore, the velocity distribution is resolved from a time-of-flight (TOF) measurement.

A trivial way to measure the velocity distribution $f(v)$ is achieved by cutting the beam in such a way that no molecule package would overlap before reaching the detector. The distribution would be retrieved by calculating the velocity from the time of flight knowing the distance. However, the disadvantage is the immense loss in signal.

TOF measurements are always a compromise between resolution and intensity. Here, the pseudorandom chopper method is applicable and has been efficiently used in similar experiments [62]. Hence, a pseudorandom chopper disk is mounted on a linear stage close to the molecule's source. Respectively, it can be driven into the beam path [60]. That provides two additional advantages. First, mechanical vibrations are as far away from the gratings as possible and the examined flight time is maximized. In principle, the disk spins chopping the beam according to the slits as shown in figure 2.3. A photodiode records the pattern of the opened and closed slits from the chopper while simultaneously the molecules are detected.

Vibrations of the chopper motor limit its frequency to $f = 15\,\text{Hz}$. The disk's minimal bin width defines the resolution of the chopper function. For constructional reasons, the number of bins on the chopper is limited. If the analysis treats the chopper as an ideal delta function modulator, it produces a binary sequence [63, 64]. To maximise the length of the binary sequence, a linear feedback shift register is used as pseudorandom generators, which results in the specific maximum length of $n = (2^8 - 1) = 255$ for the number of bins [65]. The pseudorandom pattern of bins on the disks results in 64 physical slits with different width as illustrated in figure 2.3. Thus, the time resolution $\mathrm{d}t$ can be estimated form the frequency f and the number of bins n : $\mathrm{d}t = (f \cdot n)^{-1} \cong 250\,\mu\text{s}$. As a consequence of that limit, the sampling rate, or better the integration time of the detector, should be respectfully reasonable.

Here, the Nyquist-Shannon sampling theorem is used as a reference point for

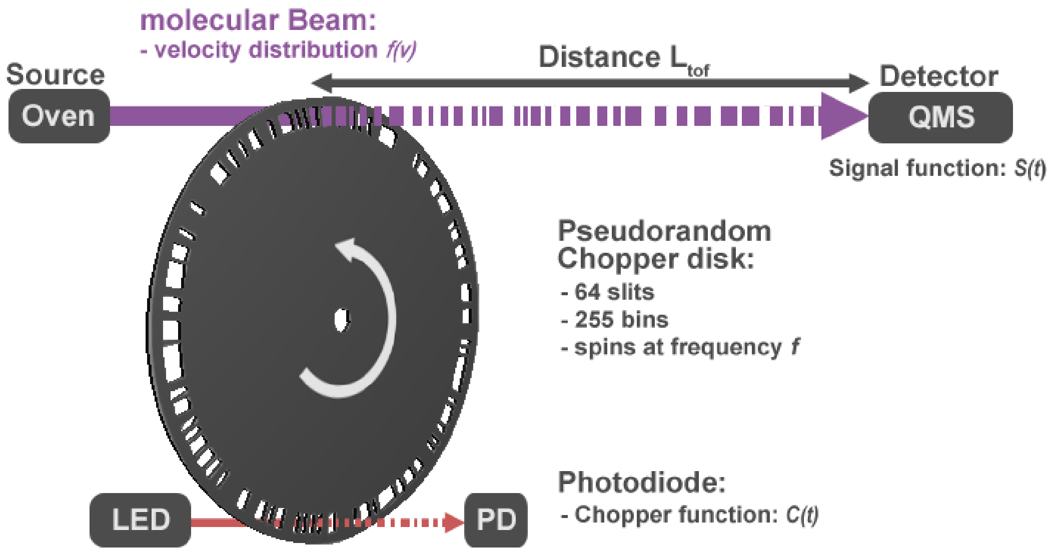

Figure 2.3: The figure shows the pseudorandom chopper disk which is used for time-of-flight (TOF) measurements. The chopper disk is placed inside the molecular beam in front of the oven, where the molecules with a velocity distribution $f(v)$ are emitted from. The spinning disk chops the beam according to the open slits. The photodiode measures the sequence of the disk being open or closed in an angle of 180° to the molecular beam. The time-of-flight of the molecules is calculated from the deconvolution of the photodiode signal $C(t)$ and the molecular beam signal $S(t)$ measured from the QMS (see equation 2.13).

the integration time [66]. The theorem says, that if a signal is perfectly limited to a bandwidth of the frequency f_0, no information is lost to recover f_0 sampling with a frequency greater than or equal to $2f_0$. As a result, the integration time of the detector is depending on the frequency of the chopper wheel. The new control software measures this frequency and automatically provides a recommended integration time. How the software allocates the data from the experiment is described in section 4.4.

Before the data can be analysed, the mathematical background needs to be investigated before further processing. Figure 2.3 demonstrates the principle of the TOF measurement, where the signal function $S(t)$ and the chopper function $C(t)$ are recoded in the data. The relation from the data to the velocity distribution is expressed in equation 2.12, where $B(t)$ is the background signal including for example dark counts from the QMS or noise from the chopper. Additionally, a proportionality constant K represents aberrations caused by e.g. the ionization cross section or amplifier gain during the detection process (see section 2.2.5). In the next step, the velocity distribution is transformed into a time-of-flight distribution by a simple substitution:

$$S(t) = K \int_0^t C(t - Lv^{-1}) f(v)\,\mathrm{d}v + B(t) \tag{2.12}$$

$$\text{Substitution :} \quad T = Lv^{-1} \quad \longrightarrow \quad g(T) = f(v) \left| \frac{\partial v}{\partial T} \right|$$

$$S(t) = K \int_0^t C(t - T) g(T)\,\mathrm{d}T + B(t) \tag{2.13}$$

The TOF is extracted by deconvoluting the two measured signals from the photodiode and the detector. Multiple methods for this extraction are available [63]. One method is to apply a Fourier transformation, which is convincing due to its simplicity. However, some assumptions and approximations have to be made beforehand. First, any background noise is not taken into account. The limits of the integral have to be extended to ∞ and $-\infty$. As a consequence, frame overlap may be neglected and noise adds a high-frequency components to $\mathcal{F}(S(t))$, causing $\mathcal{F}(C(t-T))$ go to zero faster than $\mathcal{F}(S(t))$, which results in $\mathcal{F}(g(T))$ diverging for high frequencies [63]. Employing the Fourier transformation method, the convolution theorem is used to obtain the time-of-flight distribution $g(T)$ from the data [67]. This method is used in the analysis in section 5.2.2:

$$S(t) = K \int_{-\infty}^{\infty} C(t - T) g(T)\,\mathrm{d}T \tag{2.14}$$

$$\mathcal{F}(S) = \mathcal{F}(C)\,\mathcal{F}(g)$$

$$g(T) = \mathcal{F}^{-1}\left[\frac{\mathcal{F}(S)}{\mathcal{F}(C)}\right] \tag{2.15}$$

In practice, this approach might give too vague results for noisy data [63]. In that case, other methods are more suitable like smoothing data or a Laplace transformation. A general method of obtaining a deconvolution of TOF data would be fitting a parameterized convolution, which works even for complicated situations of TOF signal and it avoids the problems of noisy data [63]. A common method to deconvolute the signal is the cross-correlation method, which is used on similar experimental setups to the KDTLI or with a similar chopper disk [62, 63, 64, 68].

In conclusion, general improvements to the resolution limits of the TOF measurements can be achieved both in hardware adjustments and in analytical revisions. The TOF measurements are essential to the overall experimental results, because the molecules interaction with the gratings of the interferometer are velocity dependent as the next sections will show.

2.2.3 The gratings

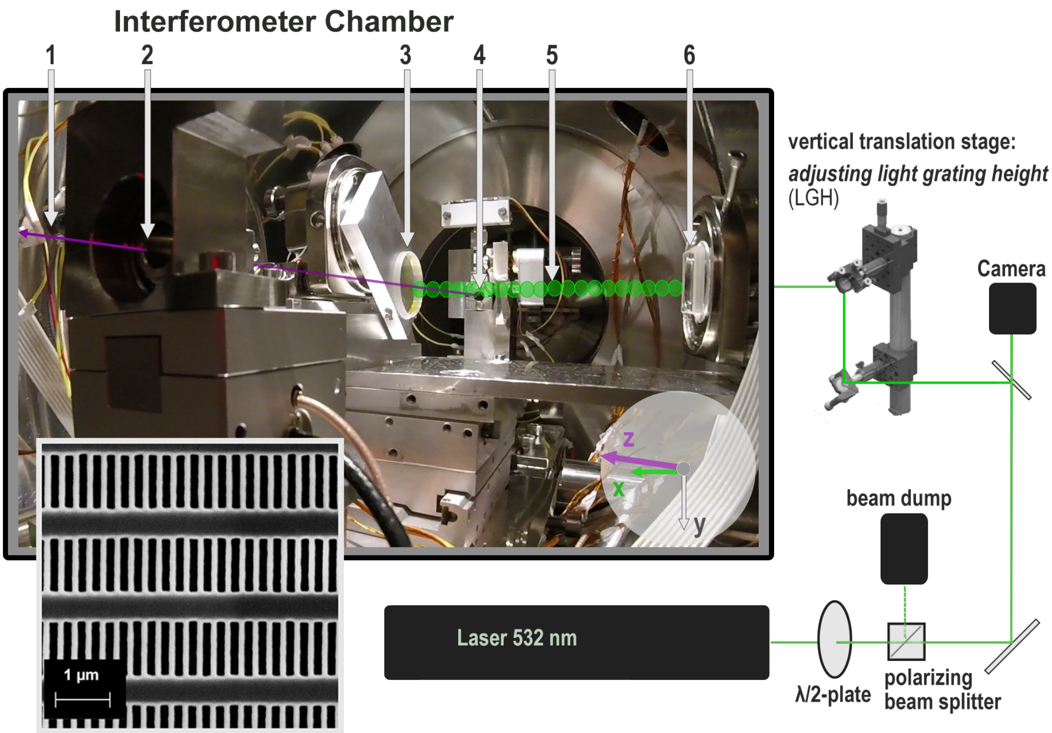

Figure 2.4: The photo is taken from inside the KDTLI's interferometer chamber. 1: The molecular beam, 2: Material grating G3, 3: 0° mirror, 4: Material grating G1, 5: Illustrated standing laser light wave G2, 6: Focal lens (adapted from [69]). The coordinate system defined in this thesis has the z-axis pointing in the direction of the molecular beam, the y-axis towards gravity and the x-axis along the standing light wave.
On the bottom left is an image of the material grating taken with an electron microscope (adapted from [70]).
On the right, the laser beam path before the chamber is sketched. Mirrors and translation stages are used to adjust the standing laser light wave. A rotational $\lambda/2$-plate controls the light intensity of the standing wave due to the polarizing beam splitter afterwards and a CMOS camera is used to monitor the laser beam profile [71].

The heart of the KDTLI is the interferometer setup consisting of three equidistantly positioned gratings. The two material gratings are photolithographically etched into a 190-nm-thick silicon nitride (SiN_x) membrane [4], which is at the cutting edge of current technology. They have a period of $d = (266.38 \pm 0.05)\,\mathrm{nm}$ and a support structure of 1.5 µm, as shown in figure 2.4. The opening fraction is approximately $f = \frac{d_s}{d} = 42\,\%$ and the entire grating has a size of (3×3) mm [53, 60]. The transit time through the material gratings amounts to approximately 125 ns for TPP molecules at a molecular temperature of 665 K. Conclusively, the molecule interactions with the grating walls are averaged over the molecular starting conditions and orientations, because the conformations interconvert on the time scale of (1–10) ps for thermally excited molecules [38]. The molecule-grating interaction has been under experimental tests to study the transmission behaviour of molecules. As a result backed by theoretical predictions, the grating openings effectively appear more narrow to the molecules mainly due to the van der Waals interactions, which are velocity and polarizability dependent [72, 73].

In contrast to the material gratings, the main advantages of the light grating are first the lack of van der Waals forces acting between the grating and the molecules. Secondly, there is no loss in transmission, which results in an increased signal compared to an all-material grating interferometer. In this experiment, the optical phase grating is realized by retro-reflecting, commercial CW laser from Coherent (Verdi V20, $\lambda_L = 532$ nm) with a linewidth of < 5 MHz rms [74]. The laser wavelength is slightly and slowly tunable between 532.18 nm and 532.32 nm by changing the intra-cavity etalon temperature. The laser beam inside the interferometer chamber is focused onto a 0° mirror with a cylindrical, plano-convex lens (focal length: $f_{\text{lens}} = 100$ mm) to a waist of $w_z = 17$ µm ($w = f_{\text{lens}} \cdot \lambda_L / (\pi \cdot w_0)$) along the molecular beam axis (see figure 2.4). The smaller the waist w_z, the easier it gets to achieve the required parallelism between the molecular beam and the mirror. However, if the resulting Rayleigh length of $z_R = \pi w^2/\lambda_L = 1.7$ mm [75] is reduced too much, one cannot operate with the full available horizontal width of the molecular beam [53]. Outside the range of the Rayleigh length, the radius of curvature of the wavefronts decreases very rapidly. Therefore, the molecule beam must cross the laser grating close to its waist, where the wavefronts are sufficiently planar.

The standing light wave can be repositioned by adjusting translational stages and the intensity is controlled by rotating a $\lambda/2$-plate as illustrated in figure 2.4. The three gratings are spaced equidistantly with a distance of $L = 105$ mm between each material grating and the light grating, which was set up to correspond to $L \cong 4.5\,L_T$ for the fullerenes C_{60} at $v_z = 180\,\text{ms}^{-1}$ in the interferometer [12, 53].

Moreover, the periods of the material gratings G_1 and G_3 were carefully aligned to the $\lambda_L/2 = 266\,\text{nm}$ laser grating period. The difficulties and the procedure of the alignment process of the three gratings are described in previous theses [44, 53, 55]. A deviation above 0.05 nm, which is roughly the diameter of a hydrogen atom, would reduce the interference fringe visibility significantly [20, 12]. The next section motivates the theoretical prediction of the fringe visibility for the KDTLI.

2.2.4 The visibility in the KDTLI

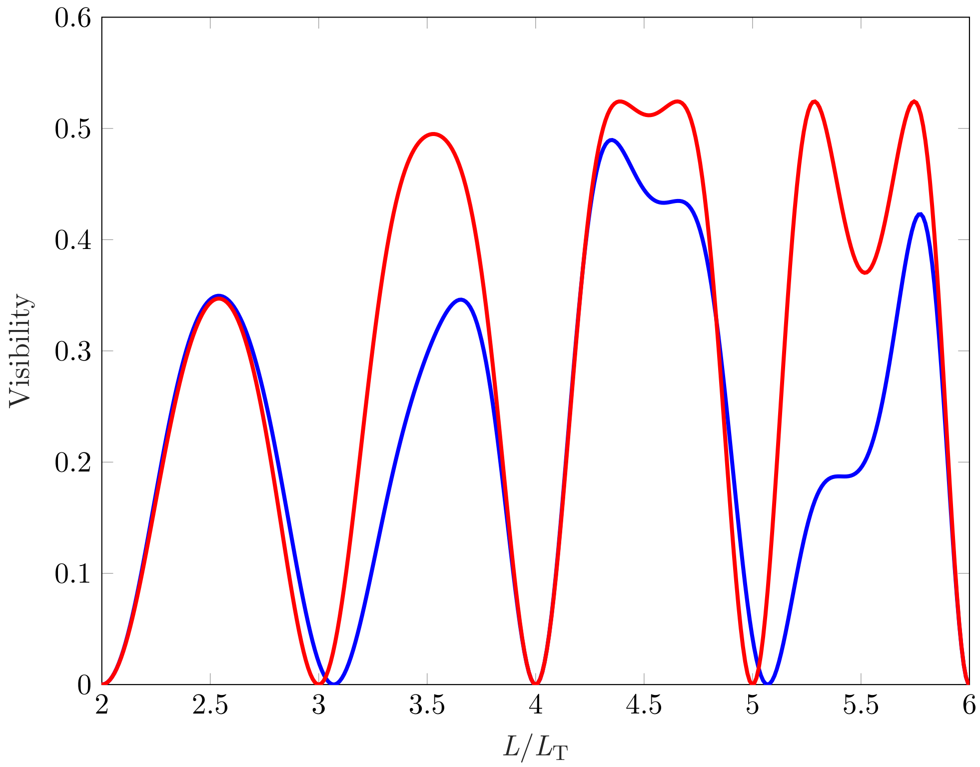

Figure 2.5: The fringe visibility was calculated for the parameters of the molecule TPP (614 amu) as a function of L/L_T (laser power: $P_L = 7.5\,\text{W}$, optical polarizability at the laser wavelength: $\alpha_L = 105\,\text{Å}^3 \times 4\pi\epsilon_0$ [76], vertical beam waist $w_y = 700\,\mu\text{m}$).
Red line: The contrast is calculated with the equation 2.18 assuming a pure phase grating ($\sigma_{abs} = 0$).
Blue line: The absorption of light grating photons is taken into account to calculate the visibility using equation 2.17 (assuming $\sigma_{abs} = 1.70 \times 10^{-21}\,\text{m}^2$ [77]).

As the interferometer itself, the theory of the KDTLI is building upon the theoretical description of the three-material grating interferometer [3, 12] incorporating the interaction with the standing light wave.

The propagation of the molecular beam through the interferometer is described by means of the phase space representation of quantum mechanics [78]. The Wigner function or Wigner quasi-probability distribution describes the transverse molecular beam state in phase space. The material gratings are represented by a rectangular transmission function, which is defined by a sinc-function in phase space including the opening fraction f of the gratings. Between the gratings, the matter wave evolves freely. The periodicity of the sinusoidal phase grating defines the Fourier transform of the transmission function and due to the Talbot-Lau effect the Fourier coefficients depend on L/L_{T}. The light grating transmission function includes the maximum phase shift ϕ_0 (see equation 2.7) induced by the Kapitza-Dirac effect. The transmission function is represented by Fourier coefficients, which are proportional to a sum over Bessel functions J_n [38]. Higher order than two of the Bessel function (J_2) are neglected safely when comparing with measured data [60, 79]. Here, $\zeta_c = \phi_0 \sin(\pi L/L_{\mathrm{T}})$ describes the diffraction effect from a phase modulation and $\zeta_a = n_0(1 - \cos(\pi L/L_{\mathrm{T}}))/2$ includes the diffraction effect due to absorption. The mean number n_0 of absorbed photons, which depends on the absorption cross section σ_{abs}, is given by:

$$n_0 = \frac{8}{\sqrt{2\pi}} \frac{\sigma_{\mathrm{abs}} P_{\mathrm{L}} \lambda_{\mathrm{L}}}{\mathrm{h\,c}\, w_{\mathrm{y}} v_{\mathrm{z}}} \tag{2.16}$$

The final molecular diffraction pattern in the KDLTI is characterized by the fringe visibility $\mathcal{V}$ incorporating the absorption effects of the light grating [60, 79]:

$$\mathcal{V} = 2\,\mathrm{sinc}^2(\pi f) \mathrm{e}^{-\zeta_a} \left(\frac{\zeta_c + \zeta_a}{\zeta_c - \zeta_a} \right) J_2 \left(\sqrt{\zeta_c^2 - \zeta_a^2} \right) \tag{2.17}$$

For a pure phase grating, there is no absorption of photons ($n_0 = 0 \rightarrow \zeta_a = 0$) and equation 2.17 simplifies to:

$$\mathcal{V}_{\mathrm{phase}} = 2\,\mathrm{sinc}^2(\pi f) J_2 \left(\phi_0 \sin \left(\pi \frac{L}{L_{\mathrm{T}}} \right) \right) \tag{2.18}$$

The equations 2.17 and 2.18 are plotted in figure 2.5 for the mass and polarizability of the molecule TPP. It demonstrates, that even a small absorption cross section affects the visibility in higher Talbot orders. In comparison, the calculated visibility in a TLI shows only maxima close to the multiples of Talbot order in between the red and blue line in figure 2.5 [1, 53].

In a three grating setup, classical Moiré fringes are expected with the same periodicity as the interference fringes in the KDTLI [20, 12]. These can be well excluded in the KDTLI for all measurements, since these classical fringes lie in a different parameter regime than the quantum interference patterns. The effects can be distinguished by observing the fringe visibility as a function of the laser power and comparing the measured curve (see figure 5.2) with the theoretical predictions for the classical and quantum model [2].
Under typical experimental conditions, the interference pattern is well described by a sine curve [19]. Therefore, the visibility $\mathcal{V}$ is defined in terms of the maximum and minimum count rate C:

$$\mathcal{V} = \frac{C_{\mathrm{max}} - C_{\mathrm{min}}}{C_{\mathrm{max}} + C_{\mathrm{min}}} = \frac{A}{C_{\mathrm{mean}}} \tag{2.19}$$

C_{mean} is the mean count rate of the recorded signal and A is the amplitude of the sine curve fitted to the data (see section 5.2.1). The ratio between amplitude and offset in the sine curve is given by the ratio between the zeroth and first Fourier component, when the signal is discrete and the sine period is fixed (see figure 5.3). The measurement of the final fringe visibility is accomplished by detecting the intensity of the molecular beam as a function of the position of the third grating G3, which is moved as illustrated in figure 1.1.

2.2.5 Detector - QMS

The last part of the experimental setup is the detection chamber [53, 60, 80, 55]. Its main components are the third delimiter for velocity selection (D3 in figure 1.1), and a commercial quadrupole mass spectrometer (QMS, Extrel Core Mass Spectrometers, Model 150-QC [81]). The working mechanism of the QMS can be separated into three main parts: the axial molecular beam ionizer [82], the quadrupole mass filter [83], and the conversion dynode electron multiplier [84] as symbolized in figure 1.1. First, the neutral molecules are ionized by electron impact. Secondly, the positive ions enter the quadrupole mass filter. Four rods with a 9.5 mm diameter form a hyperbolic electric field, because the electric potential of the neighbouring rods have opposite signs. While the ions pass the electric field, they are driven away by the electric force. An additional alternating potential at 440 kHz is applied to the rods. Therefore, the destabilization is changing in a way that a certain mass-to-charge ratio of the ions traverse the QMS. Mathematically, the equation of motion in an QMS can be expressed with Mathieu differential equations [85]. The QMS from Extrel can detect mass-to-charge ratios from zero to 16 000 amu. The resolution of the QMS can be increased lowering the mass-range by changing the rods, or the resonator, and the settings of the voltages and frequencies within the software from Extrel called Merlin [86]. The settings are saved to a tune file. Last, the positive ions are accelerated towards a dynode with negative potential up to 9 kV. The dynode produces secondary electrons, which are detected by an electron multiplier. The signal is then amplified into a TTL pulse for each count. The level of amplification determines to the dark counts, which is the mayor factor in the noise of the signal. The signal is measured by the USB-6343 device described in section 4.1 [87]. For optimization of the position of the mass spectrometer, it is mounted on a X/Y-translation stage to the experimental setup.

2.2.6 Metrology of the KDTLI

The detected density pattern of the examined molecules has a nano structure with the periodicity of the gratings. Due to the resolution of this structure small shifts or amplitude changes of the fringe pattern can be measured. Gravity, a magnetic field, an electric field, or other external forces can cause a change of the phase or the visibility of the interferogram. Therefore, the interferometer is a precise tool for metrology measurements on molecules [88].

When introducing a controlled electric field into the interferometer, the resulting phase shift or dephasing of the fringe visibility is directly related to the electric force $\mathbf{F}$ acting on the electric susceptibility χ of the molecule. The electric susceptibility χ can be calculated by the expression: $\chi = \alpha_{\text{stat}} + \mu^2/3k_\text{B}T$, where α_{stat} is the static polarizability and μ^2 is the thermal average of all squared electric dipole moment components [21]. This expression for the susceptibility is known as the Langevin-Debye formula [89]. The force acting on the molecules relevant for deflectometry in the KDTLI is proportional to the specific susceptibility χ: $\mathbf{F} \propto \chi(\mathbf{E}\nabla)\mathbf{E}/mv^2$ [90]. The expression simplifies for non-polar rigid molecules molecules, where the susceptibility χ is given only by the static polarizability α_{stat}. Floppy molecules may develop a fluctuating dipole moment on the nanosecond time scale due to thermally-induced conformational changes [21].

The molecules under investigation are thermally hot causing a large number of rotational and vibrational states to be excited. The flight time of the molecules through the electrode region is in the order of microseconds. Therefore, anisotropies of the electric polarizability are effectively cancelled out for all practical purposes considering the KDTLI.

The electric dipole moment of a molecule is generally speaking the volume integral over its charge density. For an unpolar molecule the dipole moment is given by the product of the static polarizability (α_{stat}) and the electric field **E**. In general, the polarizability is frequency-dependent. In the case of electric deflectometry in the KDTLI a DC electric field is applied, therefore the static polarizability is the relevant property.

The electrode has to provide a homogeneous force field **F**, which is the fundamental constraint of the design of the deflector. The deflector is made of two identical electrodes, which generate a maximum force uniformity in the interaction region with the molecules, where the molecular beams sees a maximum variation in the force field of $\pm 0.5\,\%$ [5].

In practice, an electrostatic deflector is inserted before the second grating in the KDTLI as illustrated in figure 2.6 and a voltage U is applied to the electrodes. The geometry of the deflector is characterized by the factor K, the lateral fringe shift Δs is then given by [60]:

$$\Delta s_x = K \alpha_{\mathrm{stat}} \frac{U^2}{m v_z^2} \tag{2.20}$$

The geometry factor K can be determined by calibration using a molecule with well known properties. As a result, the shift is proportional to the square of the voltage U, which is set by the experimenter, and the polarizability-to-mass ratio of the molecule. The working principle of the electrodes deflecting the molecular beam causing the interference pattern to be shifted along the x-axis is illustrated in figure 2.6.

This metrology method has been used in the all-material grating interferometer (TLI) to measure the absolute scalar polarizability of the fullerenes C_{60} and C_{70}

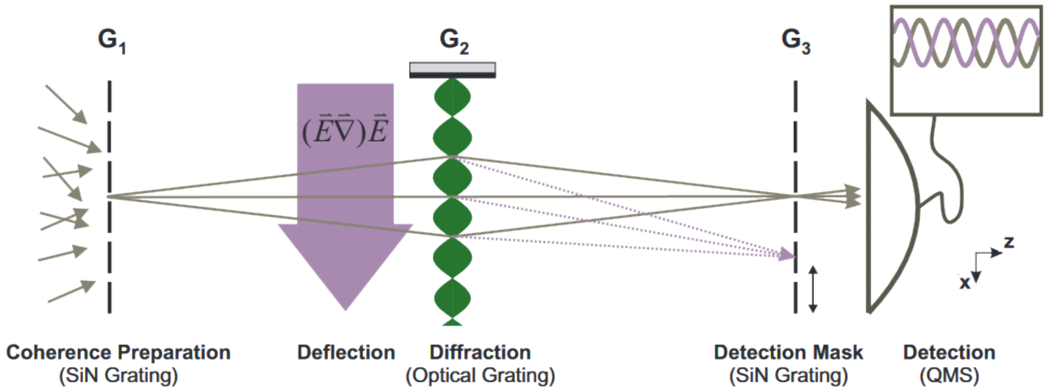

Figure 2.6: From [90]: The figure illustrates the metrology method used in the KDTLI, where a high-voltage deflection electrode is placed before the second grating inside the interferometer setup. The internal properties of the molecules such as the static polarizability α_{stat} interact with the homogeneous force field from the electrodes causing a displacement of the observed interference fringes.

[91]. In a related but different experimental implementation of a three-grating Mach-Zehnder atom interferometer, the same approach was used to measure the electric polarizability of sodium [92]. This arrangement of deflectometry is built on well established classical beam methods to characterize electric or magnetic properties of molecules and clusters [93]. It is a powerful tool, because it combines the sensitivity of near-field quantum interferometry with classical Stark deflectometry. Furthermore, the method even allows for the distinction of constitutional isomers due to the different shift they experience despite of their identical mass and chemical sum formula [94].

Deflectometry in the KDTLI also provided a quantitative comparison of a non-polar (FeTPP: 668 amu) molecule and its polar derivative (FeTPPCl: 703 amu) contrasting their quantum interference patterns [90]. The quantum contrast of polar version decays much faster with applied voltage. The non-polar rigid molecule is shifted to regions of higher field strength, while contrast stays constant.

There are many more interesting biomolecules that can be investigated by metrology in the KDTLI, for example tripeptides. However, some these molecules are rather fragile, which makes it difficult to produce a long lasting signal to preform deflectometry. The next chapter is presenting a vision, how to improve the measurement procedure from a software side to make more metrology and other measurement possible.

Chapter 3

Computer control - vision & measurement strategy

Many successful experiments have been performed on the KDTLI since its proof of principle was first demonstrated almost a decade ago [1]. Several improvements and additional features, which were presented in the previous chapter, extended the range of the experiment's applications over time. By now, the KDTLI is a sophisticated table-top experiment for the study of molecular interference.

The vision of this thesis is to amend and optimise the experiment's data acquisition, because the new features run on different PCs, within different programmes, or are not computer controlled. Therefore, a new, efficient, and consistent software application, which is comprehensible and easily extendible, was developed. Furthermore, the measurement procedures and documentation of the state of the experiment are done automatically. Conclusively, a database is continuously built up while the programme is running. In the future, this control vision is supposed to be the seed of new ideas for further development on this experiment and quantum physics in general, rather than achieving an overall automated KDTLI as a measurement machine.

This chapter initially explains the working process under nearly optimum condition. It thus provides the background knowledge to the concepts of the software development. The next section describes the experiment's peripheral and motivates its integration into the software. Afterwards, the automation of measurements is presented, which is a major aspect of the new control vision. Basic measurement procedures are being automated and joined into a unifying control application. At last, the underlying structure of the software is explained starting with a brief introduction to the programming language LabVIEW.

3.1 Optimization of the readjustment process

Given an ideally working KDTLI, the experimenter starts a day with refilling the oven to have an optimal signal of the examined molecule. The oven is detached from the experiment and filled with the molecular material of choice as for example tetraphenylporphyrin (TPP), which is available in the form of a purple powder (see figure 1.1). Afterwards, the oven is mounted back on the experiment to restore the vacuum (see figure 2.2). Minor spacial adjustments have to be made, because small deviations of the oven's position are inevitable. The oven's position is aligned to maximise the count rate while the molecules are heated. The temperature must be hot enough for the molecules to evaporate, but also low enough to avoid thermal degradation or fragmentation. Next, the slits or delimiters are moved into the molecular beam while keeping the count rate as high as possible. As a consequence of the changed molecular beam path, a slightly different velocity class of the molecules is selected and the light grating hight (LGH) has to be adjusted as well (see laser beam path in figure 2.4). At this point of the readjustment, the fringe visibility is restored. Consequently, a chosen laser power is set, which is either known from previous measurements or tested. Finally, interference patterns can be recorded, which show comparable visibility to previous measurements.
The position of the floating optical table affects the visibility. For that reason, any work on the optical table has to be done with care to not destabilise the table. Experience has shown that readjustments differ slightly every time. Therefore, automatizing this processes is not part of the control vision, because it seems to be more time-consuming than beneficial in contrast to procedures explained in section 3.3. However, there is potential for optimization in monitoring parameters of the experiment as the next section will show.

3.2 Recording of the peripherals of the KDTLI

Peripheral devices on the KDTLI are those, that are not necessary to record an interference scan. In detail, only the reading of the count rate from the QMS and the piezo-control setting the third grating's position are essential to plot an interference pattern. Nevertheless, other devices are needed to measure feedback parameters as crucial indicators for the quality and stability of the overall measurement condition. The operator might identify discrepancies to the optimal state of the experiment by keeping track of the following devices and parameters:

- The laser's properties play a central role for the interference contrast. They are monitored through different devices. First, the Verdi laser itself [74] returns parameters such as the etalon and baseplate temperature. The laser's wavelength is measured with 7 digits precision using a High Finesse wavemeter [95]. Also, the laser's beam profile is recoded as an image from a CMOS camera or a beam profiler. The laser power is measured before the light enters the main chamber either by a power meter or a calibrated photodiode.

- The temperature of the oven is measured with a thermocouple plugged into a USB data logger [96]. The temperature is set by a voltage from a power supply, which drives the heating coils of the oven.

- The vacuum pressure of the three chambers needs to be ensured to avoid collisional decoherence for example. Therefore, pressure gauges from Pfeiffer [97] and Leybold [98] are connected to each chamber.

- The table's position is measured by tilt [99] and acceleration sensors, while the optical table is floating. The pneumatic vibration isolators are inflated through pressurized nitrogen bottles or the central gas line [54].

- Two piezos are routinely addressed in the experiment. One sets the third grating's position and the other sets the width of the second delimiter for the velocity selection. Both controls need to set their position precisely. Therefore, their position is read to ensure their stability.

- The QMS detects the molecules, but a USB multifunction I/O device [87] actually transfers the signal to the PC, where an interference scan is recorded. The QMS is crucial for the reliability of the measurements, because its signal depends on various settings such as detection threshold and mass resolution. These settings consist of numerous options and are saved in a tune-file [86].

Capturing those parameters describes the state of the experiment. Automatically saving the parameters is a valuable addition to the lab book. A digital lab book has many advantages, because it allows to run scripts analysing all data. The deviations of the visibility can be correlated with any parameter's deviation determining if it is worth to invest time in stabilizing a parameter further to achieve an overall improved stability. In summary, measurement results will be more reliable and reproducible with more data to work with.

Studying mid- and long-term drifts of the experiment becomes possible as the database is continuously being built up further. As a result, malfunctioning and failure of devices can be identified and prevented by finding tendencies of parameters drifting out of range. Saving the peripherals of the experiment makes previously recorded data analytically comparable. This new way of handling the data could lead to new ideas for other experiments.

In order to use the meta data, it must be saved in a consistent way, searchable by key words. Since the programme congregates a vast amount of parameters, a well structured GUI (graphical user interface) is necessary to get all information on the screen for the operator to set up the next measurements or to quickly recognise errors. Chapter 4 shows how the control strategy is implemented. In contrast to the readjustment, some measurement processes include very repetitive working steps for the experimenter, where automations seems reasonable as the next section will show.

3.3 Automation of the KDTLI

After the alignment, the KDTLI is prepared to measure interference of molecules. Since its first demonstration, new features and measurements were added to the experiment. This section explains the work steps with a potential for automation. However, the KDTLI is an instrument for fundamental research in continuous development and is never meant to be fully automated.

During the interference experiments, automation of certain processes comes in handy. First, an optimal laser power has to be found. That is done by blocking the laser manually. Next, a lambda-half plate is rotated, which changes the ratio of the light being reflected to the beam dump or transmitted by the polarized beam splitter (see figure 2.4). A power meter measures the intensity, but it has to be placed within the beam path on the optical table. Last, the laser is unblocked and the power meter is removed. This is a time consuming and repetitive work, which also risks to destabilize the optical table. In that case, the operator has to wait until the tilt sensors show that the table is stable again.

The significance of the fringe visibility is increased by scanning multiple times and using statistical methods. However, experimental imperfections, such as a drifting a drifting third grating, have to be taken into account. Therefore, the interference scan itself is repeated several times with additional variation of parameters. The piezo step size and its scanning direction could be changed and the integration time at each grating position is adjustable. A shorter time decreases the measurement time, but longer integration improves the signal to noise ratio. In combination, one could measure the count rate multiple times before changing the piezo position taking the mean counts per position. Those options have to be chosen by the experimenter, while the computer control provides the functionality.

Seen by the control software, deflectometry measurements on the KDTLI are interference scans with an additional voltage set to the electrode. Therefore, all automated functions apply to deflectometry scans as well. Additionally, the electrode is set to different voltages before rerunning the scan, which is obviously also an easily automated procedure. Last, the time-of-flight measurements rely on data from a fast scaler card [100]. Merging those systems allowed to automate and combine all mentioned functionalities.

In conclusion, a sophisticated computer control saves a lot of time for the experimenter, ensures a more reliable and reproducible way of measuring and could open the possibility to measure interference with fast vanishing signals from biomolecules. Additionally, some automated measurements, which would take a lot of time, can be started remotely and the operator only needs to be notified. As a result, the experiment can run without being disturbed.

3.4 The programming language LabVIEW

Laboratory Virtual Instrument Engineering Workbench (LabVIEW) is the development environment for a visual, data flow programming language from National Instruments. The execution process of a LabVIEW-source code is determined by the structure of a graphical block diagram or back panel [101]. On the block diagram, the programmer connects different function-nodes by drawing wires, which propagate the variables as seen in the block diagram of the control software in figure 3.1. The wires and variables are colour-coded depending on the data type of the variable. A function node can be executed as soon as all its input data becomes available, while the data flows from the inputs through different nodes to the outputs.
In LabVIEW, the development of a graphical user interface (GUI) is already integrated into the coding process, because every new variable on the back panel creates a linked control button (input) or indicator (output) on the front panel. The block diagram contains the structures and functions, which perform operations on controls and supply the indicators with data. A virtual instrument (VI) can be run as either a stand-alone programme with the front panel or as a subroutine (subVI), when dropped onto the block diagram. In that case, its front panel defines the inputs and outputs of the subroutine. Therefore, each VI can easily be tested before being embedded as a subVI into another programme.
In general, the graphical approach also allows non-programmers to follow and understand the code due to the data flow scheme even for more complex structures.

3.5 The concept of the control software

This section explains the working principle of the new control software as a consequence of the new measurement strategy before the application's functionalities are exemplified in the next chapter. The software structure was implemented from the beginning using the LabVIEW guidelines, before the software's back panel becomes incomprehensible [102].
The new vision demands a stable all-in-one application, which runs all types of existing measurement procedures, constantly displays the state of the experiment,

and is easily adjustable and scalable. A state machine within LabVIEW [103], which is triggered by static events [104] fulfils the requirements. These two concepts, the state machine and the event handling, run within two separate while loops with independent runtimes as seen in figure 3.1. A state machine is a mathematical model of computation [105]. It is always in exactly one of a finite number of states. The machine changes from one state to another due to conditions within the state or an external input such as an event case structure, here. The user pressing a button on the front panel triggers an event, which writes a number into the state variable, which is then read by the state machine. Further, the scalability of the overall programme is achieved by making the state variable a type definition [106]. In summery, the state machine is defined by the list of all its states (see appendix). The states' content and their transitions define the workflow, while the events, which are triggered by the user, set a certain starting state.

For instance, as illustrated in figure 3.1, the user presses the button "TOF" (see section 4.4), that triggers the corresponding event, the state variable is set, and the state machine executes the state number of the variable. As another example of the workflow, the recording of the peripherals of the KDTLI is implemented into a set of states, one for each device. The first device's state points to the next device's state, and so on. Therefore, when different functionalities of the application check the condition of the experiment e.g. at the end of a measurement or to log it, the state machine only needs to be set to the first device's state.

As a summary, the new control programme starts with an initialization of the hardware, state by state as explained in the first section of chapter 4. Afterwards, the state machine reaches a "wait" state, where it reads the state variable set by a user event to perform tasks like a time-of-flight measurement. Than, it returns to the "wait" state ready for further instructions. The complete block diagram of the control software and the list of all subVIs, including the block diagram of the interference scan and the time of flight measurement can be found in the appendix of this thesis. In the next section the applications of the software on the KDTLI are presented by explaining the functionalities for the user.

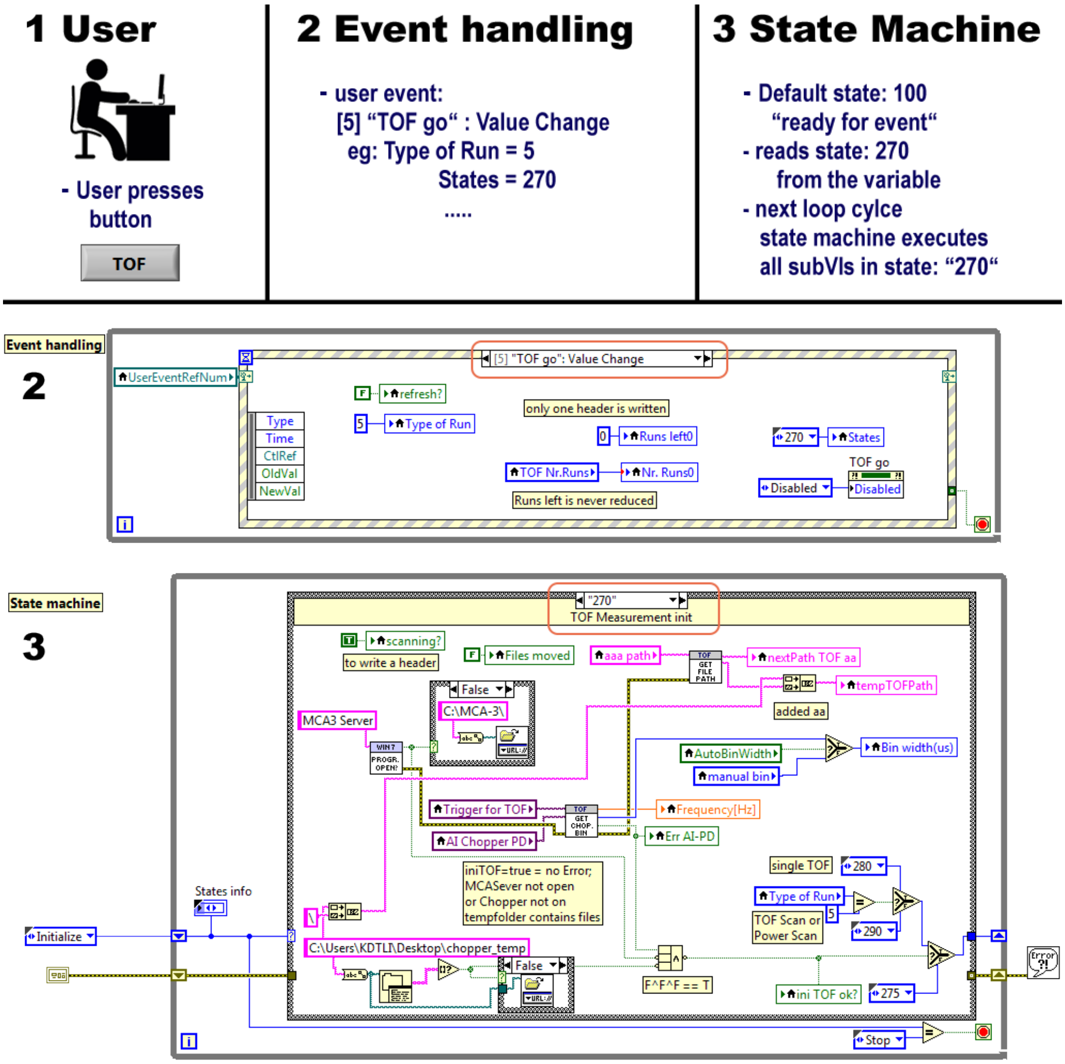

Figure 3.1: The figure illustrates the working principle of the LabVIEW code from the new control software. 1- The user presses a button on the GUI such as the "TOF"-button (see section 4.4). 2- An event is triggered by the action and within that event case the state variable is set to "270". 3- The state machine reads the state variable, transits to that state, and executes the code within.

Chapter 4

Programme guide of the KDTLI

As a result of the implementations from the previously explained measurement vision, the new stably running control software is introduced in this chapter. New features like the live display of several parameters provide an improved user experience. Moreover, data is recorded according to the new strategy of building a database. Last, some measurement routines are automatized and the software is built in a modular way. Therefore, subroutines and the software architecture can be recycled for other experiments, which are using the same hardware or having similar measurement tasks.

This chapter is a programme guide explaining the implemented software functionalities. The new programme is meant to be used by a person familiar with the KDTLI, who can properly set the parameters to run the experiment. In addition, most parameters are restricted to an applicable range within the programme code. The user interface is designed in the style of the original LabVIEW programme controlling interference scans on the KDTLI. Furthermore, the interface is sorted into different tabs as seen at the top of figure 4.1, which contain all the functionalities for a certain measurement task.

The first tab and section is about the initialization process, which does initialize all connected devices, but the main idea is an overall sanity check of the experiment. Section 4.1 is rather technical, because it explains how the devices are connected and communicate with the PC. Therefore, the acquired data's reliability is validated from a software point of view and along the way the wiring of the experiment is revealed. The next sections present the interference, deflectometry and the time-of-flight measurements according to the tabs' names of the GUI (see top of figure 4.1). The last section presents the new handling of the peripheral devices of the experiment including new functionalities and integrated applications.

4.1 Initialization

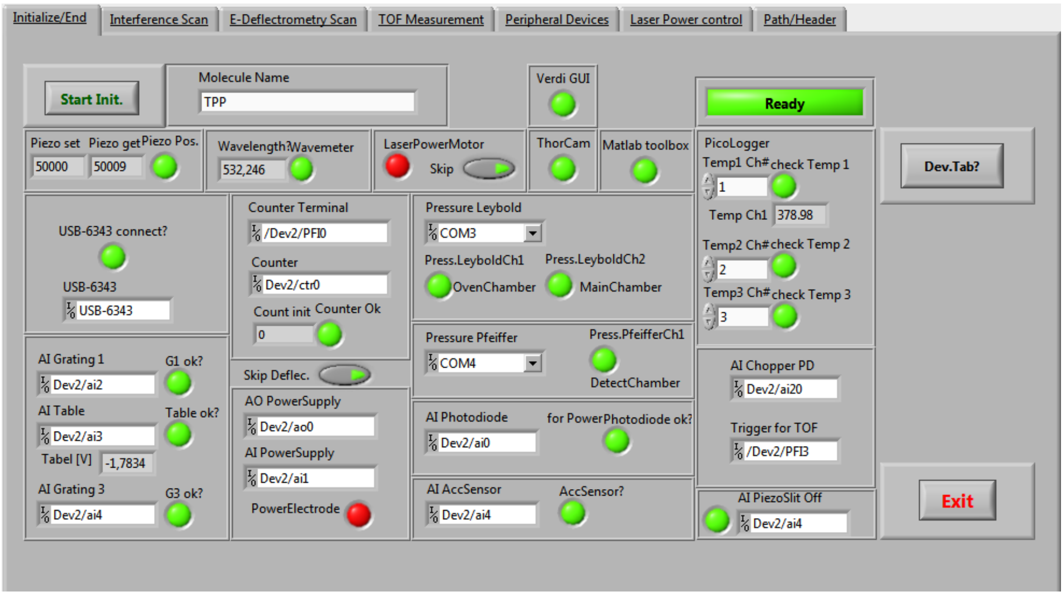

Figure 4.1: This image shows the initializing tab of the control software, where the user starts and exits the programme. Its main purpose is to get the software ready to control the experiment after a sanity check. The user can see whether all devices are corresponding correctly indicated by an LED. The other interface tabs are listed on the top and their names imply their content.

When the programme is started, the initialization tab is active as shown in figure 4.1. There are three buttons for the user; "Start Init.", "Dev.Tab?", and "Exit". On top, the other tabs of the interface are listed, which are described in the following sections.

It is mentioned here, that the window is not closable in the top right corner as typical in Windows® application, when the programme is running. The user has to 'Exit' first. Then, the programme closes all open communications and threads before enabling the regular exit button. This is important to ensure, that the programme can be opened and closed within one Windows® session without any errors occurring. Also, the "Dev.Tab?"-button makes a hidden tab visible, which contains a variety of helpful variables for debugging.

After pressing the "Start Init."-button, the procedure to get the control software ready to go begins. Step by step, LEDs are supposed to turn green, when the corresponding device was successfully initialized. As a remark to the section 3.5, the following paragraphs are in the same order as the state machine goes through the initialization process (see appendix).

First, a windows pops up and it is required to enter the molecule's name to make comparable data sets for later analysis (state 9). Next, the USB-6343 from National Instruments is the main data acquisition device containing the analogue in- and outputs and the counter [87] (States: 10, 15, 16, 20, 25, 30, 35). It will be detected automatically even if it has been re-plugged into a different USB-port. Otherwise, settings in LabVIEW's device manager, the Measurement and Automation Explorer (MAX), would have to be adjusted every time. Then, the current molecular signal counts of 500 ms are displayed (state 40). If they are greater than zero, there is signal or noise and the indicator is set green.

Next, the piezojena-system, which controls the position of the third grating, is initialized communicating via a GPIB protocol included in LabVIEW [107, 108]. The initialization command sets the position of the piezo far away from the start value used in this experiment (see state 50, subVI "Piezo-Initialize.vi", 8.2.2 system commands [107]). Therefore, the piezo is set afterwards to the start position of an interferogram (position: 50000). The position is also read and, if as set within an error range, the indicator is turned green. That procedure is an advantage to the previous LabVIEW code, which initialized the piezo before every scan. Conclusively, a scan took more time and the first two measurement points of every scan had to be neglected in the analysis. After successfully initializing the USB-6343 and the piezo-system, the machine is in principle ready to run interference scans.

The USB-6343 reads via its analogue inputs the tilt sensors [1] (state 30, see section 4.5.2), the piezo slit (state 35), the acceleration sensor, the photo diode (state 20) and the chopper signal for the TOF measurements (see section 4.4). In addition, the power supply for the deflectometry electrode is also controlled via an analogue in- and output. The power supply is tested by sending a voltage of 200 V, reading the voltage, and afterwards resetting it to zero (state 25). If no error occurs, the

[1] Electrolytic Tilt Sensors SH50050 Ceramic Series - SPECTRON GLASS AND ELECTRONICS INC.

deflectometry tab is available. The option to skip deflectometry is implemented, because the electrode is not permanently in the molecular beam path and setting the voltage is rather time consuming compared to the rest. The photo diode, piezo slit and accelerometer indicators are turned green, if a voltage greater than zero is detected. That is the case, if a cable is connected to the input of the USB-6343 device due to a noise level from the powered devices. The last analogue inputs are the three voltage readings of the tilt sensors named "Grating 1", "Table", and "Grating 3". The voltages are specific to the optical table's orientation. The software checks if the voltages are within or out of range of the non-floating position. When out of that range, it assumes a floating table and the indicators are switched to green.
In the next step, the wavemeter software is started from within LabVIEW (state 55) [109]. The Wavemeter application has to be running in the background, because the wavelength is read out via dynamic link libraries (DLLs) [110] between the control software and the manufacturers application [95]. If the wavemeter is unplugged or not well adjusted, the software returns error codes and the message can be seen in the wavemeter software. Otherwise, the wavemeter indicator is set green. The coherent laser GUI is also started (state 59) [74], enables a telnet server and the values can be read out via TCP/IP using a library from LabVIEW [111] (see appendix). If the LED is switched green, the laser shutter button is available on the "Laser Power control" tab of the main GUI (see figure 4.1).
The temperature is measured with thermocouple type K connected to the pico temperature logger device which provides a LabVIEW control software [96]. That software has been adjusted to a stable subVI ("USBtc08Thermo-ChSelect.vi") within the main programme, which can be restarted, if necessary, by re-plugging without affecting the main VI. The LED is green, if the pico logger is connected during the initialization (state 60 and 65) and the temporal progression charts (see section 4.5.5) become visible. However, it can not be detected if a thermocouple is connected, because the logger returns room temperature values from empty ports.
The pressure gauges used on the KDTLI have a RS232 connector. A USB to serial adapter is used to establish a connection to the PC. Both pressure gauges are read out using a VISA communication from LabVIEW [112], where the commands are listed in the manuals from the manufactures Leybold and Pfeiffer [98, 97]. The subVIs return the pressure values or an error message (state 70, 75, subVI "Pressure-

read-com#-ch#.vi").

The laser power is controlled by a motorized rotational stage, which turns the $\frac{\lambda}{2}$ plate. The corresponding LabVIEW software from Thorlabs (APT) requires a homing to determine its position (state 80) [113]. Thorlabs is currently working on an improved version. This process is also time consuming and only needed for power runs (also see section 4.5). Therefore, the user has the option to skip that part.

In addition to a beam profiler, which has to be placed manually into the beam path, there is a new CMOS image sensor mounted on the optical table. The CMOS sensor from Thorlabs is measuring a reflected beam from the laser and the manufacturer provides a LabVIEW software [71]. This software is adapted to be integrated into the main programme as a subVI. The subVI takes only a snapshot of the image from the sensor instead of a live view. The snapshot is taken without gain and with the shortest possible integration time to avoid manipulation and saturation of the image. It is later saved as a PNG file every time a header file is saved. The initialization process checks if the sensor is properly connected and if the software driver is corresponding correctly (state 85).

Next, the Matlab[2] toolbox group licence must be occupied from the lab computer for data fitting purposes [114]. The LED shows if a licence was available (state 95, subVI "Matlab-lic-toolbox-check.vi"). At this point of the initialization, all devices and functionalities are tested and software enables all features possible on the experiment (states 96-98). Last as a new feature, a folder for the data of the day is created automatically within the structure of year, month and day on the server, where the data is saved. Furthermore, the naming of data sets are chosen programmatically. Thus, no overwriting of any data nor data loss is possible (state 99, subVI "Filename-getnext_aaa.vi"). Finally, the user can start measuring using the other tabs of the control software.

4.2 Interference scan tab

The tab, as shown in figure 4.3, controls the interference scan. The top right corner is separated by a line from the rest of the interface, because it contains the options handling the counter application and the dark counts, which have to be set once

[2] ©1994-2018 The MathWorks, Inc.

before the first interference scan. Pressing the "Auto-Reset dark counts"-button, one measures the dark count rate automatically by averaging the signal over 10 seconds. The other button ("Set dark counts") opens a dialogue for the user to enter the dark counts. The dark count rate is needed for the calculation of the visibility and it varies depending on the QMS conditions. The third button ("GET count rate") opens a new window, the counter application, as described in the next section 4.2.1. It is usually used before continuing with the interference settings on this interface tab, which are explained in the section afterwards.

4.2.1 The counter application

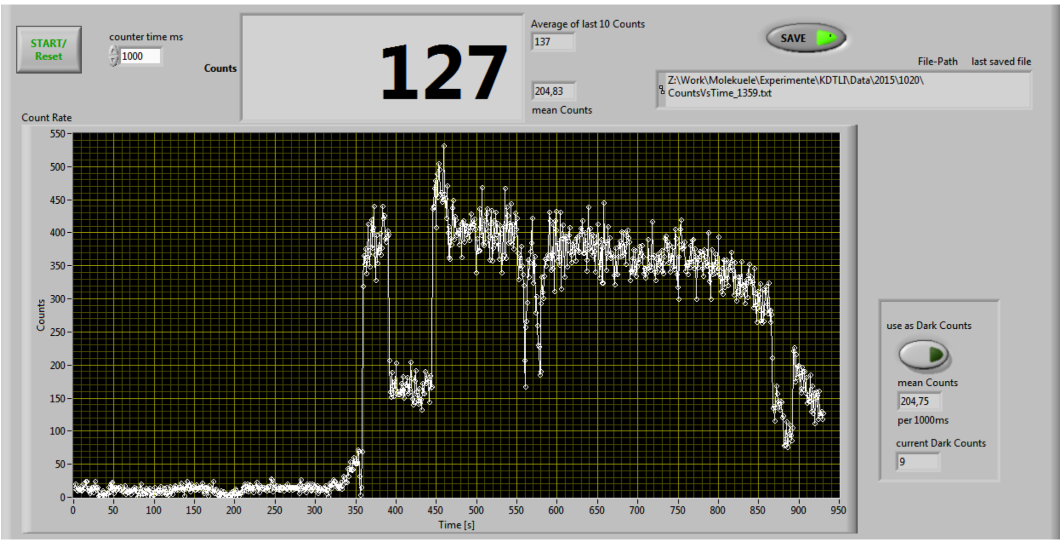

Figure 4.2: This programme monitors the current count rate depending on the integration time set by the user. The user has the options to reset or save the displayed count history and to set the dark count rate of the main VI from the currently displayed average.

The counter programme is mostly needed right after the first initialization of the experiment, when the oven of the KDTLI was changed before (see section 2.2.1). The oven's position has to be optimized to the current count rate together with the delimiters determining the free-flight parabola (see section 2.2.2). Additionally, the application is used as a sanity check of the molecular beam throughout all measurements. A stand-alone application with equal functionalities has been developed, if the count rate needs to be displayed without the entire control software to be started. The interface, seen in figure 4.2, displays the current count rate. The window and font size are important, because it must be readable from a distance while working on the KDTLI. The user can adjust the integration time, save the graph's data in a text file, and monitor the oven temperature simultaneously underneath (not included in this figure, but similar to figure 4.9). The currently averaged count rate can be set as the dark counts to the main VI. When the user successfully arranged the oven's position, this application is closed, and the software is set to measure interference pattern on the main GUI.

4.2.2 Measuring interference

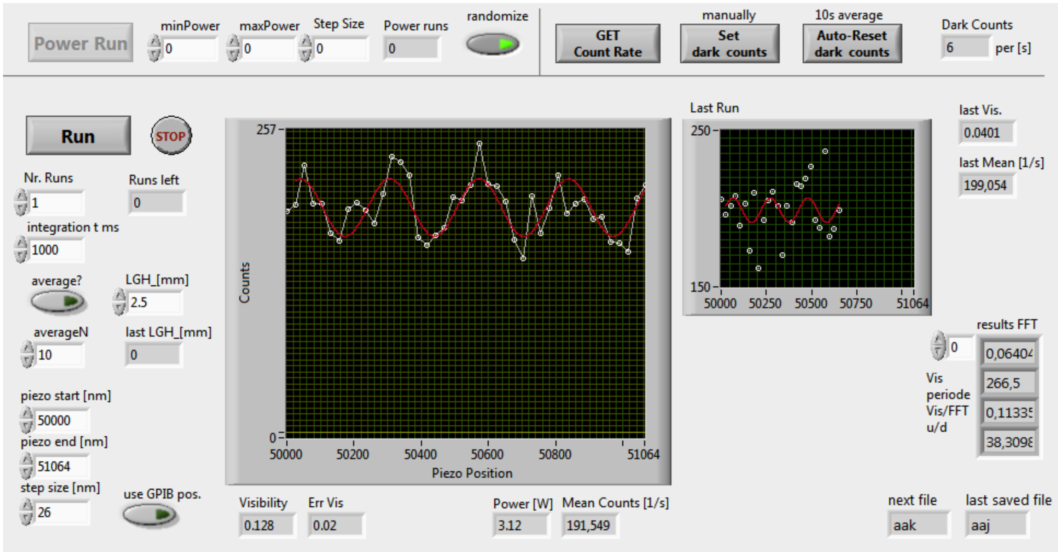

Figure 4.3: This tab of the main programme controls an interference scan with any parameter settings chosen by the user. The amount of runs, how the third grating is scanning, and the integration time can be chosen separately. It can be combined with a "Power Run", where all settings for the "Run"-button are applied to each laser power set on the top left of the GUI. The interference pattern is plotted on the graph, while recording it. Afterwards, a sinusoidal function is fitted with the data and plotted. On the right, the previous scan is shown in a smaller graph.

To measure an interference pattern, the user enters the parameters for scanning the third grating in a similar style to the previous LabVIEW programme. The scanning itself is implemented into a subVI named "ScanInterference_new.vi". The piezo's position is set in nanometres and converted into a position the piezo-system expects (pos[nm]x0.818925 +180 = pos[piezosystem], see appendix "Calib_convertPiezoPos.vi"). The position together with the count rate are written into the data file (.dat), named, and saved automatically as shown underneath the graph in figure 4.3. The "Use GPIB"-option writes the piezo position, as read by the piezo-system itself, to the data file, instead of the position sent to the piezo-system. The reading from the piezo position is averaged over the reading before and after the measurement of the count rate before the position is changed. That option is useful to investigate the piezo' stability over time.

The integration time is the time the counts are recorded at each piezo position. The averaging option splits the integration time into N intervals. Then, N measurements of the count rate are taken at each position. The average is then used to calculate and return the total count rate at each position.

Pressing "Run" starts the amount of interference scans as chosen by "Nr. Runs", which is written into the header file to group the measurements. A running measurement can be called off by the "Stop"-button and afterwards be restarted without any further actions resetting anything. In any case, a header file and data file is written into the folder of the day. In addition, the parameter "Completed?" in the header file indicates, if the measurement was either completed ("1") or interrupted ("0") (see table 4.1). Another parameter, saved to the header file, is the LGH, which has to be set manually on the front panel. The operator can combine the LGH parameter and the "user tag" on the path/header tab (see section 4.5.6) to calculate the optimal light grating height easily from the data (see section 5.1.1).

When the motor to control the laser power has been initialized correctly, a "Power Run" can be executed. A regular interference scan will then start with the settings on the panel. Afterwards, the laser power is automatically changed as set on the interface and the interference scan is repeated. The laser powers are determined by the start and end power and the step size. The order, in which the powers are set, can be randomized if desired.

The measured count rate at each piezo position is plotted on the GUI (see figure 4.3) while running a scan. At the end, a sinusoidal function is fitted and plotted (subVI "Matlab-sinfit.vi"). The results of a FFT-analysis (see chapter 5), the visibility calculated from the fitted function, the mean counts, the laser power, and the name of the file saved is displayed on the bottom of the tab. For comparison, the previous scan is shown in the smaller diagram on the side.

In general, the interference scan is a core functionality of the KDTLI. For example, the interference scans with functionalized TPP entail the current mass record [2].

The interference contrast varies with the power of the laser for the optical grating due to the optical polarizability of the molecules causing the phase shift. Therefore, the optical polarizability of the fullerenes C_{60} and C_{70} have been extracted from the fringe visibilities dependency on the power [12]. Furthermore, the KDTLI may complement mass spectrometry, because molecular properties of neutral particles in the gas phase can be probed [115]. Therefore, no manipulation on the probe, like ionization, is necessary for mass spectroscopy, which is a powerful tool to study molecular structures and properties, besides the mass. Moreover, interference scans with large molecules can be used to investigate quantitative tests of quantum decoherence due to the high internal complexity of biomolecules and their coupling to the environment (see section 2.1.4).
Near-field matter wave interferometry combined with classical Stark deflectometry paves the way to many more possibilities for quantum-assisted measurements of biomolecules [90], as the next section explains the deflectometry tab of the GUI.

4.3 Deflectometry interference scan

The deflectometry tab is very similar to the interference scan tab as described before. The electrode has to be placed into the beam path manually before the software is of any use. The programme needs to be initialized with the deflectometry activated (see figure 4.1). Otherwise, this tab is not available to the user to avoid accidentally applying voltage to the electrode.
The user sets the voltage and the reference voltage displayed in figure 4.4. For each piezo position a count rate is recorded with the reference voltage and the high voltage applied, before the grating is moved. As for the interference scan, the measured counts are continuously plotted on the user panel. At the end of the scan, the data and header file is saved, including the sinusoidal fit for each voltage, which is also displayed. The phase shift of the two fringe visibilities is of interest, because internal properties like the static polarizability of the molecule can be derived from it (see section 2.2.6).
The tolerance is the accepted voltage difference in reading and writing the electrodes voltage before the programme continues and 50 V is the default value. Due to the capacities of the electrode, the voltage crawl only slowly to the desired decreased

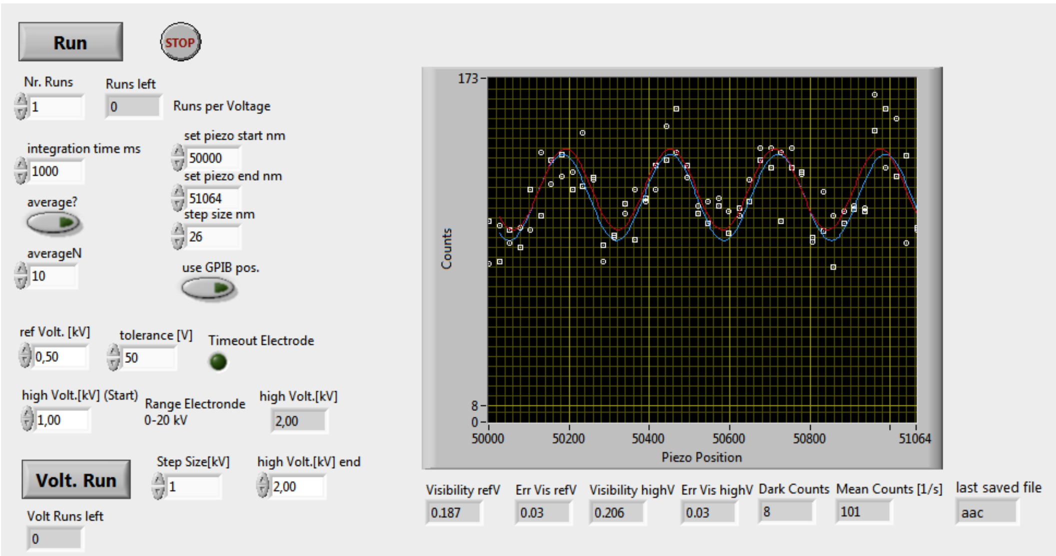

Figure 4.4: This tab of the main programme controls metrology measurements of the KDTLI, where an electrode has to be included into the beam path as described in section 2.2.6. The control settings are similar to an interference scan with additional options to set the electrode's voltage. Moreover, the "Volt. Run" starts an interference scan with the settings above, afterwards the voltage is increased by the voltage "Step Size[kV]", and the run is repeated until the value from the "high Volt.[kV] end"-control is reached. During the measurement, the count rate relating to the high and reference voltage is plotted for each position of the third grating. Last, a sinusoidal function is fitted to each count rate determining the visibility. Results and other parameters are displayed underneath the graph.

value. A "Volt. Run" repeats a "Run" with the same settings, additionally it changes the "high" voltage after every "Run" from the start to the end value in chosen steps. In general, it is possible to collect information on internal properties of molecules using deflectometry on the KDTLI while the molecules are delocalized [116]. Properties like the static polarizability or susceptibility have been measured for different molecules like the fullerenes C_{60} and C_{70} [91, 90] and even for the first time for provitamin A, vitamin E, and vitamin K1 [117]. These properties are encoded in the shift of the matter-wave interference pattern depending on the different voltages set to the electrode. In principle, even the permanent dipole moment is extractable from such a measurement [55]. Furthermore, time-of-flight resolved measurements, as the next section presents the controlling tab, offer more accurate results instead of summing over the entire selected velocity class of the molecules (see section 2.2.2).

4.4 Time of flight measurement

This tab of the main GUI, as shown in figure 4.5, holds all options preforming time of flight measurements (TOF), which uses a different hardware, the fast card [100]. That fast card achieves a fast enough sample rate, recording the molecules, for the analysis. That hardware's driver (MCA) includes LabVIEW routines, which are integrated into the main programme. It is crucial to the measurement principle to simultaneously equally record the chopper signal and the molecular beam to convolute the flight time from both input signals (equation 2.15). Therefore, the chopper, accurately the photodiode's signal, starts with fast card via the "in sync" channel [118, 100].

The "TOF"-button starts a single time-of-flight measurement with chosen the "Bin width [μs]" (integration time) and "Range" (amount of bins). The bin width can be set to automatic. In that case, the width is than determined by the current speed of the chopper wheel, which has to be placed into the molecule beam by the experimenter before (see set-up and equations in section 2.2.2). The estimated time of the complete measurement is displayed on the panel, because it might be not trivial to guess the total time including all options. After a measurement, part of the signal from the chopper and fast card (MCA data) are displayed in the diagrams as seen in figure 4.5. Writing the data from the MCA software directly to server used

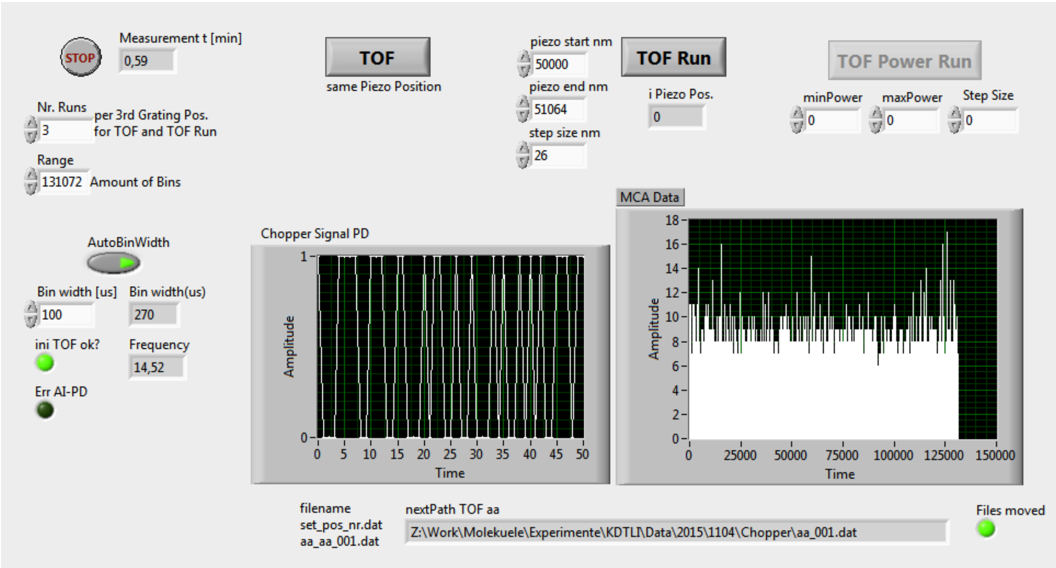

Figure 4.5: This tab of the main programme controls time-of-flight measurements (TOF). As explained in section 2.2.2, the count rate and the shutter function have to be measured simultaneously in order to extracted the time-of-flight distribution. The shutter function describes how the chopper disk, which has to be inserted into the beam path manually, cuts off the molecular beam. The user sets the "Bin width [μs]" and the amount of bins (range) before starting a "TOF" measurement. The "Auto Bin Width" is determined by the spinning speed of the chopper disk, because it limits the resolution of the TOF distribution. The "TOF Run" repeats the TOF measurement for every grating position set and the "TOF Power Run" again repeats a TOF run for every laser power. After a "TOF" measurement, part of the chopper and molecule (MCA Data) signal are displayed to the user as a sanity check of the signals.

to be troubling. However, it is solved by temporarily saving the data files on the local PC and moving the files to the server into a sub folder of the folder of the day after the complete TOF measurement. The successful process is indicated by the green LED on the bottom. The file names consist of first two letters indicating the measurement set like the interference scan (aa, ab, ...), followed by two letters for a different piezo position, which is started by pressing the "TOF Run"-button, and last a number according to the "Nr. Runs" (e.g. "aa_aa_001.dat"). The TOF-run can be combined with a "TOF Power Run" as with the interference scan.
Accurate velocity resolved interference fringes offer a much more detailed understanding of the beam-splitting mechanisms of the KDTLI, which is the corner stone of the quantum-mechanical interaction of the molecules [46].

4.5 The peripheral devices of the KDTLI

A main aspect of the new control software is the integration of the peripheral devices. This section includes the new software features and applications of the peripheral. First is the tab of the GUI, where all measured values of the devices are displayed. The next paragraphs introduce the applications with their user panel controlling devices like the tilt sensors, the accelerometer, and the beam camera. Next, the new temporal progression charts are presented, which are attached to the bottom of the tabs of the main GUI. Last is the path and header tab with some new features and an example header file, which are used to build the new data base (see section 5).
The "Laser Power Control" tab is not explicitly presented due technical problems on the optical table affecting the calibration of the photodiode measuring the laser power. The manufacture Thorlabs were also working on important bug fixes of their software driver for the motor that rotates the λ-half-plate changing the laser power. However, the preliminary implementation proved the working principle recording several "power runs". The laser tab has the options to shutter the laser on the Verdi itself and further commands could be send to Verdi from the subVI "Telnet-Verdi20-getPara2.vi". Further, a software controlled laser blocking aperture had been planed to be included onto this tab.

4.5.1 Peripheral devices tab

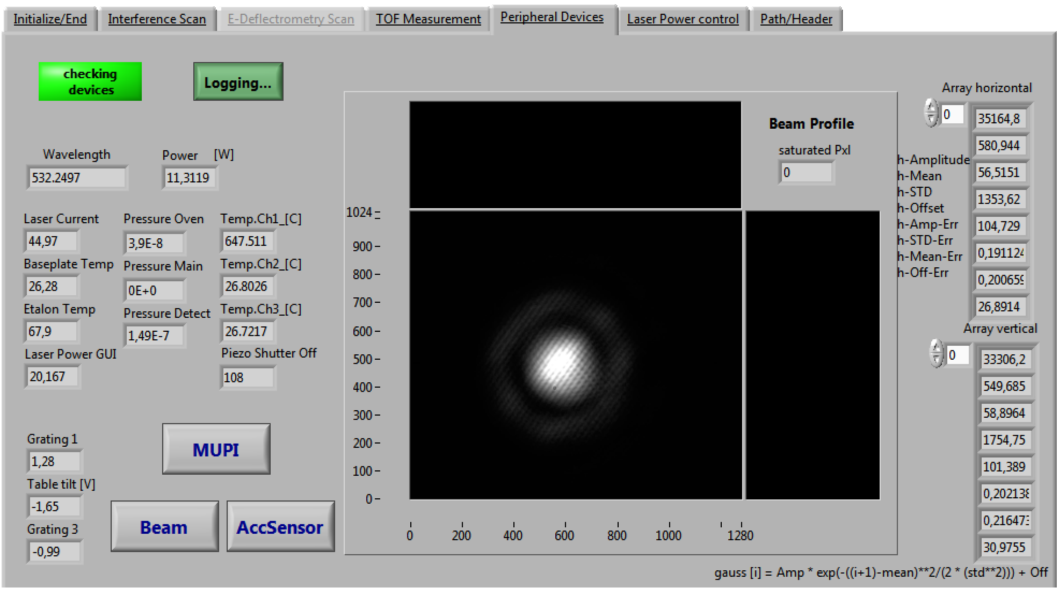

Figure 4.6: This tab of the main programme displays the currently measured values of the peripheral devices of the experiment for the user to assess the measurement conditions. On the left, there are the laser's parameters, the pressure readings, the temperature, the tilt sensors and the offset of the piezo-controlled delimiter. The image shows the laser profile taken with a CMOS chip. Additionally, the operator can start the "MUPI", which are the tilt sensors, the "AccSenosr" (accelerometer), and the "Beam" profiler using the CMOS chip. On the top left is a, here activated, button "logging", which continuously saves the shown values, while no measurements are being recorded.

The readings of all peripheral devices like the pressures gauges, the thermometer, and the ones reading the laser's properties e.g. the laser current or its wavelength, are displayed on this tab of the main GUI (figure 4.6). These gathered parameters build the header files. The operator can also start a logging option as shown in figure 4.6, when there is no measurement process running. The programme will then write files similar to the header file in a sub folder and name them automatically with a time step ("...\logging\log_*HHMM*.txt"). Later, the analysis of the logging files could reveal informations about the experiment's stability, because periodically recorded data over time might show possible drifts or correlated perturbations of these feedback parameters.

Also, this tab holds the start buttons to the "MUPI"-, "Beam"- and "AccSensor"-applications, which will be explained in the next sections. These programmes open their user interface in a new window on top when started, but the main programme keeps running in the background.

4.5.2 The tilt sensor application - MUPI

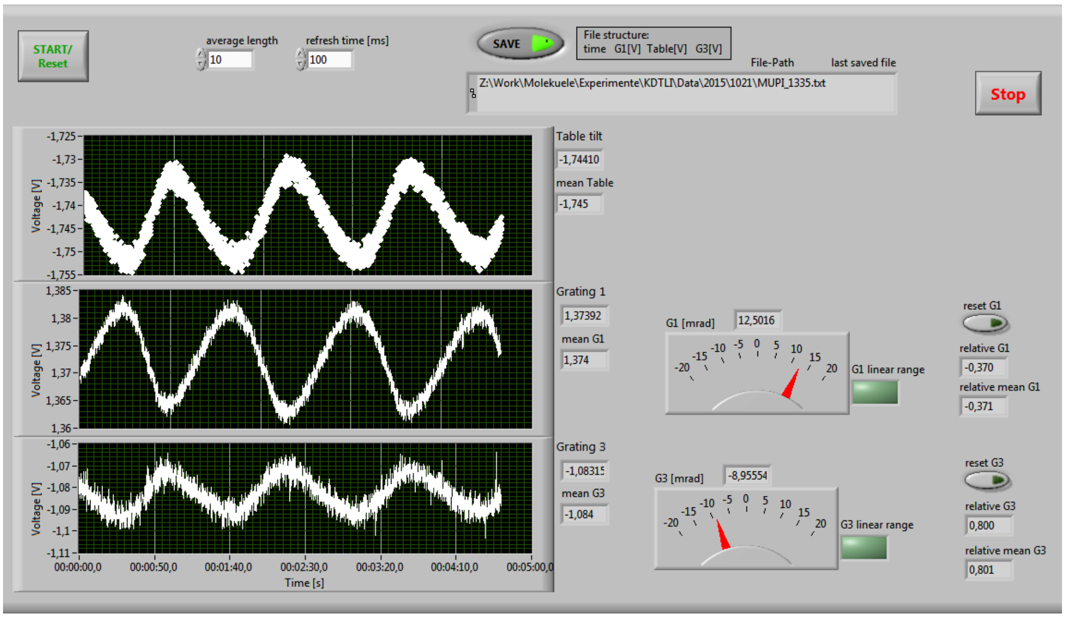

Figure 4.7: There are three tilt sensors; one the optical table and one on each material gratings (G1 and G3). The voltage readouts of these sensors are displayed on the charts. The operator can average, reset, and save the displayed measurements, while e.g. adjusting the optical table or aligning the gratings.

The user interface, seen in figure 4.7, pops up, after the button "MUPI" was pressed on the "Peripheral Devices" tab. The name originates from the manufactures calibration procedure of the tilt sensors. The interface is very similar to the previous LabVIEW programme. It monitors the voltage of the tilt sensors, that are connected to the optical table and the two material gratings (G1 and G3) of the KDTLI. The optical table has to levitate, because the experiment must be decoupled from external vibrations. The tilt sensors are sensitive enough to show the slightest movements of the table. Monitoring the sensors over time enables the experimenter to see perturbations, periodic movements or drifts. The displayed measurements can be saved to a text file and the plots can be reset by restarting.
On the right side of user panel, the sensor's voltage is converted into milliradian (mrad) and the gratings' position can be measured relative to the table's. It is duplicated from the original programme code into the new LabVIEW application ("PopUp-MUPI2.vi"), but the new VI runs in parallel to the main control software.

This applications runs on a daily base to check the table's floating position, while adjusting the pressure on the valves of the vibrations isolators. Furthermore, this user interface is the main feedback to the experimenter, when aligning the interferometer, which has to be considered carefully, because the KDTLI operates with de Broglie wavelengths in the regime of picometers and grating periods as small as a few hundred nanometers [53]. The alignment of the grating's respective position require certain constraints for their pitch, roll and yaw angle [53, 12]. A height- and velocity-dependent phase shifts will reduce the contrast, which limits the roll angle to 14 mrad deviation. The effective slit width of the gratings is decreased by a yaw angle, which results in a constraint of 10 mrad for that angle to ensure a sufficient fringe visibility. The height depending variation of the grating separation implies a less strict constraint of 250 mrad to the pitch angle [12]. After achieving the parallelism of the gratings, they also need to be orientated to gravity, because the gravitational acceleration causes a phase shift, if the grating bars are not aligned perpendicular to the horizontal direction [53, 12]

At last, it is mentioned here, the position is changed by motors controlled on an old PC using a MS-DOS application, which is not compatible with the new measurement PC. Therefore, it is not integrated into this control software, but also because it is only used for the delicate alignment process in contrast to the beam profile explained in the next section.

4.5.3 The beam profiler application

In addition to the commercial beam profiler (Beam-Master), there is a CMOS image sensor included into the laser beam path [71]. In the current setup, the Beam-Master has to be placed manually into the beam path blocking the laser before the main chamber. Also, the Beam-Master' software has to run on other older PC due to its outdated hard- and software. The new sensor enables a constant and not invasive measuring of the laser profile at least additionally to the Beam-Master.

When the user starts the new beam profiling application from the peripheral devices tab, a new user panel, more detailed compared to the image on right of figure 4.6, is popping up ("PopUp-BeamProfile-Cam.vi"). The interface shows an image of the laser and graphs with computed Gaussian fits in vertical and horizontal direction to judge the laser profile. The shape of the laser's profile is crucial, because it forms the standing light wave for diffraction. The Gaussian fit sums over all pixel values (0 to 255) in each direction. As a result, the position of the centre and the widths are calculated and converted into units of micrometers (pixel: square of $5.2\,\mu$m [71]). Therefore, relative and absolute movements of the laser can be frequently recorded to detect drifts of the laser position during a measurement day. The image can be saved in a PNG file as raw date. Independent of this interface panel, the image is saved with every header file, into which the results of the Gaussian fit are written (see example header 4.1).

4.5.4 The acceleration sensor application

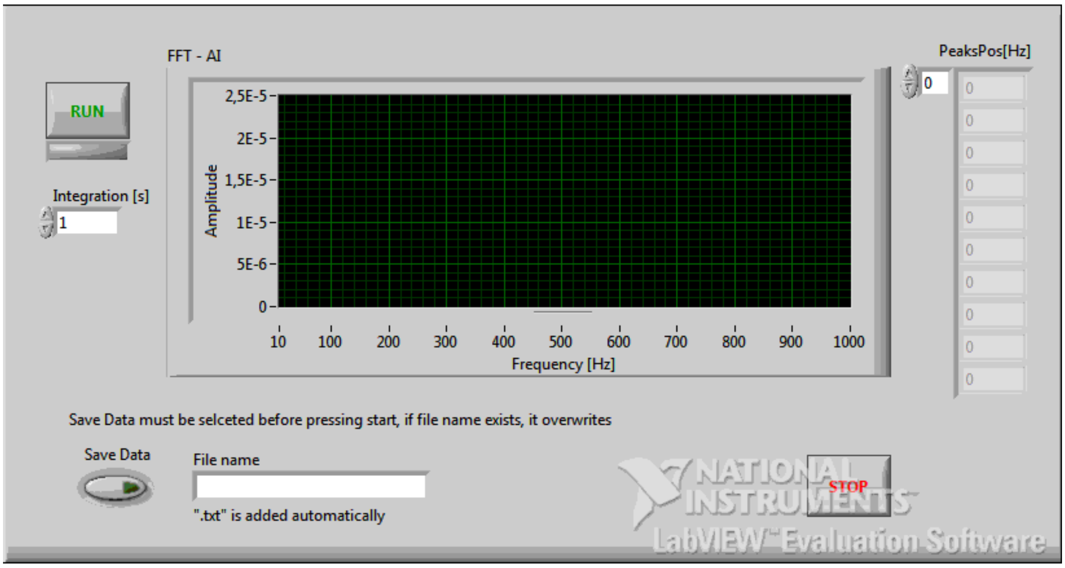

Figure 4.8: The shown user panel controls the accelerometer, which is placed on the optical table. The "Run"-button starts recording the voltage of the sensor for the time chosen ("Integration [s]"), calculates a FFT to show the frequency spectrum. The result can be saved to the folder of the day.

The acceleration sensor is battery driven and it has to be turned on manually. The operator can open the interface (shown in figure 4.8) from the peripheral devices tab by pressing "AccSensor". The "Run"-button on this GUI starts recording the voltage of the sensor for the chosen "Integration [s]" time. Next, a Fourier transformation (power spectrum, PSD within LabVIEW) is computed on the measured data. The results for the PSD are shown in the graph on the GUI and they can be saved to a text file before closing this user panel and returning to the main programme.

The strong influence of acoustic vibrations has been demonstrated [51]. Especially frequencies between 50 and 1000 Hz affect the fringe visibility the most due to the molecule's passage time through the interferometer. If the displacement of the grating exceeds 10 nm, a reduction of the contrast above 5 % is to be expected [53]. Higher vibration frequencies of the gratings can be treated as constant from the molecules point of view. Further, many oscillation modes and low frequencies may be neglected, because only large amplitudes affect visibility.
However, the vibrational spectrum of interest is dominated by the effects from the presence of vacuum pumps, and other experimental equipment on the optical table. Therefore, this application helps to find the cause of perturbation frequencies and to improve the vibrational decoupling of the experiment as the corresponding amplitudes in the spectrum are reduced.

4.5.5 Temporal progression charts

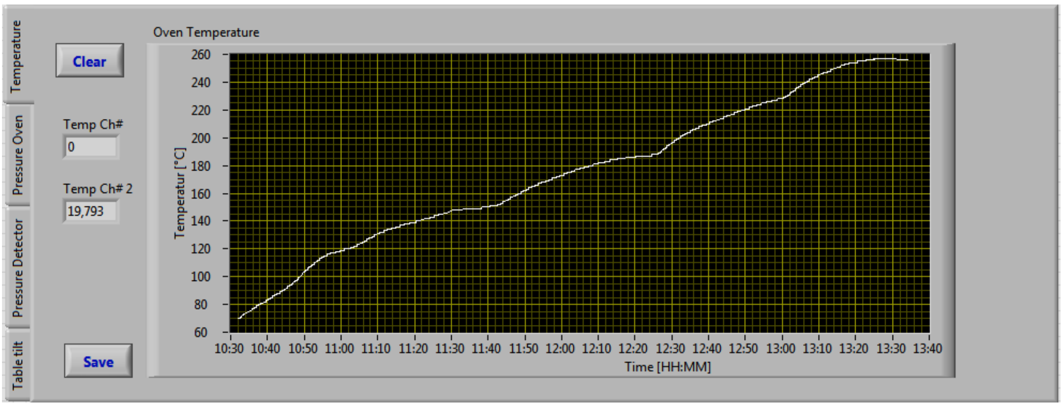

Figure 4.9: The shown user interface is actually attached underneath the main GUI and always displayed to the user. The interface contains four very similar tabs displayed vertically on the left; temperature, oven and detection chamber pressure, and the optical table's tilt sensor. Each shows a graph of the parameters progression over time. The operator can save and reset each chart.

The interface shown in figure 4.9 is part of the main GUI (see figure 4.1) and placed underneath. The charts show a parameter's progression over time and are continuously updated. On the left, there are several tabs; temperature, oven and detection chamber pressure, and the optical table's tilt sensor, which the user can chose from. On each chart, the operating person can save the data to a text file or reset it. The temporal progression chats making it possible for the user to recognize an unexpected change or drift of a crucial parameter right away without any analysis of header or logging files.

4.5.6 Path and header file

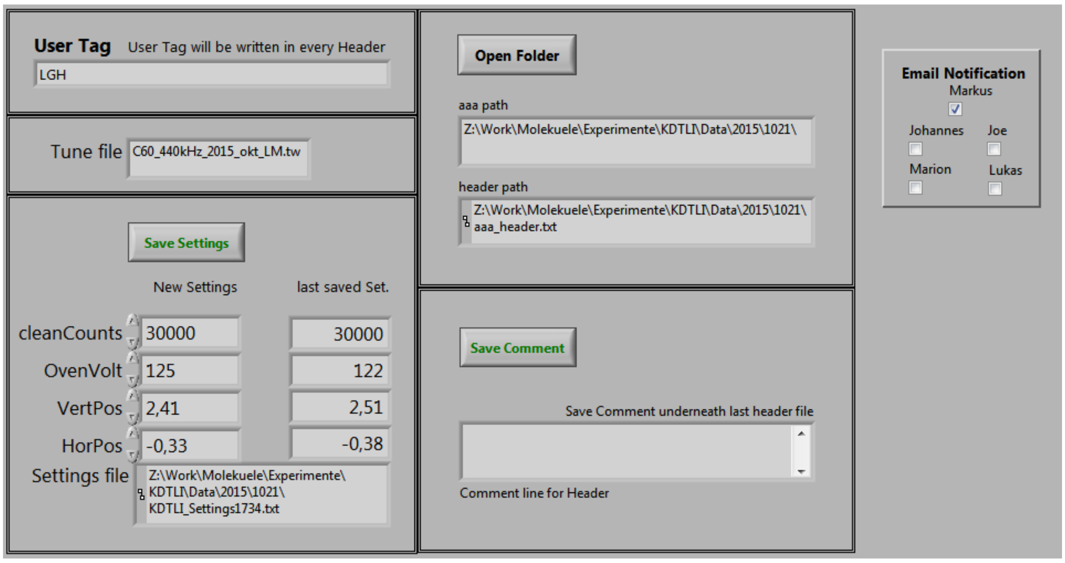

Figure 4.10: This tab of the main programme, named "Path/Header", includes additional features to the header file. The "User Tag" and "Save Comment" options add the content of the boxes to the last header file. The "Save Settings"-button creates a file with the chosen values from the front panel. The email notification boxes can be ticked to send an email to the corresponding person, when the next started measurement is finished.

The last tab of the main GUI, shown in figure 4.10, contains new features and options to the header file, which are presented in this section.

One new feature is the email notification on the right side of this tab, that sends an email to the person of a checked box, when the next measurement is finished. Therefore, the experimenter could start a time consuming measurements e.g. a TOF run with the maximum range and leave the experiment to avoid perturbations. The boxes are unchecked programmatically afterwards. Moreover, the file path of the folder of the day, and the last saved header are displayed and the button "Open Folder" opens that path in the file explorer.

On the top left, a phrase, typed into the "User Tag" box, will be saved to all future header files. That is used for example when optimising the LGH. The experimenter enters a specific user tag (e.g. "LGHscan1") before starting, and also the chosen LGH into the proper box on the interference scan tab (see figure 4.3) before every measurement. Afterwards, a script can automatically plot the LGH over the visibility and calculate the optimal LGH as shown in section 5.1.1, because the user tag groups the measurements.

Another new feature is the "Save Comment"-option, which writes the text from the box into the last saved header file underneath all entries. The experimenter can leave notes directly connected to a specific measurement. The option "Save Settings" digitalizes the part of the lab book, where the experimenter wrote down the parameter values, which describe the optimization process of the oven's position e.g. "OvenVolt" or "cleanCounts". A setting file is saved to the folder of the day and the last saved values are displayed. In conclusion, a better comparability of the results of different oven fillings with the same molecule is given.

The section 2.2.5 explained the working principle of the QMS, which stores its settings into a tune file. Due to technical difficulties of the QMS software [86] writing on the server as mentioned in section 4.4, it seemed reasonable to copy the applied tune file into a specific folder, where the QMS loads it from. Therefore, this control software checks the tune file's existence, displays the name to the user on the header tab (see figure 4.10), and adds the tune file's name to the header. If the file is not found, the experimenter should be warned to inspect the QMS.

A complete header file is presented as table 4.1 as a result of the new control software of the KDTLI. The header is a table with two columns delimited by tabs. The second column contains the values, which are not rounded, because the KDTLI control software only collects the values from the different devices without manipulating them. The parameter "ScanType" encodes, which type of measurement the user selected (1 interference scan, 2 deflectometry scan, 3 interference scan with "Power Run", 4 deflectometry "Volt Run", 5 "TOF" measurement, 6 TOF scan "Run", 7 "TOF Power Run"). In conclusion, the header file enables a new way of analysing measurement results and evaluating the condition and development of the state of the experiment, which will be presented next, in section 5.

Programme	KDTLI-Control... ...Version 2.2
Filename	aag
Date	27.11.2015
Time	00:39
Molecule	c60
Scan_type	1.000000
Nr.of_Runs	15.000000
Run_Nr	1.000000
LGH_[mm]	0.000000
Dark_Counts	10.000000
Integration_T_[s]	1.000000
Visibility	0.100813
Err_Visibility	0.024834
Mean_Counts_[1/s]	222.000000
h-Amplitude	45112.393908
h-Mean	753.802384
h-STD	78.591217
h-Offset	898.480491
h-Amp-Err	42.071693
h-Mean-Err	0.082441
h-STD-Err	0.088853
h-Off-Err	13.450812
v-Amplitude	43172.940717
v-Mean	644.819919
v-STD	80.165430
v-Offset	1329.609097
v-Amp-Err	59.922871
v-Mean-Err	0.123674
v-STD-Err	0.137589
v-Off-Err	22.962050
⋮	⋮

⋮	⋮
Wavelength_[nm]	532.250809
Temp.Ch1_[C]	692.029968
Temp.Ch2_[C]	26.041775
Temp.Ch3_[C]	26.082094
Power_[W]	6.858711
P_Main_[nbar]	0.000000
P_Oven_[nbar]	0.120000
P_Detector_[nbar]	0.011800
Pos_G1_[V]	2.100385
Pos_G3_[V]	-1.857095
TableTilt_[V]	-2.512674
Electrode_Voltage_[kV]	0.000000
Electrode_Voltage_ref_[kV]	0.000000
Visibility_V	0.000000
Err_Visibility_V	0.000000
Laser_Current_[A]	44.500000
Baseplate_Temp_[C]	26.330000
Etalon_Temp_[C]	67.390000
PowerVerdi_[W]	20.443000
Piezo_slit_Off	109.000000
User_Tag	static2
Tunefile	C60_440kHz_... ...2015_okt_LM.tw
Completed?	1.000000

Table 4.1: The table shows an example header text file. A text file like this one is created and saved from the LabVIEW programme every time the user runs a measurement or logs the experiment's parameters. It is human readable and can easily be imported into any analysis software. The values of the parameters are not rounded, because they are the raw data as collected by the KDTLI control software programme from the different devices.

Chapter 5

Analytical applications of the software

This chapter presents new possibilities to investigate the understanding and the measurement results of the Kapitza-Dirac-Talbot-Lau interferometer based on the header file created by the new control software. The analysis of the data is performed with the analysis software Matlab.

First, some advantages for daily operating purposes are illustrated in the section 5.1. It shows how the header file is used to find the optimal light grating height and the optimal laser power while readjusting the experiment (see section 4.2.2).

Secondly, a Matlab script was written to find all header files from the directory, where the control software saved the data. Afterwards, the script collects all entries from all header files in a single table. The table's columns are the parameters in a header file (see example header 4.1) and each row contains the values of a single header file. Further, that table includes the path to every measurement data and all meta data collected together with the measurements. Completely new advantages arise from this new database, which are motivated and presented in section 5.2 and 5.3.

For example, one can search analytically or manually through all measurements and filter them by a parameter of interest. Measurements with the same molecule, comparable laser parameters, or a similar setup of the experiment can be linked and summarized. This is a major improvement for trouble shooting even over longer

time periods, because the meta data for various parameters is readily available. Also combing data sets from different measurements is now easier, allowing for improvement of statistical relevance for measurement results.
In section 5.2, a selection of interference and time-of-flight measurements from the database are shown in figure 5.3 and 5.4.
Last, the database is used to correlate parameters and to look at some parameters' stability over time. That might be one of the most significant improvements of the KDTLI using the new control software. The control software saved all data in a consistent and automated algorithmic way. In summary from section 4.5, there is also data from the logging option, the temporal progression charts, and the other sensors; the table tilt, the accelerometer, and the beam profiler. The file names of the data were also programmatically generated, when saved from the user. These files were summarized in tables such as the header file database by another script enabling automated numerical analysis. In section 5.3, the stability of the laser parameters are under investigation and some parameters of interest are checked for how much they correlate with the fringe visibility. Last, the change in the position of the laser is illustrated using the beam camera (see section 4.5.3).

5.1 Regular applications

This section presents new applications resulting directly from the header file. These applications are mostly relevant during a measurement session while operating the experiment.
A light grating height scan (section 5.1.1) and a laser power scan (section 5.1.2) are plotted and evaluated in the next two paragraphs. Furthermore, the mean count rate, also saved in the header file, can be plotted over time enabling the experimenter to foresee the signal decreasing as the molecules in the oven run out. Similarly, the other parameters being saved (see example header 4.1) can be plotted during a measurement day as a direct feedback, if the associated device responds accordingly or suspiciously.

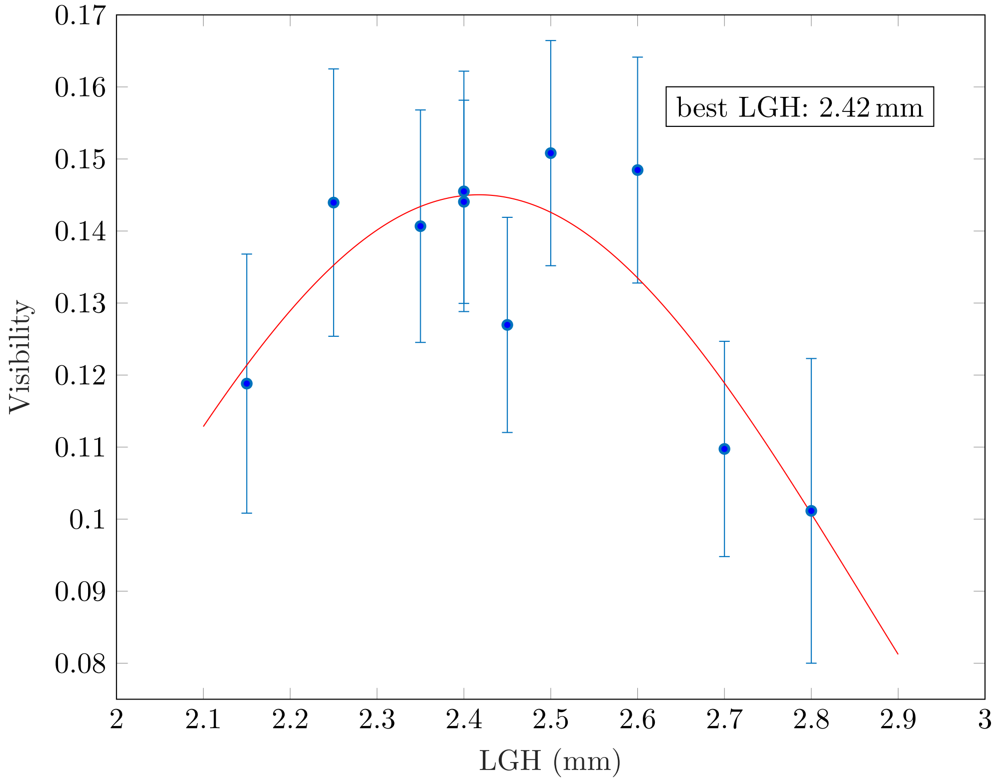

Figure 5.1: The fringe visibility of TPP is plotted in blue as a function the light grating height (LGH). The error bars for the visibility are read from the header file entry ”Err_Visibility”. Afterwards, a Gaussian function (red) is fitted into the data to find the optimal LGH (at 2.42 mm) to maximise the visibility (data from: 20.11.2015, User_Tag: LGH5).

5.1.1 Light grating height scan

The header file's entry "LGH_[mm]" in combination with the entry "User_Tag" are convenient on a daily basis determining the best light grating height during the readjustment procedure (see section 3.1). Both must be written manually into the appropriate control box on the front panel of the software (see section 4.2.2 and 4.5.6). As a result, a script can collect the files belonging to the same light grating scan to plot and fit the data. The visibility is plotted over the light grating height and a Gaussian function is fitted into the data as seen in figure 5.1.
Only at a low laser power, the LGH as a function of the visibility has a Gaussian shape. Otherwise, if the laser power is to intensive, the visibility would decrease at the optimal light grating height, because the molecular beam is seeing more than the optimal power to maximize the interference contrast.
In the figure 5.1, the error bars for the visibility are read from the header file as well, which are a result from the sine-function fit as shown on the front panel after a measurement (see figure 4.3). The resulting peak from the Gaussian function determines the optimal light grating height, which is then used for further measurements.

5.1.2 Laser power scan

The laser power scan option on the front panel of the interference tab sets the type of scan in the header file to "6" (see section 4.2.2). This is used to collect and bunch measurements and plot the visibility as a function of the laser power as shown in figure 5.2. The error for the visibility is given by the error in the sine-fit in the same manner as for the previous the LGH scan plot. The statistical error for the power reading with the photodiode is in the range of milliwatts comparing repetitive readings and therefore neglected here. However, it has a significant systematic error depending on the calibration of the photodiode (see section 4.5) and it might depend on environmental factors like the temperature. That error is important if comparing the absolute value of the power reading, but it has no influence on the optimal laser power if the photodiode is the feedback to set the laser power. The data is fitted with a Gaussian function to derive the optimal laser power for the experimental setup at the time. This assumes that the data is close to the maximum of the curve

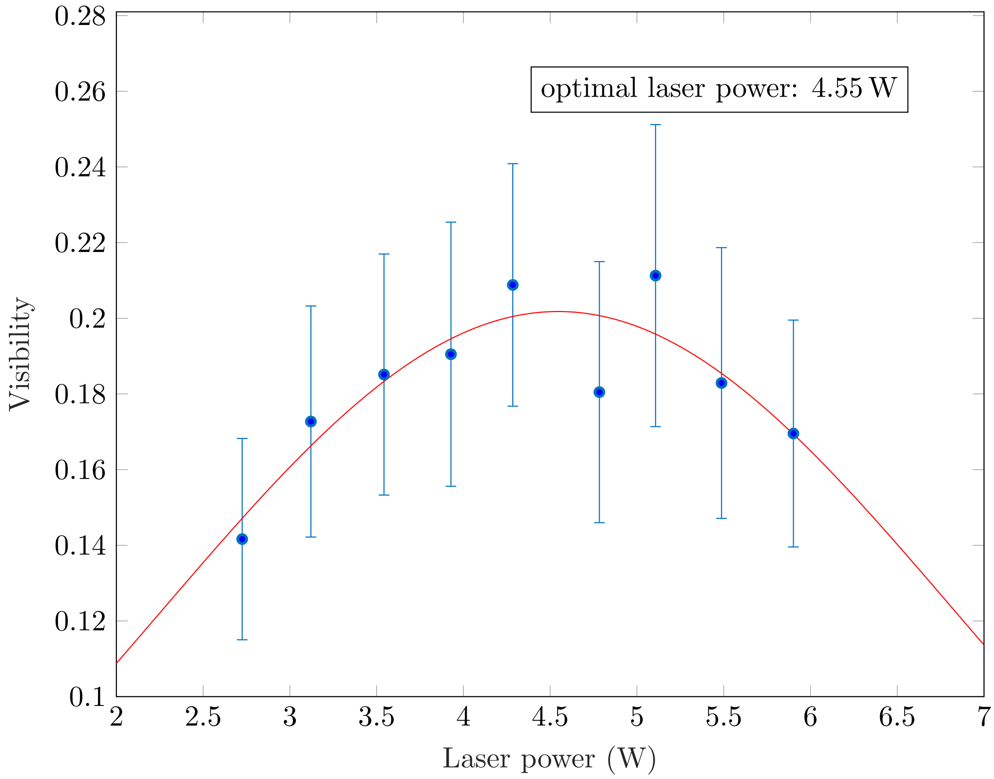

Figure 5.2: The fringe visibility of TPP is plotted as a function of the laser power (blue). The data is taken from an automated "Power Run" (see section 4.2.2), where two interference patterns were recorded per laser power and averaged. The error bars for the visibility are read from the header file entry "Err_Visibility". Afterwards, a Gaussian function (red) is fitted to the data points to derive the optimal laser power (data from: 09.10.2015).

and that only the position of the maximum is searched for. Otherwise, one has to use a Bessel function (equation 2.17 described in section 2.2.4) to fit the visibility as a function of the power.

In general, the visibility's dependency on the laser power as shown in figure 5.2 verifies the quantum nature of the measured interference patterns when comparing with the prediction of classical Moiré fringes [21] (see section 2.2.4).

5.2 Interference results

In contrast to the previous section showing analytical applications directly from the header file, the analysis of the next two sections is based on a database of the header files. Only entries such as the date, visibility or the molecule type are used in this section.

First, this section presents an interference scan of TPP with the highest fringe visibility since the new control software was running. Secondly, the result from a time-of-flight measurement (see section 4.4) is shown. Both are core functionalities of the KDTLI. A deflectometry measurement has not been performed with TPP using the control software, which is an information quickly extracted from the database.

5.2.1 Interference scans and FFT

An interference scan collects the count rate per time interval together with the third grating's position as illustrated in figure 1.1. The interference pattern (see section: 2.2.4) is fitted with a sine curve to obtain the visibility. Before, the background detection rate (dark counts), another parameter in the header file, was subtracted. A simple fast Fourier transform analysis (FFT) already yields a visibility. However, the FFT returns the visibility only for discrete frequencies depending on the amount of steps and step size of the third grating during the measurement. Therefore, the visibility from the sine curve is more reliable, because it corresponds to the period in the signal with the highest amplitude. Drifts, small perturbations, or the alignment of the three-grating setup may vary the period of the fringe visibility. On the other hand, the FFT result is independent of fitting parameters, which makes it useful for comparisons with other measurements on the experiment. It could be

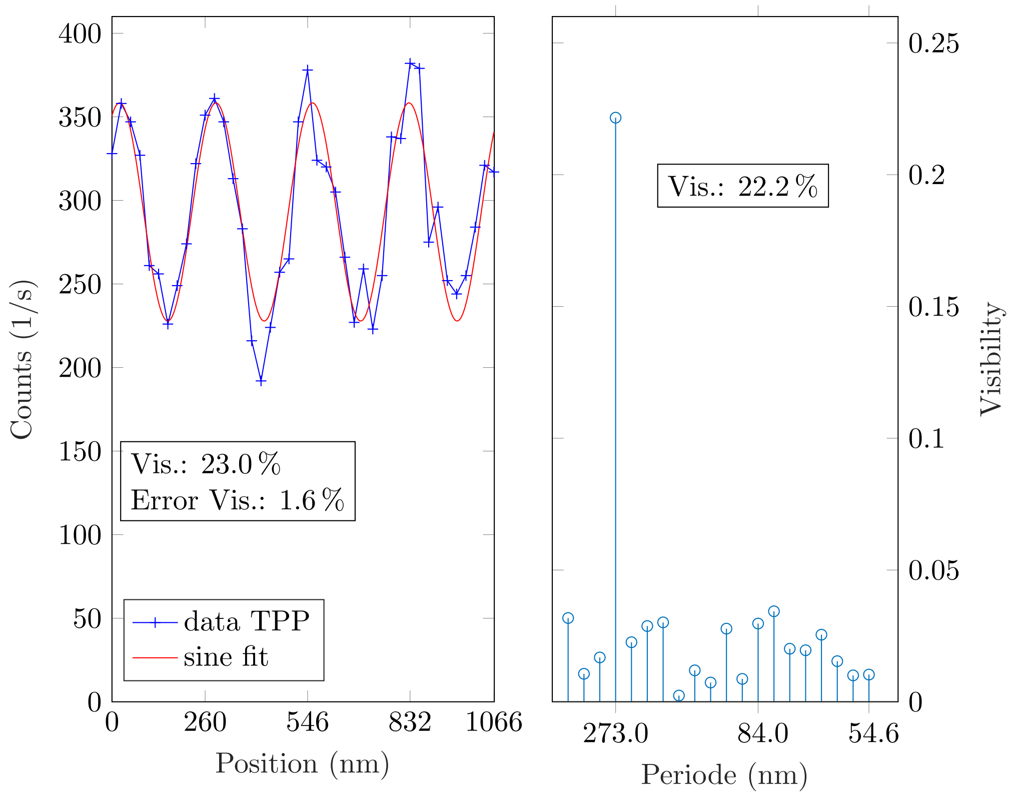

Figure 5.3: On the left, the counts per second of TPP are plotted against the third grating's position as illustrated in figure 1.1. A sinusoidal function is fitted to determine the visibility (see section 2.2.4). The fast Fourier transformation (FFT) is calculated from the data and the resulting visibility is shown on the right (data: 27/10/2015 file: aac).

used as a measure of signal-to-noise ration. For that measure, one would compare the amplitude of the expected frequency with the amplitude of the second highest frequency component in the Fourier spectra. This quick robust method could be used as a feedback parameter for the readjustment process.
The interference scan displayed in figure 5.3 is a result of a search through the database looking for the fringe visibility of TPP with the highest interference contrast.
The analysis of the interference pattern in general forms the foundation to analyse any results from the KDTLI such as deflectometry or time-resolved interference measurement. In the next section, the general analysis of a time-of-flight measurement is presented.

5.2.2 Random chopper for time-of-flight measurements

In chapter 2, introducing the theory of the KDTLI, almost every equation embodies a velocity of a molecule when describing the interaction in the interferometer. Therefore, time-of-flight (TOF) measurements are crucial to compare the fringe visibility with theoretical predictions.
The raw data of such a measurement, which is visualized on the front panel of the control software in figure 4.5, is deconvoluted with equation 2.15. The resulting TOF distributions are shown in figure 5.4.
A more substantial analysis of the noise level, and its properties, or a different method of deconvolution would improve the signal-to-noise ratio (see section 2.2.2). In this case, the molecule signal and the photodiode signal have almost equal time bins of 270 µs. The increased integration time of the scaler card towards the limit of the chopper resolution improved the signal-to-noise ratio in general.
The data, which is illustrated in figure 5.4, has the highest amplitude after the deconvolution from all TOF measurements in the database. Each of the 21 deconvoluted time-of-flight distributions was fitted with a Gaussian function to determine the maximum of the curve. As a result, (253 ± 14) m/s is the mean most probable velocity, where the error is determined by the standard deviation of the most probable velocities. The mean FWHM of the fitted distributions results in 89 m/s. Even though the Gaussian function does not consider the shift of the distribution to faster velocities (see section 2.2.1), the measured most probable velocity is much faster

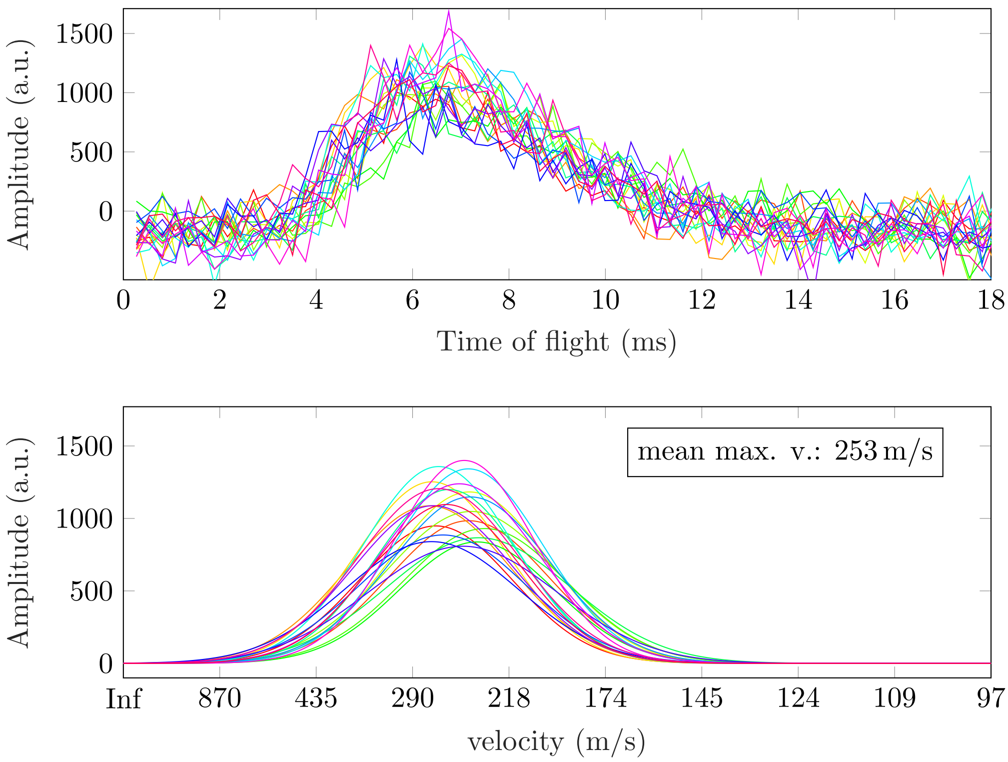

Figure 5.4: The TOF distribution is calculated from the measured signal as explained in section 2.2.2. In the diagram on the top, the data of 21 runs are plotted after the deconvolution. On the bottom, the same data is fitted with a Gaussian function and the flight time is converted to a velocity. The maxima from the fits are averaged resulting in 253 m/s for the most probable velocity of TPP with a standard deviation of the maxima of 14 m/s. The mean FWHM of the distributions results in 89 m/s (data: 11/06/2015 file: ab).

than the thermal one of 135 m/s. However, the higher mean velocity is explainable, when part of the beam was cut by delimiters preselecting a velocity class. Another reason is the opening slit of the thermal source acting as a nozzle, causing the beam to be in the partially hydrodynamic regime. Further, the position of the photodiode measuring the chopper function is assumed to be positioned exactly opposite of the molecular beam on the chopper disk as sketched in figure 2.3. The offset from the photodiode of (180°) is included into this analysis of the deconvolution. A variation in that position would shift the resulting velocity distribution. Experimental issues must also be taken into account. Checking the state of the experimental setup might lead to different explanations to the deviation, which can be done by analysing the meta data.

5.3 Meta data analysis

This chapter demonstrates the new access to a quantitative analysis of the state of the experiment, which became only possible with the new control software saving a header file automatically with every measurement containing the readings of different sensors on the KDTLI. Therefore, all data is saved in a consistent way. As mentioned earlier in this chapter, a script collected all header files and stored their content into a single database.

Besides the header file, the new control software saved more data from peripheral devices of the experiment such as, when the user saved temporal progression charts (see section 4.5.5), the data displayed in the tilt sensor application (see section 4.5.2), or other applications of the software such as the logging option (see section 4.5.1). The automatically generated file names make it possible to study the behaviour of the optical table's position in section 5.3.1 from the data from the tilt sensor application. Next, the stability of the laser is investigated in section 5.3.2 first by looking at the parameters from the laser itself and secondly by observing the position of the laser on an image taken with the beam camera (see figure 2.4).

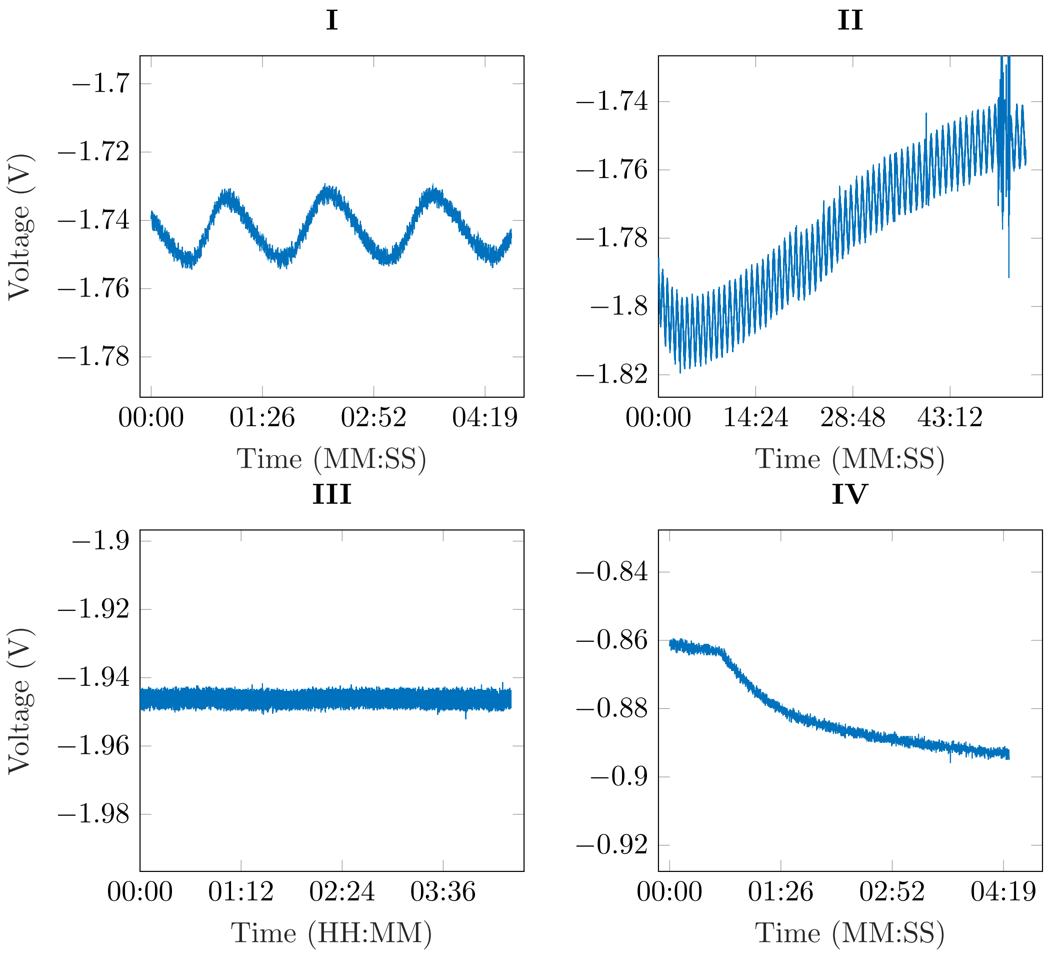

Figure 5.5: Four measurements of the table tilt sensor are plotted over time, each representing a different scenario (see section 2.2). For comparison, the vertical ranges of all figures are identical (data file).
I: The pneumatic feet of the table are supplied by the nitrogen out of the gas line with a central compressor. Therefore, the table is oscillating with a period of roughly 65 s (21.10.2015 13:35).
II: The table's position is moving slowly on time scales of an hour if the position is unstable. The last spike at the end is probably caused by the experimenter gently touching the table. The feet were supplied as in I and the same oscillations are noticeable (22.01.2016 12:54).
III: Gas from a bottle is supporting the feet without visible oscillations. On top, this measurement shows a particularly stable table position over several hours (7.12.2016 14:50).
IV: This plot shows that the table can slowly drift on the time and amplitude scales like in plot I even when the gas bottle is supplying the feet (26.11.2015 17:45).

5.3.1 Table tilt

The optical table plays a crucial role to measure interference. The table needs to be decoupled from external vibrations and the gratings need to be aligned with respect to gravity using the tilt sensors (see section 2.2). During the readjustment process (see section 3.1), the table's tilt serves as an absolute measure to reproduce the previous alignment when the table is floating again.

The feet of the optical table are pneumatic vibration isolators, which are supplied with compressed air either from a gas line or from a gas bottle. The effect on the table's stability is illustrated in figure 5.5. Only when the gas line supply is being used an oscillation of the table is visible with a frequency slightly above 60 s (see I in figure 5.5). This is a clear argument to use gas bottles. However, in the past decent fringe visibilities have also been measured using the gas line. Other factors affect the visibility more than that oscillation with a rather small amplitude. A reproducible position and stability during the complete measurement session is more important comparing the plots II and III in figure 5.5. The experimenter needs to avoid any interaction with the table if possible not to risk to destabilize the position.

The effect of the table's position on the visibility is visualized in figure 5.6. Displaying the table tilt over the period of a year allows to find preferable positions, where good measurement results were achieved. The variation of the absolute position of the table has no noticeable effect on the visibility. However, the reading of the table tilt sensor is done after each measurement and therefore it is not clear if the table was moving during that time. That would strongly affect the visibility. In order to study the moving of the table during a measurement, one can use the acceleration sensor (see section 4.5.4) or have the tilt sensor application running during a scan.

In general, the stability of the table guaranteed by the pneumatic feet relies strongly on the position of the centre of mass (COM) of the experiment on the optical table. A too highly elevated COM can cause the table to perform oscillations analogously to a swaying sailing boat [54].

In conclusion, the new data can help to find drifts and compare results of long time periods. The same idea is applied to study the stability of the laser in the next paragraph.

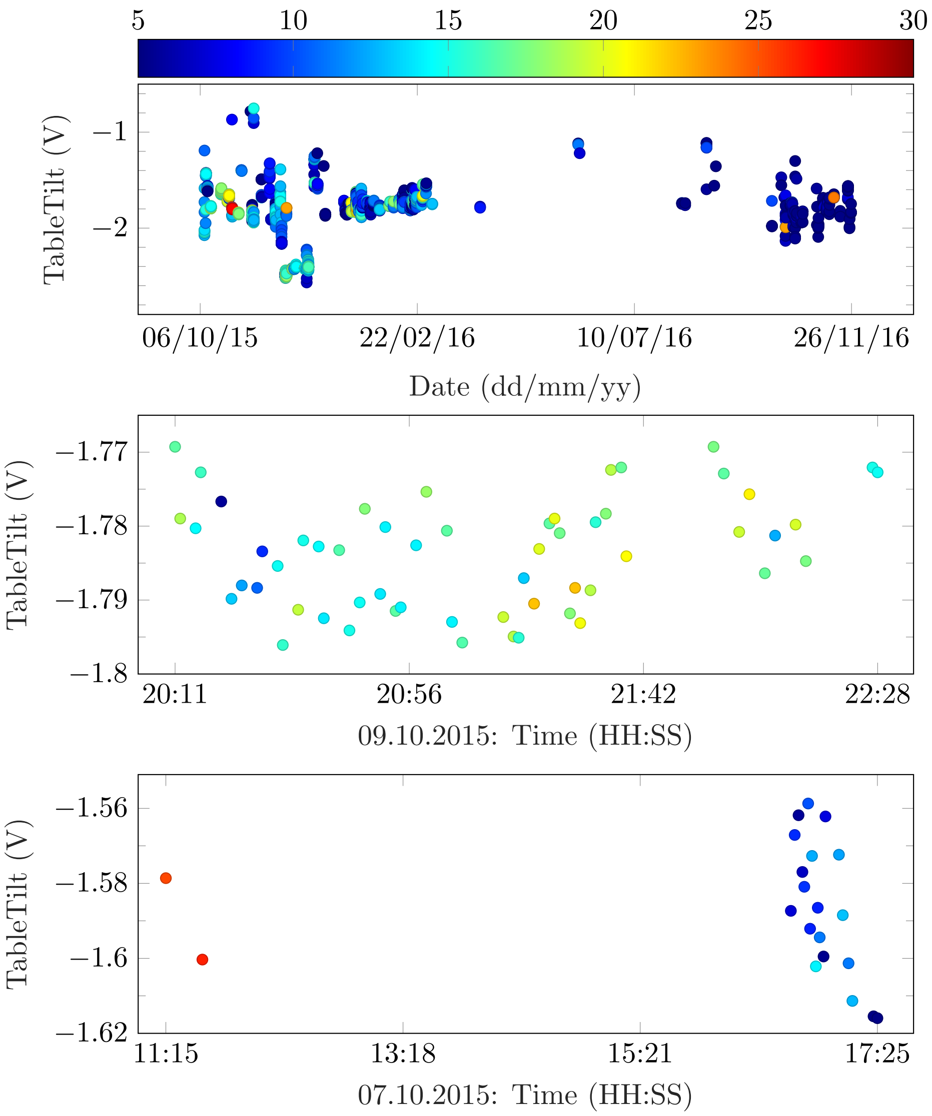

Figure 5.6: The table tile voltage is plotted, where each point is colour-coded with the respective visibility from 5 % to 30 % as illustrated by the colour bar on top. The graph right underneath shows the tilt of the table over the period of a year. The others graphs display the change during a single day with a higher resolution in the voltage scale. The date of the measurement day of the graph in the middle was chosen, because there were the most visibility measurements. The bottom graph shows the data of the day, where the table's tilt varies the most.

5.3.2 Laser properties and correlations

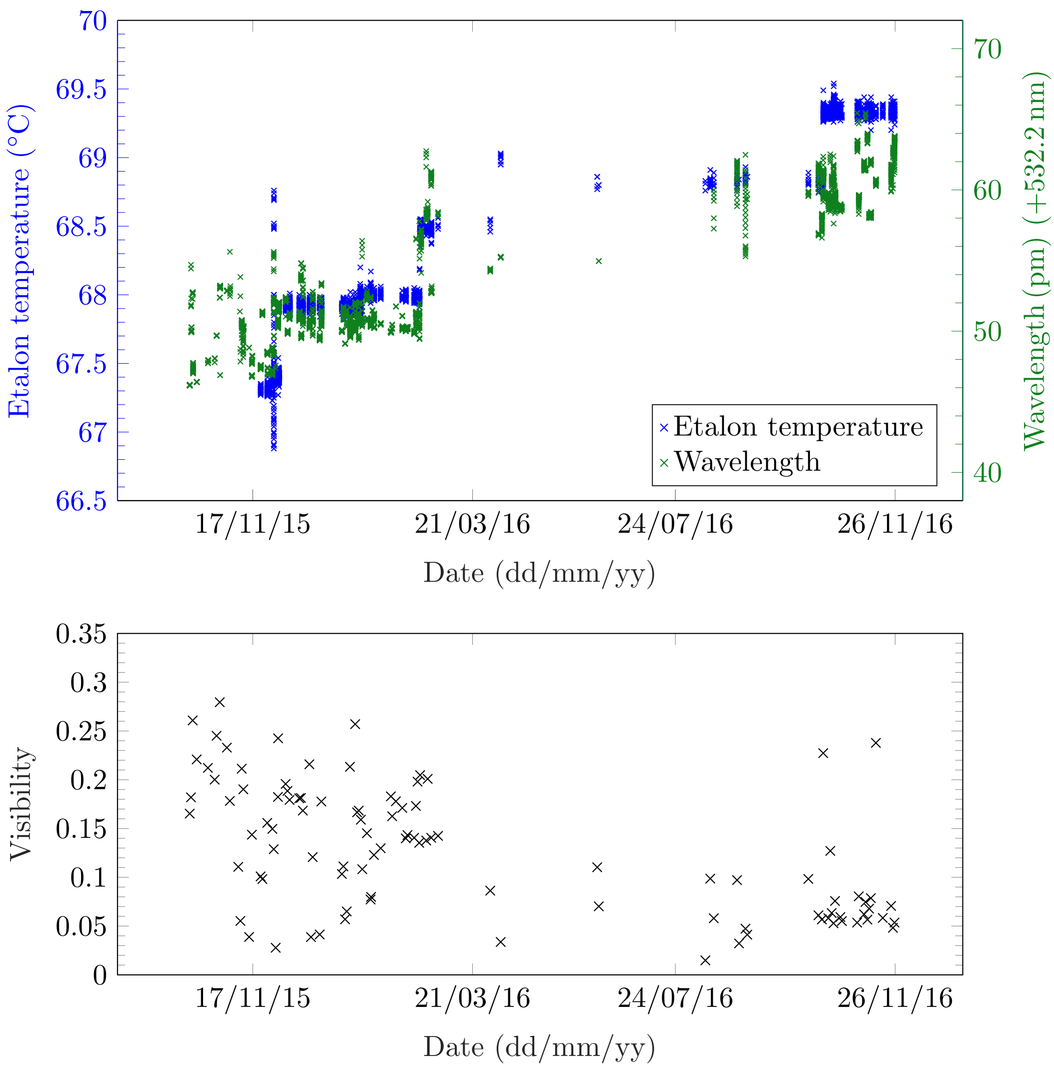

Figure 5.7: On top, the etalon temperature (blue) and the wavelength λ_L (green) of the laser are plotted over the time period of a year. On the bottom, the maximum visibility measured during a single day is plotted over the same time period. A correlation between the etalon temperature and the wavelength is well noticeable, which is directly resulting from the working mechanism of the laser. In contrast, both seem to be uncorrelated from the visibility even though a correlation is rooted into the working mechanism of the interferometer using a standing laser light wave as a grating.

The second diffraction grating in the KDTLI is made of a standing laser light wave. In the Talbot-Lau setup of the KDTLI, the grating periods of all grating must match. A deviation of only 0.05 nm would already cause a strong reduction of the visibility. Therefore, the absolute stability of the laser wavelength is crucial to be able to detect molecular interference. The laser light with a wavelength of $\lambda_L = 532\,\text{nm}$ is produced by a CW diode pumped 20 W laser [74]. The output of the laser is set to stay at maximum power, otherwise the laser system makes slow temperature changes. The etalon temperature is the parameter with which the experimenter can control the wavelength.

Therefore, the etalon temperature and the wavelength are plotted over the period of roughly a year in figure 5.7. An increase and a correlation between both parameters is evident. However, there is no clear correlation to the visibility recognizable if comparing with the best visibility of each measurement day plotted over the same time period. It does make sense, because there are many other parameters which determine the interference contrast.

The laser power forming the standing light wave is controlled by the position of a rotatable $\lambda/2$-plate in combination of a polarizing beam splitter cube (see figure 2.4). If the laser power would be set by the laser control unit, it regulates other parameters to achieve the desired power and the wavelength might change over time. The laser current is also a parameter saved to the header file. Sometime the laser system settles at a non-stable current set to the diodes. For that reason, the visibility is plotted as a function of the laser current in figure 5.8. The database was filtered to find sets of measurements with a decent and comparable visibility and no indication, that other parameter were changed. Only five different sets were found and plotted in different colours in figure 5.8. The result of the figure suggests a correlation between the laser current and the visibility, but one has to take into account, that the error of the visibility is in the range of the change in visibility being correlated and the fact, that the data sets are rather short.

Another interesting parameter is the position of the laser and its behaviour, because the molecular beam has to be aligned to the position of the standing laser wave accordingly to section 5.1.1. During the course of this thesis, a camera was placed into the beam path as illustrated in figure 2.4 [71].

It can serve multiple purposes. First, it complements the knife edge beam profiler used to determine the spatial beam profile by constantly taking pictures of a reflected part of the laser beam. Secondly, the camera can be calibrated to measure the power of the laser if it is not saturating from the maximum laser power reaching the camera. Last, the picture of the laser profile is analysed by control software. All horizontal and vertical lines are fit with a Gaussian function to determine the

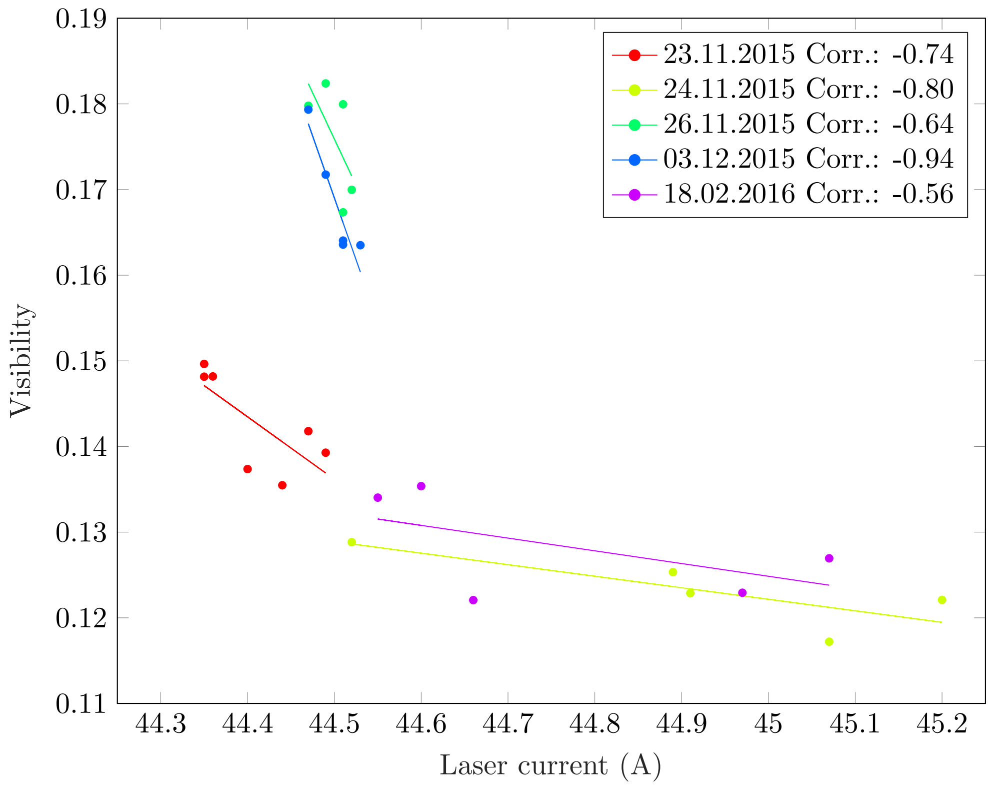

Figure 5.8: There are only five measurement days out of all in the database, where there were laser current readings saved and at least five well comparable interference scans within a day. Those scans had to have at least 10 % visibility, a variation of maximum 10 %, and no "User Tag" or lab book entries suggesting the variation of any parameter on the experiment.
From the remaining interference scans, the visibility is plotted over the laser current in different colours and a linear fit is inserted. A correlation between the visibility and a small variation in the laser current is observable and the resulting correlations are listed in the right corner. However, the result is to be interpreted with caution, because the error in the visibility is typically in the range of 1.5 %.

position of the maximum intensity. Therefore, the camera can detect a movement in the laser pointing.

The behaviour of the laser position is visualized in figure 5.9. Plot I and II are histograms showing the occurrences of the horizontal position of the laser on the camera. The number of occurrences with a position close to zero is most likely resulting from Gaussian fits to images being to dark, which is the case when the camera is not properly positioned. Therefore, plot II is a rescaled version of plot I showing the movement of the laser over all measurements in the database. Plot III shows an example image of the laser taken from the camera. The pixel size is converted to units of millimetres for all plots. The last plot IV displays all mean horizontal and vertical positions during a single measurement day. The visibility is colour-coded into each point to be able to judge the correlation to the visibility.

The visibility is the core result to all measurements of the KDTLI and therefore, the software development and analysis aim to achieve improvement.

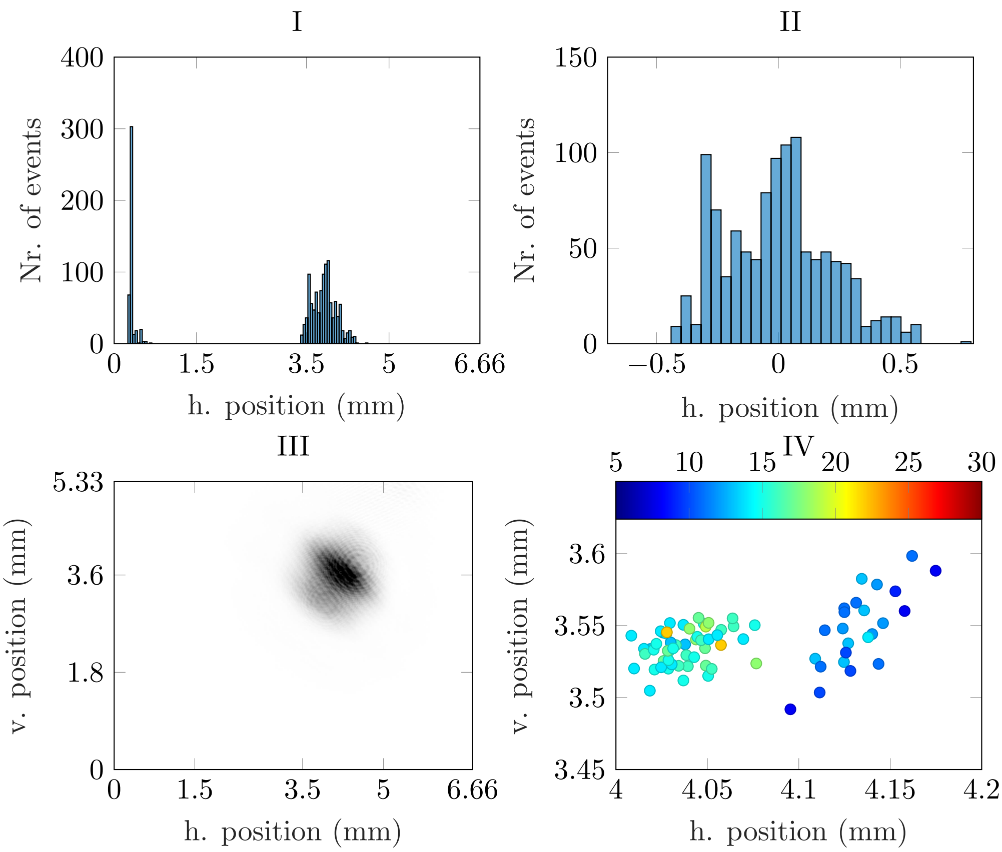

Figure 5.9: The position of the laser pointing is analysed using the header file entries ("h-Mean" and "v-Mean") of the result from the beam camera (see section 4.5.3). A picture of the beam profile is taken as in plot III. The position is determined by a Gaussian function summing horizontally and vertically. The axes are converted into a scale of millimetres (pixel size: $(5.2\,\mu m)^2$ [71]).
Plot I is a histogram of all mean horizontal position occurrences with a bin width of 100 pixel. Plot II zooms in plot I with a x-axis being zero at the mean position of the bulk at $3.82\,\mu m$.
Plot IV shows the vertical and horizontal mean position during the measurement day with the most beam photos taken. The visibility is colour-coded into each marker as the colour bar visualizes from 5 % to 30 % (data of III and IV: 15.12.2015)

Chapter 6

Conclusions and outlook

The new control software successfully united all existing measurement procedures and a data base has been built up using the header files. Aspects for improvement will come up as the software and the data base are routinely used. The software development included the control of the light grating hight, but that was not fully implemented due to other technical difficulties on the experiment. For a safer working environment on the optical table, a laser blocking aperture has already been tested to be implemented into the software. This would unblock the laser only for the measuring time and if explicitly chosen by the experimenter. In addition to the tilt sensors, which read the optical table's position, a digital pressure gauge could be installed before the valves of the vibration isolators. Its reading would be included into the header file to improve the reproducibility of the table's position.
The control vision, which motivated the new software, did not include the control of the motors used during alignments of the interferometer such as the motor for the oven's position and the grating's motor controlling their pitch, roll and yaw angle. Hardware updates and realignment for testing might be necessary, but one would gain a more reliable and expandable system, which can be backed up.
The general modular concept of the software offers to implement new and quickly adapt features, or combine the existing procedures such as time-resolved deflectometry measurements plus an additional laser power run option. This is relevant for biomolecules, when the signal is not lasting long enough to complete the desired measurement sequences.

Furthermore, the software modules (subVIs), which acquire date from hardware, could be exchanged by subVIs reading that data from files. As a result, the software would complement the simulated interactive software of the KDTLI [119], which serves as an educational tool for advanced science to understand the working principle and experimental setup of the KDTLI. Including the actual control software would make the simulation of experiment more realistic, and enables the possibility to analyse real data for educational purposes.

The future of molecular interferometers opens unknown possibilities to perform research on almost individual biomolecules, which are probed in the gas phase without perturbations or affections. For example, the absolute absorption cross section has been extracted from the quantum interference using photon recoil on the KDTLI [45].

In general, understanding the transition from the quantum world to the classical one is a promising field with the potential of discovering ground-breaking scientific news. The currently built long baseline universal matter-wave interferometer (LUMI), which will first operate as a Kapitza-Dirac-Talbot-Lau interferometer, is particularly suitable for large molecules to claim a new mass record [120]. This might also be the future of this control software due to the similarity of the experiments in their used hardware, their measurement procedures, and consequently their analysis with an akin data base concept.

Bibliography

[1] Stefan Gerlich, Lucia Hackermüller, Klaus Hornberger, Alexander Stibor, Hendrik Ulbricht, Michael Gring, Fabienne Goldfarb, Tim Savas, Marcel Müri, Marcel Mayor, et al. A Kapitza–Dirac–Talbot–Lau interferometer for highly polarizable molecules. *Nature Physics*, 3(10):711, 2007.

[2] Sandra Eibenberger, Stefan Gerlich, Markus Arndt, Marcel Mayor, and Jens Tüxen. Matter–wave interference of particles selected from a molecular library with masses exceeding 10000 amu. *Physical Chemistry Chemical Physics*, 15(35):14696–14700, 2013.

[3] Björn Brezger, Lucia Hackermüller, Stefan Uttenthaler, Julia Petschinka, Markus Arndt, and Anton Zeilinger. Matter-wave interferometer for large molecules. *Physical Review Letters*, 88(10):100404, 2002.

[4] TA Savas, Satyen N Shah, ML Schattenburg, JM Carter, and Henry I Smith. Achromatic interferometric lithography for 100-nm-period gratings and grids. *Journal of Vacuum Science & Technology B: Microelectronics and Nanometer Structures Processing, Measurement, and Phenomena*, 13(6):2732–2735, 1995.

[5] André Stefanov, Martin Berninger, and Markus Arndt. A novel design for electric field deflectometry on extended molecular beams. *Measurement Science and Technology*, 19(5):055801, 2008.

[6] Klaus Hornberger, Stefan Uttenthaler, Björn Brezger, Lucia Hackermüller, Markus Arndt, and Anton Zeilinger. Collisional decoherence observed in matter wave interferometry. *Physical Review Letters*, 90(16):160401, 2003.

[7] Franz Hasselbach. Progress in electron-and ion-interferometry. *Reports on Progress in Physics*, 73(1):016101, 2009.

[8] SA Werner and H Rauch. *Neutron interferometry: Lessons in Experimental Quantum Physics*. Oxford University Press, Oxford, 1st edition, 2000.

[9] O. Carnal and J. Mlynek. Young's double-slit experiment with atoms: A simple atom interferometer. *Phys. Rev. Lett.*, 66:2689–2692, May 1991.

[10] Alexander D Cronin, Jörg Schmiedmayer, and David E Pritchard. Optics and interferometry with atoms and molecules. *Reviews of Modern Physics*, 81(3):1051, 2009.

[11] Ch J Bordé, N Courtier, F Du Burck, AN Goncharov, and M Gorlicki. Molecular interferometry experiments. *Physics Letters A*, 188(3):187–197, 1994.

[12] Klaus Hornberger, Stefan Gerlich, Hendrik Ulbricht, Lucia Hackermüller, Stefan Nimmrichter, Ilya V Goldt, Olga Boltalina, and Markus Arndt. Theory and experimental verification of Kapitza–Dirac–Talbot–Lau interferometry. *New Journal of Physics*, 11(4):043032, 2009.

[13] Thomas Young. *A Course of Lectures on Natural Philosophy and the Mechanical Arts: In Two Volumes*, volume 2. Johnson, 1807.

[14] Immanuel Estermann and Otto Stern. Beugung von Molekularstrahlen. *Zeitschrift für Physik*, 61(1-2):95–125, 1930.

[15] Wieland Schöllkopf and J Peter Toennies. The nondestructive detection of the helium dimer and trimer. *The Journal of chemical physics*, 104(3):1155–1158, 1996.

[16] Michael S Chapman, Christopher R Ekstrom, Troy D Hammond, Richard A Rubenstein, Jörg Schmiedmayer, Stefan Wehinger, and David E Pritchard. Optics and interferometry with Na_2 molecules. *Physical Review Letters*, 74(24):4783, 1995.

[17] Markus Arndt, Olaf Nairz, Julian Vos-Andreae, Claudia Keller, Gerbrand Van der Zouw, and Anton Zeilinger. Wave–particle duality of C_{60} molecules. *Nature*, 401(6754):680, 1999.

[18] Louis de Broglie. Ondes et quanta. *Comptes Rendus des Sciences*, 177:507–510, 1923.

[19] Markus Arndt and Klaus Hornberger. Quantum interferometry with complex molecules. *arXiv:0903.1614*, 2009.

[20] Klaus Hornberger, Stefan Gerlich, Philipp Haslinger, Stefan Nimmrichter, and Markus Arndt. Colloquium: Quantum interference of clusters and molecules. *Reviews of Modern Physics*, 84(1):157, 2012.

[21] M Arndt, N Dörre, S Eibenberger, P Haslinger, J Rodewald, K Hornberger, S Nimmrichter, and M Mayor. *Matter-wave interferometry with composite quantum objects*, volume 188. IOS Press: Amsterdam, The Netherlands, 2014.

[22] Bahaa E. A. Saleh and Malvin Carl Teich. *Statistical Optics, Fundamentals of Photonics*, chapter 10, pages 342–380. John Wiley & Sons, Inc., 1st edition, 1991.

[23] A. Khintchine. Korrelationstheorie der stationären stochastischen Prozesse. *Mathematische Annalen*, 109(1):604–615, Dec 1934.

[24] Olaf Nairz, Markus Arndt, and Anton Zeilinger. Quantum interference experiments with large molecules. *American Journal of Physics*, 71(4):319–325, 2003.

[25] C. W. McCutchen. Generalized Source and the van Cittert–Zernike Theorem: A Study of the Spatial Coherence Required for Interferometry. *J. Opt. Soc. Am.*, 56(6):727–733, Jun 1966.

[26] David Attwood and Anne Sakdinawat. *X-rays and extreme ultraviolet radiation: principles and applications*. Cambridge university press, 2017.

[27] Gang Xiong, Oussama Moutanabbir, Manfred Reiche, Ross Harder, and Ian Robinson. Coherent x-ray diffraction imaging and characterization of strain in silicon-on-insulator nanostructures. *Advanced Materials*, 26(46):7747–7763, 2014.

[28] Pieter Hendrik van Cittert. Die wahrscheinliche Schwingungsverteilung in einer von einer Lichtquelle direkt oder mittels einer Linse beleuchteten Ebene. *Physica*, 1(1-6):201–210, 1934.

[29] Max Born and Emil Wolf. Elements of the theory of diffraction. In *Principles of Optics*, chapter VIII. Pergamon Press, 4th edition, 1970.

[30] Wolfgang Demtröder. *Interferenz, Beugung und Streuung*, chapter 10. Springer-Verlag, 5th edition, 2009.

[31] quantum interactive: explore modern experimental physics. The Talbot-Effect. `http://interactive.quantumnano.at/wp-content/uploads/2014/04/talbot-transition_EN.jpg` [Accessed: 06.04.2018].

[32] Henry Fox Talbot. Lxxvi. facts relating to optical science. no. iv. *The London and Edinburgh Philosophical Magazine and Journal of Science*, 9(56):401–407, 1836.

[33] Lord Rayleigh F.R.S. Xxv. on copying diffraction-gratings, and on some phenomena connected therewith. *The London, Edinburgh, and Dublin Philosophical Magazine and Journal of Science*, 11(67):196–205, 1881.

[34] Ernst Lau. Beugungserscheinungen an Doppelrastern. *Annalen der Physik*, 437(7-8):417–423, 1948.

[35] K Patorski. Incoherent superposition of multiple self-imaging lau effect and moiré fringe explanation. *Optica Acta: International Journal of Optics*, 30(6):745–758, 1983.

[36] William B Case, Mathias Tomandl, Sarayut Deachapunya, and Markus Arndt. Realization of optical carpets in the talbot and talbot-lau configurations. *Optics Express*, 17(23):20966–20974, 2009.

[37] Olaf Nairz, Markus Arndt, and Anton Zeilinger. Experimental verification of the Heisenberg uncertainty principle for fullerene molecules. *Physical Review A*, 65(3):032109, 2002.

[38] Christian Brand, Sandra Eibenberger, Ugur Sezer, and Markus Arndt. Matter-wave physics with nanoparticles and biomolecules. *arXiv:1703.02129*, 2017.

[39] P. L. Kapitza and P. A. M. Dirac. The reflection of electrons from standing light waves. In *Mathematical Proceedings of the Cambridge Philosophical Society*, volume 29, pages 297–300. Cambridge University Press, 1933.

[40] Daniel L Freimund, Kayvan Aflatooni, and Herman Batelaan. Observation of the kapitza–dirac effect. *Nature*, 413(6852):142, 2001.

[41] Olaf Nairz, Björn Brezger, Markus Arndt, and Anton Zeilinger. Diffraction of complex molecules by structures made of light. *Physical Review Letters*, 87(16):160401, 2001.

[42] Phillip L Gould, George A Ruff, and David E Pritchard. Diffraction of atoms by light: The near-resonant Kapitza-Dirac effect. *Physical Review Letters*, 56(8):827, 1986.

[43] Peter J Martin, Bruce G Oldaker, Andrew H Miklich, and David E Pritchard. Bragg scattering of atoms from a standing light wave. *Physical Review Letters*, 60(6):515, 1988.

[44] Sandra Isolde Eibenberger. Kapitza-Dirac-Talbot-Lau Interferometrie mit komplexen molekülen. diploma thesis, University of Vienna, 2010.

[45] Sandra Eibenberger, Xiaxi Cheng, JP Cotter, and Markus Arndt. Absolute absorption cross sections from photon recoil in a matter-wave interferometer. *Physical Review Letters*, 112(25):250402, 2014.

[46] JP Cotter, S Eibenberger, L Mairhofer, X Cheng, P Asenbaum, M Arndt, K Walter, S Nimmrichter, and K Hornberger. Erratum: Coherence in the presence of absorption and heating in a molecule interferometer. *Nature Communications*, 6:10121, 2015.

[47] Philippe Blanchard, Domenico Giulini, Erich Joos, Claus Kiefer, and Ion-Olimpiu Stamatescu. I. General Introduction. In *Decoherence: Theoretical, Experimental, and Conceptual Problems: Proceedings of a Workshop Held at Bielefeld Germany, 10–14 November 1998*. Springer Science & Business Media, 2000.

[48] Lucia Hackermüller, Klaus Hornberger, Björn Brezger, Anton Zeilinger, and Markus Arndt. Decoherence in a Talbot–Lau interferometer: the influence of molecular scattering. *Applied Physics B*, 77(8):781–787, 2003.

[49] Lucia Hackermüller, Klaus Hornberger, Björn Brezger, Anton Zeilinger, and Markus Arndt. Decoherence of matter waves by thermal emission of radiation. *Nature*, 427(6976):711, 2004.

[50] Jens Ulrik Andersen and E Bonderup. Classical dielectric models of fullerenes and estimation of heat radiation. *The European Physical Journal D-Atomic, Molecular, Optical and Plasma Physics*, 11(3):413–434, 2000.

[51] A Stibor, K Hornberger, L Hackermüller, A Zeilinger, and M Arndt. Talbot-lau interferometry with fullerenes: Sensitivity to inertial forces and vibrational dephasing. *arXiv:0411118*, 2004.

[52] C Jess Riedel and Itay Yavin. Decoherence as a way to measure extremely soft collisions with dark matter. *Physical Review D*, 96(2):023007, 2017.

[53] Stefan Gerlich. *Interferometry and Metrology with Macromolecules*. PhD thesis, University of Vienna, 2011.

[54] Newport Corporation. Technical Note: Instability Oscillation of High CG Table Systems. `https://www.newport.com/n/instability-oscillation-of-high-cg-table-systems` [Accessed: 22.03.2018].

[55] Lukas Mairhofer. *Quantum-interference assisted Metrology with complex Biomolecules*. PhD thesis, University of Vienna, 2017.

[56] James William Rohlf. *Modern Physics from α to Z*, chapter II. Wiley-VCH, 1st edition, 1994.

[57] Wolfgang Demtröder. *Experimentalphysik 1: Mechanik und Wärme*, chapter 7, pages 210–214. Springer-Verlag, 5th edition, 2008.

[58] Lukas Mairhofer. Photo from the oven used inside the KDTLI. taken with a Fujifilm X-E2 camera: DSCF2198.JPG, 07 2017.

[59] Precision Ceramics. Shapal Hi-M Soft Material Properties. `http://www.precision-ceramics.co.uk/materials/shapal/material-properties/` [Accessed: 07.03.2018].

[60] Sandra Isolde Eibenberger. *Quantum interference experiments with complex organic molecules*. PhD thesis, University of Vienna, 2015.

[61] Robert C Dunbar. Deriving the Maxwell distribution. *Journal of Chemical Education*, 59(1):22, 1982.

[62] G Comsa, R David, and BJ Schumacher. Magnetically suspended cross-correlation chopper in molecular beam-surface experiments. *Review of Scientific Instruments*, 52(6):789–796, 1981.

[63] Daniel J. Auerbach. Velocity measurements by time-of-flight methods. In Giacinto Scoles, editor, *Atomic and Molecular Beam Methods*, chapter 14, pages 362–379. Oxford University Press, 1992.

[64] VL Hirschy and JP Aldridge. A cross correlation chopper for molecular beam modulation. *Review of Scientific Instruments*, 42(3):381–383, 1971.

[65] G Wilhelmi and F Gompf. Binary sequences and error analysis for pseudo-statistical neutron modulators with different duty cycles. *Nuclear Instruments and Methods*, 81(1):36–44, 1970.

[66] Abdul J Jerri. The shannon sampling theoremits various extensions and applications: A tutorial review. *Proceedings of the IEEE*, 65(11):1565–1596, 1977.

[67] John W. Dettman. *Mathematical Methods in Physics and Engineering*, volume 1 of *International series in pure and applied mathematics*, chapter 6, pages 266–282. MacGraw-Hill, New York, 1962.

[68] F. Gompf, W. Reichardt, W. Glaser, and K.H. Beckurts. The use of a pseudo-statistical chopper for time-of-flight measurements. In *Proceedings of a Symposium on Neutron Inelastic Scattering*, volume II, pages 417–428. International Atomic Energy Agency, 1968.

[69] Maxime Debiossac. Photo from inside the KDTLI's main chamber. snapshot from a video: GOPR0064.MP4, 04 2016.

[70] Marion Romirer. Image of the material grating taken with an electron microscope at 5kv. Photo No. = 30407, 05 2016.

[71] Thorlabs. CMOS Cameras: USB 2.0 and USB 3.0. camera: DCC1545M, software: ThorlabsDCx_camera_V4.20 `https://www.thorlabs.com/newgrouppage9.cfm?objectgroup_id=4024` [Accessed: 13.06.2018].

[72] RE Grisenti, W Schöllkopf, JP Toennies, JR Manson, TA Savas, and Henry I Smith. He-atom diffraction from nanostructure transmission gratings: The role of imperfections. *Physical Review A*, 61(3):033608, 2000.

[73] RE Grisenti, W Schöllkopf, JP Toennies, GC Hegerfeldt, and T Köhler. Determination of atom-surface van der waals potentials from transmission-grating diffraction intensities. *Physical Review Letters*, 83(9):1755, 1999.

[74] Coherent. Verdi V Series. Diode-Pumped Solid-State Lasers, High-Power CW Output at 532 nm, 20 `https://www.coherent.com/lasers/laser/verdi-v-series` [Accessed: 13.06.2018].

[75] Wolfgang Demtröder. *Interferenz, Beugung und Streuung*, chapter 11. Springer-Verlag, 5th edition, 2009.

[76] Sarayut Deachapunya, André Stefanov, Martin Berninger, Hendrik Ulbricht, Elisabeth Reiger, Nikos L Doltsinis, and Markus Arndt. Thermal and electrical properties of porphyrin derivatives and their relevance for molecule interferometry. *The Journal of chemical physics*, 126(16):164304, 2007.

[77] Scott Prahl. Tetraphenylporphyrin, [TPP], 2017. `https://omlc.org/spectra/PhotochemCAD/html/099.html` [Accessed: 19.06.2018].

[78] Stefan Nimmrichter and Klaus Hornberger. Theory of near-field matter-wave interference beyond the eikonal approximation. *Physical Review A*, 78(2):023612, 2008.

[79] Kai Walter, Stefan Nimmrichter, and Klaus Hornberger. Multiphoton absorption in optical gratings for matter waves. *Physical Review A*, 94(4):043637, 2016.

[80] Xiaxi Cheng. Exploration of matter wave interferometry in the Talbot-Lau design. master's thesis, University of Vienna, 2014.

[81] Extrel CMS. Quadrupole Mass Spectrometers and Residual Gas Analyzers, 1964. `http://www.extrel.com/Module/Catalog/ProductsCategory/default/Quadrupole_Mass_Spectrometers_and_Residual_Gas_Analyzers?id=31` [Accessed: 22.02.2018].

[82] Extrel CMS. User Manual, 2004. Mass Separation and Focusing.

[83] Extrel CMS. User Manual, 2004. Axial Molecular Beam Ionizer.

[84] Extrel CMS. User Manual, 2004. Electron Multiplier and Mounting Flange.

[85] Wolfgang Demtröder. *Experimentalphysik 3: Atome, Moleküle und Festkörper*, chapter 2.7.7, pages 52–56. Springer-Verlag, 3rd edition, 2005.

[86] Extrel CMS. User Manual, 2004. Merlin Automation Quick Start Guided Tour.

[87] National Instruments. USB-6343: 32 AI (16-Bit, 500 kS/s), 4 AO (900 kS/s), 48 DIO USB Multifunction I/O Device. `http://www.ni.com/de-at/support/model.usb-6343.html` [Accessed: 23.02.2018].

[88] M Arndt, M Berninger, S Deachapunya, S Gerlich, L Hackermüller, AG Major, M Marksteiner, A Stéfanov, and H Ulbricht. On the prospects of interferometry and deflectometry for characterizing large molecules. *The European Physical Journal Special Topics*, 159(1):1–9, 2008.

[89] J. H. Van Vleck. Classical theory of the Langevin-Debye formula. In *The Theory Of Electric And Magnetic Susceptibilities*, chapter II. Oxford At The Clarendon Press, 1st edition, 1932.

[90] Sandra Eibenberger, Stefan Gerlich, Markus Arndt, Jens Tüxen, and Marcel Mayor. Electric moments in molecule interferometry. *New Journal of Physics*, 13(4):043033, 2011.

[91] Martin Berninger, André Stefanov, Sarayut Deachapunya, and Markus Arndt. Polarizability measurements of a molecule via a near-field matter-wave interferometer. *Physical Review A*, 76(1):013607, 2007.

[92] Christopher R Ekstrom, Jörg Schmiedmayer, Michael S Chapman, Troy D Hammond, and David E Pritchard. Measurement of the electric polarizability of sodium with an atom interferometer. *Physical Review A*, 51(5):3883, 1995.

[93] Keith D Bonin and Vitaly V Kresin. *Electric-dipole polarizabilities of atoms, molecules, and clusters*. World Scientific, 1997.

[94] Jens Txen, Stefan Gerlich, Sandra Eibenberger, Markus Arndt, and Marcel Mayor. Quantum interference distinguishes between constitutional isomers. *Chem. Commun.*, 46:4145–4147, 2010.

[95] High Finesse Laser and Electronic Systems. Wavelength Meter WS 7 616. `http://www.highfinesse.com/en/wavelengthmeter` [Accessed: 24.04.2018].

[96] pico Technology. USB TC-08 Temperature Logger, 2013. User's Guide `https://www.picotech.com/data-logger/tc-08/thermocouple-data-logger` [Accessed: 22.03.2018].

[97] Pfeiffer Vacuum. DualGauge^{TM}, Dual-Channel Measurement and Control Unit for Compact Gauges. Communication Protocol: TPG 262 `http://www.idealvac.com/files/ManualsII/Pfeiffer_TPG262_Operating_Instructions.pdf` [Accessed: 27.04.2018].

[98] œrlikon leybold vacuum. CENTER TWO CENTER THREE Mehrkanal-Messgerät. Gebrauchsanleitung GA 09.035/5.01.

[99] SPECTRON GLASS AND ELECTRONICS INC. SH50050 Series Ceramic Tilt Sensor. Application Note: Installation Guidelines and Thermal Considerations `www.spectronsensors.com/datasheets/SDS-116-3106.pdf` [Accessed: 27.03.2018].

[100] FAST ComTech GmbH. MCA-3 Series/P7882, 2016. Multichannel Analyzer/ Dual Input Multiscaler User Manual.

[101] Wolfgang Georgi and Ergun Metin. *Einführung in LabVIEW*. Carl Hanser Verlag GmbH Co KG, 2012.

[102] National Instruments. LabVIEW - Development Guidelines, 2003. http://www.ni.com/pdf/manuals/321393d.pdf [Accessed: 13.08.2018].

[103] National Instruments. Tutorial: State Machines. http://www.ni.com/tutorial/7595/en/ [Accessed: 19.06.2018].

[104] National Instruments. Event-Driven Programming in LabVIEW. http://www.ni.com/white-paper/3331/en/ [Accessed: 23.06.2018].

[105] Marvin L. Minsky. *Computation: Finite and Infinite Machines*, chapter 2. Prentice-Hall, Inc., Upper Saddle River, NJ, USA, 1967.

[106] National Instruments. Creating Custom Controls, Indicators, and Type Definitions. https://zone.ni.com/reference/en-XX/help/371361H-01/lvconcepts/custom_cont_ind_type/#Type_Definitions_and_Strict_Type_Definitions [Accessed: 23.06.2018].

[107] piezosystem jena. Instruction manual EDA. Interface card for amplifier system ENV, "EDAeng.pdf".

[108] National Instruments. Connecting Instruments via GPIB. https://www.ni.com/getting-started/set-up-hardware/instrument-control/gpib-connect [Accessed: 13.06.2018].

[109] National Instruments. Windows API Function Utilities (32-bit) for LabVIEW. http://www.ni.com/example/29935/en/ [Accessed: 13.06.2018].

[110] National Instruments. An Overview of Accessing DLLs or Shared Libraries from LabVIEW. http://www.ni.com/tutorial/3009/en/ [Accessed: 01.06.2018].

[111] National Instruments. LabVIEW Internet Toolkit 2012. http://www.ni.com/download/labview-internet-toolkit-2012/3122/en/ [Accessed: 01.06.2018].

[112] National Instruments. NI-VISA Overview. http://www.ni.com/tutorial/3702/en/ [Accessed: 01.06.2018].

[113] Thorlabs. Motorized Precision Rotation Stage with DC Servo Motor. Thorlabs APT (32BIT), product version 3.9.0 https://www.thorlabs.com/NewGroupPage9_PF.cfm?Guide=10&Category_ID=31&ObjectGroup_ID=4134 [Accessed: 13.06.2018].

[114] National Instruments. MATLAB script. http://zone.ni.com/reference/en-XX/help/371361P-01/gmath/matlab_script_node/ [Accessed: 13.06.2018].

[115] Stefan Gerlich, Michael Gring, Hendrik Ulbricht, Klaus Hornberger, Jens Tüxen, Marcel Mayor, and Markus Arndt. Matter-wave metrology as a complementary tool for mass spectrometry. *Angewandte Chemie International Edition*, 47(33):6195–6198, 2008.

[116] Michael Gring, Stefan Gerlich, Sandra Eibenberger, Stefan Nimmrichter, Tarik Berrada, Markus Arndt, Hendrik Ulbricht, Klaus Hornberger, Marcel Müri, Marcel Mayor, et al. Influence of conformational molecular dynamics on matter wave interferometry. *Physical Review A*, 81(3):031604, 2010.

[117] Lukas Mairhofer, Sandra Eibenberger, Joseph P Cotter, Marion Romirer, Armin Shayeghi, and Markus Arndt. Quantum-assisted metrology of neutral vitamins in the gas-phase. *Angewandte Chemie International Edition*, 2017.

[118] National Instruments. Tips and Techniques in Data Acquisition Triggering - NI-DAQmx. In *Getting Started with NI-DAQmx Series*. NI, Apr 12, 2012. updated: `http://www.ni.com/tutorial/4329/en/` [Accessed: 17.06.2018].

[119] Mathias Tomandl, Thomas Mieling, Christiane M Losert-Valiente Kroon, Martin Hopf, and Markus Arndt. Simulated interactive research experiments as educational tools for advanced science. *Scientific reports*, 5:14108, 2015.

[120] University of Vienna Quantum Nanophysics Group. Long baseline Universal Matter-wave Interferometer (LUMI). `https://www.quantumnano.at/research/matter-wave-technologies/lumi-interferometry/` [Accessed: 18.04.2018].

Appendix

1 – Control Software documentation
2 – List of SubVIs

1 - KDTLI-Control.vi

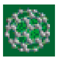

State machine - main measurement programme
The underlying concept to this VI lies in the labview state machine (check further information online). A second loop checking for user events is running parallel. A user event will be triggered by pressing a button, which will set a state for the state machine. A list of all states is on the block diagramm (State description).
In principle, it starts with an initializing the hardware (checking if everything is connected). Afterwards, it waits for the state to be changed by the user event loop. The state machine has different loops or paths to go through a number of states fulfilling a certain task.
Additional features can be included by defining new frames in the state machine (change type def.).

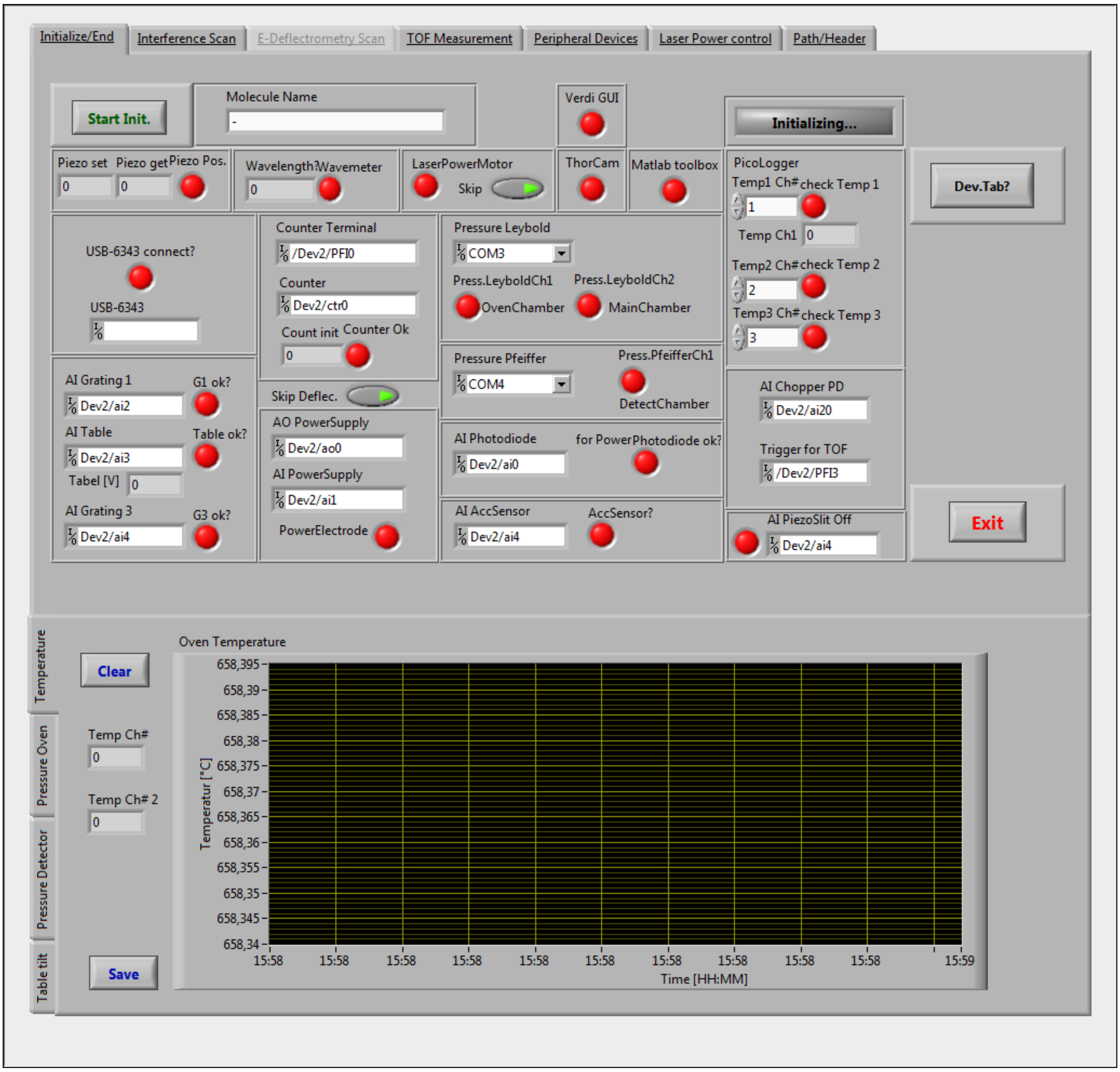

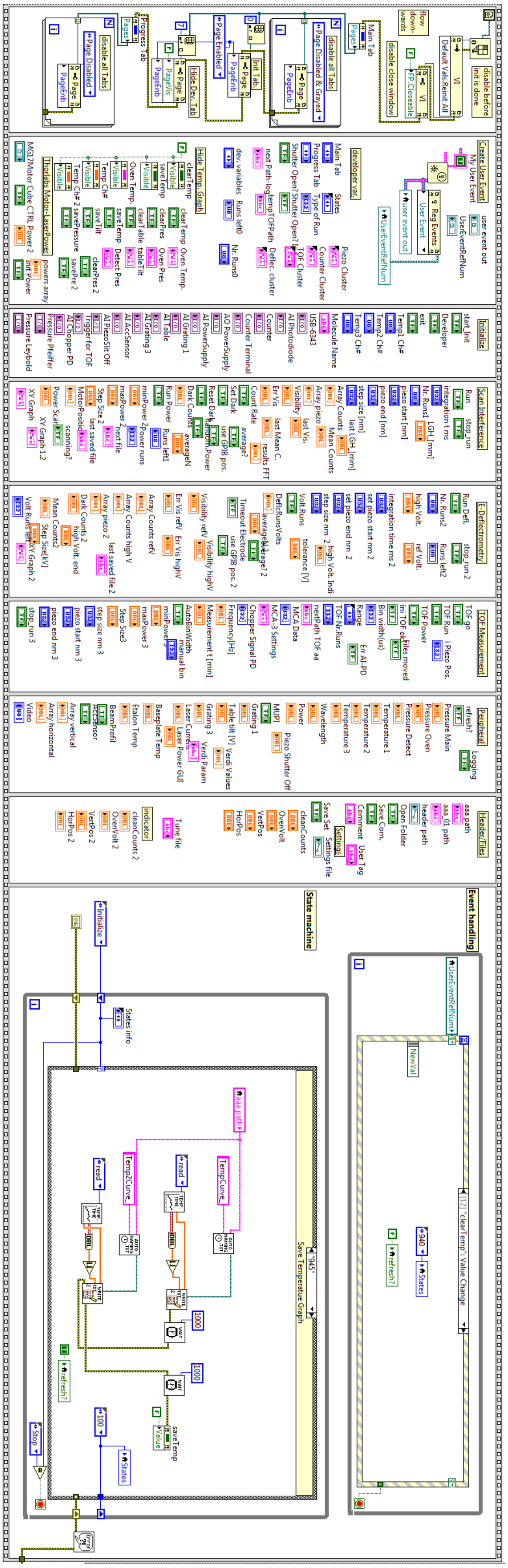

The block diagram of the control software is shown on the left. It is a frame structure with all controls and indicators on the front panel sorted by the tab on which it appears.
This VI is the framework to the control. In the last frame it contains two parallel loops. The event loop, which determine the state or the called "pop-up"-VI depending on the button pressed by the user.
First all events are listed and secondly the states.

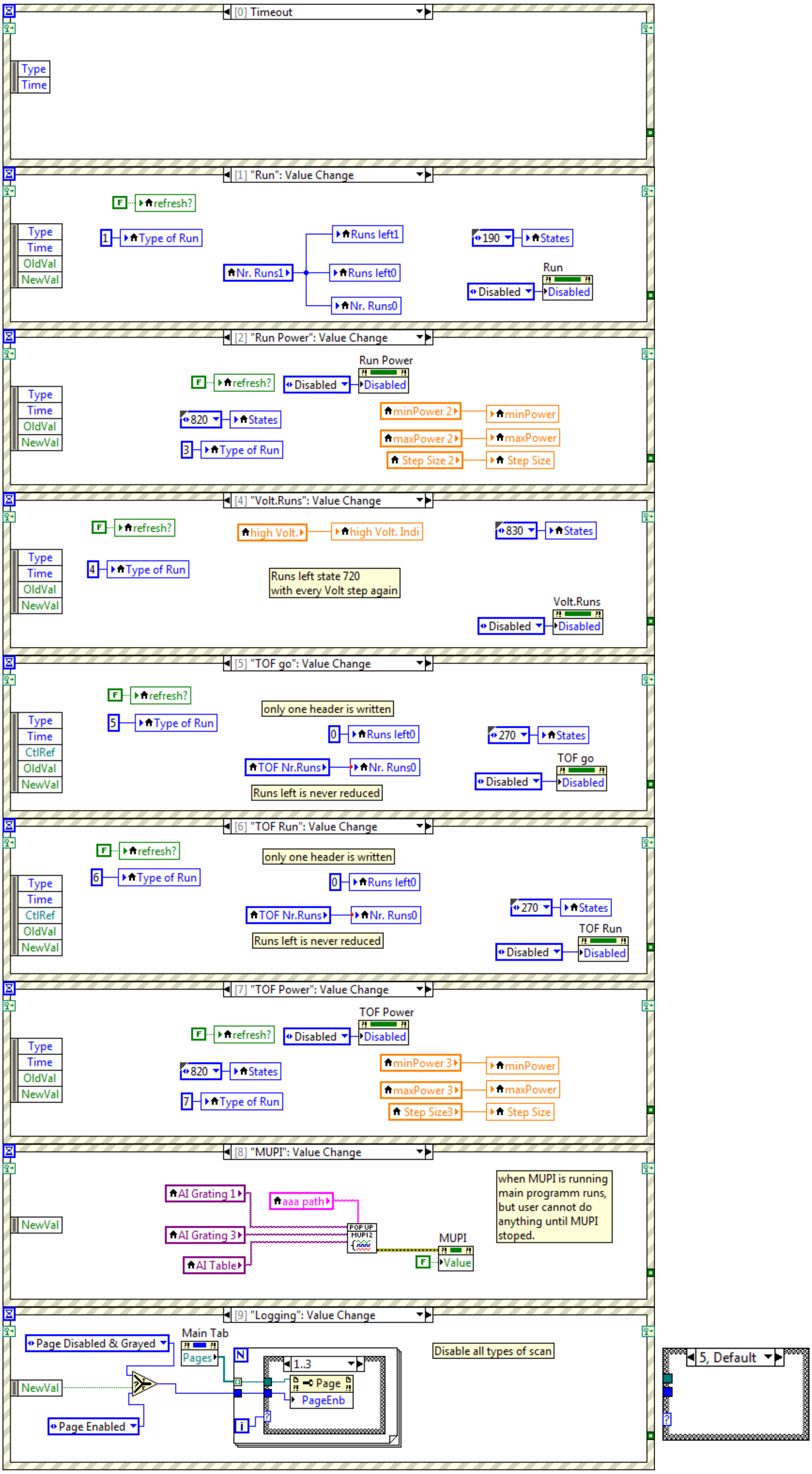
[0] Timeout
Type
Time
[1] "Run": Value Change
refresh?
Type of Run
Runs left1
Nr. Runs1
Runs left0
Nr. Runs0
190
States
Run
Disabled
[2] "Run Power": Value Change
Run Power
minPower 2
minPower
maxPower 2
maxPower
Step Size 2
Step Size
820
[4] "Volt.Runs": Value Change
high Volt.
high Volt. Indi
830
Runs left state 720
with every Volt step again
Volt.Runs
[5] "TOF go": Value Change
only one header is written
TOF Nr.Runs
270
TOF go
Runs left is never reduced
CtlRef
OldVal
NewVal
[6] "TOF Run": Value Change
TOF Run
[7] "TOF Power": Value Change
TOF Power
minPower 3
maxPower 3
Step Size3
[8] "MUPI": Value Change
AI Grating 1
aaa path
AI Grating 3
AI Table
POP UP MUPI2
MUPI
Value
when MUPI is running
main programm runs,
but user cannot do
anything until MUPI
stoped.
[9] "Logging": Value Change
Page Disabled & Grayed
Main Tab
Pages
1..3
Page
PageEnb
Page Enabled
Disable all types of scan
5, Default

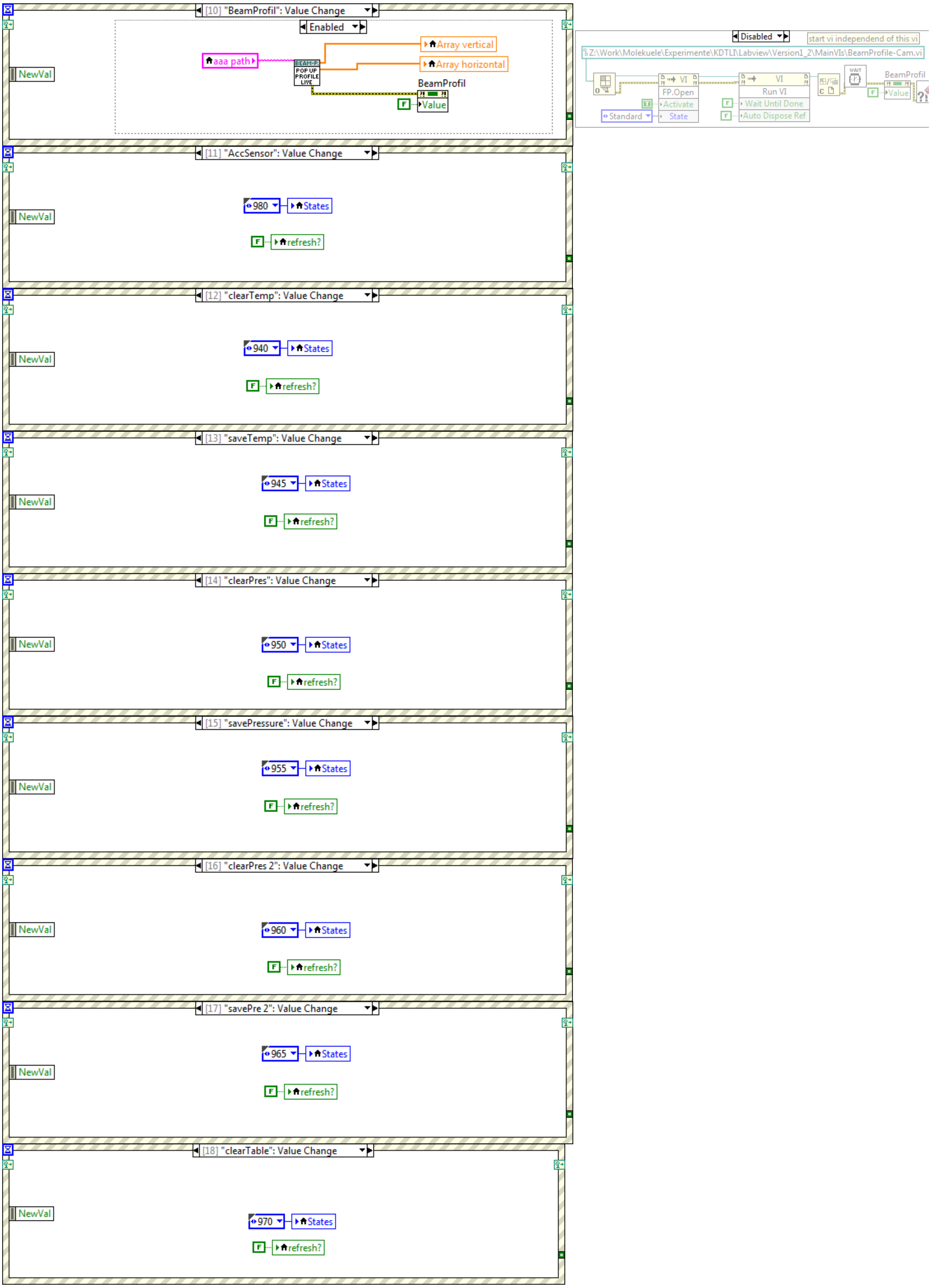
[10] "BeamProfil": Value Change
Enabled
NewVal
aaa path
Array vertical
Array horizontal
BeamProfil
Value
Disabled
start vi independend of this vi
Z:\Work\Molekuele\Experimente\KDTLI\Labview\Version1_2\MainVIs\BeamProfile-Cam.vi
FP.Open
Activate
State
Standard
Run VI
Wait Until Done
Auto Dispose Ref
[11] "AccSensor": Value Change
NewVal
980
States
refresh?
[12] "clearTemp": Value Change
NewVal
940
States
refresh?
[13] "saveTemp": Value Change
NewVal
945
States
refresh?
[14] "clearPres": Value Change
NewVal
950
States
refresh?
[15] "savePressure": Value Change
NewVal
955
States
refresh?
[16] "clearPres 2": Value Change
NewVal
960
States
refresh?
[17] "savePre 2": Value Change
NewVal
965
States
refresh?
[18] "clearTable": Value Change
NewVal
970
States
refresh?

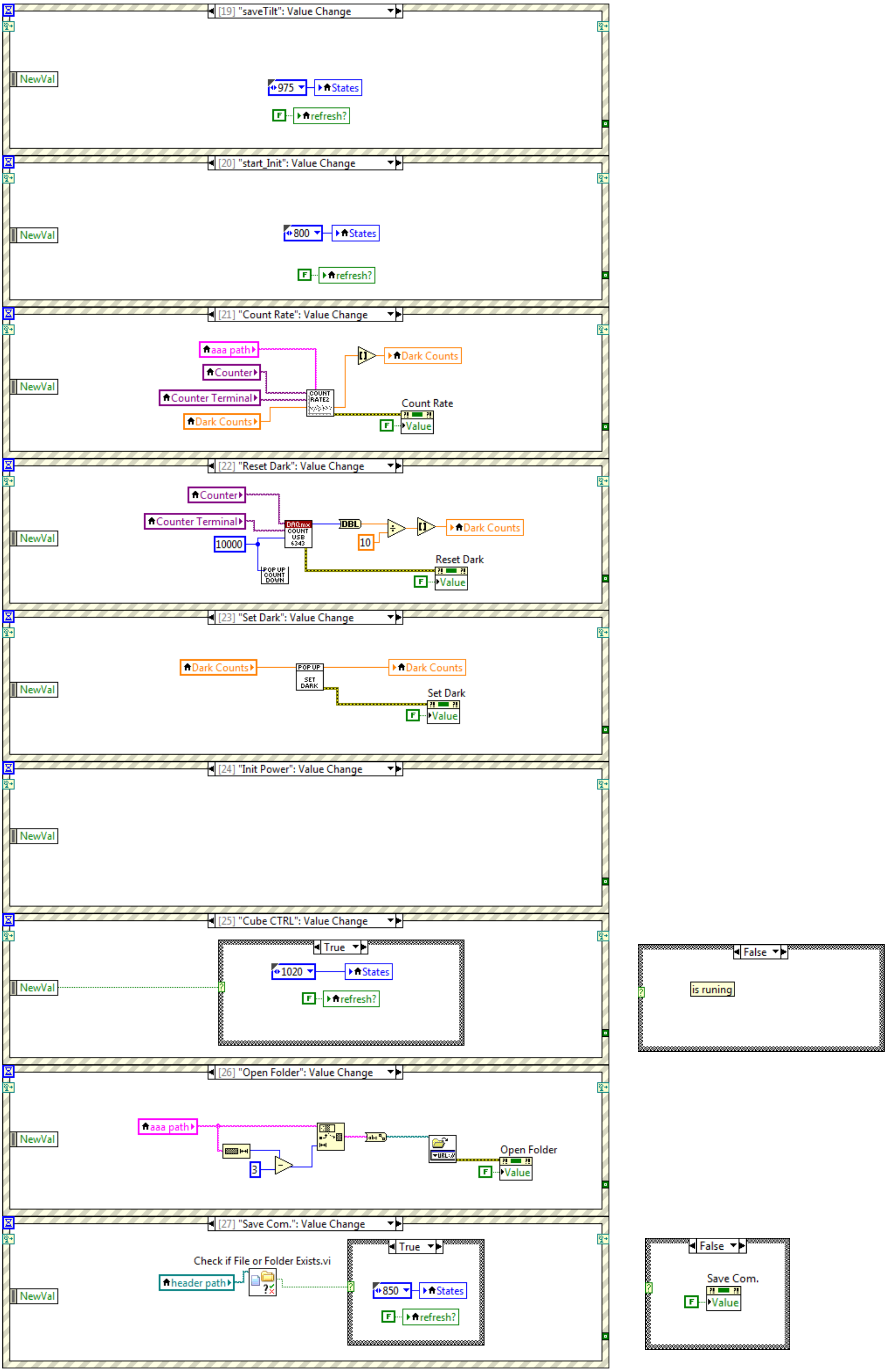
[19] "saveTilt": Value Change
NewVal
975
States
refresh?
[20] "start_Init": Value Change
NewVal
800
States
refresh?
[21] "Count Rate": Value Change
NewVal
aaa path
Counter
Counter Terminal
Dark Counts
COUNT RATE2
Dark Counts
Count Rate
Value
[22] "Reset Dark": Value Change
NewVal
Counter
Counter Terminal
10000
DAQmx COUNT USB 6343
POP UP COUNT DOWN
DBL
10
Dark Counts
Reset Dark
Value
[23] "Set Dark": Value Change
NewVal
Dark Counts
POP UP SET DARK
Dark Counts
Set Dark
Value
[24] "Init Power": Value Change
NewVal
[25] "Cube CTRL": Value Change
NewVal
True
1020
States
refresh?
False
is runing
[26] "Open Folder": Value Change
NewVal
aaa path
3
Open Folder
Value
[27] "Save Com.": Value Change
NewVal
Check if File or Folder Exists.vi
header path
True
850
States
refresh?
False
Save Com.
Value

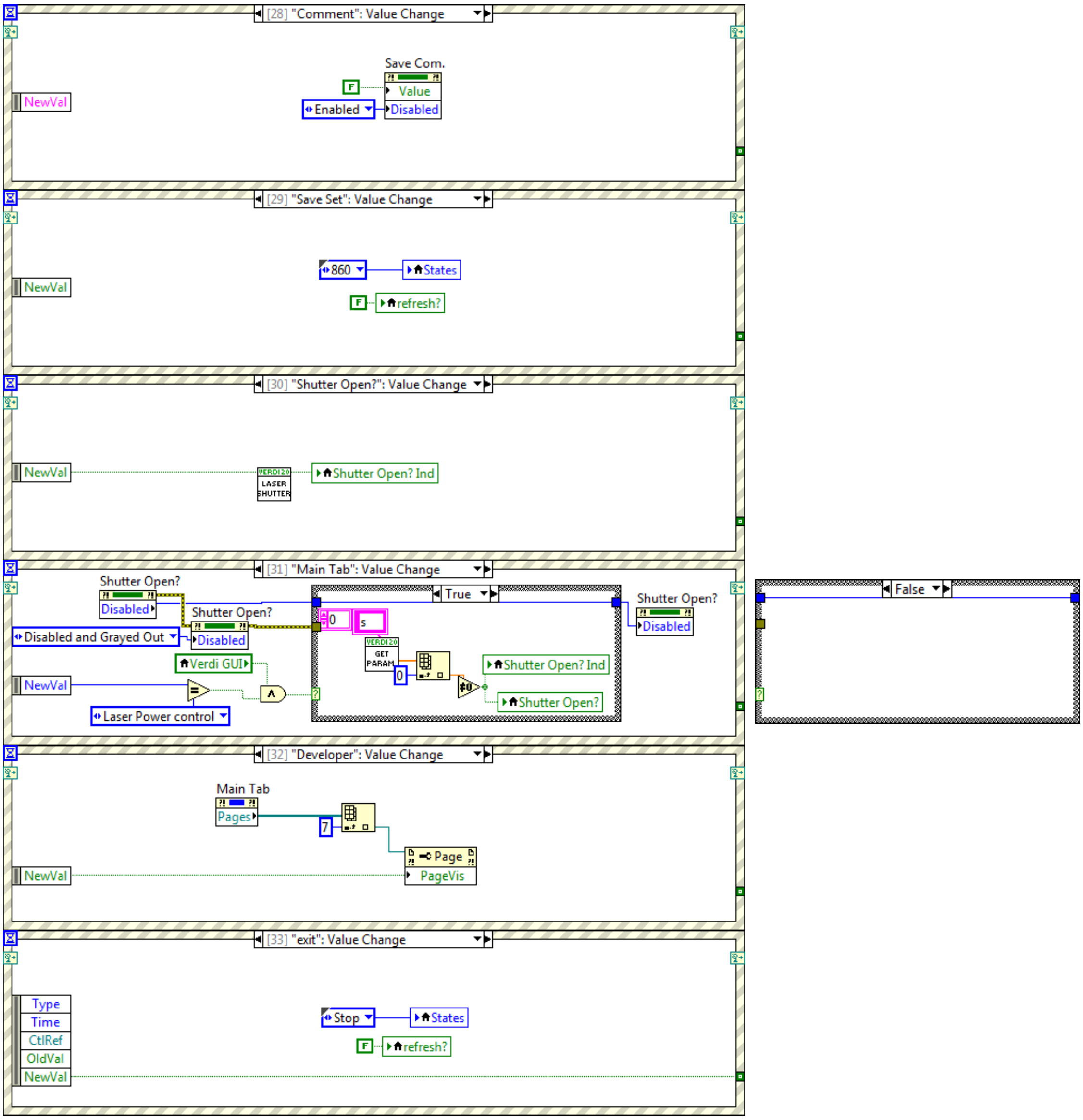
[28] "Comment": Value Change
NewVal
Save Com.
Value
Enabled
Disabled
[29] "Save Set": Value Change
NewVal
860
States
refresh?
[30] "Shutter Open?": Value Change
NewVal
Shutter Open? Ind
[31] "Main Tab": Value Change
Shutter Open?
Disabled
Disabled and Grayed Out
Verdi GUI
NewVal
Laser Power control
True
Shutter Open? Ind
Shutter Open?
False
[32] "Developer": Value Change
Main Tab
Pages
7
Page
PageVis
NewVal
[33] "exit": Value Change
Type
Time
CtlRef
OldVal
NewVal
Stop
States
refresh?

State description

Initialize
Initialize waiting for user

9 get molecule/tune name
10 USB-6343 connected

USB-6343:
AI0 Photodiode
AI1 Electrode read
AI2 Grating1 I
AI3 Table II
AI4 Grating2 III
AI5 Acc. Sensor
AI 20 Chopper PD
AO0 Electrode write
Ctr0 Counter
Ctr3 Trigger from FastCard

15 creating USB6343 ch.
20 Photodiode
25 PowerSuppy Deflect.
30 MUPI
35 Piezo Shutter
40 Counter

50 Piezo Init.
55 Wavemeter
59 Verdi GUI
60 Temp. ch#-> naming
65 Picco logger USB
70 Pressure Leybold
75 Pressure Pfeifer
80 ThorCube Motor
85 ThorCamera
95 Matlab toolbox license

96 disable tabs USB 6343
97 disable tabs Piezo
98 disable tabs Motor
disable tabs deflect.
99 create path (file)

WAIT
100 and ready

Scan

190 Check if Dark is 0

200 Interference Scan
210 Analysis Scan Data
220 Writing Scan Data File
230 Deflectometry
240 Analysis refVolt
245 Analysis DeflecVolt
250 Writing Deflc. Data
270 TOF ini
280 TOF ini failed
285 TOF single Pos.
290 TOF Scan prepare
295 TOFScan Piezo
299 move TOF-files to server

Peripheral devices
300
310 Thorcam BeamPorfile
(with Matlab)
320Thromocouple
330 Photodiode
340 Pressure Leybold
345 Pressure Pfeiffer
350 Wavemeter
360 Table Position MUPI
370 Verdi GUI Parameter
380 Piezo Slit Monitor
390 Refresh Mode?

Save Header
500 Save Snap as JPG
510 Create Header
515 Scan Type
520 Run Info
525 LGH
528 DarkCounts
530 Interation time
535 Save Visibility
540 Save BeamProfile results
550 Save Wavelength
560 Save Temperatures
570 Save Laser Power
580 Save Pressure
590 Save MUPI results
600 Electrode Voltages
610 Electrode Visibilty
620 Verdi GUI data
630 Piezo Slit Offset
640 ScanPiezo Parameter
650 fft resutls from scan
670 User Tag
680 Tunefile Path
690 Run Complete?

End of Scan

700 End of run new aaa
710 next Power - MotorControl
720 next Voltage - Deflectometry
780 Email Notification
790 End of any Scan

User Events
800 reset initializing
810 Open Folder
820 SetUp Power
830 Set up Volt Run Deflect.
850 Save Comment to header
860 Save KDTLI Settings
870 last saved Settings

More Features

900 Reset dark Count(event case)
910 Current Counter(event case)
930 Set DarkCount(event case)
xxx Shutter Laser (event case)

940 clear Temp. graph
945 save Temp. graph
950 clear Pres.Oven graph
955 save Pres.Oven graph
960 clear Pres.Detect graph
965 save Pres.Detect graph
970 clear Table_tilt. graph
975 save Table_tilt. graph

980 Acc.Sensor FFT
990 MUPI Display (event case)
1000 Reinit Laser Power Ctrl
1010 Reset Ctrl Buttons
1020 Laser Power Control

Error:
2nd Devices
Matlab
Path/Saving
Scan
Other?

Stop

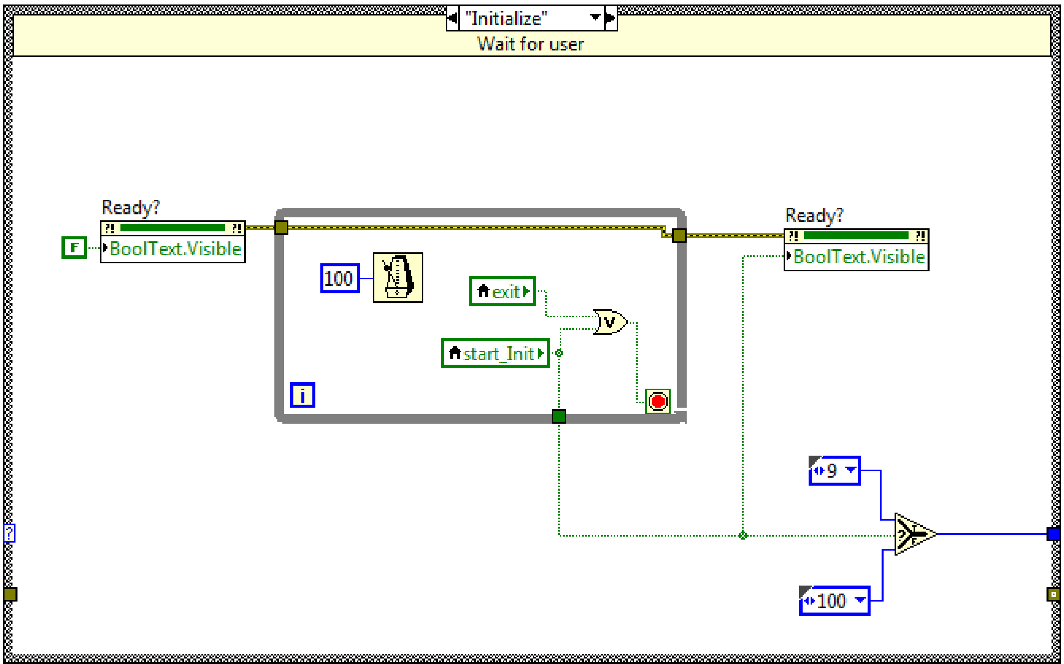
"Initialize"
Wait for user
Ready?
BoolText.Visible
F
100
exit
start_Init
i
Ready?
BoolText.Visible
9
100

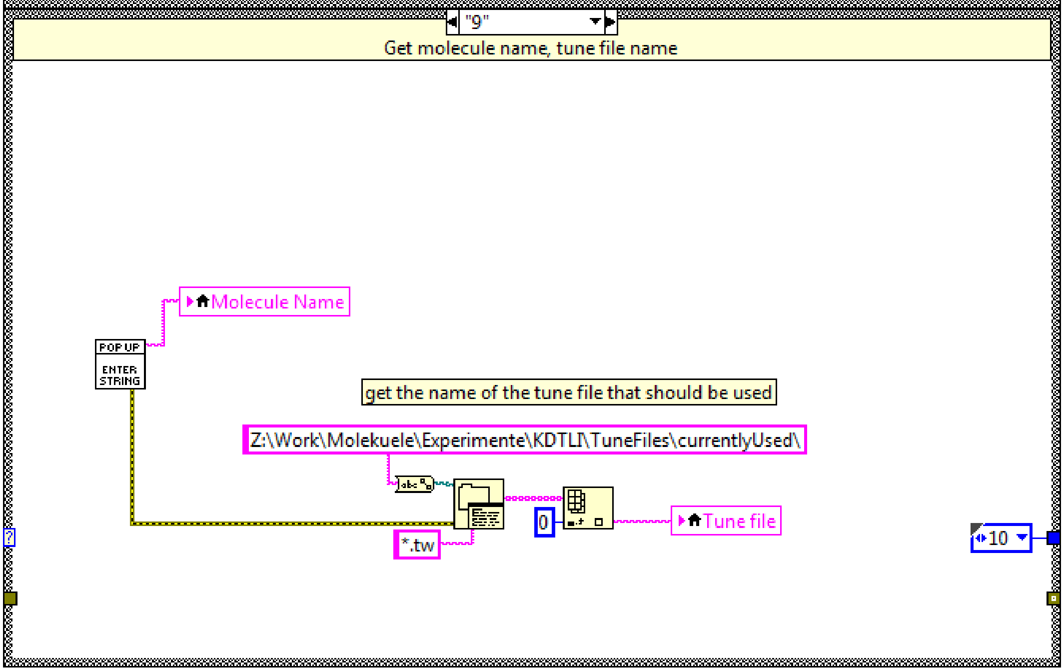
"9"
Get molecule name, tune file name
Molecule Name
POP UP
ENTER STRING
get the name of the tune file that should be used
Z:\Work\Molekuele\Experimente\KDTLI\TuneFiles\currentlyUsed\
*.tw
0
Tune file
10

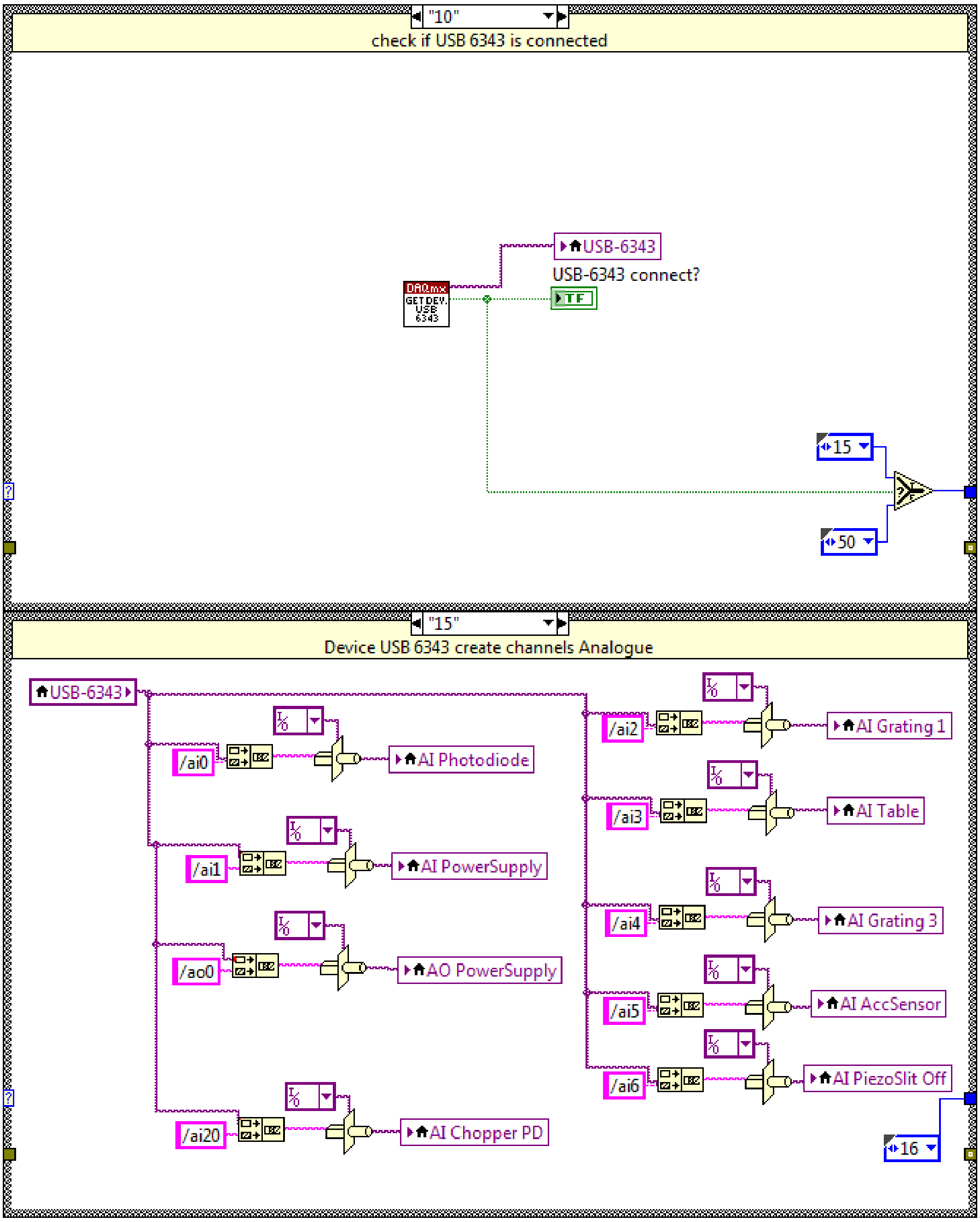
"10"
check if USB 6343 is connected
USB-6343
USB-6343 connect?
15
50
"15"
Device USB 6343 create channels Analogue
USB-6343
/ai0
AI Photodiode
/ai1
AI PowerSupply
/ao0
AO PowerSupply
/ai20
AI Chopper PD
/ai2
AI Grating 1
/ai3
AI Table
/ai4
AI Grating 3
/ai5
AI AccSensor
/ai6
AI PiezoSlit Off
16

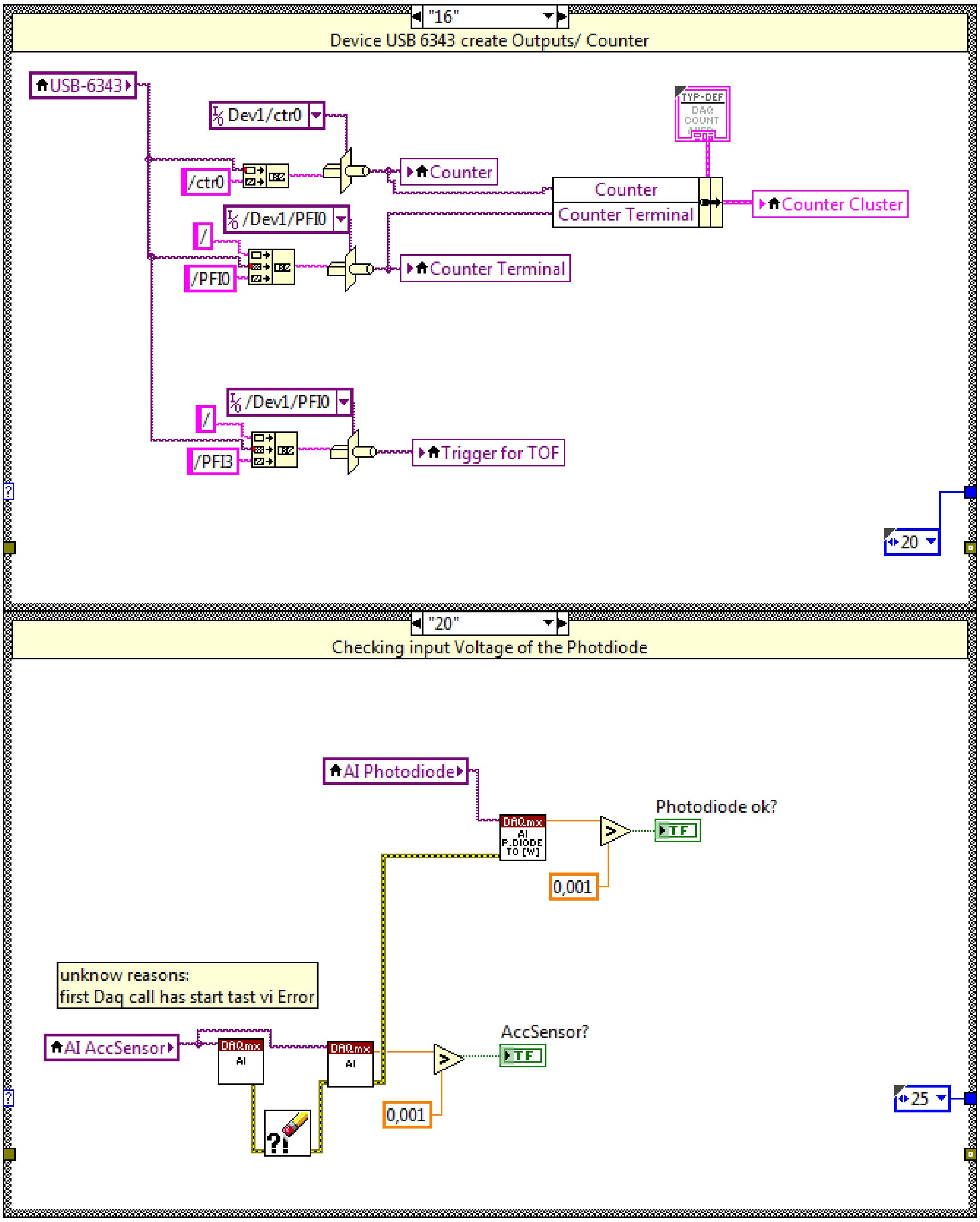
"16"
Device USB 6343 create Outputs/ Counter
USB-6343
Dev1/ctr0
/ctr0
Counter
/Dev1/PFI0
/
/PFI0
Counter Terminal
TYP-DEF DAQ COUNT
Counter
Counter Terminal
Counter Cluster
/Dev1/PFI0
/
/PFI3
Trigger for TOF
20
"20"
Checking input Voltage of the Photdiode
AI Photodiode
DAQmx
AI P.DIODE TO [W]
Photodiode ok?
TF
0,001
unknow reasons:
first Daq call has start tast vi Error
AI AccSensor
DAQmx
AI
DAQmx
AI
AccSensor?
TF
0,001
25

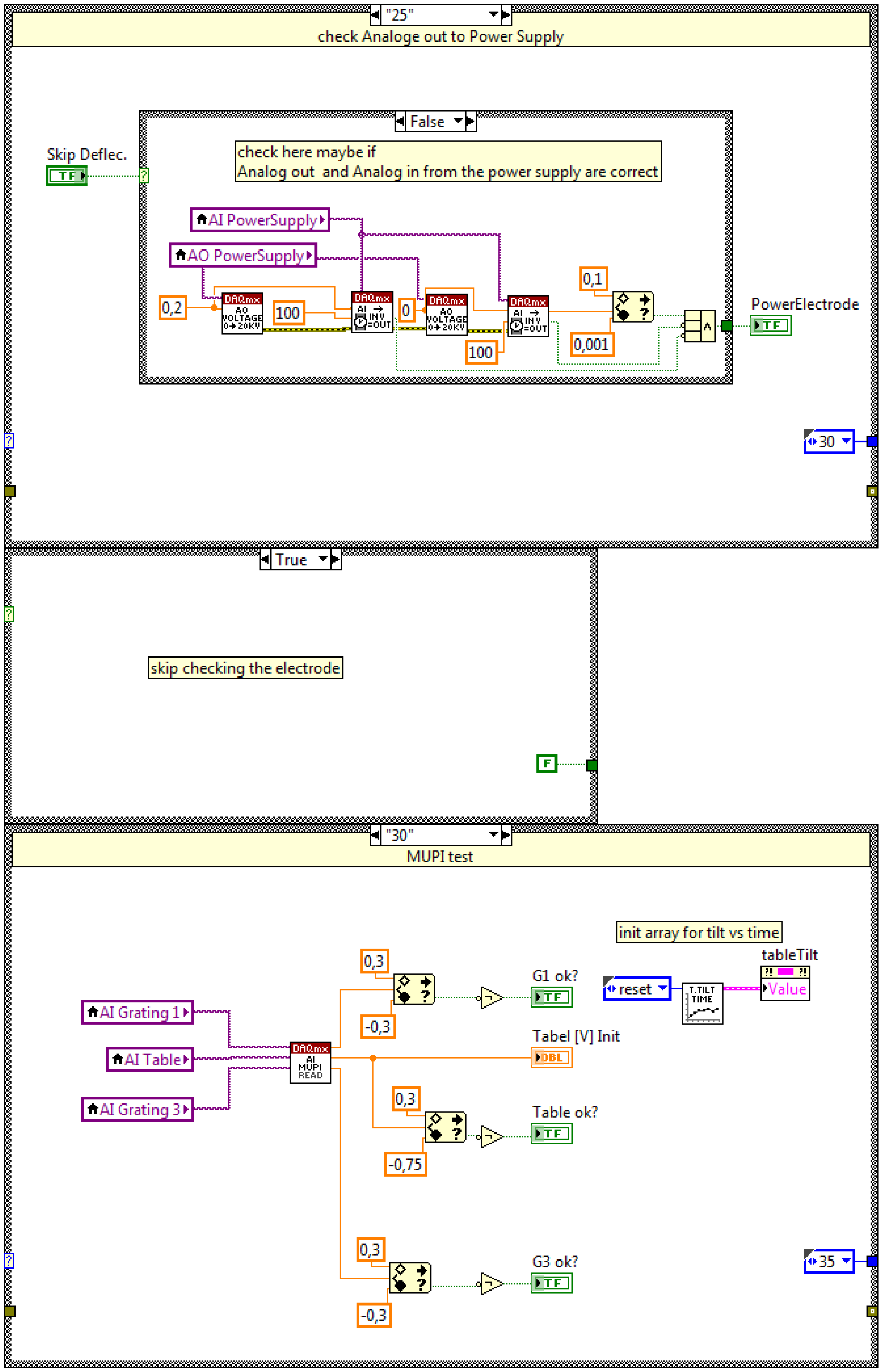

"25"
check Analoge out to Power Supply
False
Skip Deflec.
check here maybe if
Analog out and Analog in from the power supply are correct
AI PowerSupply
AO PowerSupply
0,2
100
0
100
0,1
0,001
PowerElectrode
30
True
skip checking the electrode
"30"
MUPI test
init array for tilt vs time
tableTilt
0,3
-0,3
G1 ok?
reset
Value
AI Grating 1
AI Table
AI Grating 3
Tabel [V] Init
0,3
-0,75
Table ok?
0,3
-0,3
G3 ok?
35

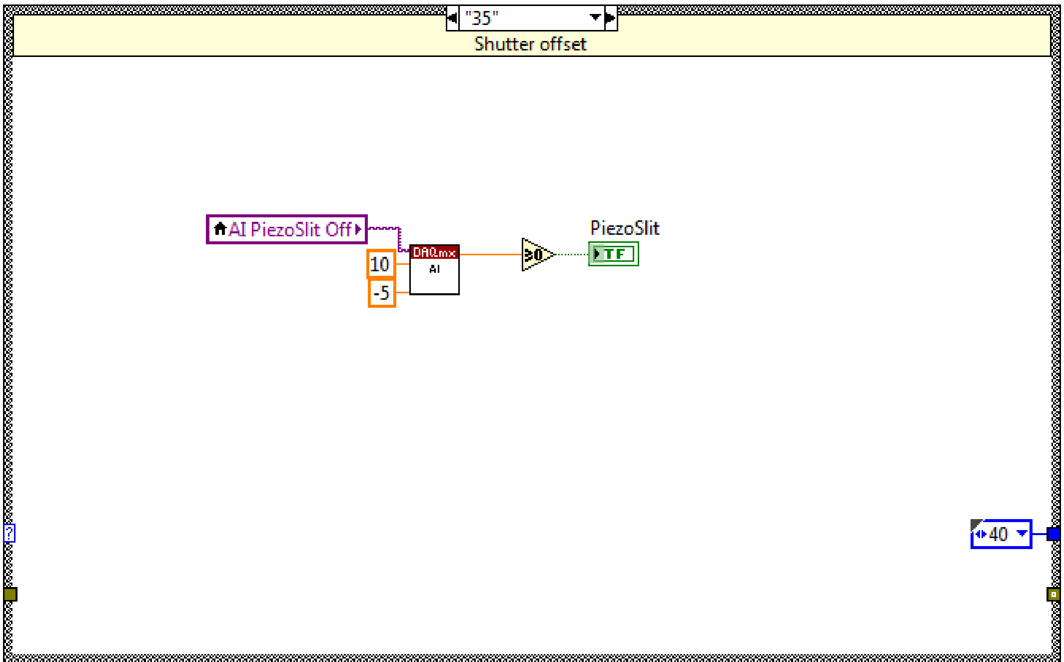
"35"
Shutter offset
AI PiezoSlit Off
10
-5
DAQmx
AI
PiezoSlit
TF
40

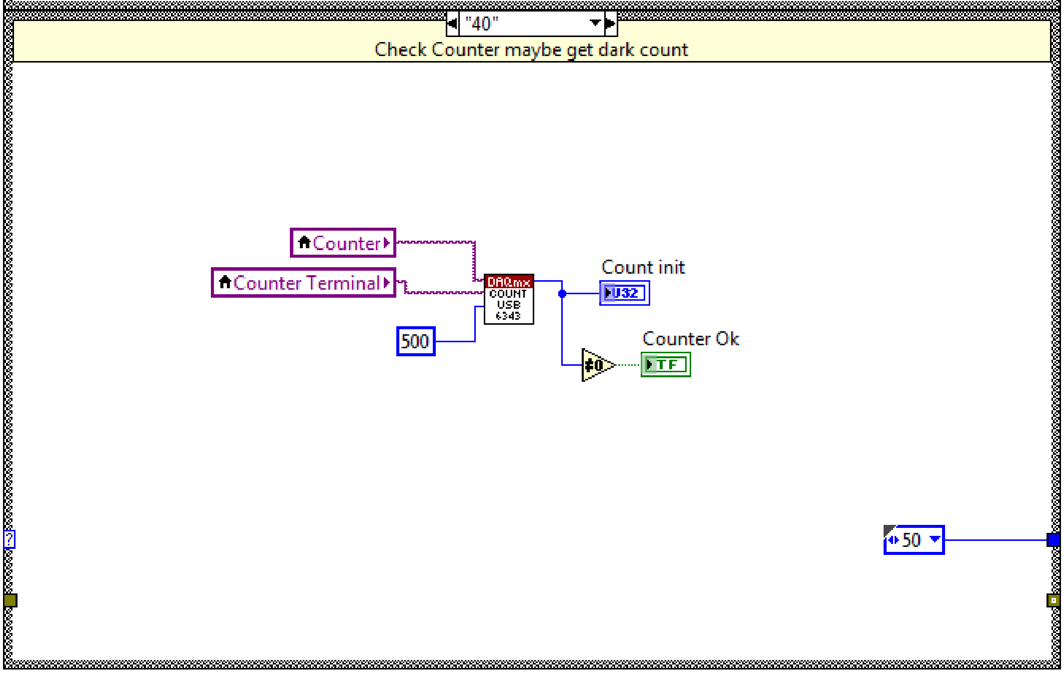
"40"
Check Counter maybe get dark count
Counter
Counter Terminal
500
DAQmx
COUNT
USB
6343
Count init
U32
Counter Ok
TF
50

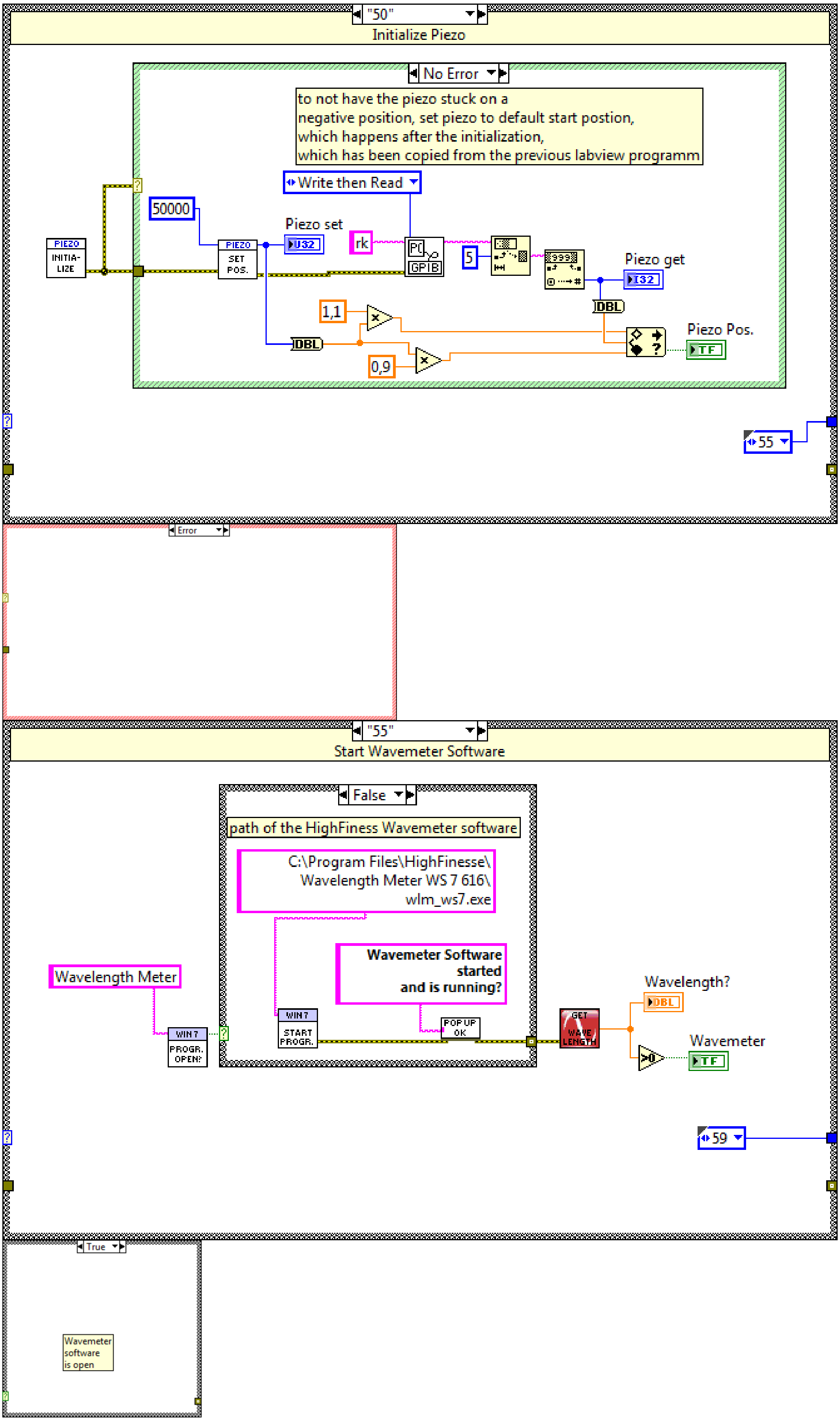

"50"
Initialize Piezo
No Error
to not have the piezo stuck on a
negative position, set piezo to default start postion,
which happens after the initialization,
which has been copied from the previous labview programm
Write then Read
50000
PIEZO INITIA-LIZE
PIEZO SET POS.
Piezo set
U32
rk
GPIB
5
Piezo get
I32
DBL
1,1
DBL
0,9
Piezo Pos.
TF
55
Error
"55"
Start Wavemeter Software
False
path of the HighFiness Wavemeter software
C:\Program Files\HighFinesse\
Wavelength Meter WS 7 616\
wlm_ws7.exe
Wavemeter Software
started
and is running?
Wavelength Meter
WIN 7 PROGR. OPEN?
WIN 7 START PROGR.
POP UP OK
GET WAVE LENGTH
Wavelength?
DBL
Wavemeter
TF
59
True
Wavemeter
software
is open

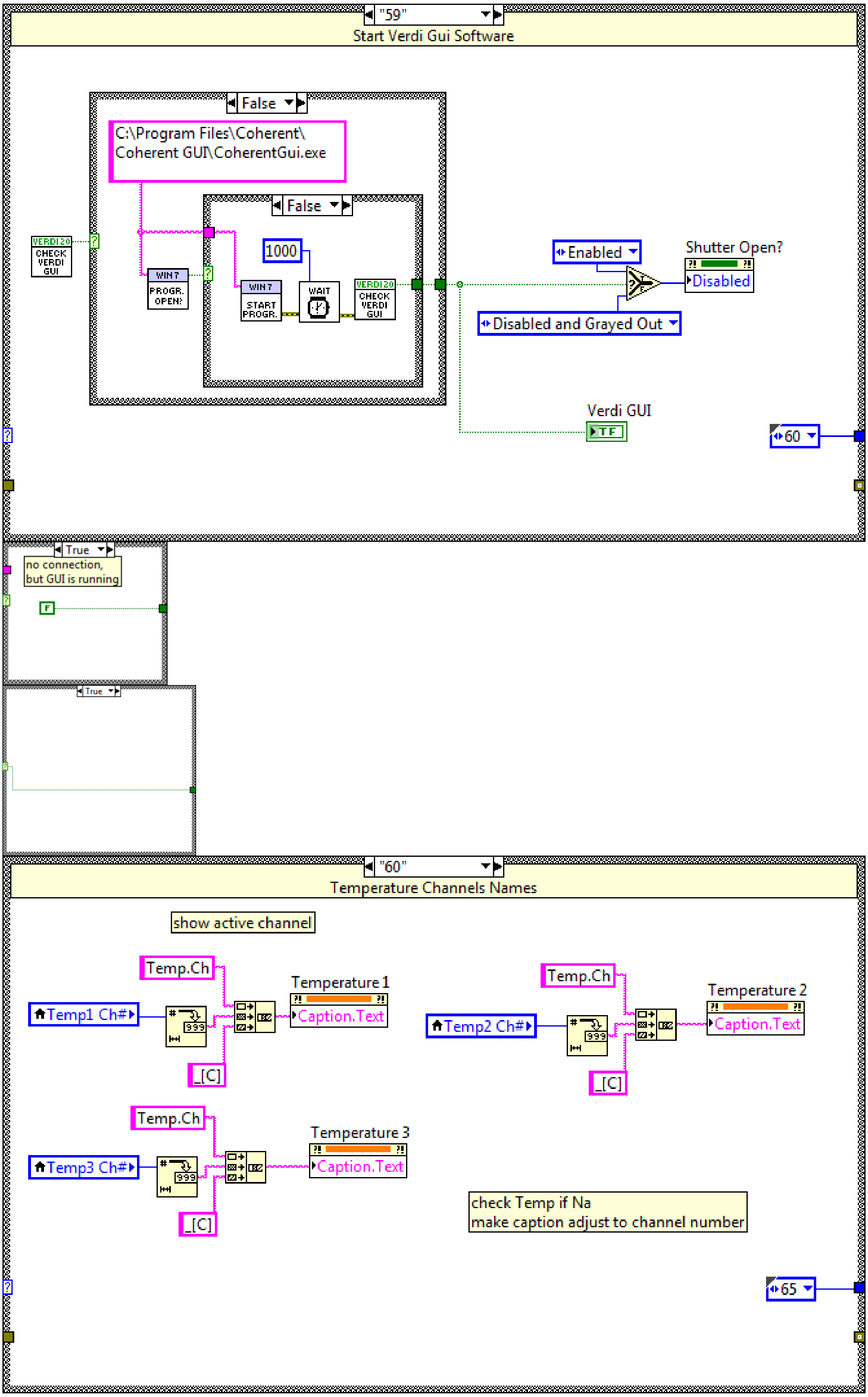
"59"
Start Verdi Gui Software
False
C:\Program Files\Coherent\
Coherent GUI\CoherentGui.exe
False
1000
VERDI 20 CHECK VERDI GUI
WIN7 PROGR. OPEN?
WIN7 START PROGR.
WAIT
VERDI 20 CHECK VERDI GUI
Enabled
Shutter Open?
Disabled
Disabled and Grayed Out
Verdi GUI
TF
60
True
no connection,
but GUI is running
F
True
"60"
Temperature Channels Names
show active channel
Temp.Ch
Temp1 Ch#
999
_[C]
Temperature 1
Caption.Text
Temp.Ch
Temp2 Ch#
999
_[C]
Temperature 2
Caption.Text
Temp.Ch
Temp3 Ch#
999
_[C]
Temperature 3
Caption.Text
check Temp if Na
make caption adjust to channel number
65

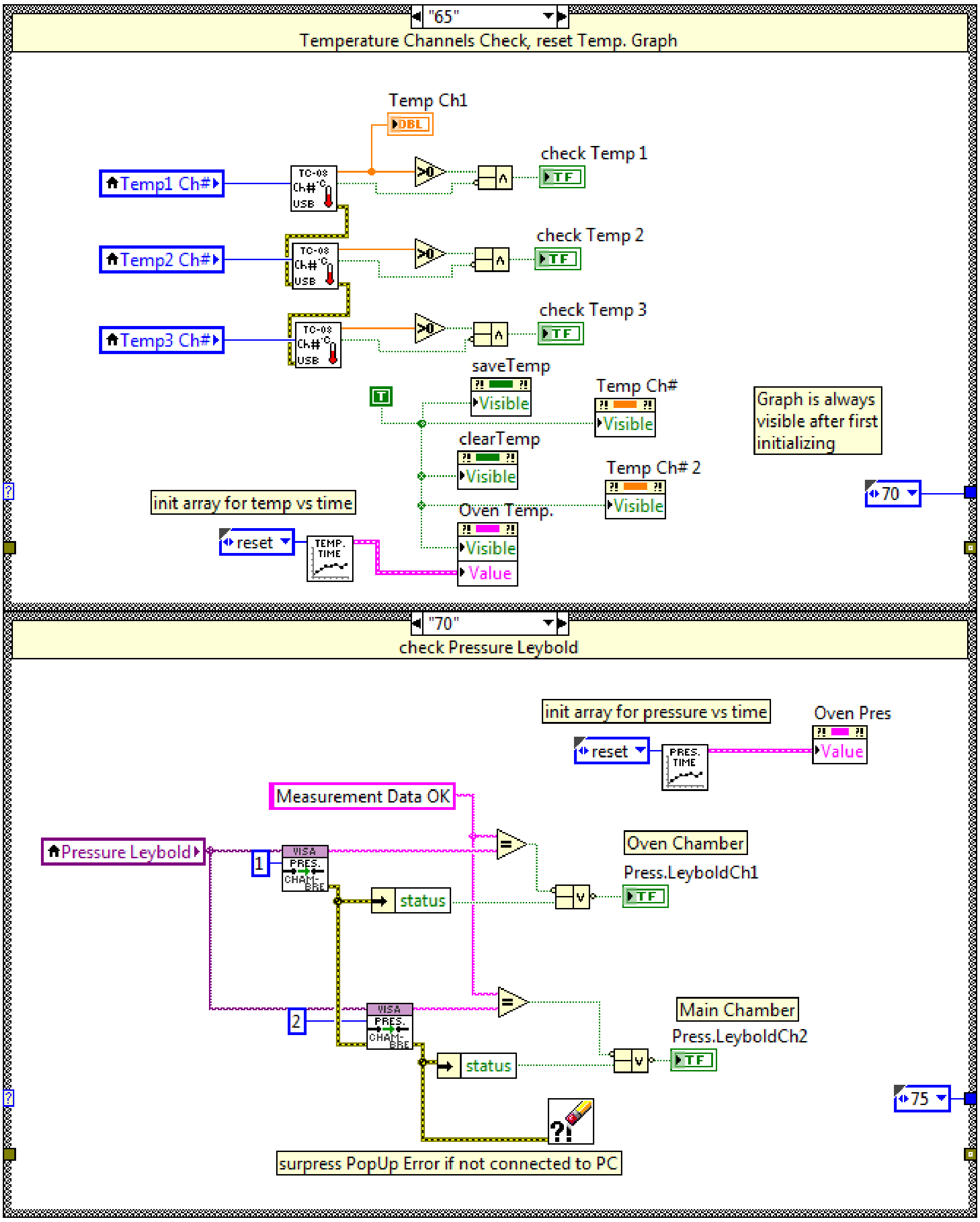
"65"
Temperature Channels Check, reset Temp. Graph
Temp Ch1
DBL
Temp1 Ch#
check Temp 1
Temp2 Ch#
check Temp 2
Temp3 Ch#
check Temp 3
saveTemp
Visible
Temp Ch#
Visible
clearTemp
Visible
Temp Ch# 2
Visible
Graph is always visible after first initializing
70
init array for temp vs time
reset
Oven Temp.
Visible
Value
"70"
check Pressure Leybold
init array for pressure vs time
Oven Pres
reset
Value
Measurement Data OK
Pressure Leybold
1
status
Oven Chamber
Press.LeyboldCh1
2
status
Main Chamber
Press.LeyboldCh2
75
surpress PopUp Error if not connected to PC

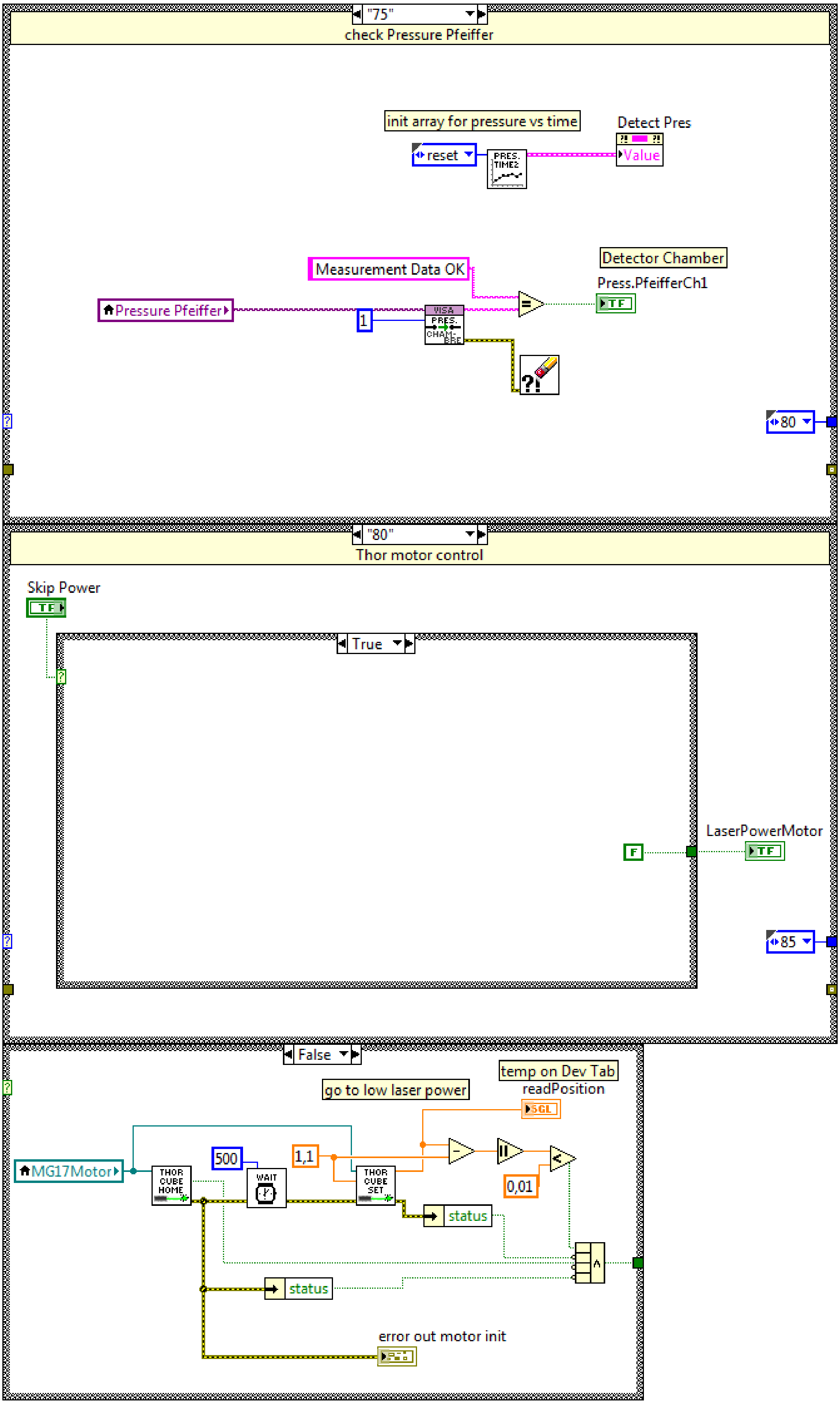
"75"
check Pressure Pfeiffer
init array for pressure vs time
Detect Pres
reset
PRES. TIME2
Value
Measurement Data OK
Detector Chamber
Press.PfeifferCh1
Pressure Pfeiffer
1
VISA
PRES.
80
"80"
Thor motor control
Skip Power
True
LaserPowerMotor
F
85
False
temp on Dev Tab
readPosition
go to low laser power
SGL
MG17Motor
THOR CUBE HOME
500
WAIT
1,1
THOR CUBE SET
0,01
status
status
error out motor init

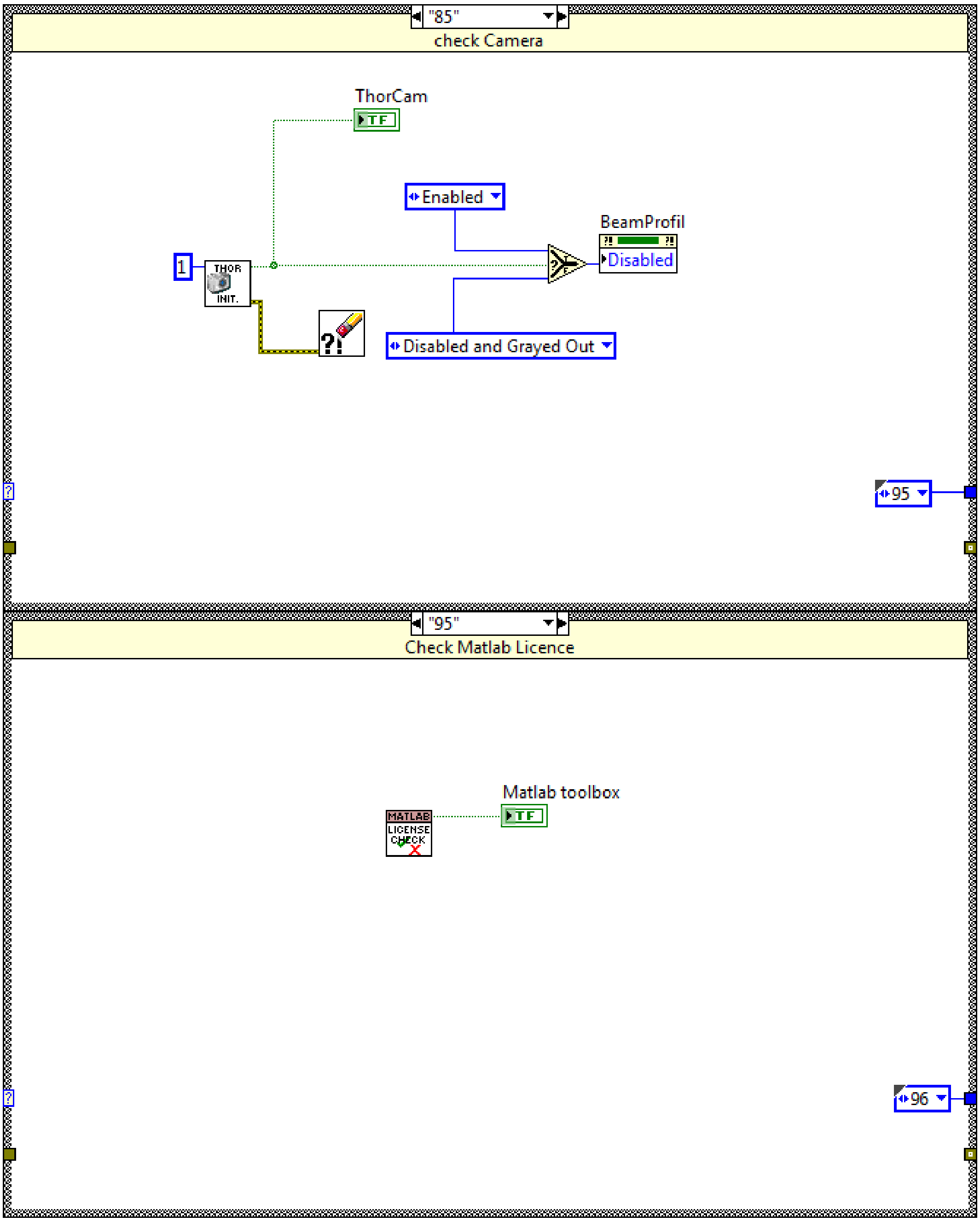
"85"
check Camera
ThorCam
TF
Enabled
BeamProfil
Disabled
1
THOR
INIT.
Disabled and Grayed Out
95
"95"
Check Matlab Licence
Matlab toolbox
MATLAB
LICENSE
CHECK
TF
96

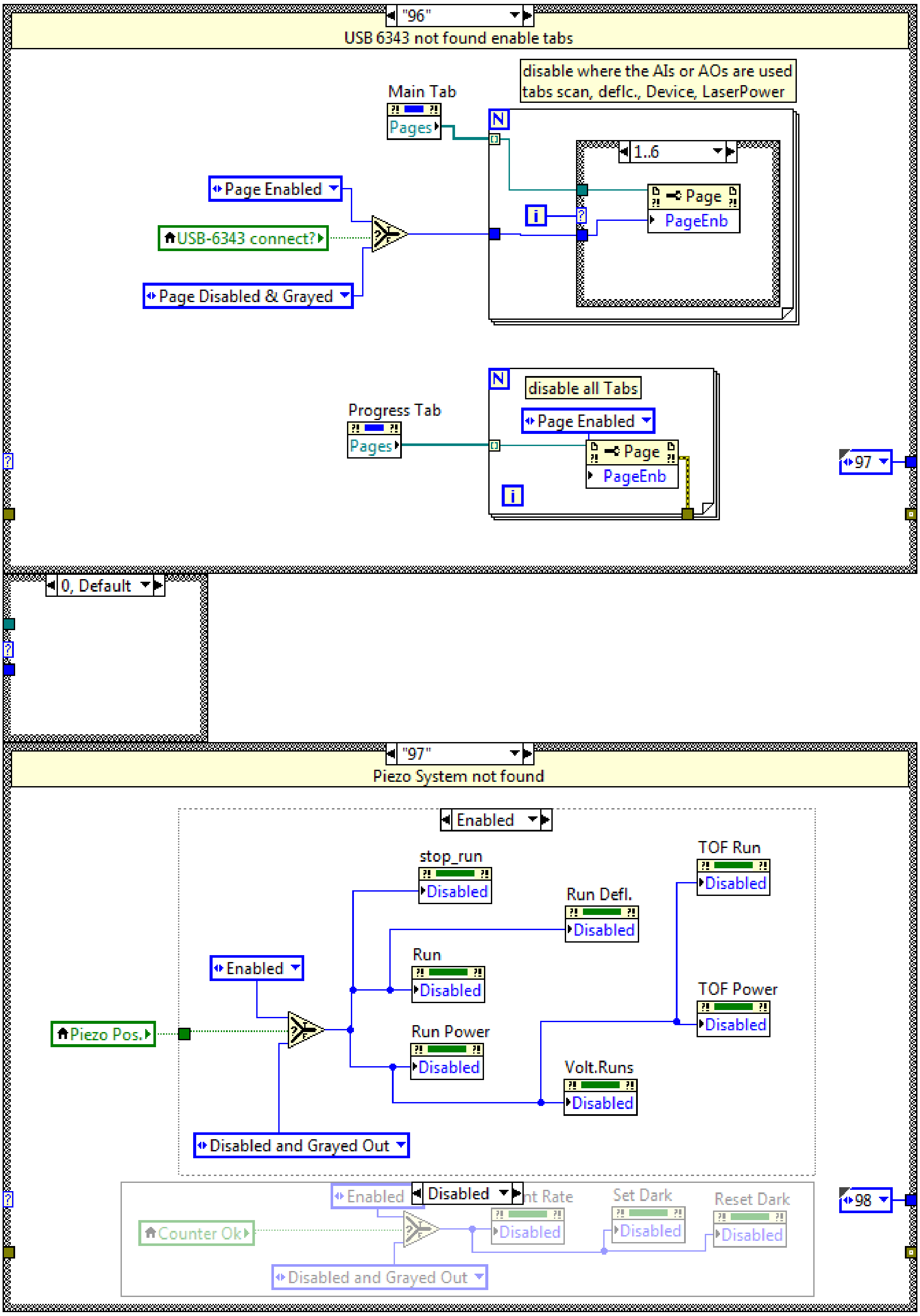
"96"
USB 6343 not found enable tabs
disable where the AIs or AOs are used
tabs scan, deflc., Device, LaserPower
Main Tab
Pages
1..6
Page
PageEnb
Page Enabled
USB-6343 connect?
Page Disabled & Grayed
disable all Tabs
Progress Tab
Pages
Page Enabled
Page
PageEnb
97
0, Default
"97"
Piezo System not found
Enabled
stop_run
Disabled
TOF Run
Disabled
Run Defl.
Disabled
Enabled
Run
Disabled
TOF Power
Disabled
Piezo Pos.
Run Power
Disabled
Volt.Runs
Disabled
Disabled and Grayed Out
Enabled
Disabled
nt Rate
Set Dark
Reset Dark
Disabled
Counter Ok
Disabled and Grayed Out
98

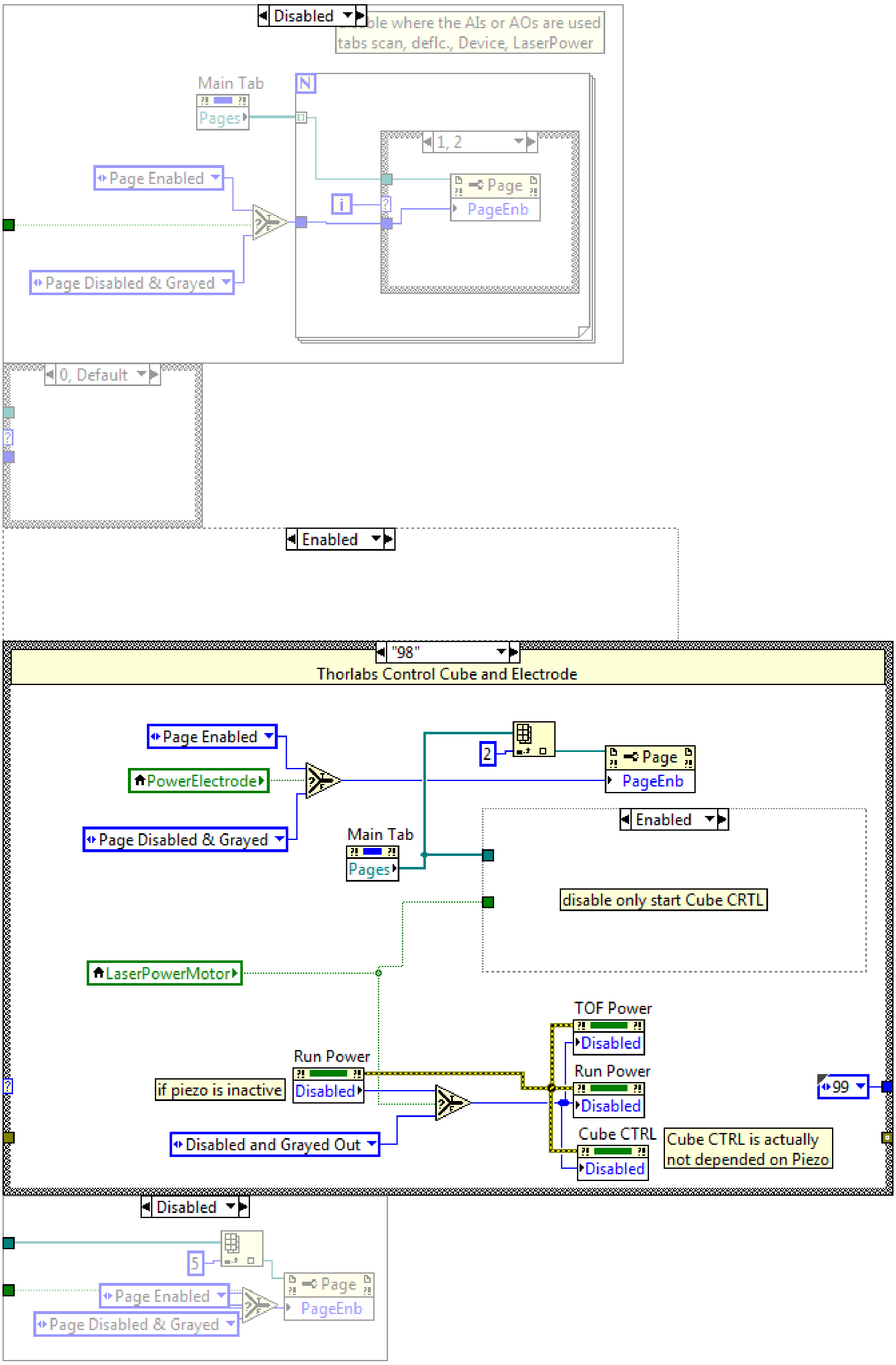
Disabled
tabs scan, deflc., Device, LaserPower
Main Tab
Pages
N
1, 2
Page
PageEnb
Page Enabled
Page Disabled & Grayed
0, Default
Enabled
"98"
Thorlabs Control Cube and Electrode
Page Enabled
PowerElectrode
Page Disabled & Grayed
2
Page
PageEnb
Main Tab
Pages
Enabled
disable only start Cube CRTL
LaserPowerMotor
TOF Power
Disabled
Run Power
if piezo is inactive
Disabled
Run Power
Disabled
Disabled and Grayed Out
Cube CTRL
Disabled
Cube CTRL is actually
not depended on Piezo
99
Disabled
5
Page Enabled
Page Disabled & Grayed
Page
PageEnb

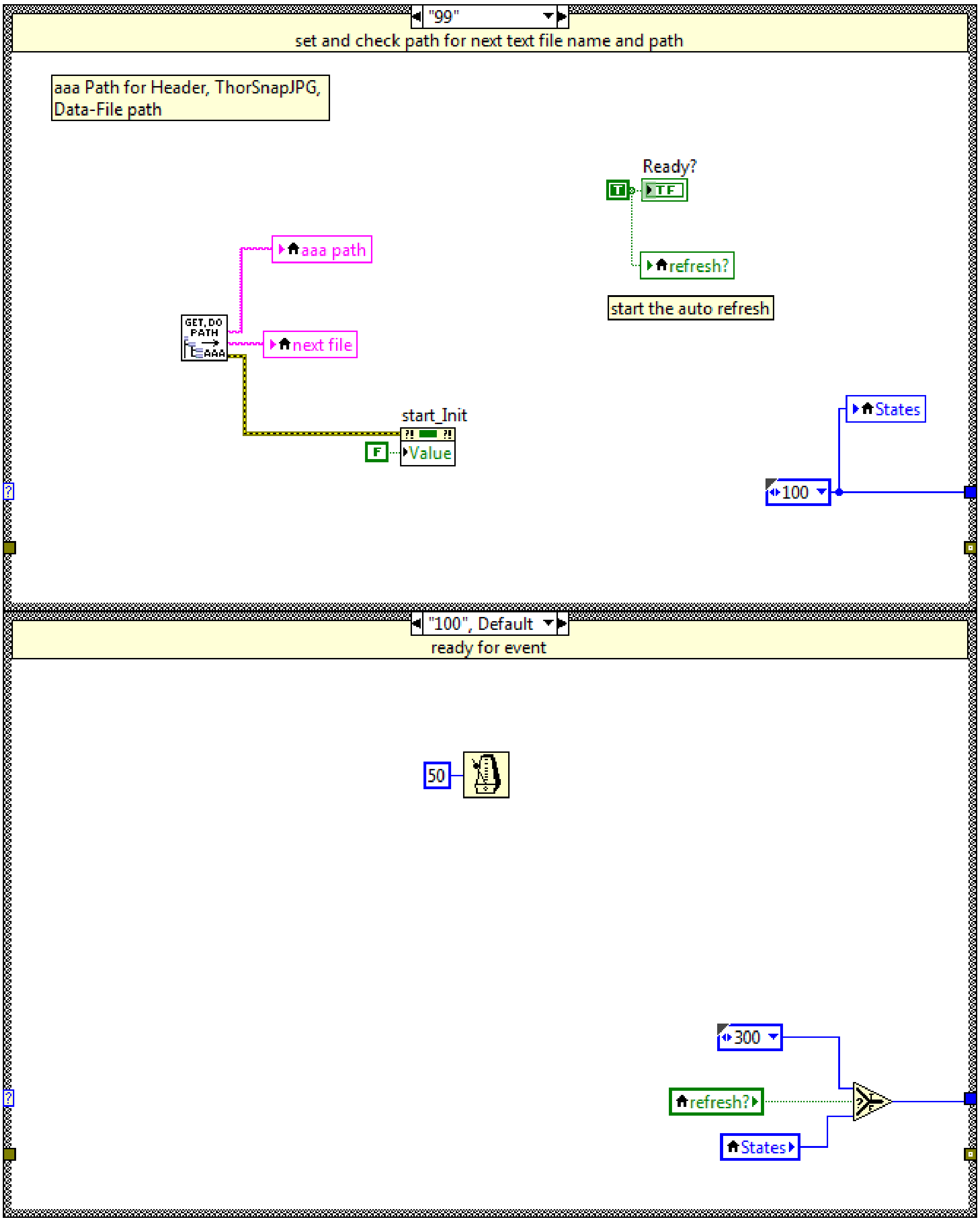
"99"
set and check path for next text file name and path
aaa Path for Header, ThorSnapJPG, Data-File path
Ready?
refresh?
start the auto refresh
aaa path
GET, DO PATH
next file
start_Init
Value
States
100
"100", Default
ready for event
50
300
refresh?
States

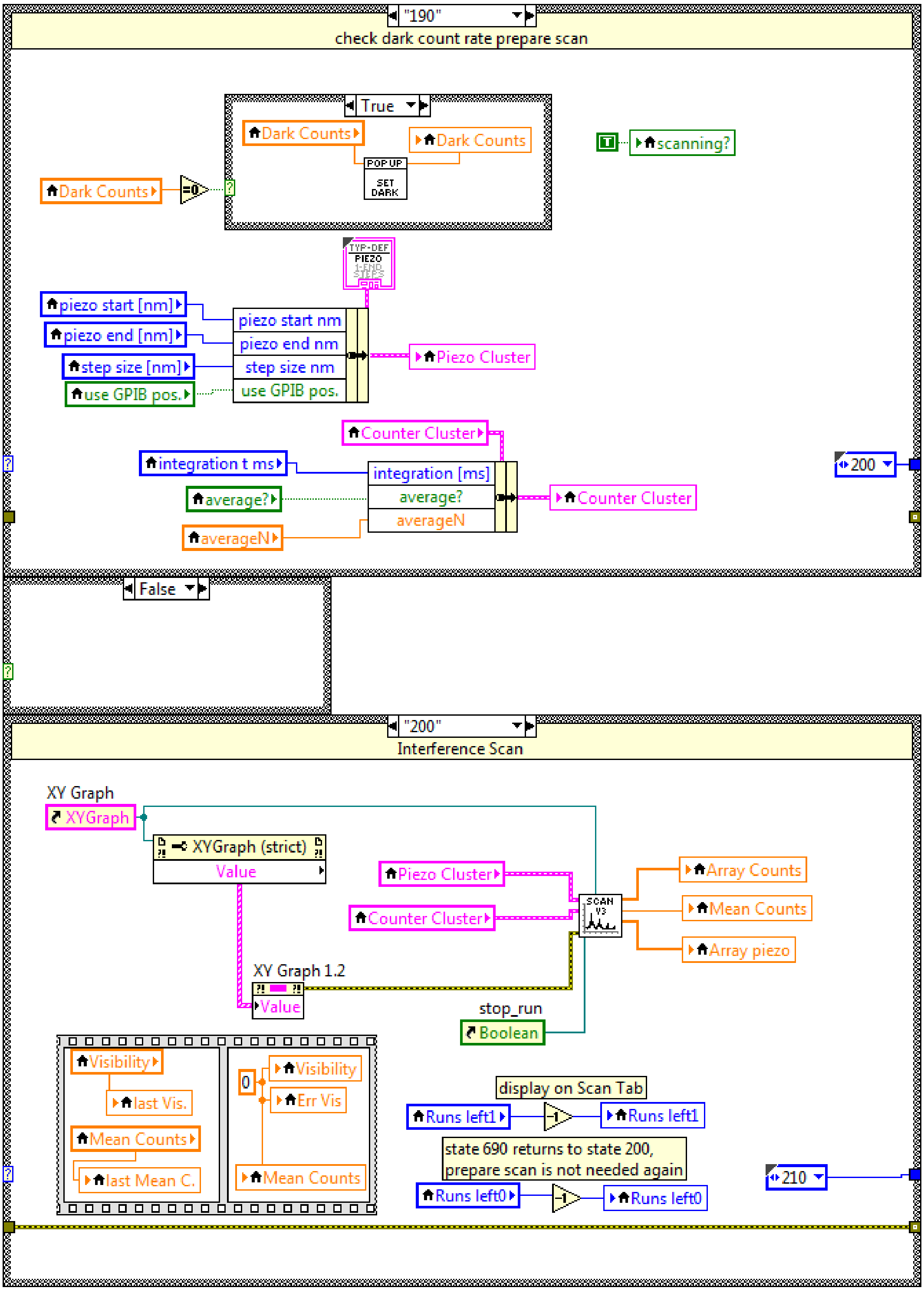
"190"
check dark count rate prepare scan
True
Dark Counts
Dark Counts
POP UP
SET DARK
Dark Counts
scanning?
TYP-DEF PIEZO
piezo start [nm]
piezo end [nm]
step size [nm]
use GPIB pos.
piezo start nm
piezo end nm
step size nm
use GPIB pos.
Piezo Cluster
Counter Cluster
integration t ms
average?
averageN
integration [ms]
average?
averageN
Counter Cluster
200
False
"200"
Interference Scan
XY Graph
XYGraph
XYGraph (strict)
Value
Piezo Cluster
Counter Cluster
SCAN V3
Array Counts
Mean Counts
Array piezo
XY Graph 1.2
Value
stop_run
Boolean
Visibility
last Vis.
Mean Counts
last Mean C.
0
Visibility
Err Vis
Mean Counts
display on Scan Tab
Runs left1
Runs left1
state 690 returns to state 200,
prepare scan is not needed again
Runs left0
Runs left0
210

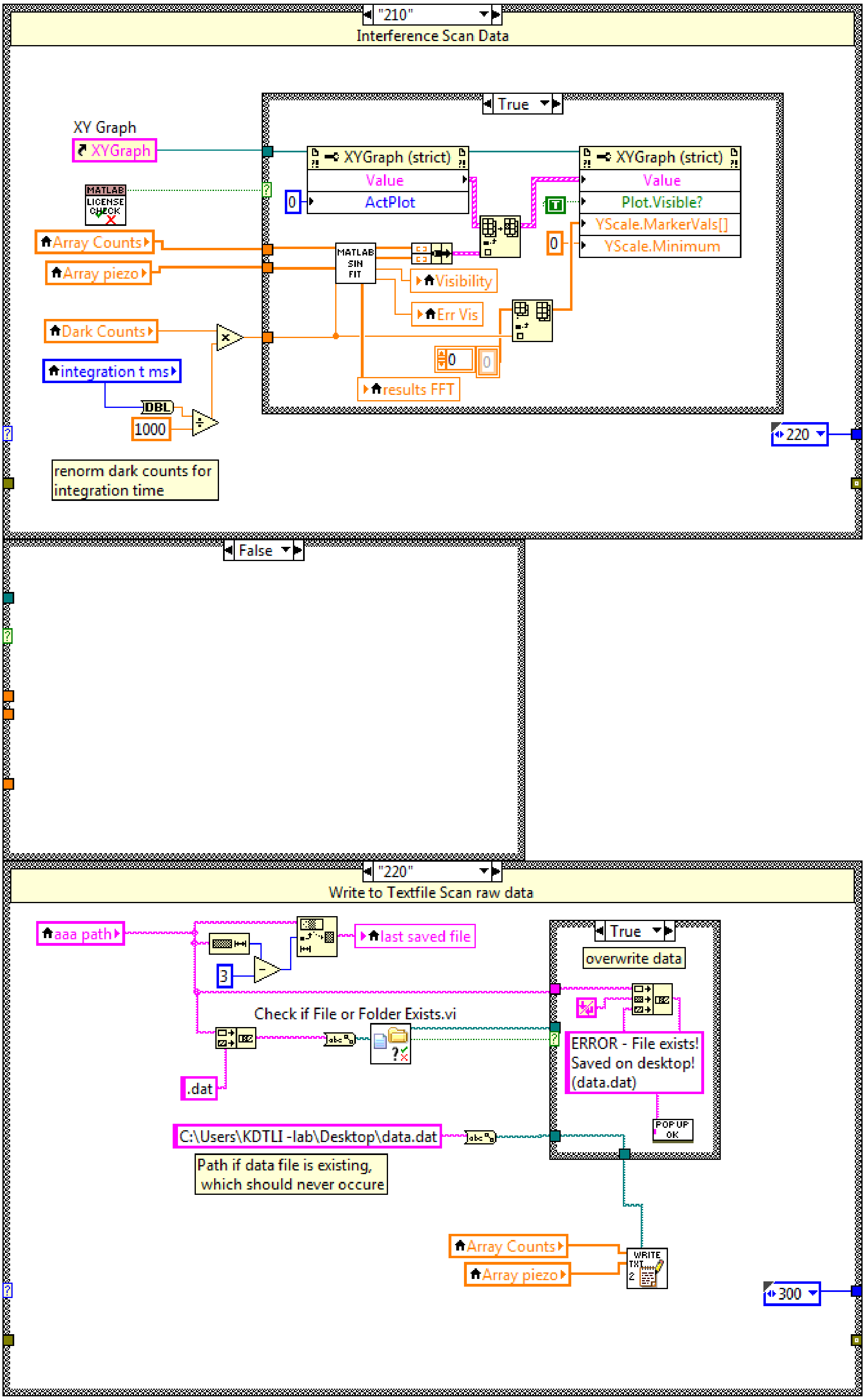

"210"
Interference Scan Data
True
XY Graph
XYGraph
XYGraph (strict)
Value
ActPlot
XYGraph (strict)
Value
Plot.Visible?
YScale.MarkerVals[]
YScale.Minimum
MATLAB LICENSE CHECK
Array Counts
Array piezo
MATLAB SIN FIT
Visibility
Err Vis
Dark Counts
integration t ms
DBL
1000
results FFT
220
renorm dark counts for integration time
False
"220"
Write to Textfile Scan raw data
aaa path
last saved file
3
Check if File or Folder Exists.vi
.dat
True
overwrite data
ERROR - File exists! Saved on desktop! (data.dat)
POP UP OK
C:\Users\KDTLI -lab\Desktop\data.dat
Path if data file is existing, which should never occure
Array Counts
Array piezo
WRITE TXT
300

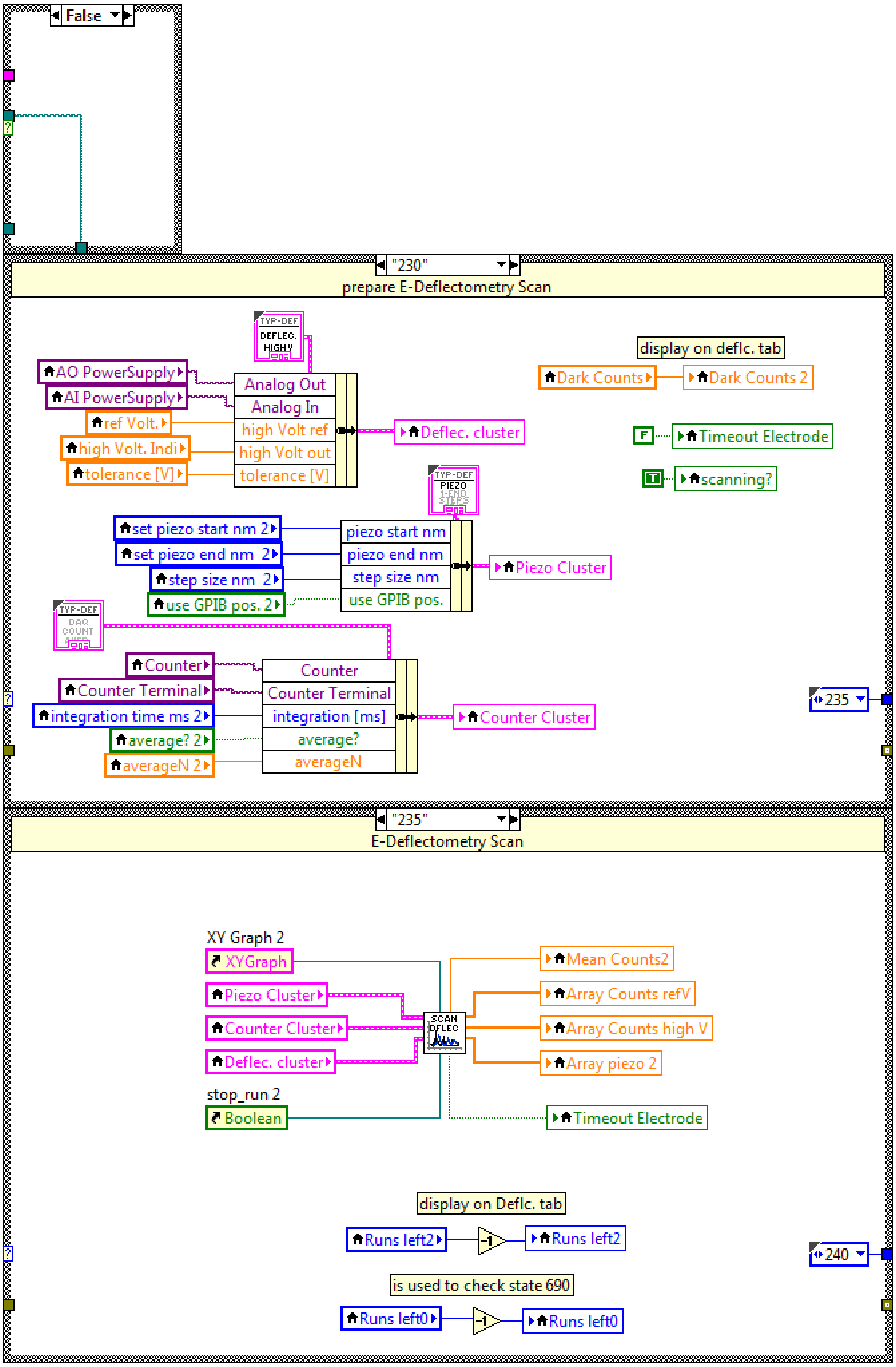
False
"230"
prepare E-Deflectometry Scan
TYP-DEF DEFLEC. HIGHV
AO PowerSupply
AI PowerSupply
ref Volt.
high Volt. Indi
tolerance [V]
Analog Out
Analog In
high Volt ref
high Volt out
tolerance [V]
Deflec. cluster
display on deflc. tab
Dark Counts
Dark Counts 2
Timeout Electrode
scanning?
set piezo start nm 2
set piezo end nm 2
step size nm 2
use GPIB pos. 2
piezo start nm
piezo end nm
step size nm
use GPIB pos.
Piezo Cluster
Counter
Counter Terminal
integration time ms 2
average? 2
averageN 2
Counter
Counter Terminal
integration [ms]
average?
averageN
Counter Cluster
235
"235"
E-Deflectometry Scan
XY Graph 2
XYGraph
Piezo Cluster
Counter Cluster
Deflec. cluster
stop_run 2
Boolean
SCAN DFLEC
Mean Counts2
Array Counts refV
Array Counts high V
Array piezo 2
Timeout Electrode
display on Deflc. tab
Runs left2
Runs left2
is used to check state 690
Runs left0
Runs left0
240

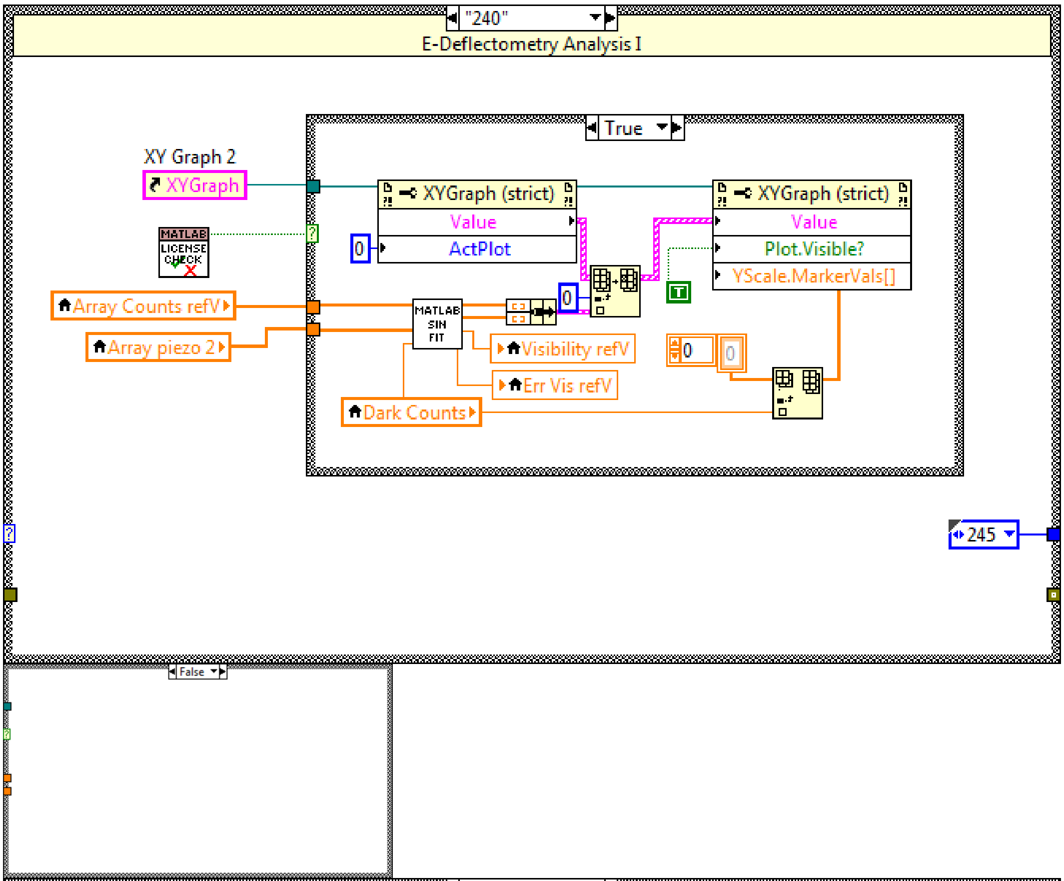
"240"
E-Deflectometry Analysis I
True
XY Graph 2
XYGraph
MATLAB LICENSE CHECK
XYGraph (strict)
Value
ActPlot
0
Plot.Visible?
YScale.MarkerVals[]
Array Counts refV
Array piezo 2
MATLAB SIN FIT
Visibility refV
Err Vis refV
Dark Counts
245
False

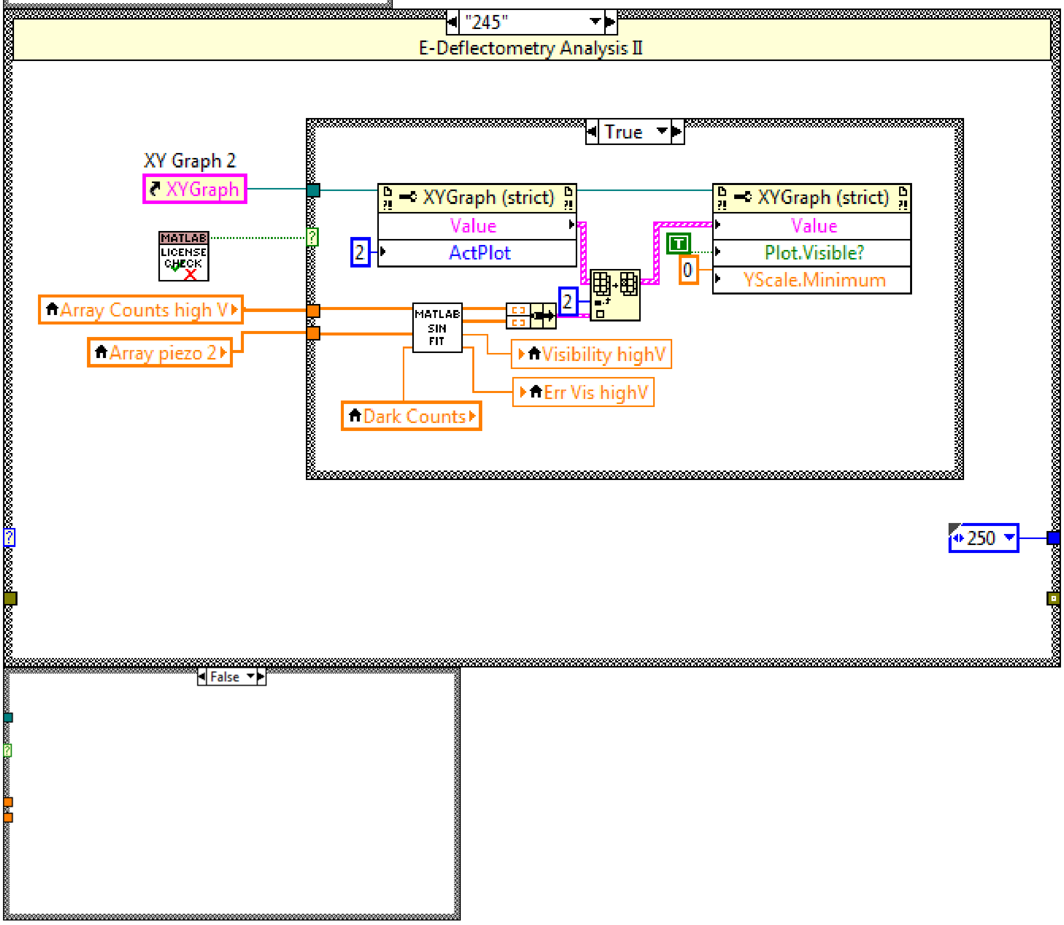
"245"
E-Deflectometry Analysis II
True
XY Graph 2
XYGraph
MATLAB LICENSE CHECK
XYGraph (strict)
Value
ActPlot
2
Plot.Visible?
YScale.Minimum
Array Counts high V
Array piezo 2
MATLAB SIN FIT
Visibility highV
Err Vis highV
Dark Counts
250
False

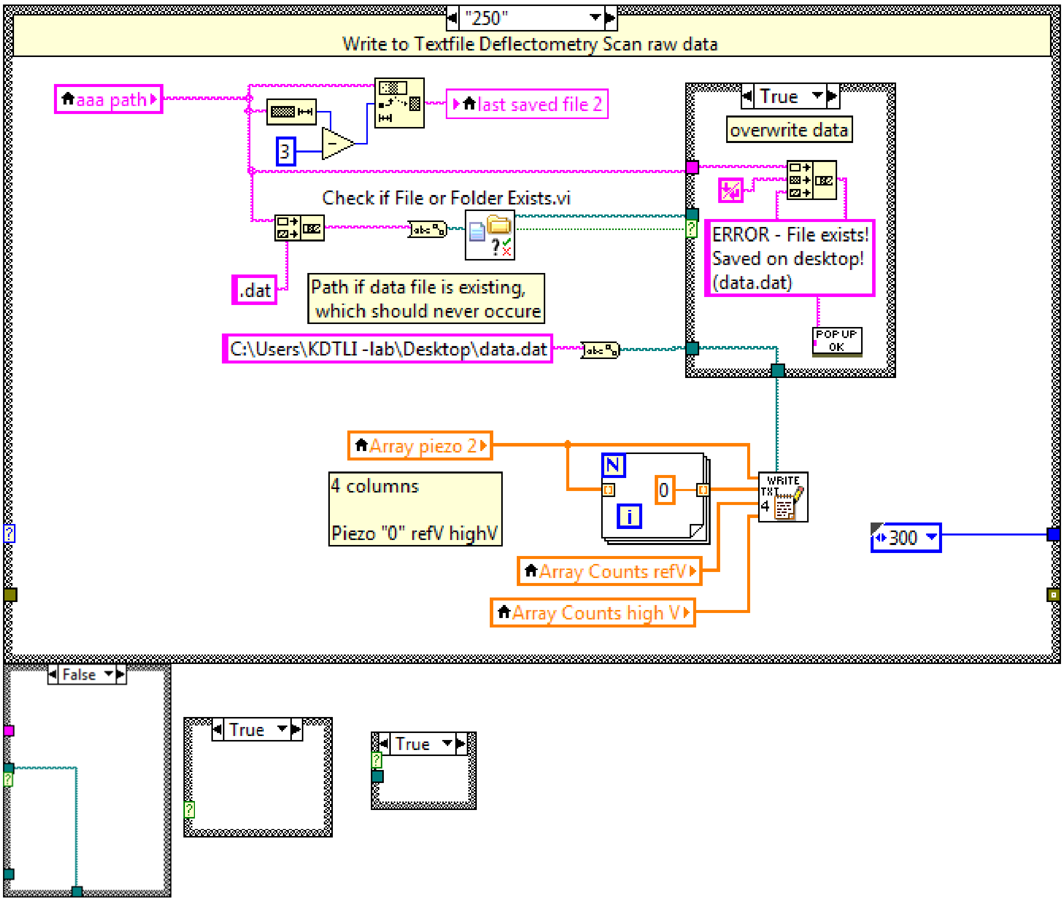
"250"
Write to Textfile Deflectometry Scan raw data
aaa path
last saved file 2
3
True
overwrite data
Check if File or Folder Exists.vi
ERROR - File exists!
Saved on desktop!
(data.dat)
.dat
Path if data file is existing,
which should never occure
C:\Users\KDTLI -lab\Desktop\data.dat
POP UP
OK
Array piezo 2
4 columns
Piezo "0" refV highV
N
0
i
WRITE
TXT
4
300
Array Counts refV
Array Counts high V
False
True
True

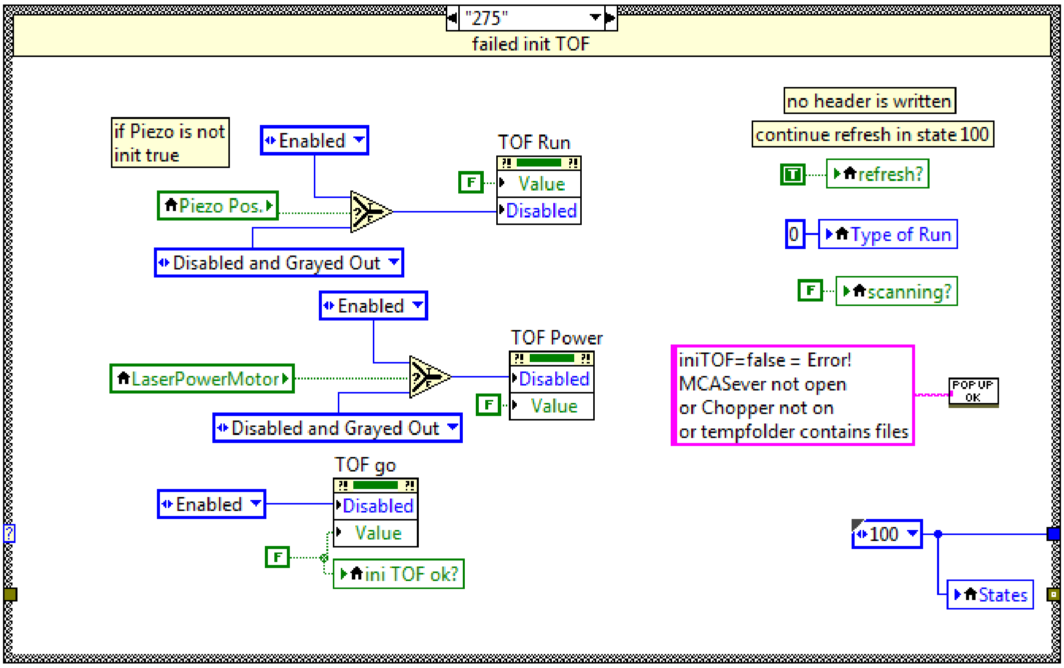
"275"
failed init TOF
no header is written
continue refresh in state 100
if Piezo is not
init true
Enabled
TOF Run
F
Value
Disabled
Piezo Pos.
Disabled and Grayed Out
T
refresh?
0
Type of Run
F
scanning?
Enabled
TOF Power
LaserPowerMotor
Disabled
F
Value
Disabled and Grayed Out
iniTOF=false = Error!
MCASever not open
or Chopper not on
or tempfolder contains files
POP UP
OK
TOF go
Enabled
Disabled
Value
F
ini TOF ok?
100
States

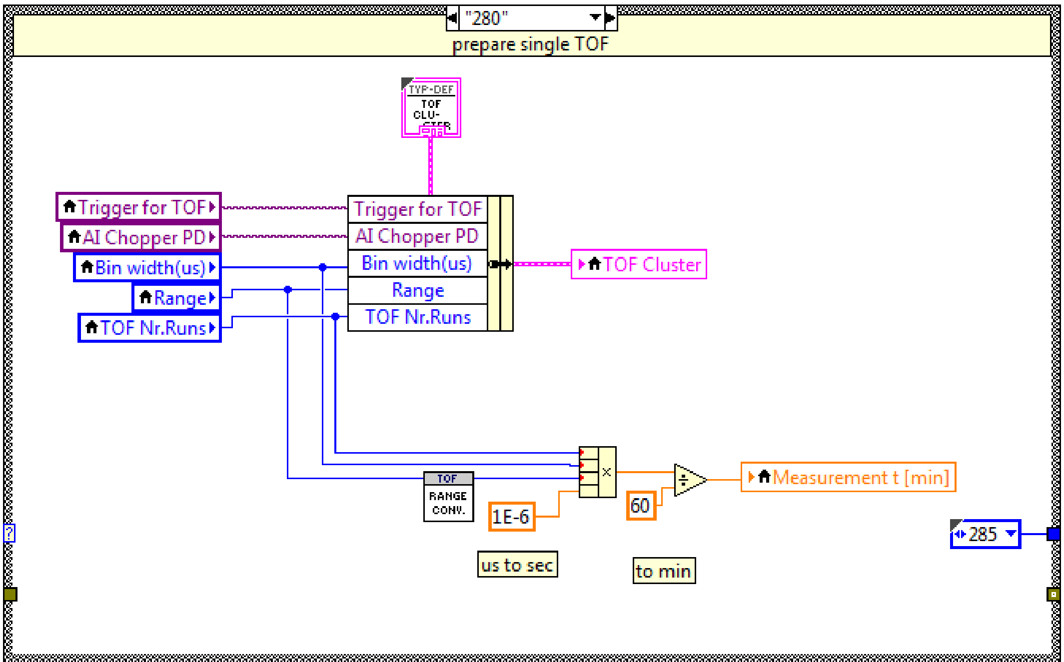

"280"
prepare single TOF
TYP-DEF TOF CLUSTER
Trigger for TOF
AI Chopper PD
Bin width(us)
Range
TOF Nr.Runs
Trigger for TOF
AI Chopper PD
Bin width(us)
Range
TOF Nr.Runs
TOF Cluster
TOF RANGE CONV.
1E-6
60
Measurement t [min]
285
us to sec
to min

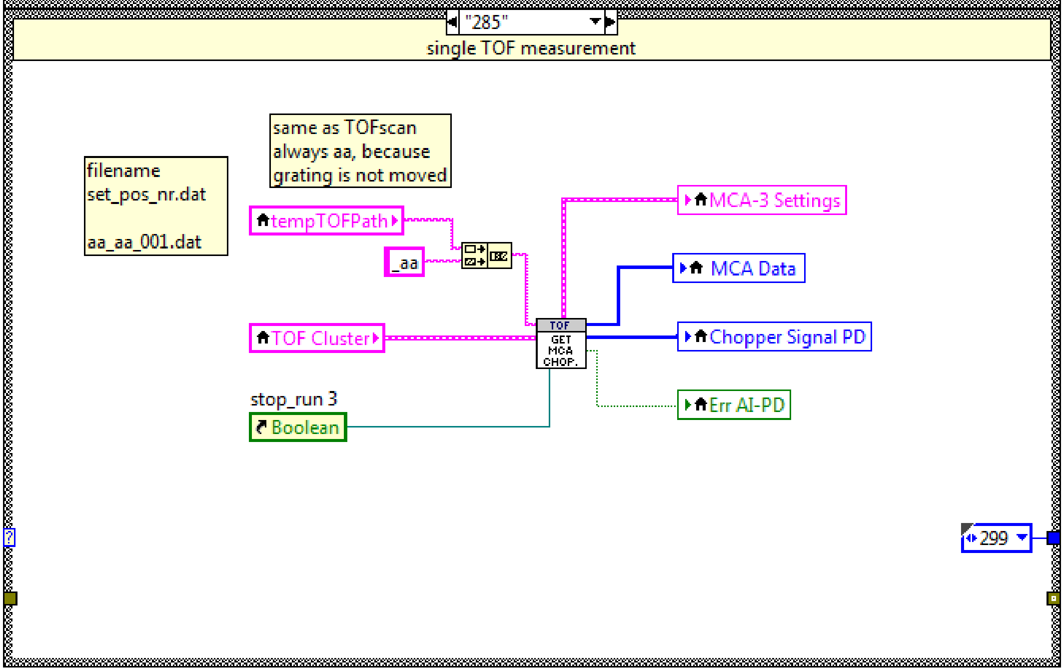

"285"
single TOF measurement
filename
set_pos_nr.dat
aa_aa_001.dat
same as TOFscan
always aa, because
grating is not moved
tempTOFPath
_aa
MCA-3 Settings
MCA Data
TOF Cluster
TOF GET MCA CHOP.
Chopper Signal PD
Err AI-PD
stop_run 3
Boolean
299

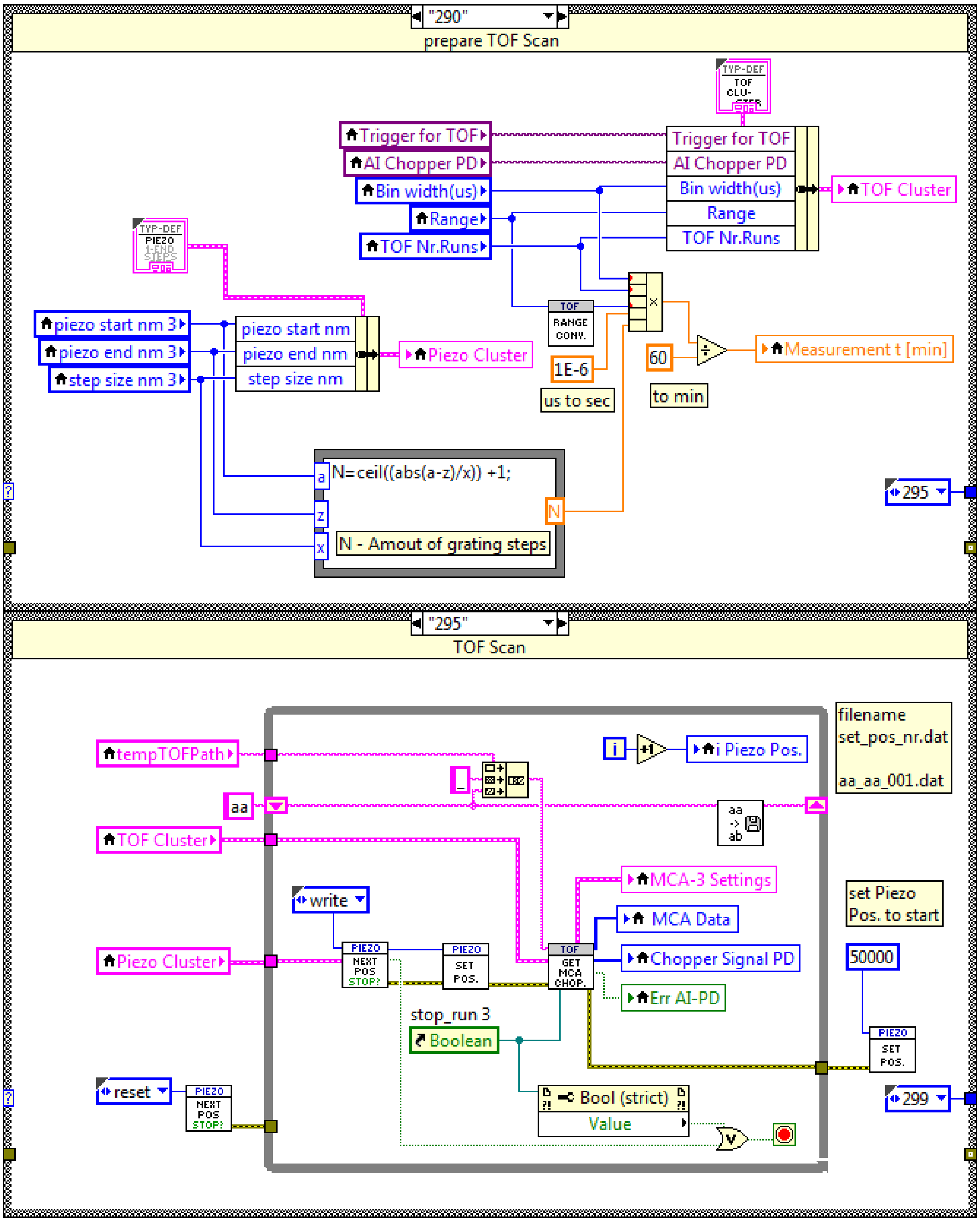

"290"
prepare TOF Scan
TYP-DEF TOF CLUSTER
Trigger for TOF
AI Chopper PD
Bin width(us)
Range
TOF Nr.Runs
TOF Cluster
TYP-DEF PIEZO 1-END STEPS
piezo start nm 3
piezo end nm 3
step size nm 3
piezo start nm
piezo end nm
step size nm
Piezo Cluster
TOF RANGE CONV.
1E-6
us to sec
60
to min
Measurement t [min]
N=ceil((abs(a-z)/x)) +1;
N - Amout of grating steps
295
"295"
TOF Scan
tempTOFPath
aa
TOF Cluster
Piezo Cluster
reset
write
i Piezo Pos.
filename
set_pos_nr.dat
aa_aa_001.dat
MCA-3 Settings
MCA Data
Chopper Signal PD
Err AI-PD
stop_run 3
Boolean
Bool (strict)
Value
set Piezo
Pos. to start
50000
299

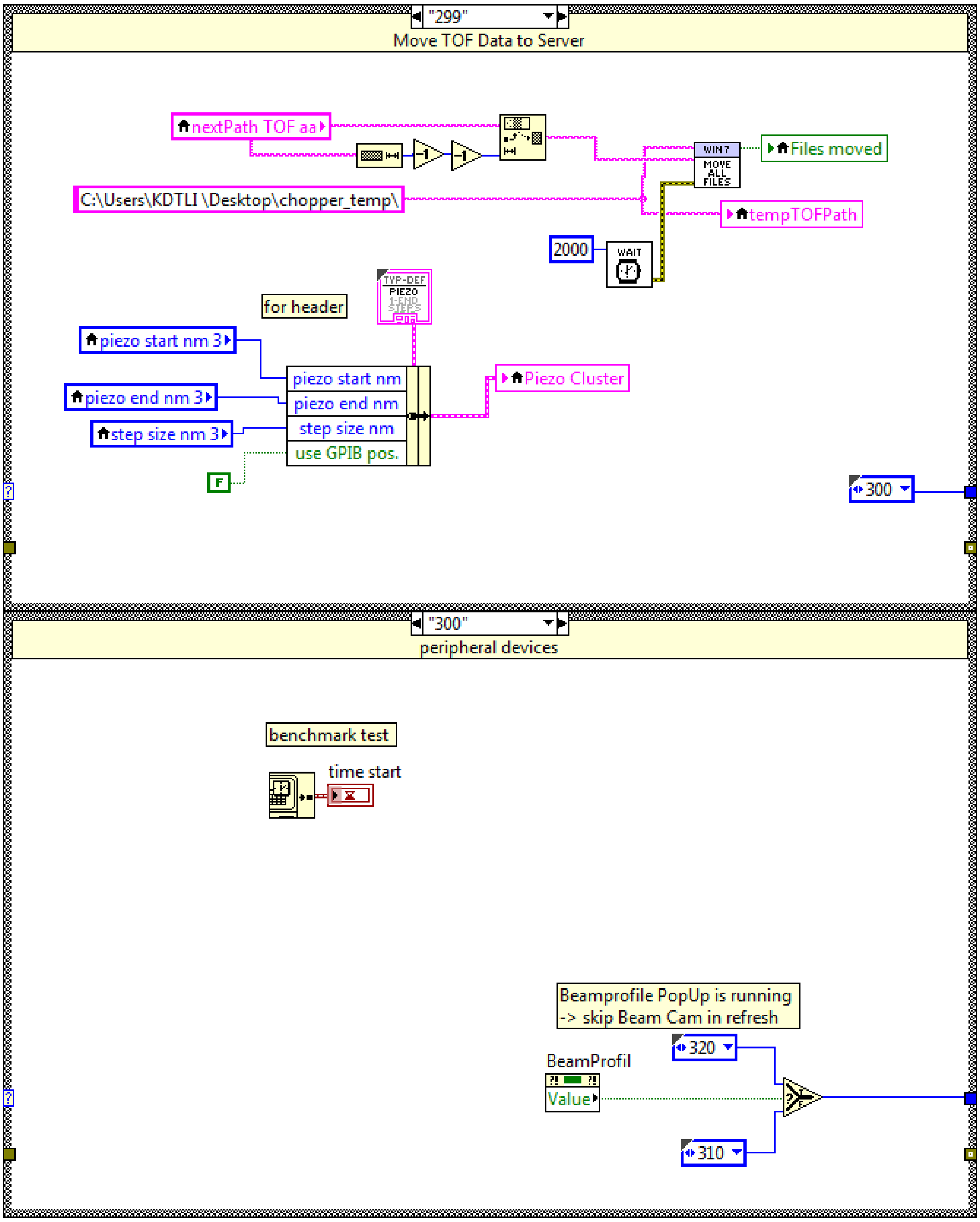

"299"
Move TOF Data to Server
nextPath TOF aa
C:\Users\KDTLI \Desktop\chopper_temp\
Files moved
tempTOFPath
2000
WAIT
for header
piezo start nm 3
piezo end nm 3
step size nm 3
piezo start nm
piezo end nm
step size nm
use GPIB pos.
Piezo Cluster
300
"300"
peripheral devices
benchmark test
time start
Beamprofile PopUp is running
-> skip Beam Cam in refresh
BeamProfil
Value
320
310

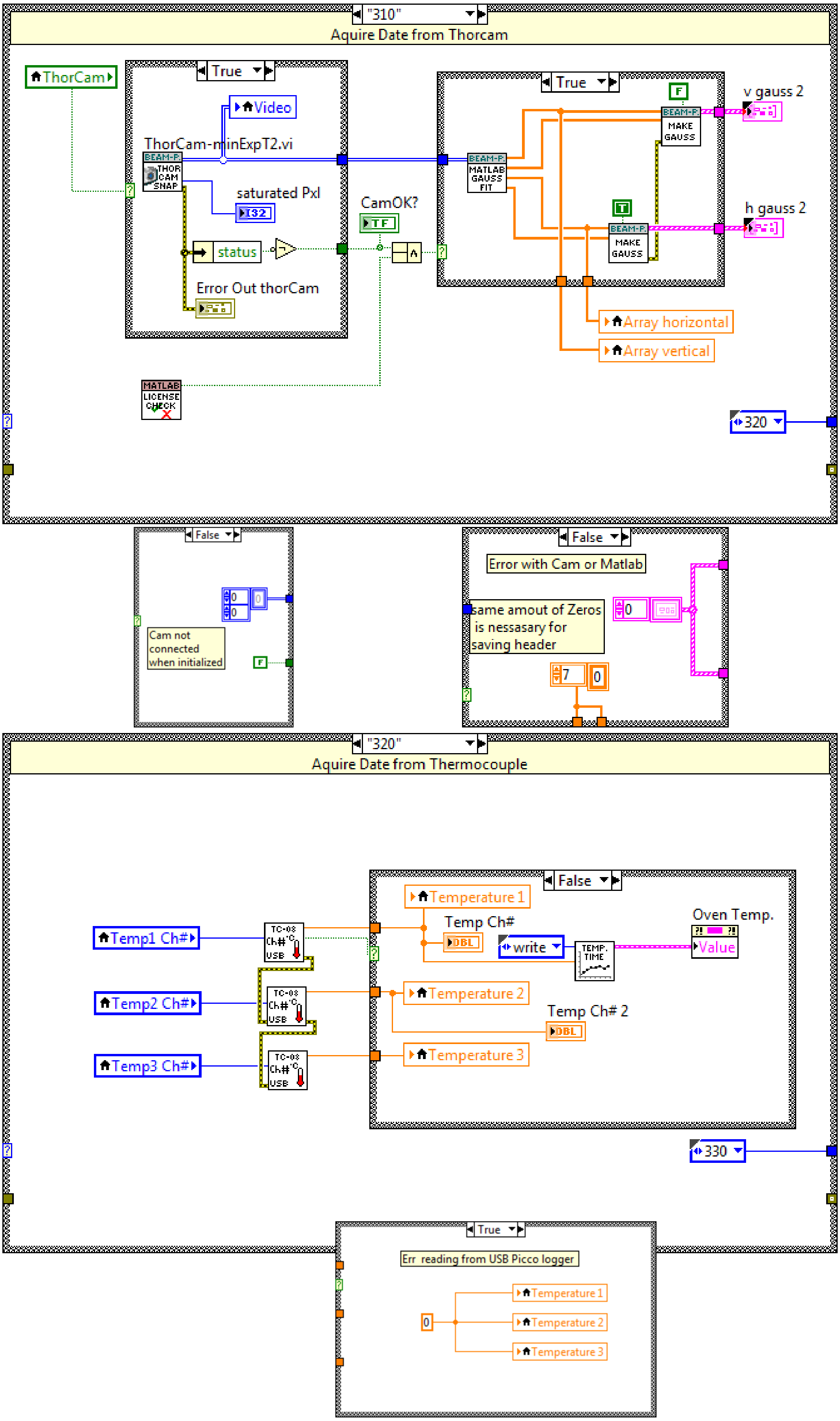
"310"
Aquire Date from Thorcam
ThorCam
True
Video
ThorCam-minExpT2.vi
saturated Pxl
status
Error Out thorCam
CamOK?
True
v gauss 2
h gauss 2
Array horizontal
Array vertical
320
False
Cam not connected when initialized
False
Error with Cam or Matlab
same amout of Zeros is nessasary for saving header
7
"320"
Aquire Date from Thermocouple
Temp1 Ch#
Temp2 Ch#
Temp3 Ch#
False
Temperature 1
Temp Ch#
write
Oven Temp.
Value
Temperature 2
Temp Ch# 2
Temperature 3
330
True
Err reading from USB Picco logger
Temperature 1
Temperature 2
Temperature 3

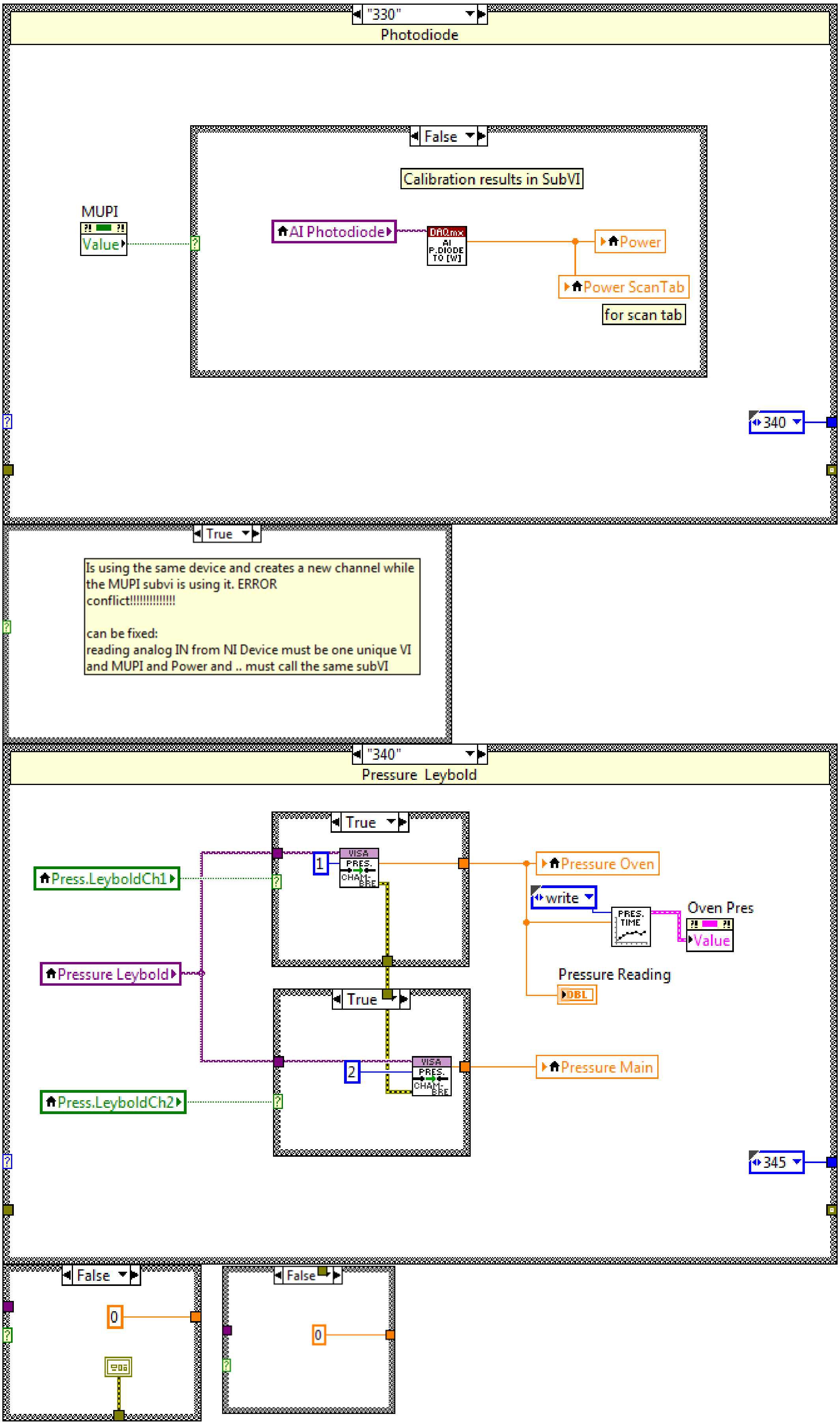

"330"
Photodiode
False
Calibration results in SubVI
MUPI
Value
AI Photodiode
DAQmx
AI P.DIODE TO [W]
Power
Power ScanTab
for scan tab
340
True
Is using the same device and creates a new channel while the MUPI subvi is using it. ERROR conflict!!!!!!!!!!!!!!
can be fixed:
reading analog IN from NI Device must be one unique VI and MUPI and Power and .. must call the same subVI
"340"
Pressure Leybold
True
Press.LeyboldCh1
Pressure Leybold
Press.LeyboldCh2
1
2
VISA PRES. CHAM-BRE
Pressure Oven
write
PRES. TIME
Oven Pres
Value
Pressure Reading
DBL
Pressure Main
345
False
0

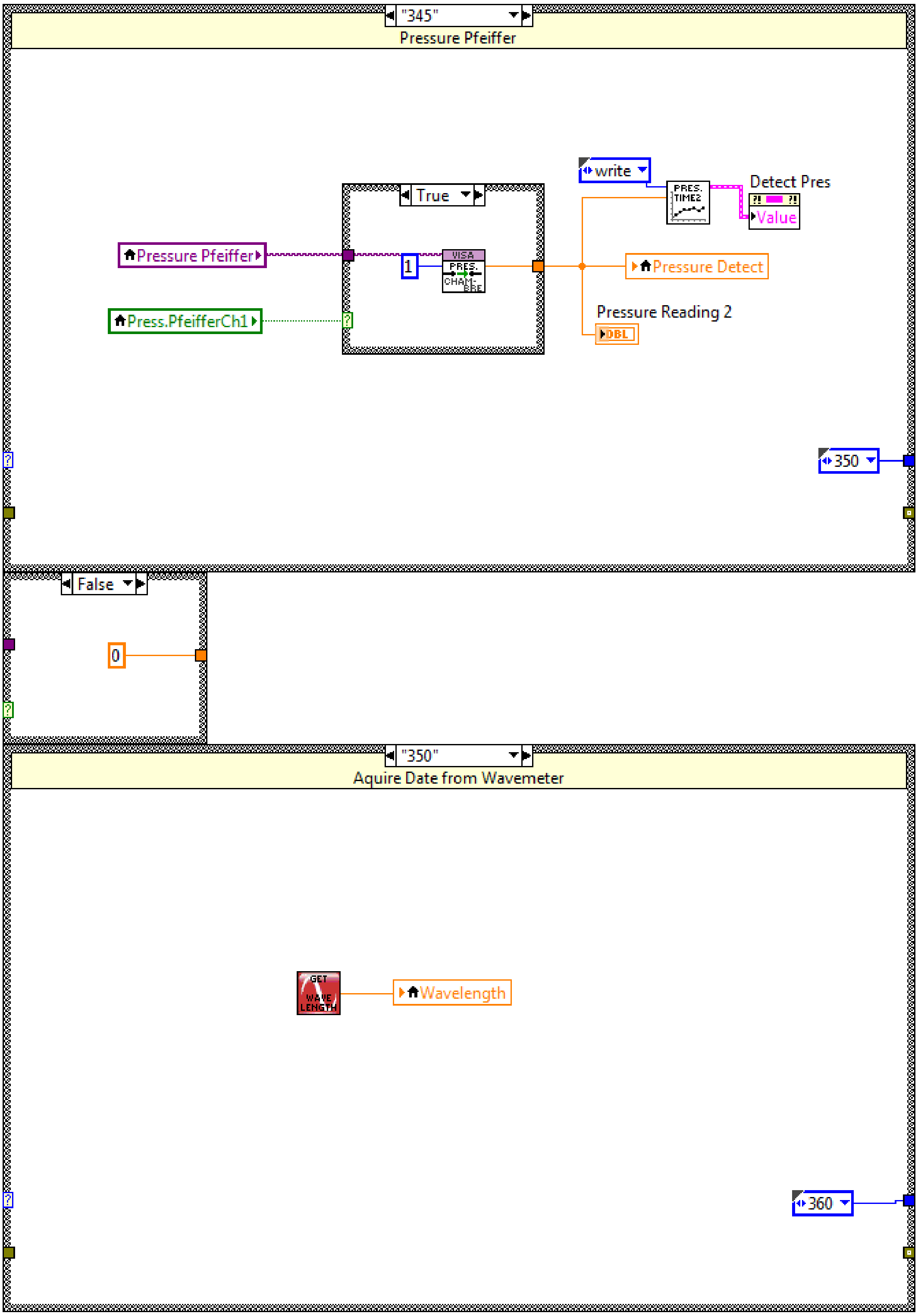
"345"
Pressure Pfeiffer
True
write
Detect Pres
Value
Pressure Pfeiffer
1
Press.PfeifferCh1
Pressure Detect
Pressure Reading 2
DBL
350
False
0
"350"
Aquire Date from Wavemeter
GET WAVE LENGTH
Wavelength
360

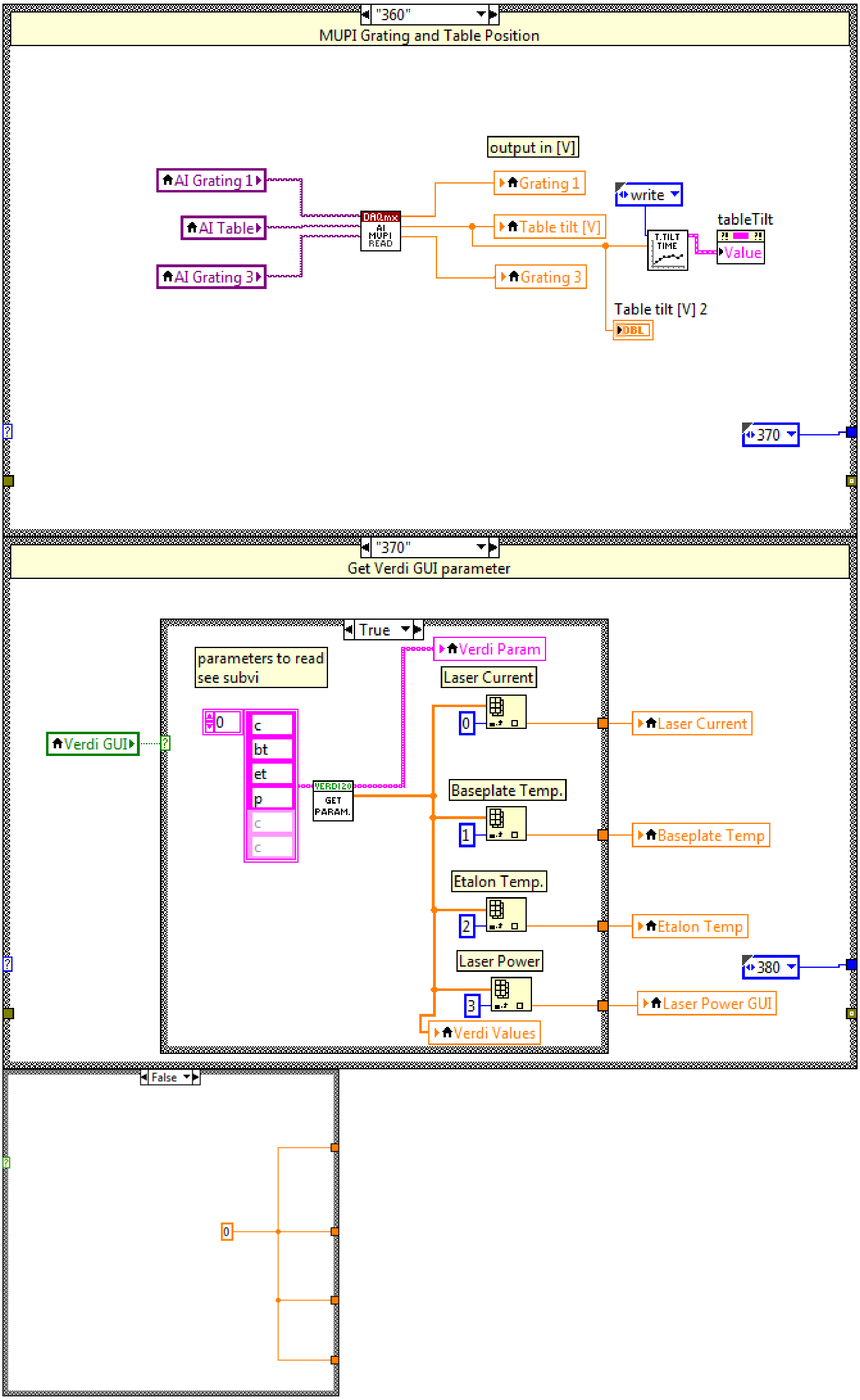
"360"
MUPI Grating and Table Position
output in [V]
AI Grating 1
AI Table
AI Grating 3
DAQmx AI MUPI READ
Grating 1
Table tilt [V]
Grating 3
write
T.TILT TIME
tableTilt
Value
Table tilt [V] 2
DBL
370
"370"
Get Verdi GUI parameter
True
parameters to read see subvi
Verdi Param
Laser Current
Verdi GUI
0
c
bt
et
p
VERDI20 GET PARAM.
Laser Current
Baseplate Temp.
1
Baseplate Temp
Etalon Temp.
2
Etalon Temp
Laser Power
380
3
Laser Power GUI
Verdi Values
False
0

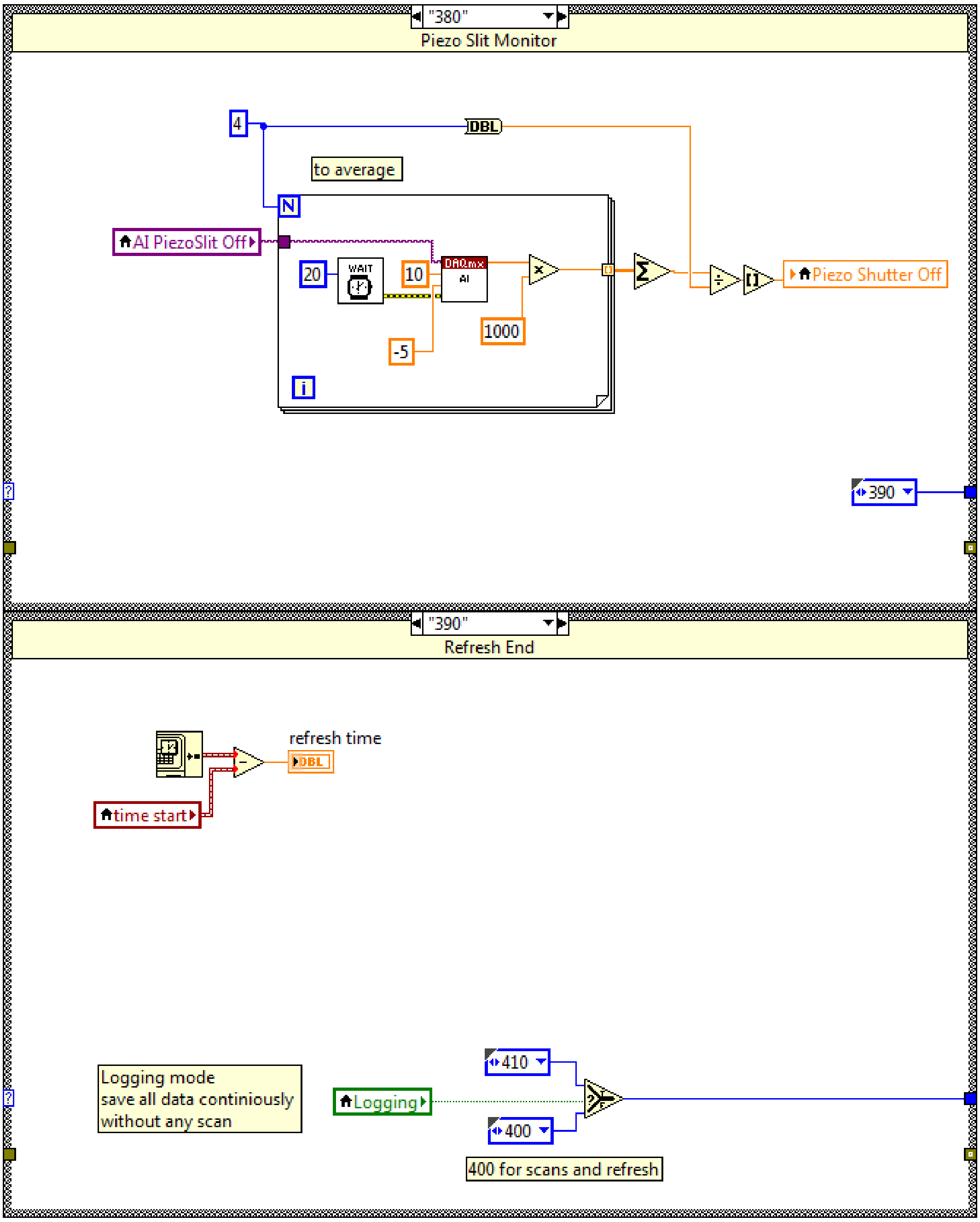
"380"
Piezo Slit Monitor
4
DBL
to average
N
AI PiezoSlit Off
20
WAIT
10
DAQmx
AI
1000
-5
i
Piezo Shutter Off
390
"390"
Refresh End
refresh time
DBL
time start
Logging mode
save all data continiously
without any scan
Logging
410
400
400 for scans and refresh

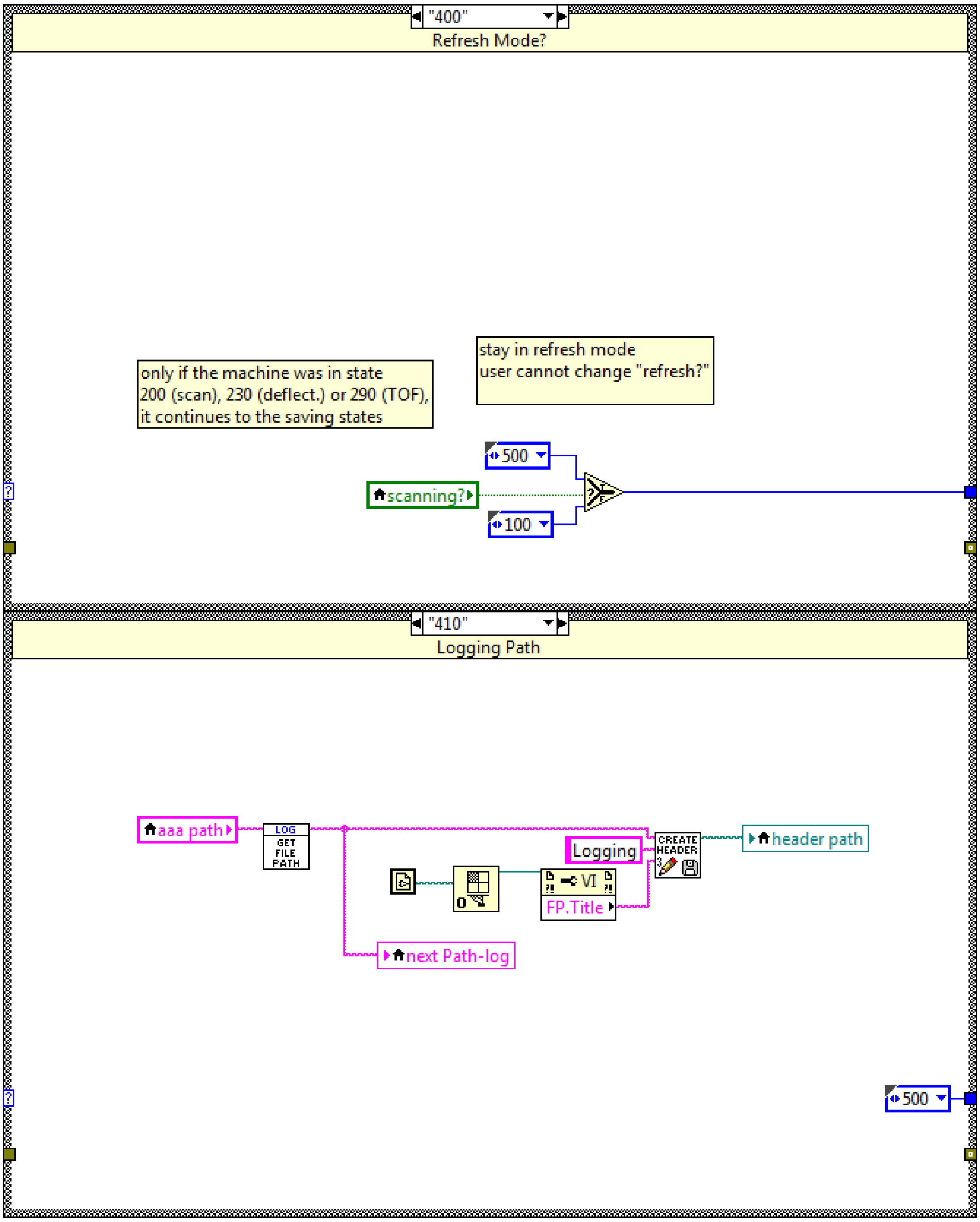

"400"
Refresh Mode?
only if the machine was in state
200 (scan), 230 (deflect.) or 290 (TOF),
it continues to the saving states
stay in refresh mode
user cannot change "refresh?"
500
scanning?
100
"410"
Logging Path
aaa path
LOG GET FILE PATH
Logging
CREATE HEADER
header path
VI
FP.Title
next Path-log
0
500

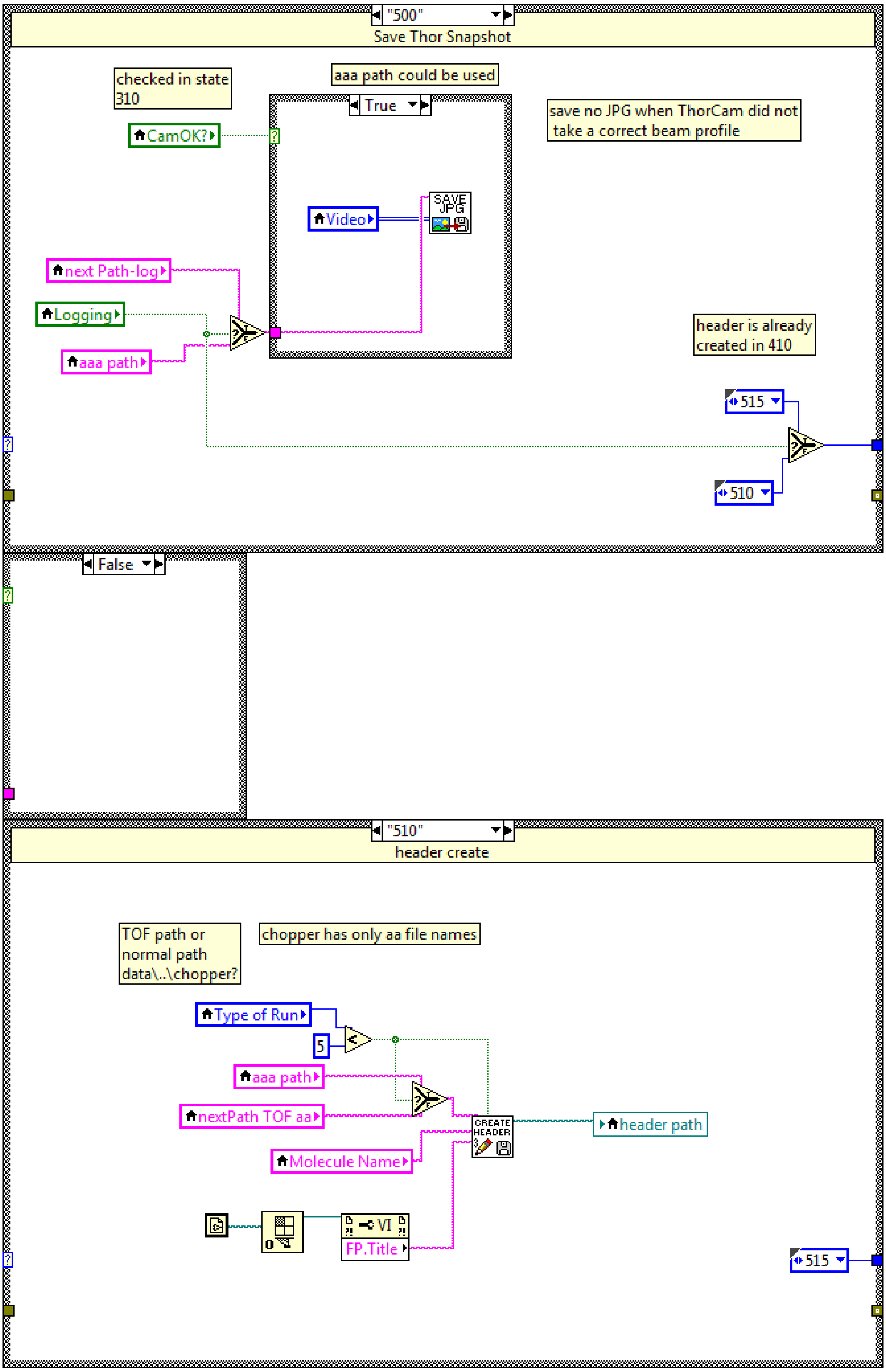
"500"
Save Thor Snapshot
checked in state 310
aaa path could be used
True
save no JPG when ThorCam did not take a correct beam profile
CamOK?
Video
SAVE JPG
next Path-log
Logging
aaa path
header is already created in 410
515
510
False
"510"
header create
TOF path or normal path data\..\chopper?
chopper has only aa file names
Type of Run
5
aaa path
nextPath TOF aa
Molecule Name
CREATE HEADER
header path
VI
FP.Title
515

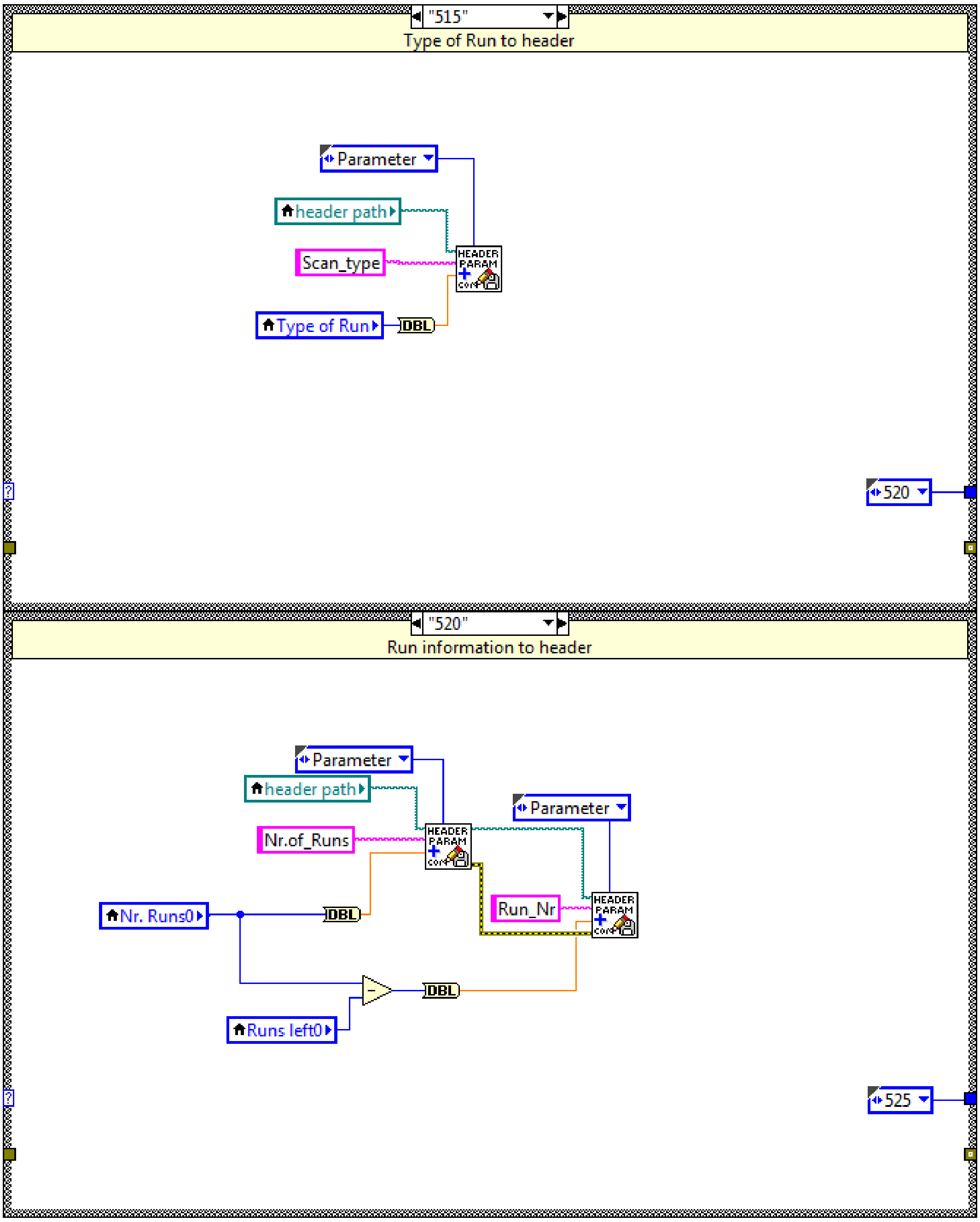
"515"
Type of Run to header
Parameter
header path
Scan_type
HEADER PARAM
Type of Run
DBL
520
"520"
Run information to header
Parameter
header path
Nr.of_Runs
HEADER PARAM
Parameter
Run_Nr
HEADER PARAM
Nr. Runs0
DBL
DBL
Runs left0
525

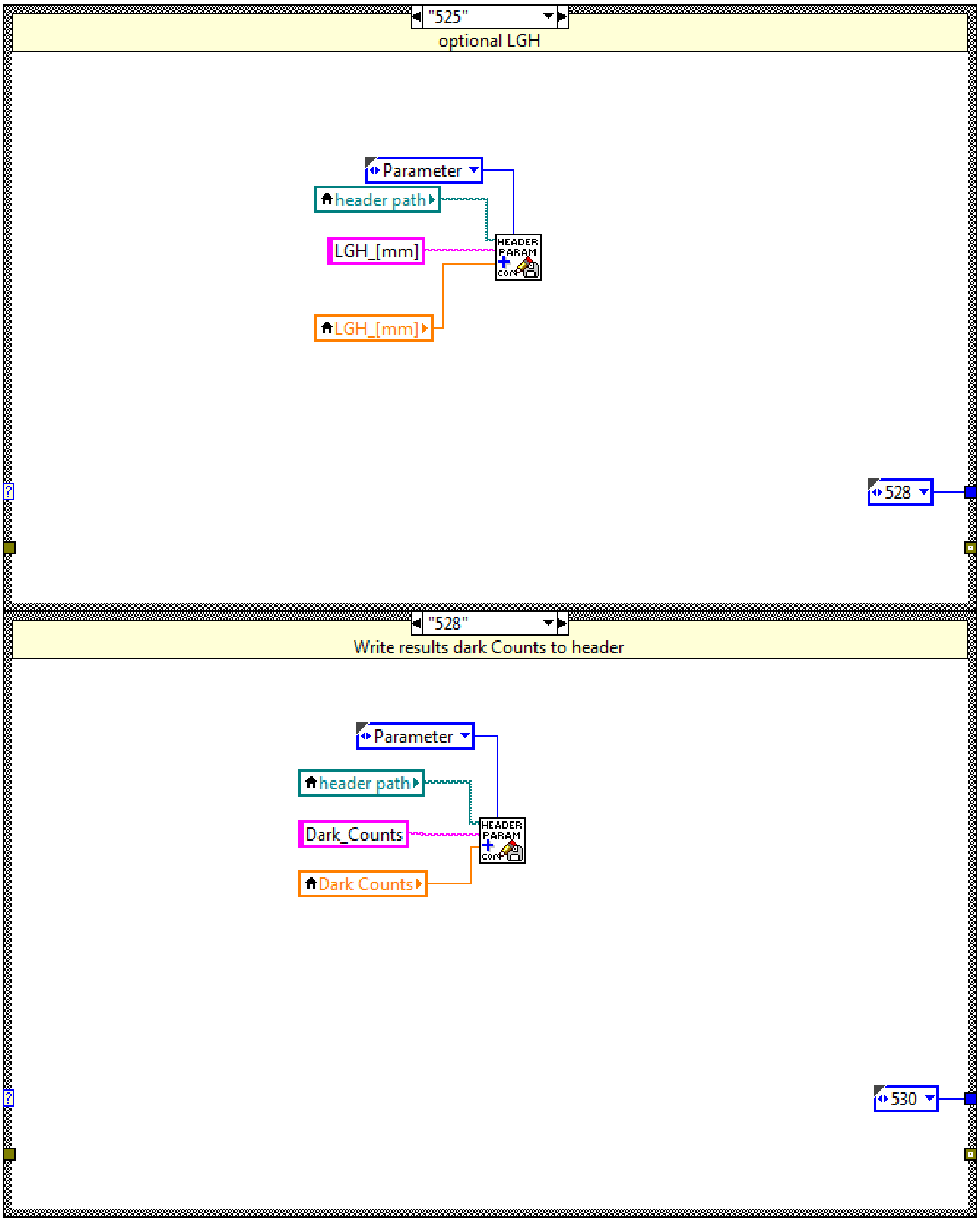
"525"
optional LGH
Parameter
header path
LGH_[mm]
LGH_[mm]
HEADER PARAM
528
"528"
Write results dark Counts to header
Parameter
header path
Dark_Counts
Dark Counts
HEADER PARAM
530

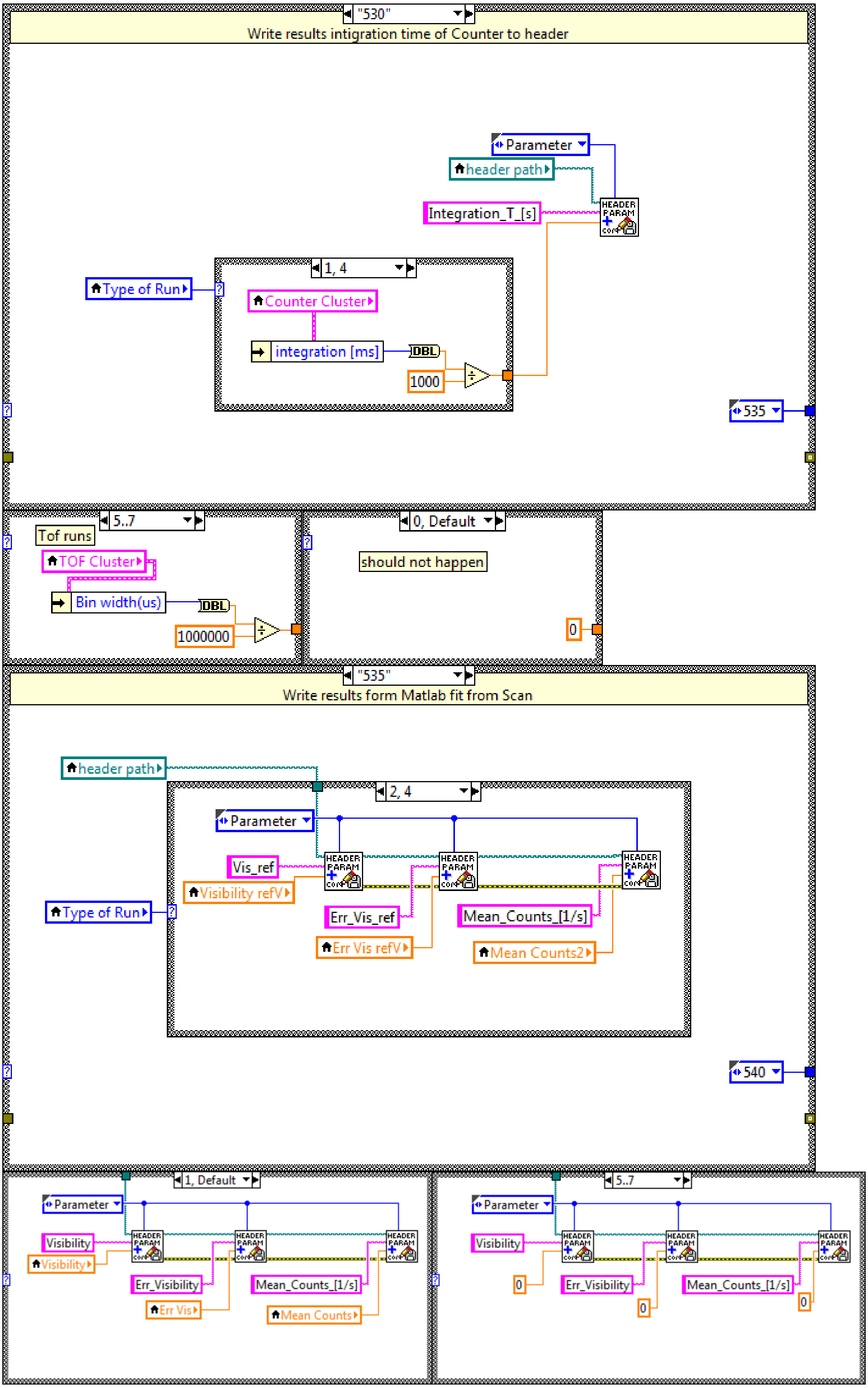
"530"
Write results intigration time of Counter to header
Parameter
header path
Integration_T_[s]
HEADER PARAM
Type of Run
1, 4
Counter Cluster
integration [ms]
DBL
1000
535
5..7
Tof runs
TOF Cluster
Bin width(us)
DBL
1000000
0, Default
should not happen
0
"535"
Write results form Matlab fit from Scan
header path
2, 4
Parameter
Vis_ref
Visibility refV
Type of Run
Err_Vis_ref
Err Vis refV
Mean_Counts_[1/s]
Mean Counts2
540
1, Default
Parameter
Visibility
Visibility
Err_Visibility
Err Vis
Mean_Counts_[1/s]
Mean Counts
5..7
Parameter
Visibility
0
Err_Visibility
0
Mean_Counts_[1/s]
0

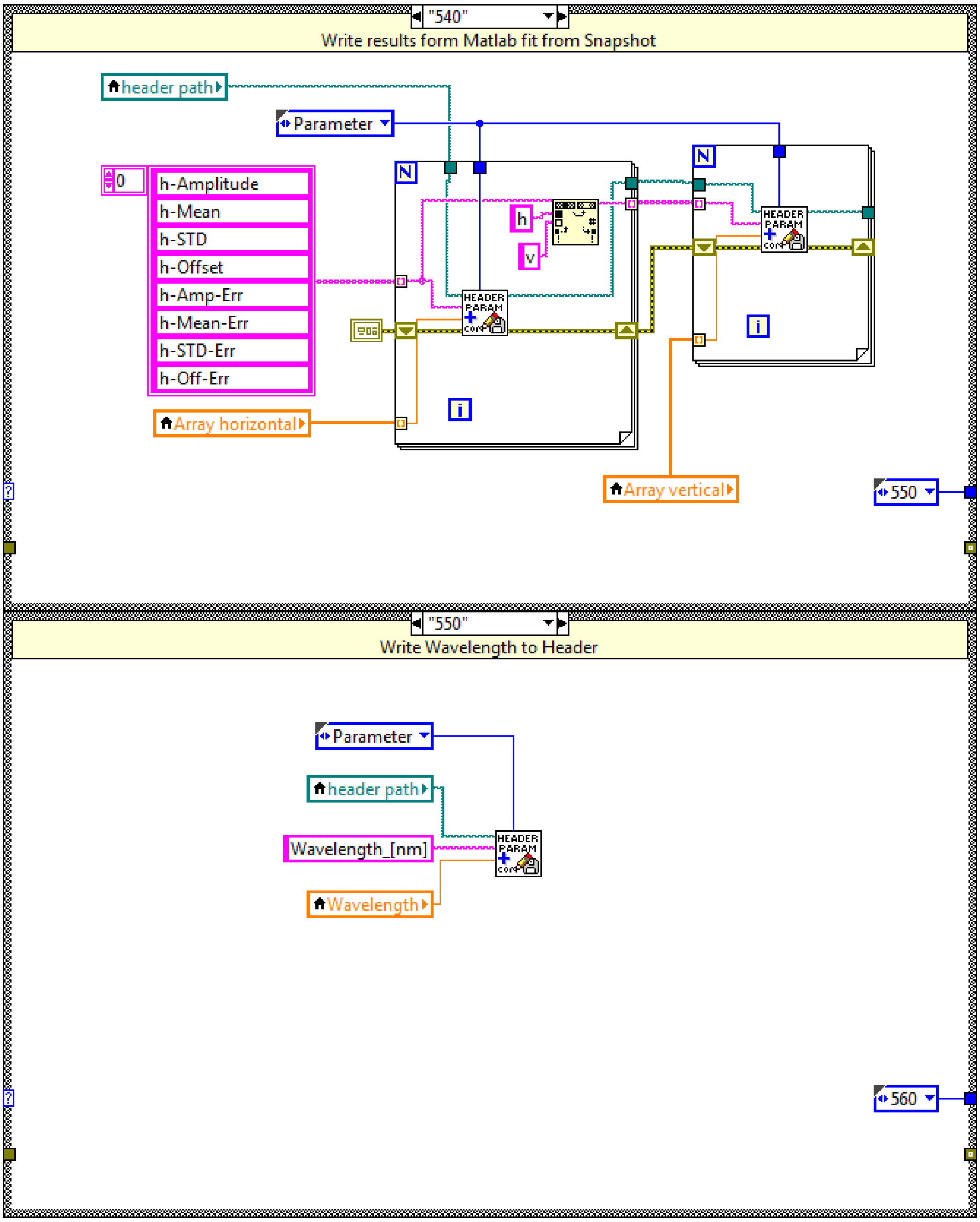
"540"
Write results form Matlab fit from Snapshot
header path
Parameter
0
h-Amplitude
h-Mean
h-STD
h-Offset
h-Amp-Err
h-Mean-Err
h-STD-Err
h-Off-Err
N
h
v
HEADER PARAM
i
Array horizontal
Array vertical
550
"550"
Write Wavelength to Header
Parameter
header path
Wavelength_[nm]
HEADER PARAM
Wavelength
560

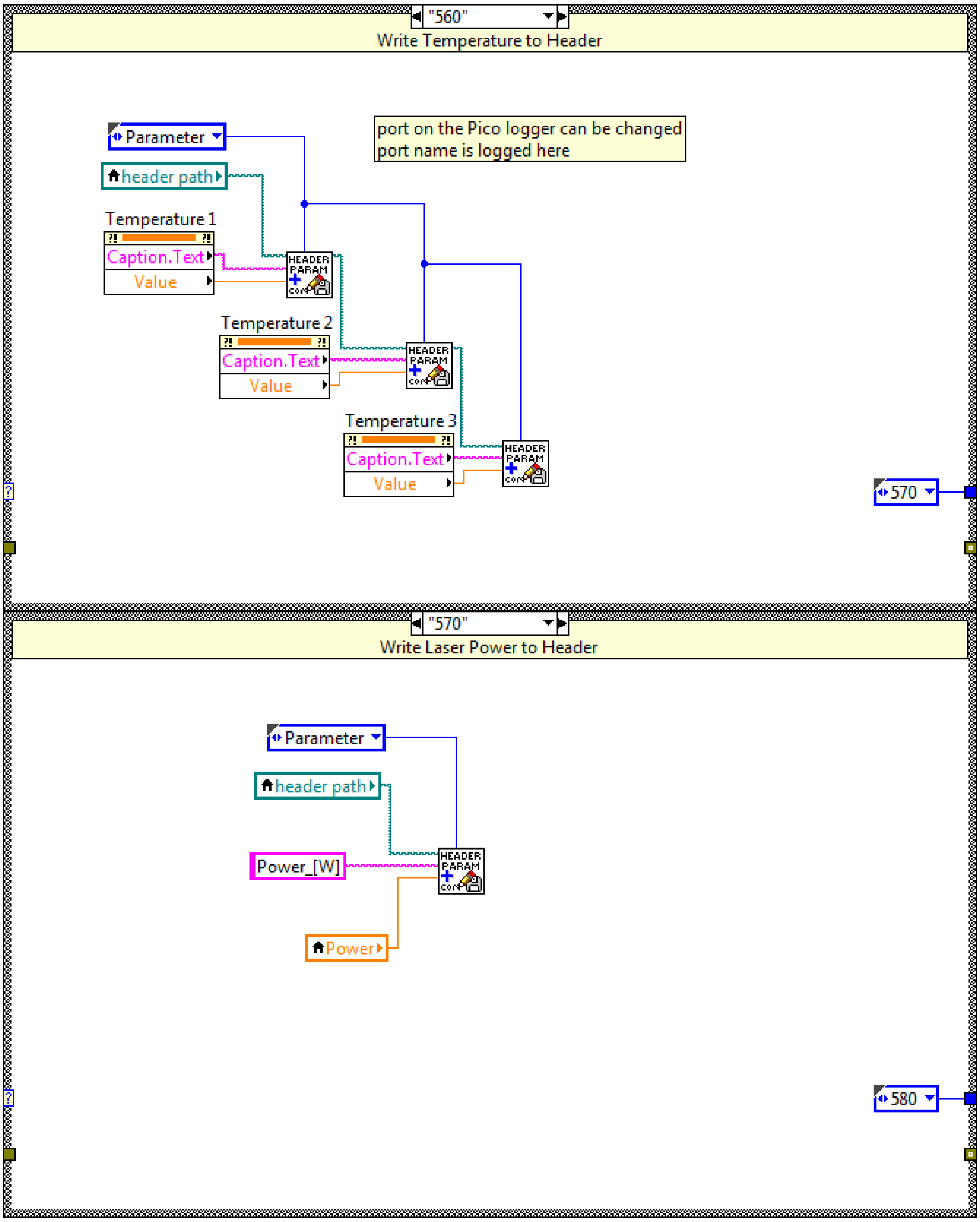
"560"
Write Temperature to Header
port on the Pico logger can be changed
port name is logged here
Parameter
header path
Temperature 1
Caption.Text
Value
Temperature 2
Caption.Text
Value
Temperature 3
Caption.Text
Value
HEADER PARAM
570
"570"
Write Laser Power to Header
Parameter
header path
Power_[W]
Power
HEADER PARAM
580

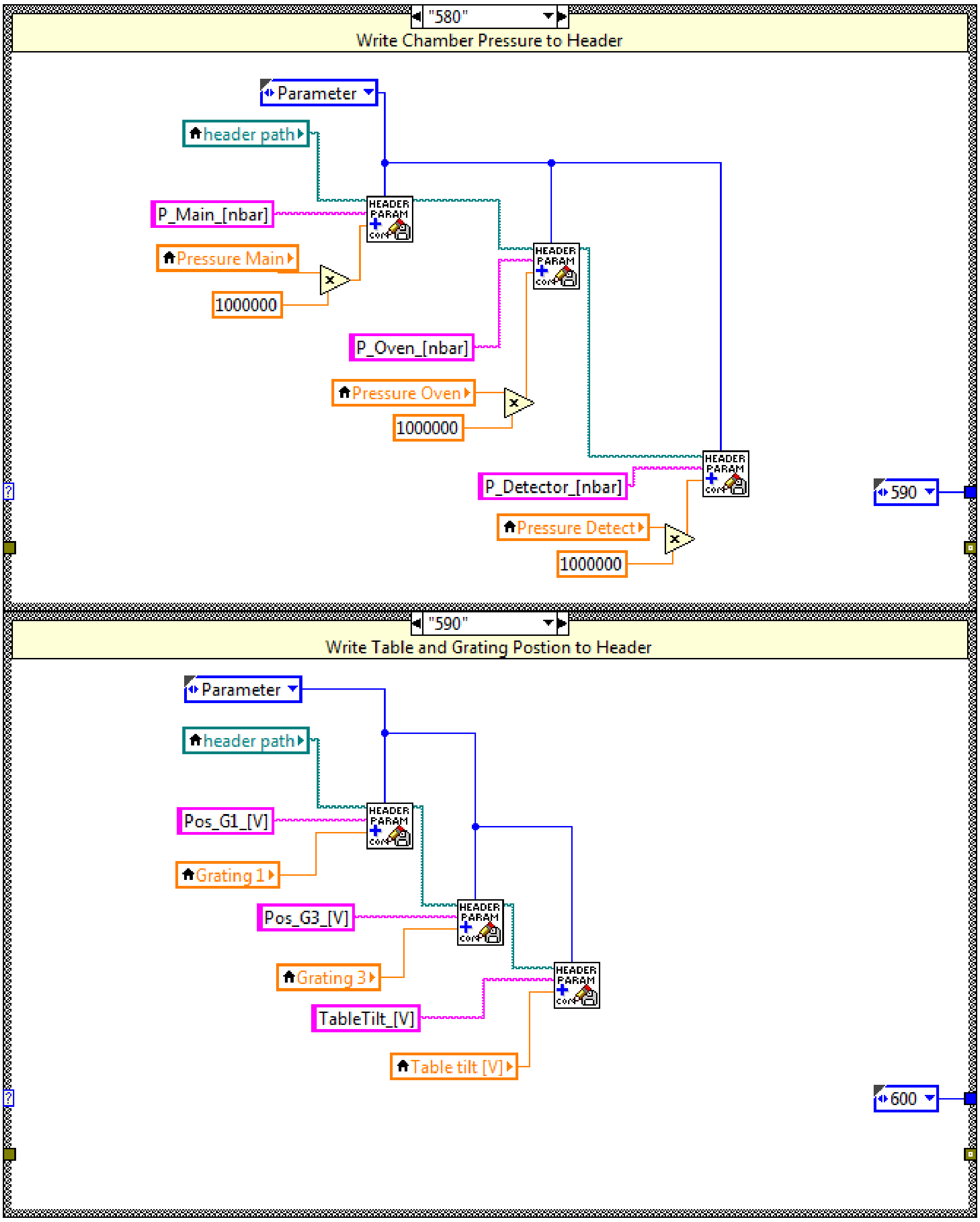
"580"
Write Chamber Pressure to Header
Parameter
header path
P_Main_[nbar]
Pressure Main
1000000
P_Oven_[nbar]
Pressure Oven
1000000
P_Detector_[nbar]
Pressure Detect
1000000
590
"590"
Write Table and Grating Postion to Header
Parameter
header path
Pos_G1_[V]
Grating 1
Pos_G3_[V]
Grating 3
TableTilt_[V]
Table tilt [V]
600

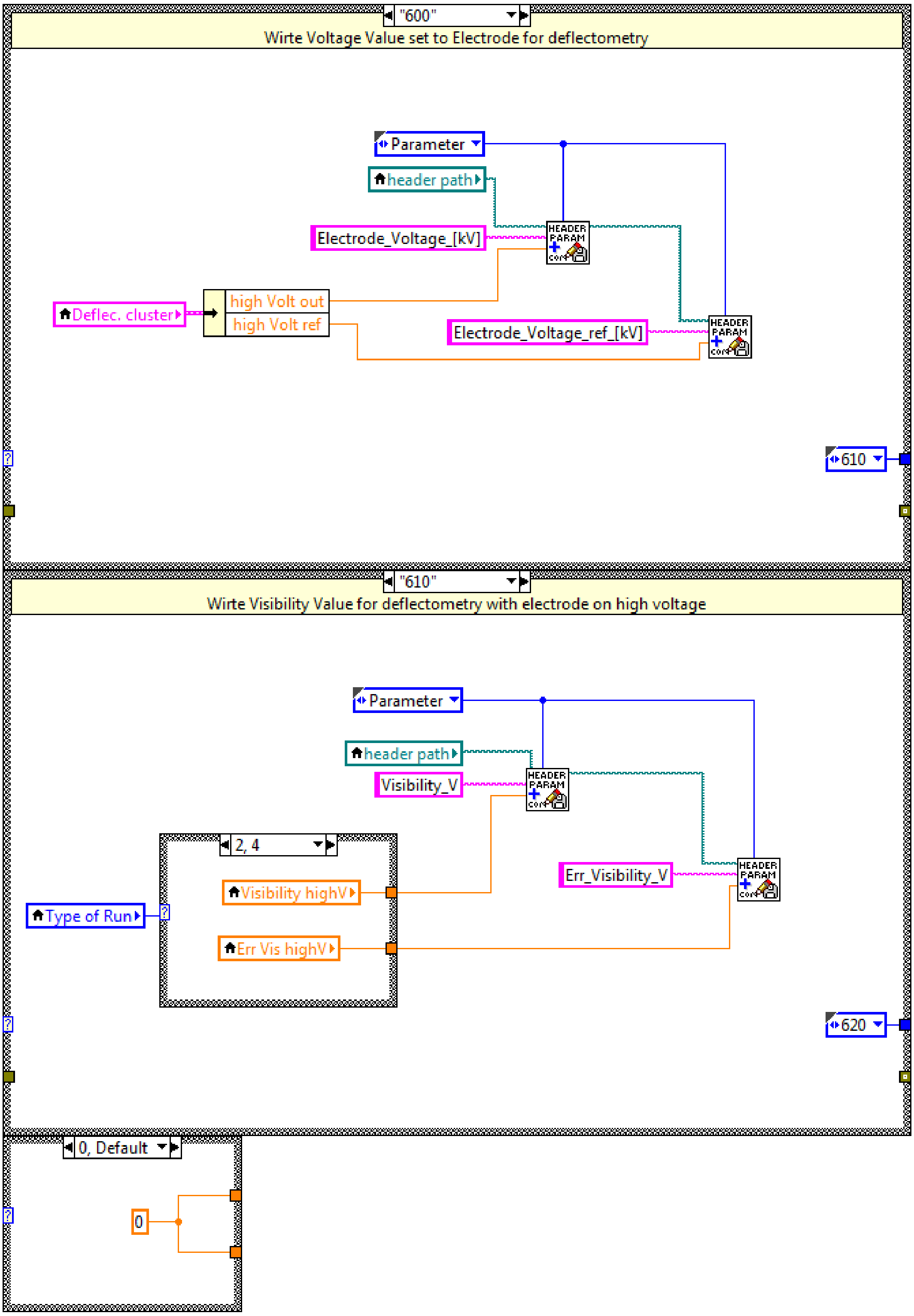
"600"
Wirte Voltage Value set to Electrode for deflectometry
Parameter
header path
Electrode_Voltage_[kV]
HEADER PARAM
Deflec. cluster
high Volt out
high Volt ref
Electrode_Voltage_ref_[kV]
610
"610"
Wirte Visibility Value for deflectometry with electrode on high voltage
Parameter
header path
Visibility_V
2, 4
Visibility highV
Err_Visibility_V
Type of Run
Err Vis highV
620
0, Default
0

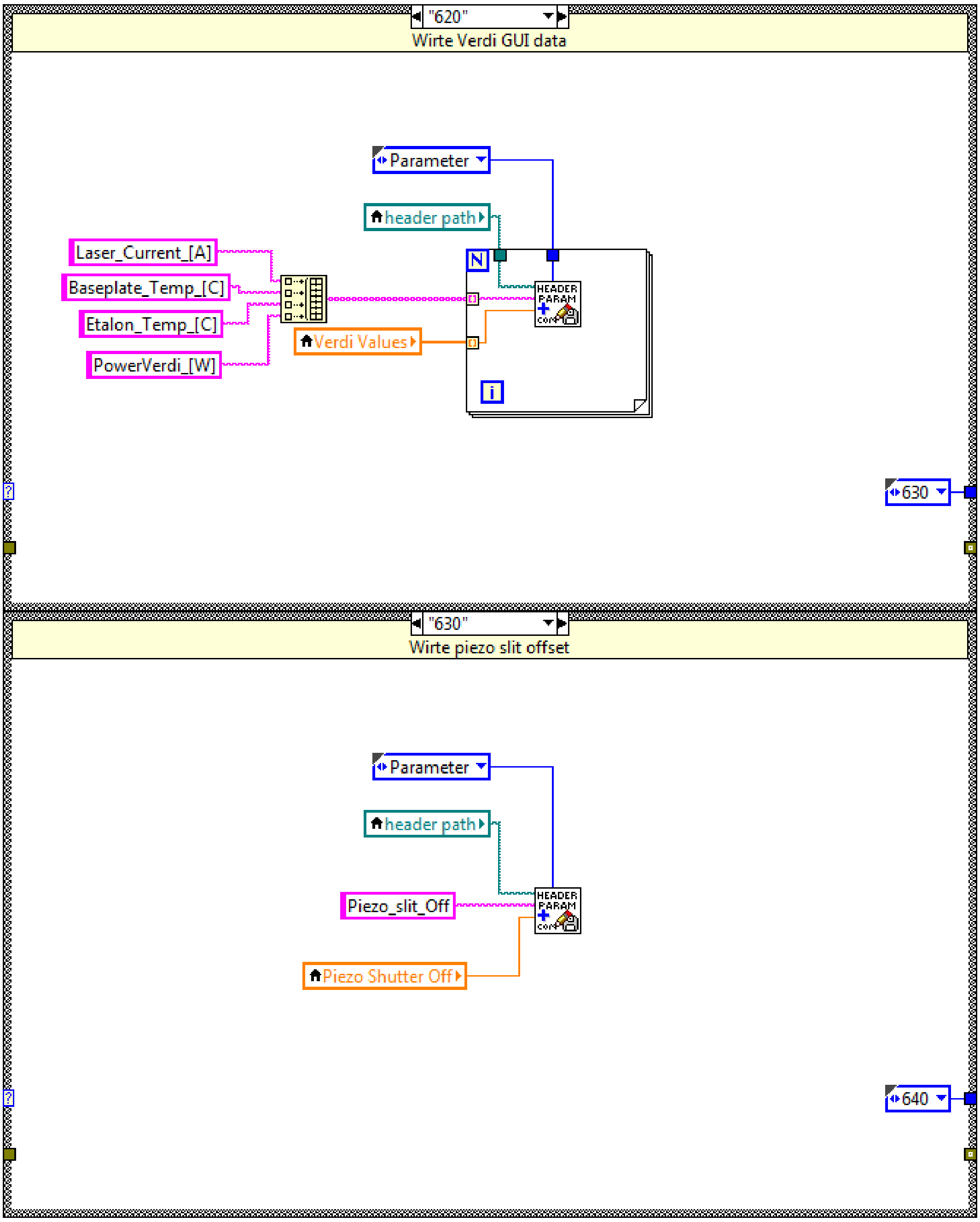
"620"
Wirte Verdi GUI data
Parameter
header path
Laser_Current_[A]
Baseplate_Temp_[C]
Etalon_Temp_[C]
PowerVerdi_[W]
Verdi Values
N
i
630
"630"
Wirte piezo slit offset
Parameter
header path
Piezo_slit_Off
Piezo Shutter Off
640

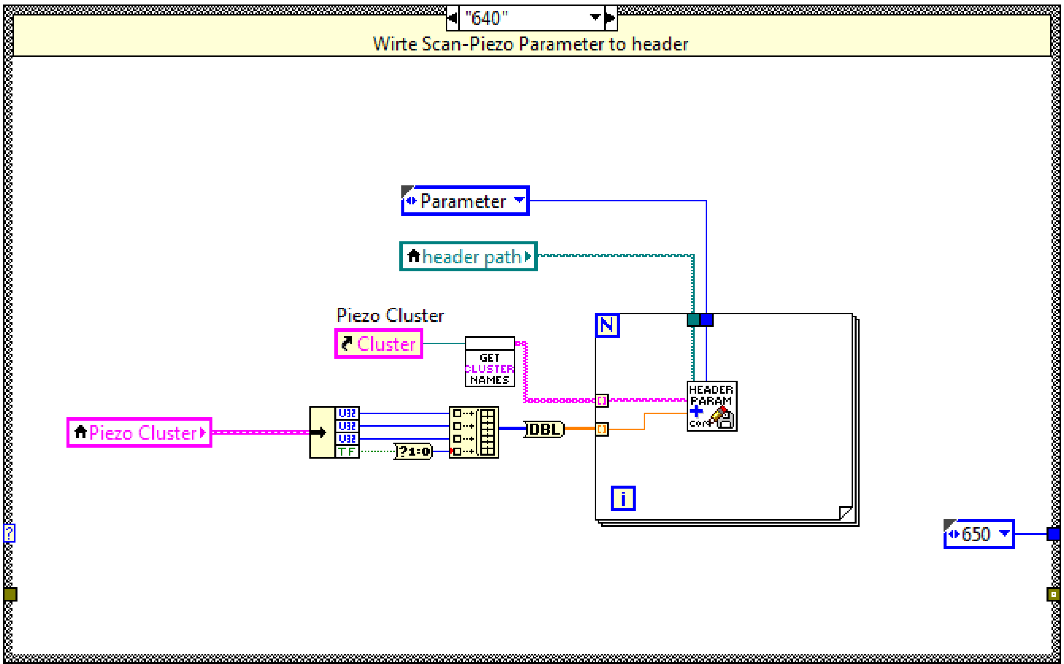
"640"
Wirte Scan-Piezo Parameter to header
Parameter
header path
Piezo Cluster
Cluster
GET CLUSTER NAMES
Piezo Cluster
DBL
N
i
HEADER PARAM
650

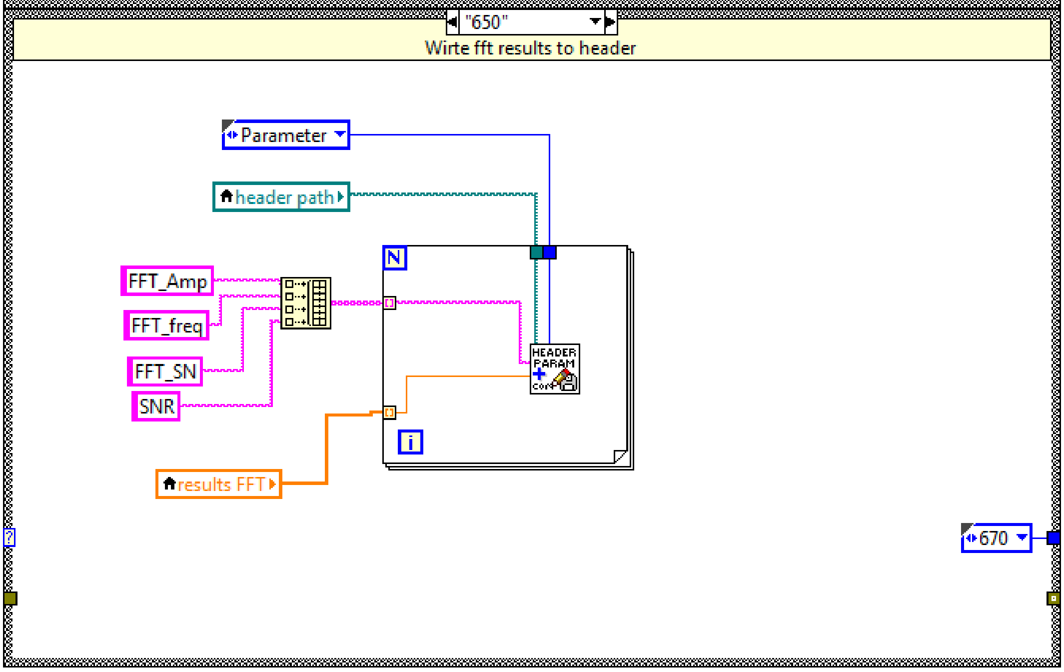
"650"
Wirte fft results to header
Parameter
header path
FFT_Amp
FFT_freq
FFT_SN
SNR
results FFT
N
i
HEADER PARAM
670

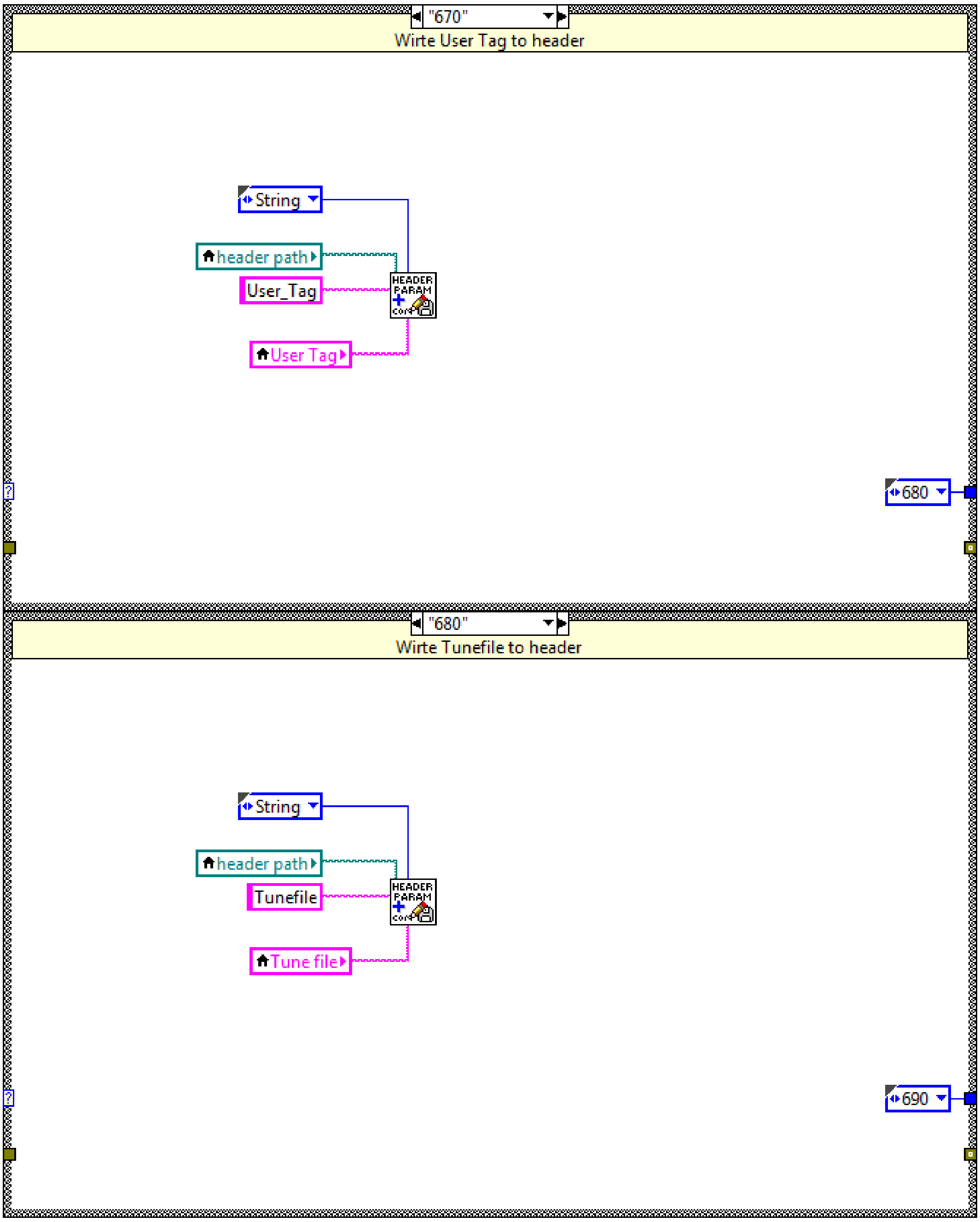
"670"
Wirte User Tag to header
String
header path
User_Tag
HEADER PARAM
User Tag
680
"680"
Wirte Tunefile to header
String
header path
Tunefile
HEADER PARAM
Tune file
690

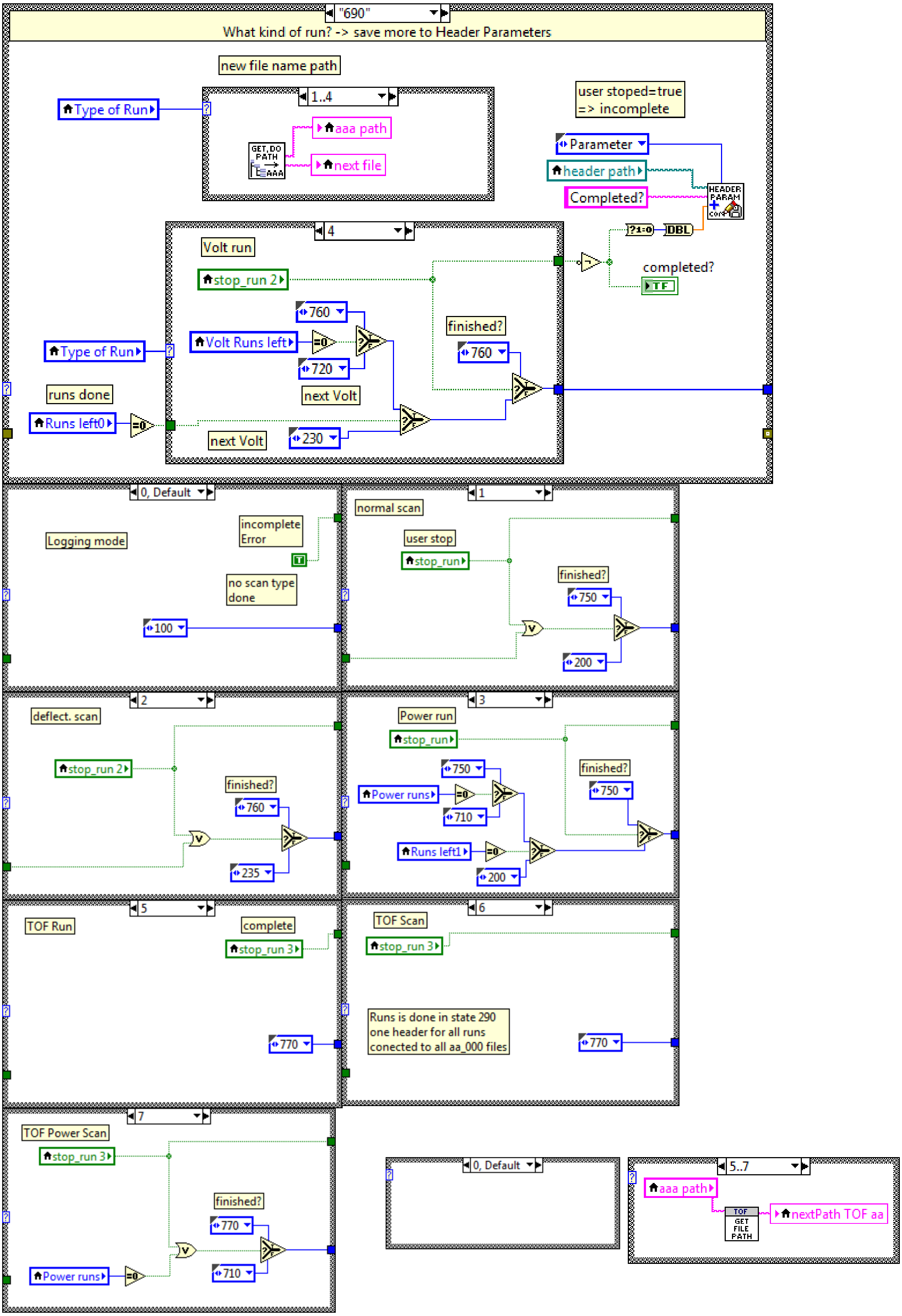
"690"
What kind of run? -> save more to Header Parameters
new file name path
1..4
Type of Run
aaa path
next file
user stoped=true
=> incomplete
Parameter
header path
Completed?
HEADER PARAM
4
Volt run
stop_run 2
760
Volt Runs left
720
finished?
760
completed?
Type of Run
runs done
next Volt
Runs left0
next Volt
230
0, Default
Logging mode
incomplete
Error
no scan type
done
100
1
normal scan
user stop
stop_run
finished?
750
200
2
deflect. scan
stop_run 2
finished?
760
235
3
Power run
stop_run
750
Power runs
710
finished?
750
Runs left1
200
5
TOF Run
complete
stop_run 3
770
6
TOF Scan
stop_run 3
Runs is done in state 290
one header for all runs
conected to all aa_000 files
770
7
TOF Power Scan
stop_run 3
finished?
770
Power runs
710
0, Default
5..7
aaa path
TOF GET FILE PATH
nextPath TOF aa

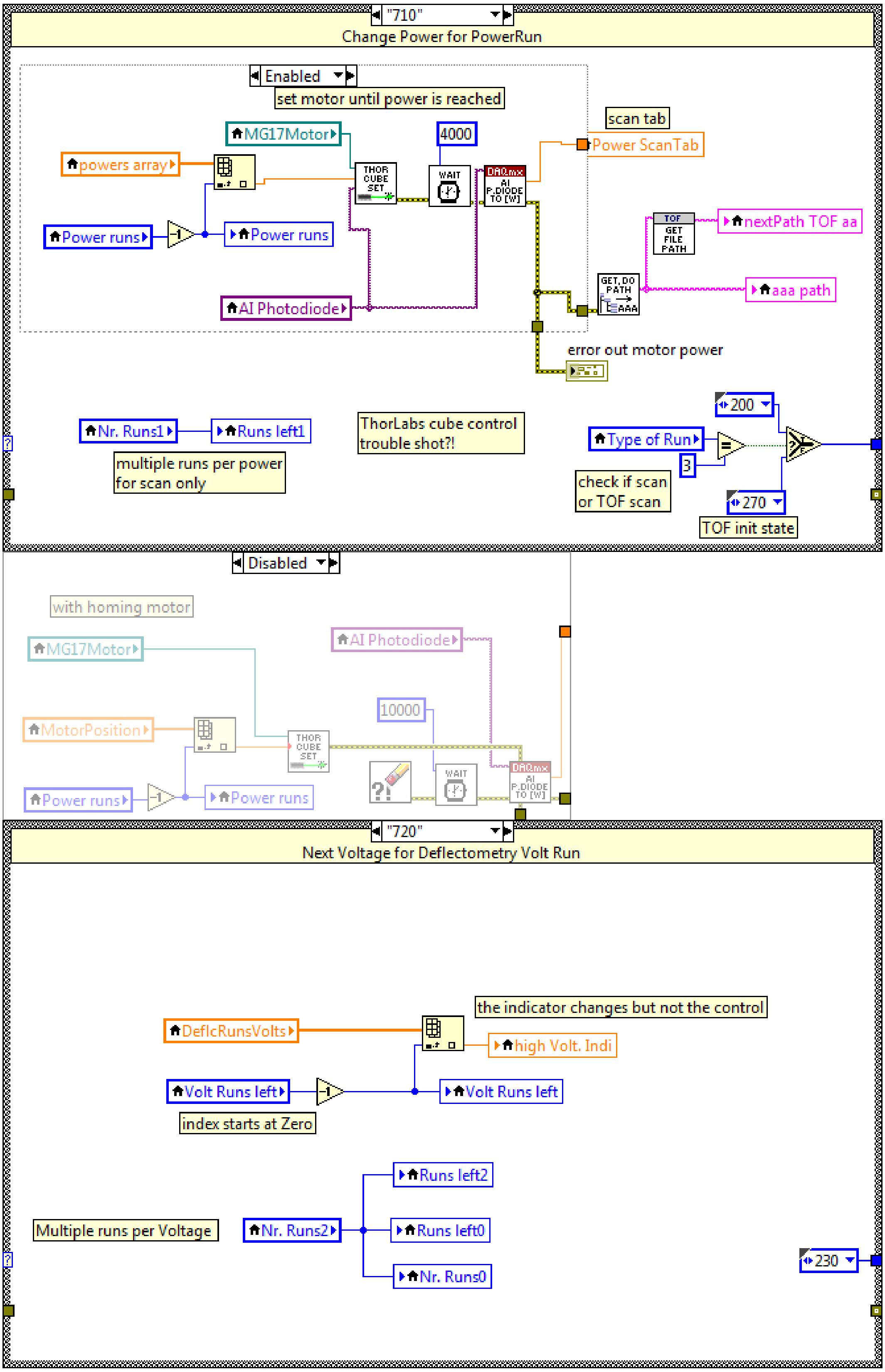
"710"
Change Power for PowerRun
Enabled
set motor until power is reached
MG17Motor
4000
powers array
Power runs
Power runs
AI Photodiode
scan tab
Power ScanTab
nextPath TOF aa
aaa path
error out motor power
200
Nr. Runs1
Runs left1
ThorLabs cube control
trouble shot?!
multiple runs per power
for scan only
Type of Run
3
check if scan
or TOF scan
270
TOF init state
Disabled
with homing motor
MG17Motor
AI Photodiode
10000
MotorPosition
Power runs
Power runs
"720"
Next Voltage for Deflectometry Volt Run
the indicator changes but not the control
DeflcRunsVolts
high Volt. Indi
Volt Runs left
Volt Runs left
index starts at Zero
Runs left2
Multiple runs per Voltage
Nr. Runs2
Runs left0
Nr. Runs0
230

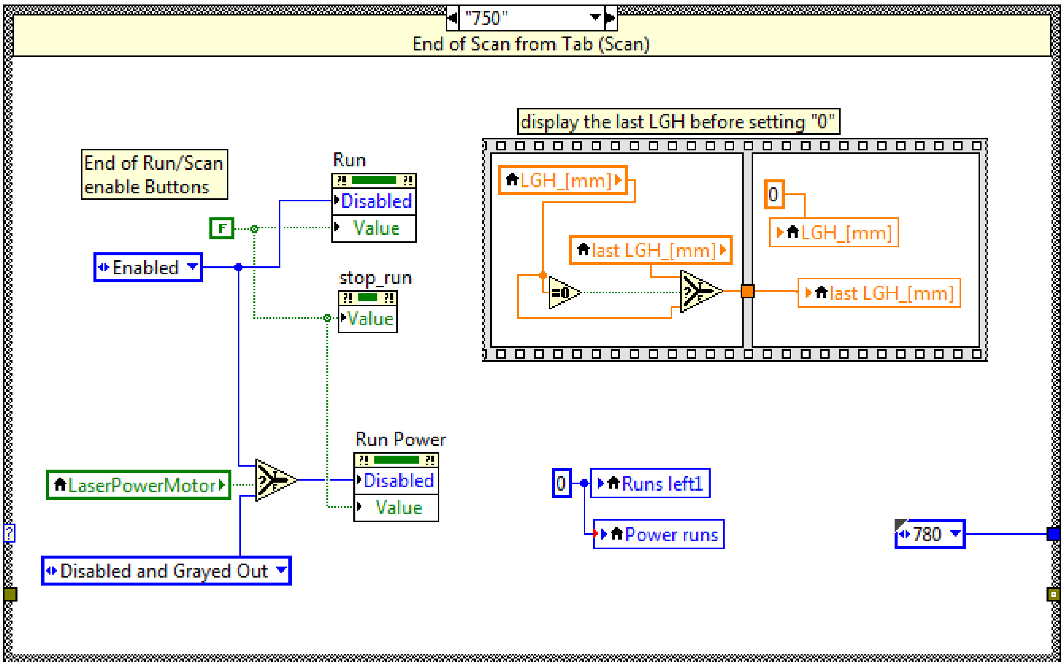
"750"
End of Scan from Tab (Scan)
display the last LGH before setting "0"
LGH_[mm]
last LGH_[mm]
0
LGH_[mm]
last LGH_[mm]
End of Run/Scan
enable Buttons
Run
Disabled
Value
F
Enabled
stop_run
Value
LaserPowerMotor
Run Power
Disabled
Value
Disabled and Grayed Out
0
Runs left1
Power runs
780

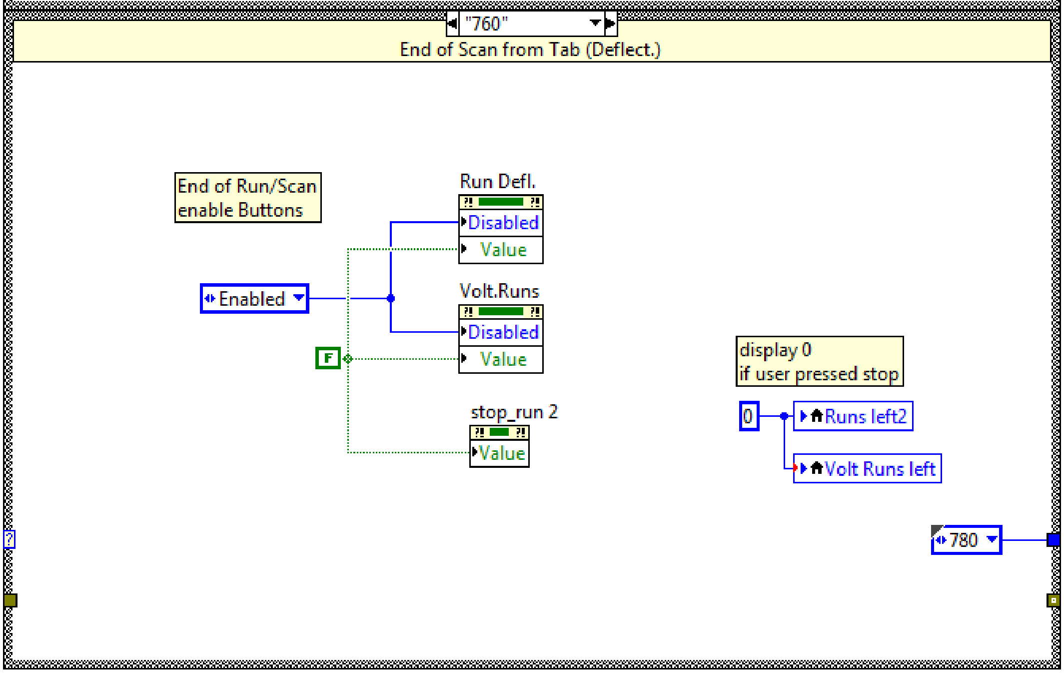
"760"
End of Scan from Tab (Deflect.)
End of Run/Scan
enable Buttons
Run Defl.
Disabled
Value
Enabled
Volt.Runs
Disabled
Value
F
stop_run 2
Value
display 0
if user pressed stop
0
Runs left2
Volt Runs left
780

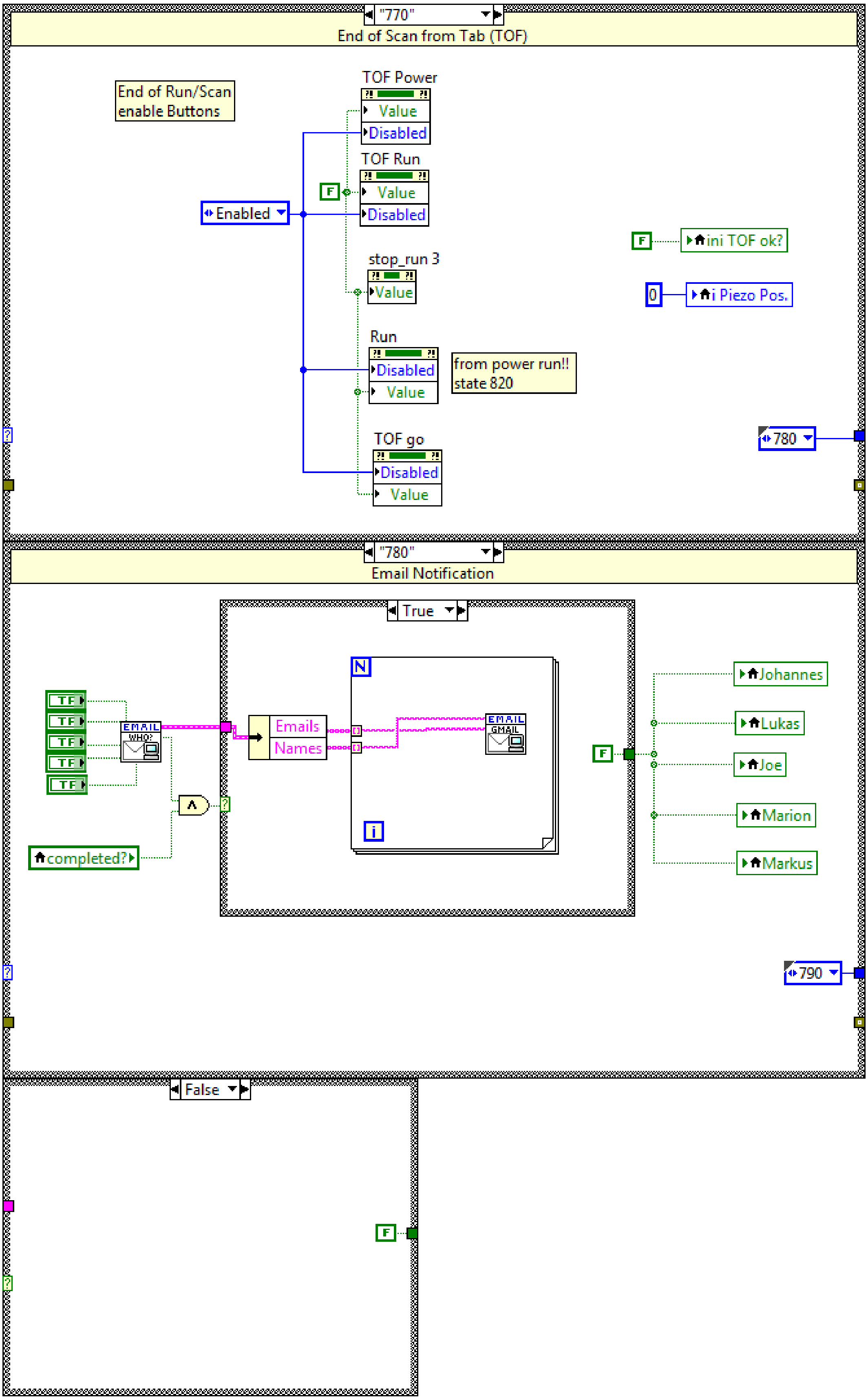
"770"
End of Scan from Tab (TOF)
End of Run/Scan enable Buttons
TOF Power
Value
Disabled
TOF Run
Value
Disabled
Enabled
F
stop_run 3
Value
Run
Disabled
Value
from power run!! state 820
TOF go
Disabled
Value
F
ini TOF ok?
0
i Piezo Pos.
780
"780"
Email Notification
True
N
Emails
Names
EMAIL WHO?
EMAIL GMAIL
completed?
i
F
Johannes
Lukas
Joe
Marion
Markus
790
False
F

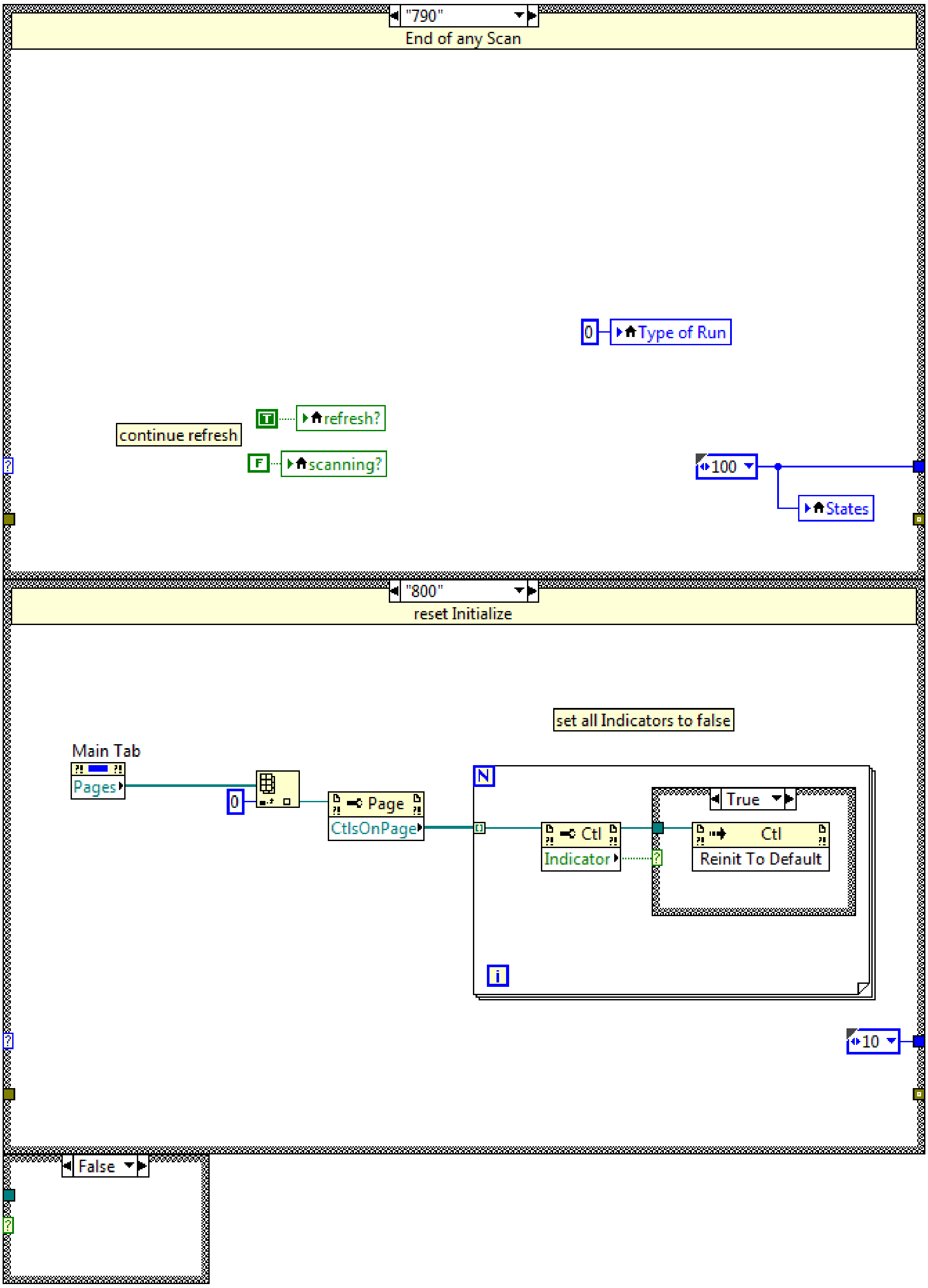
"790"
End of any Scan
0
Type of Run
continue refresh
T
refresh?
F
scanning?
100
States
"800"
reset Initialize
set all Indicators to false
Main Tab
Pages
0
Page
CtlsOnPage
N
Ctl
Indicator
True
Ctl
Reinit To Default
i
10
False

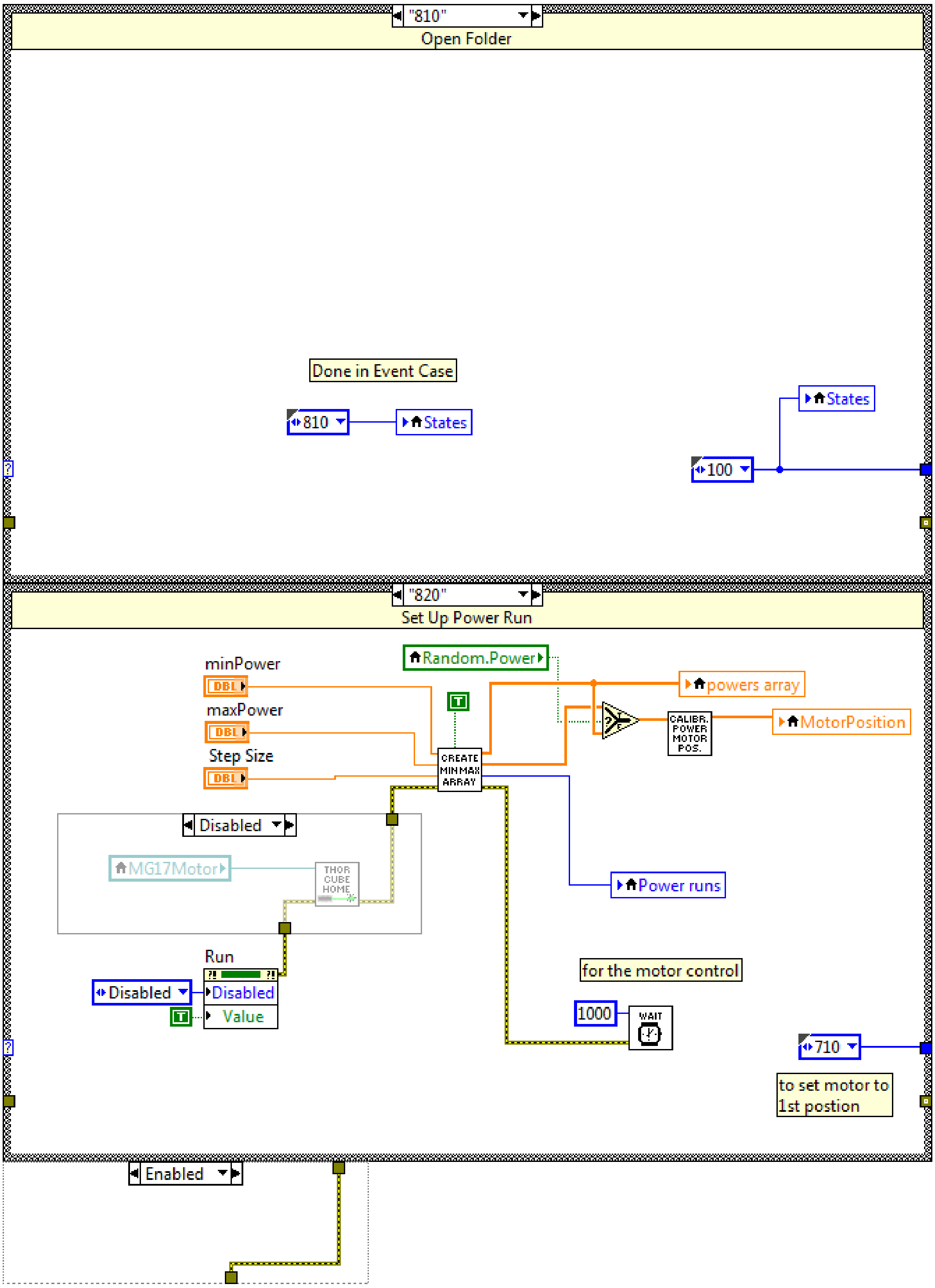

"810"
Open Folder
Done in Event Case
810
States
States
100
"820"
Set Up Power Run
minPower
maxPower
Step Size
Random.Power
powers array
MotorPosition
CREATE MIN MAX ARRAY
CALIBR. POWER MOTOR POS.
Disabled
MG17Motor
THOR CUBE HOME
Power runs
Run
Disabled
Disabled
Value
for the motor control
1000
WAIT
710
to set motor to 1st postion
Enabled

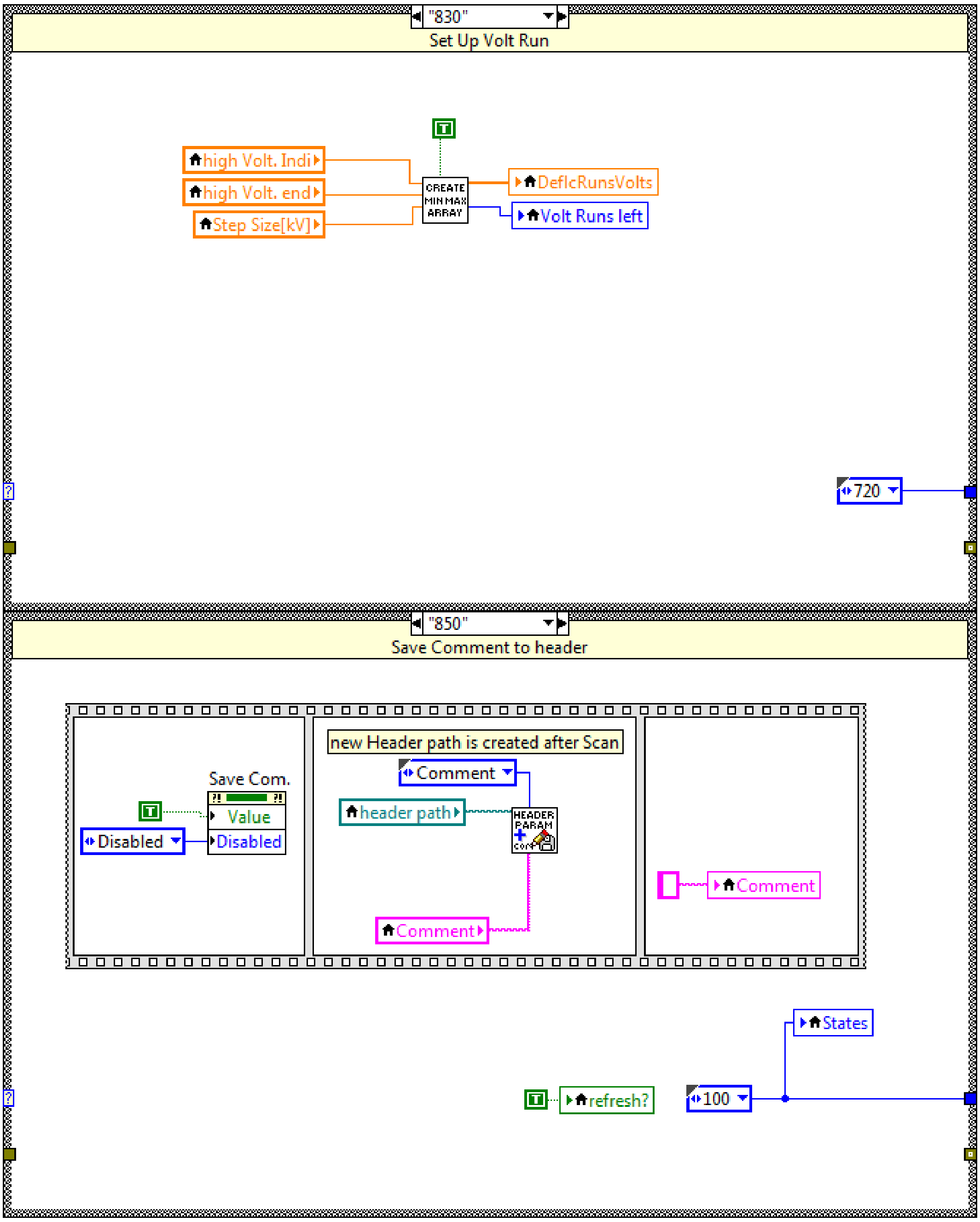

"830"
Set Up Volt Run
high Volt. Indi
high Volt. end
Step Size[kV]
CREATE MIN MAX ARRAY
DeflcRunsVolts
Volt Runs left
720
"850"
Save Comment to header
Save Com.
Value
Disabled
Disabled
new Header path is created after Scan
Comment
header path
HEADER PARAM
Comment
Comment
States
refresh?
100

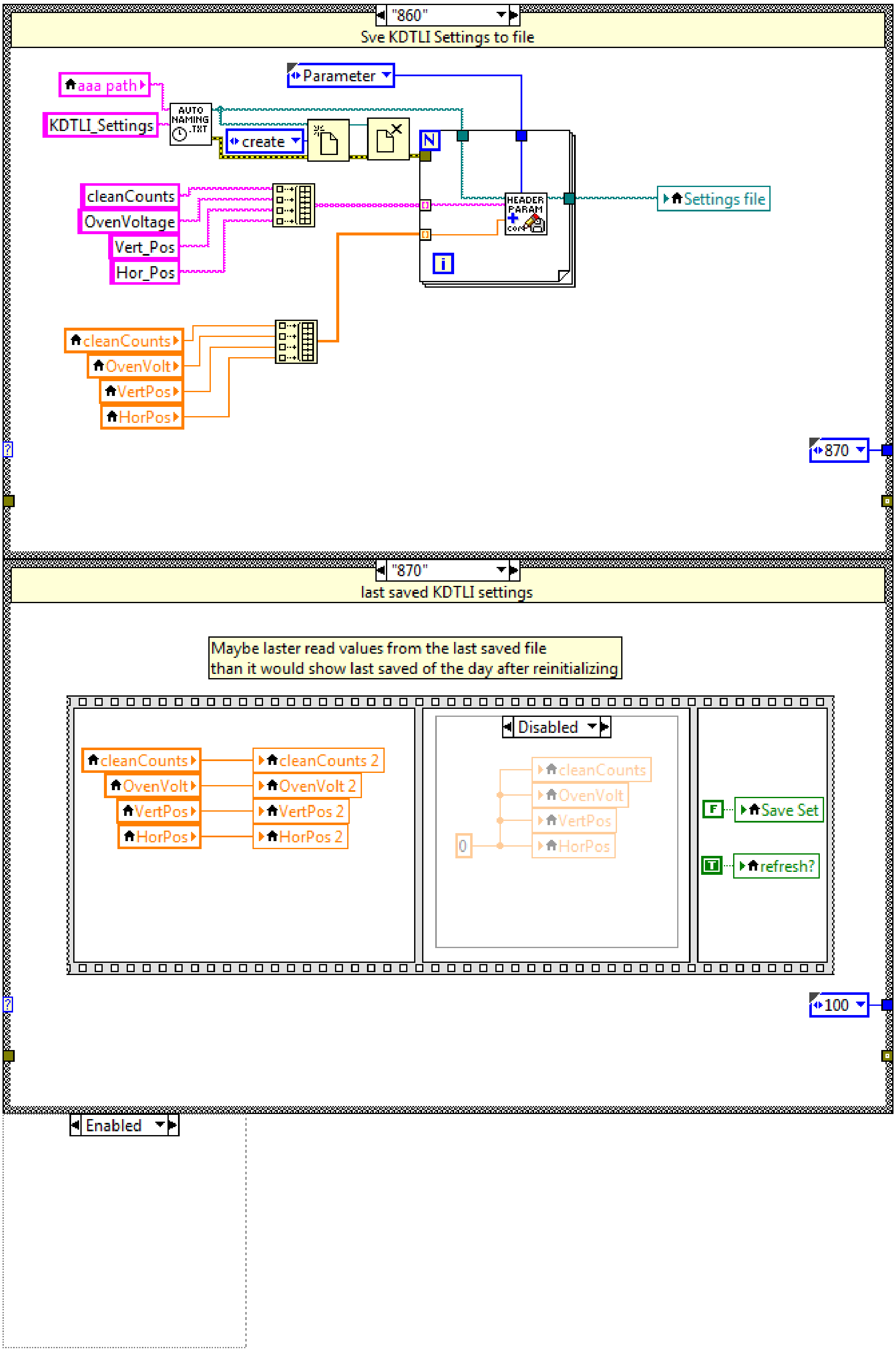

"860"
Sve KDTLI Settings to file
aaa path
KDTLI_Settings
AUTO NAMING .TXT
create
Parameter
N
HEADER PARAM
Settings file
cleanCounts
OvenVoltage
Vert_Pos
Hor_Pos
i
cleanCounts
OvenVolt
VertPos
HorPos
870
"870"
last saved KDTLI settings
Maybe laster read values from the last saved file
than it would show last saved of the day after reinitializing
cleanCounts
OvenVolt
VertPos
HorPos
cleanCounts 2
OvenVolt 2
VertPos 2
HorPos 2
Disabled
cleanCounts
OvenVolt
VertPos
HorPos
0
F
Save Set
T
refresh?
100
Enabled

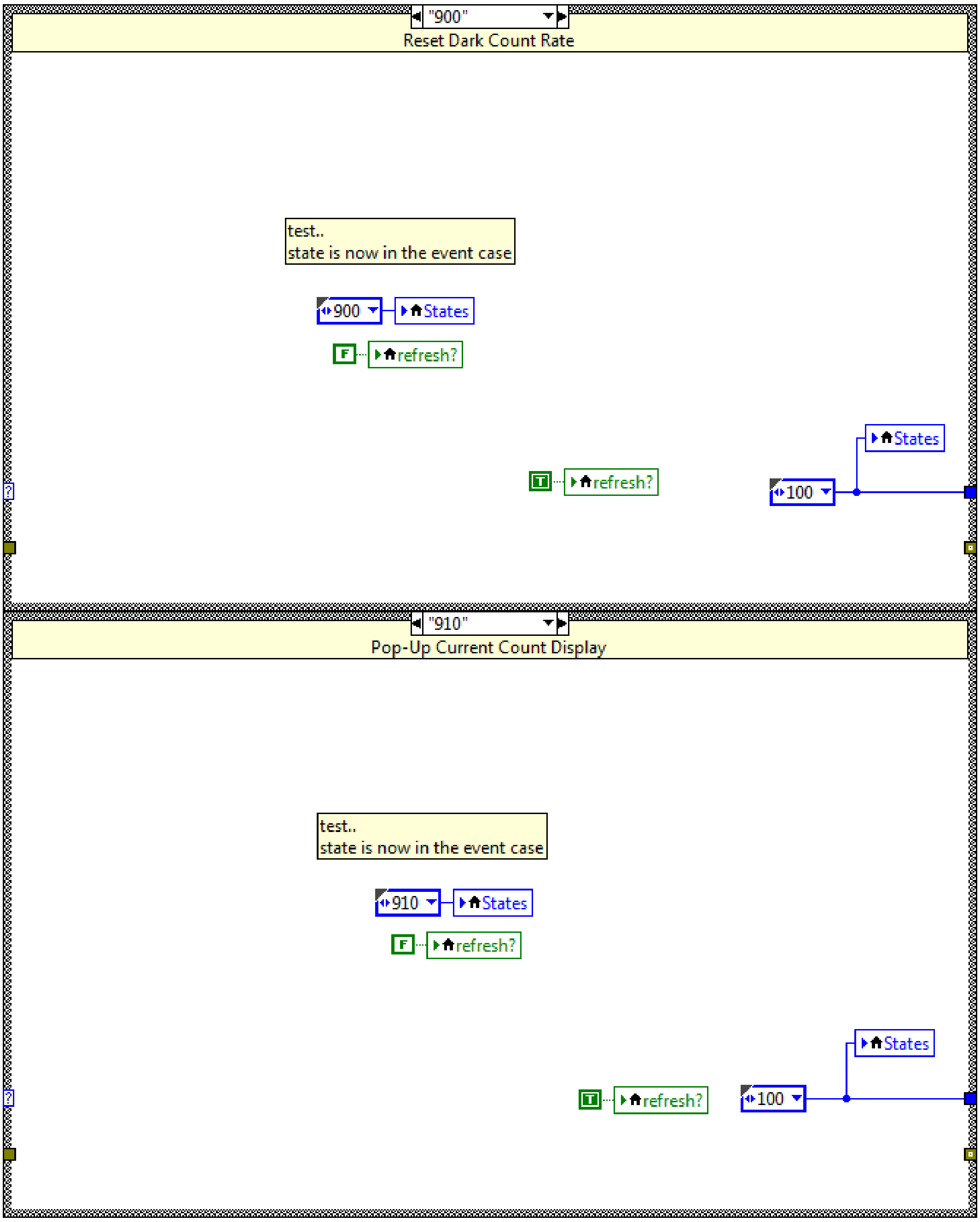

"900"
Reset Dark Count Rate
test..
state is now in the event case
900
States
F
refresh?
States
T
refresh?
100
"910"
Pop-Up Current Count Display
test..
state is now in the event case
910
States
F
refresh?
States
T
refresh?
100

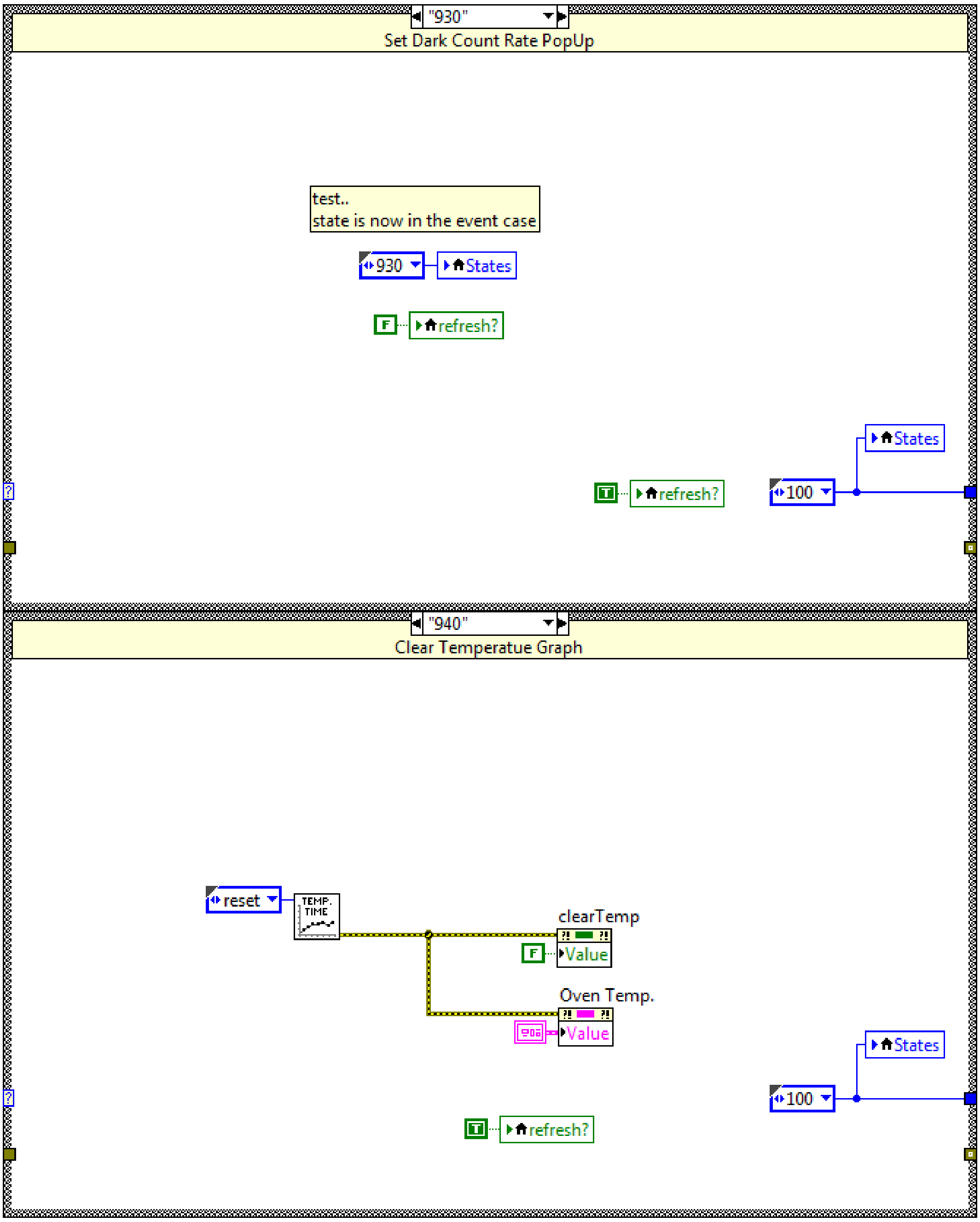
"930"
Set Dark Count Rate PopUp
test..
state is now in the event case
930
States
F
refresh?
States
T
refresh?
100
"940"
Clear Temperatue Graph
reset
TEMP. TIME
clearTemp
F
Value
Oven Temp.
Value
States
100
T
refresh?

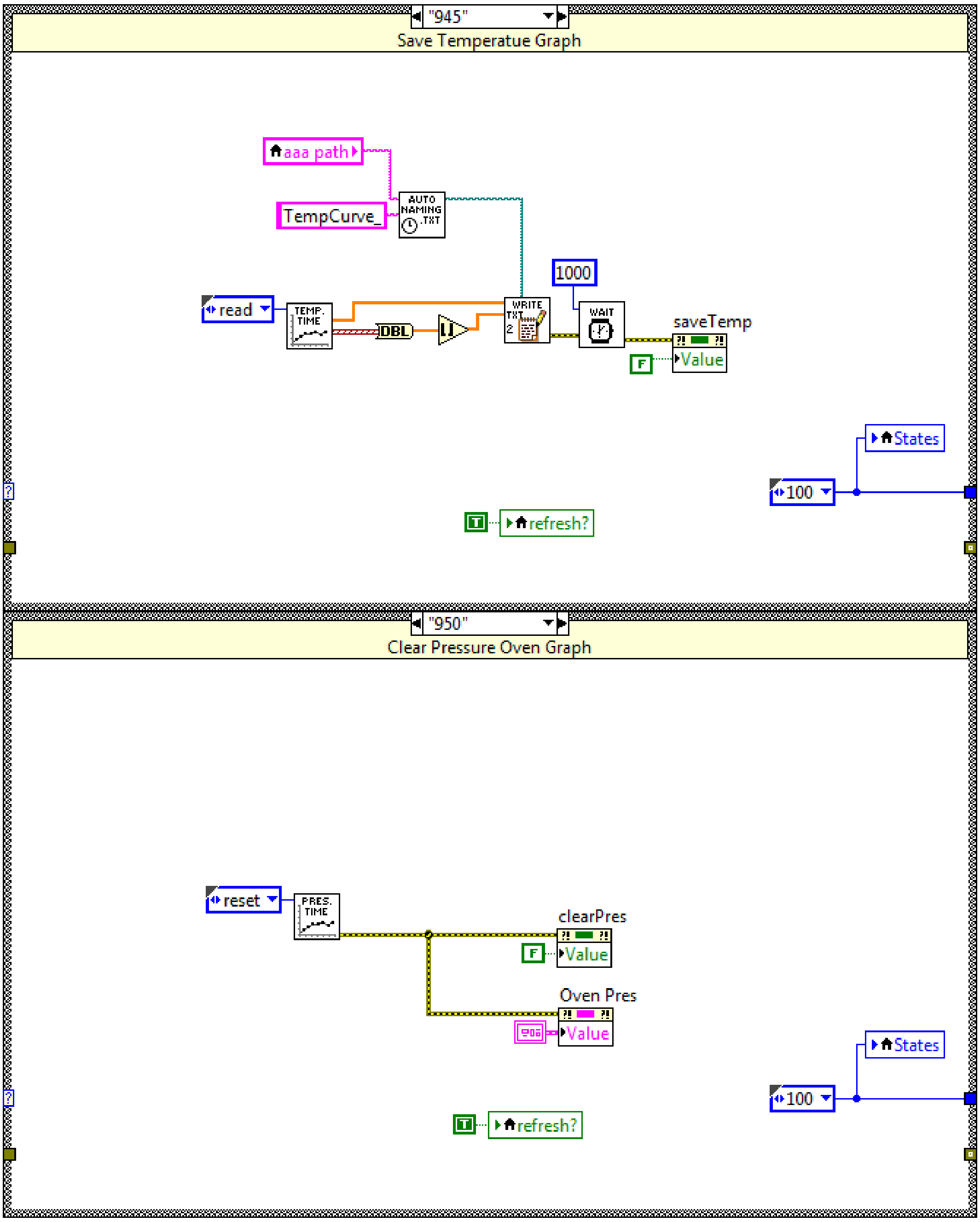

"945"
Save Temperatue Graph
aaa path
TempCurve_
AUTO NAMING .TXT
1000
read
TEMP. TIME
DBL
WRITE TXT 2
WAIT
saveTemp
F
Value
States
100
T
refresh?
"950"
Clear Pressure Oven Graph
reset
PRES. TIME
clearPres
F
Value
Oven Pres
Value
States
100
T
refresh?

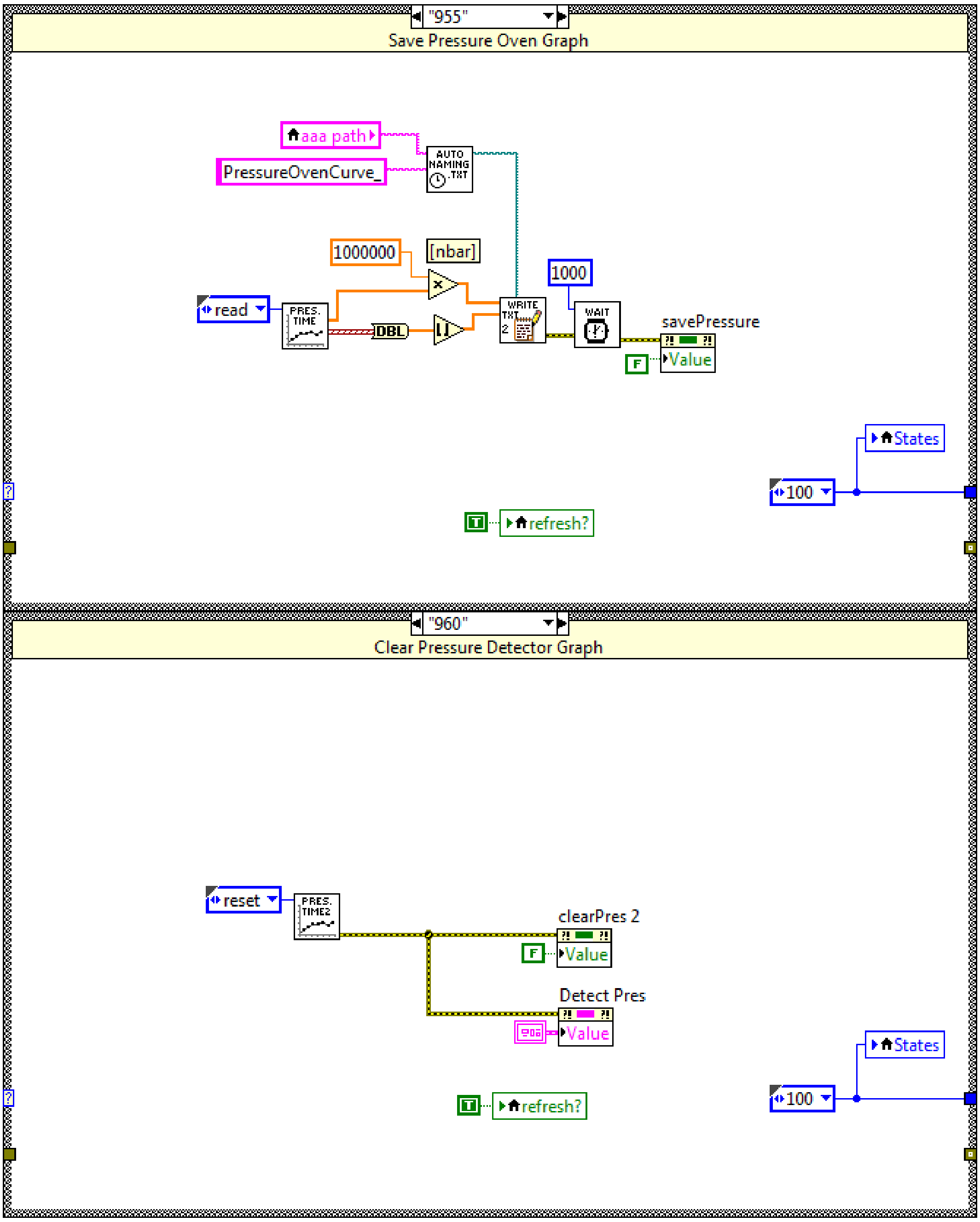
"955"
Save Pressure Oven Graph
aaa path
PressureOvenCurve_
AUTO NAMING TXT
1000000
[nbar]
read
PRES. TIME
DBL
WRITE TXT 2
1000
WAIT
savePressure
Value
F
States
100
T
refresh?
"960"
Clear Pressure Detector Graph
reset
PRES. TIME2
clearPres 2
F
Value
Detect Pres
Value
States
100
T
refresh?

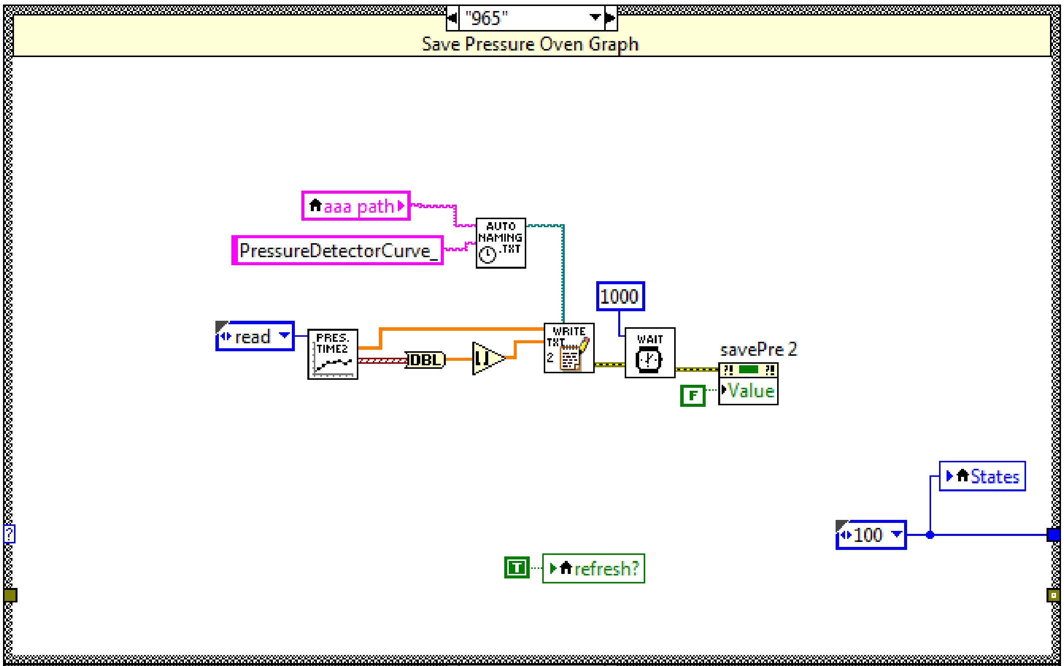
"965"
Save Pressure Oven Graph
aaa path
PressureDetectorCurve_
AUTO NAMING .TXT
1000
read
PRES. TIME2
DBL
WRITE TXT 2
WAIT
savePre 2
Value
F
States
100
T
refresh?
?

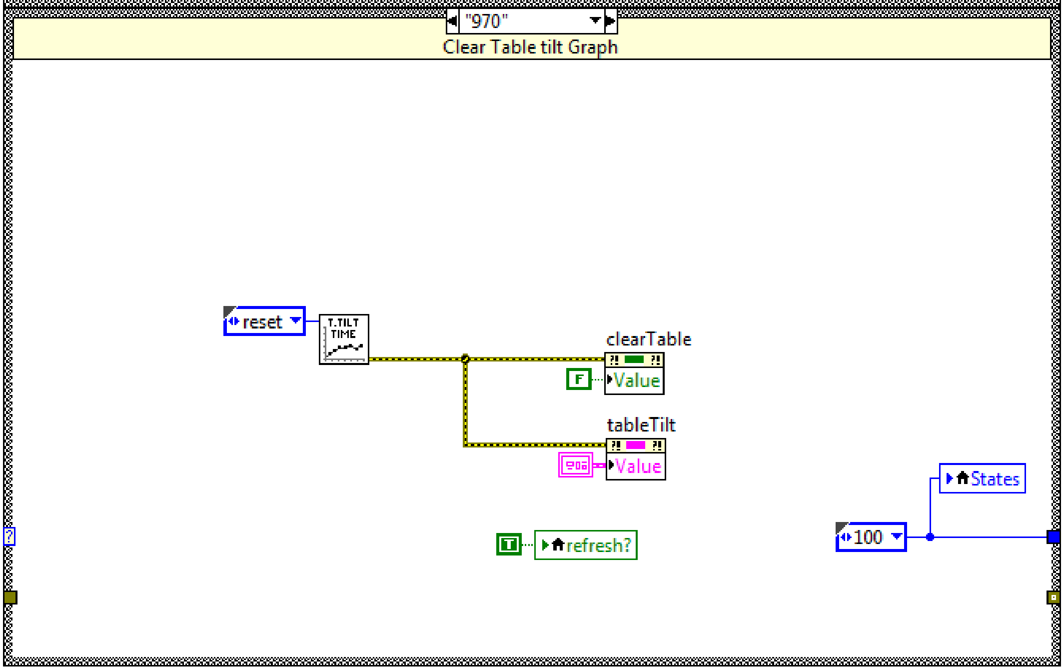
"970"
Clear Table tilt Graph
reset
T.TILT TIME
clearTable
F
Value
tableTilt
Value
States
100
T
refresh?
?

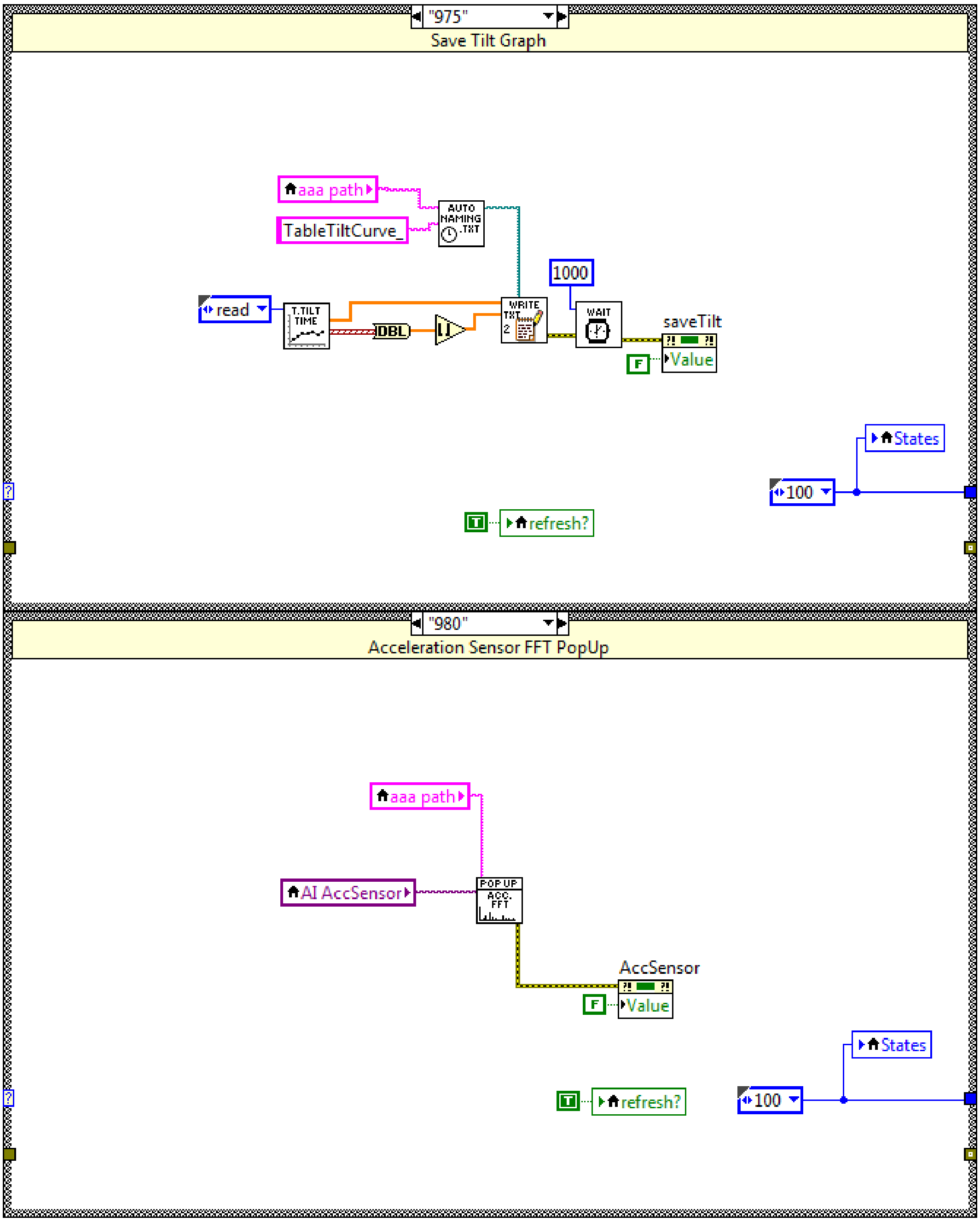
"975"
Save Tilt Graph
aaa path
TableTiltCurve_
AUTO NAMING .TXT
1000
read
T.TILT TIME
DBL
WRITE TXT 2
WAIT
saveTilt
Value
States
100
refresh?
"980"
Acceleration Sensor FFT PopUp
aaa path
AI AccSensor
POP UP ACC. FFT
AccSensor
Value
States
refresh?
100

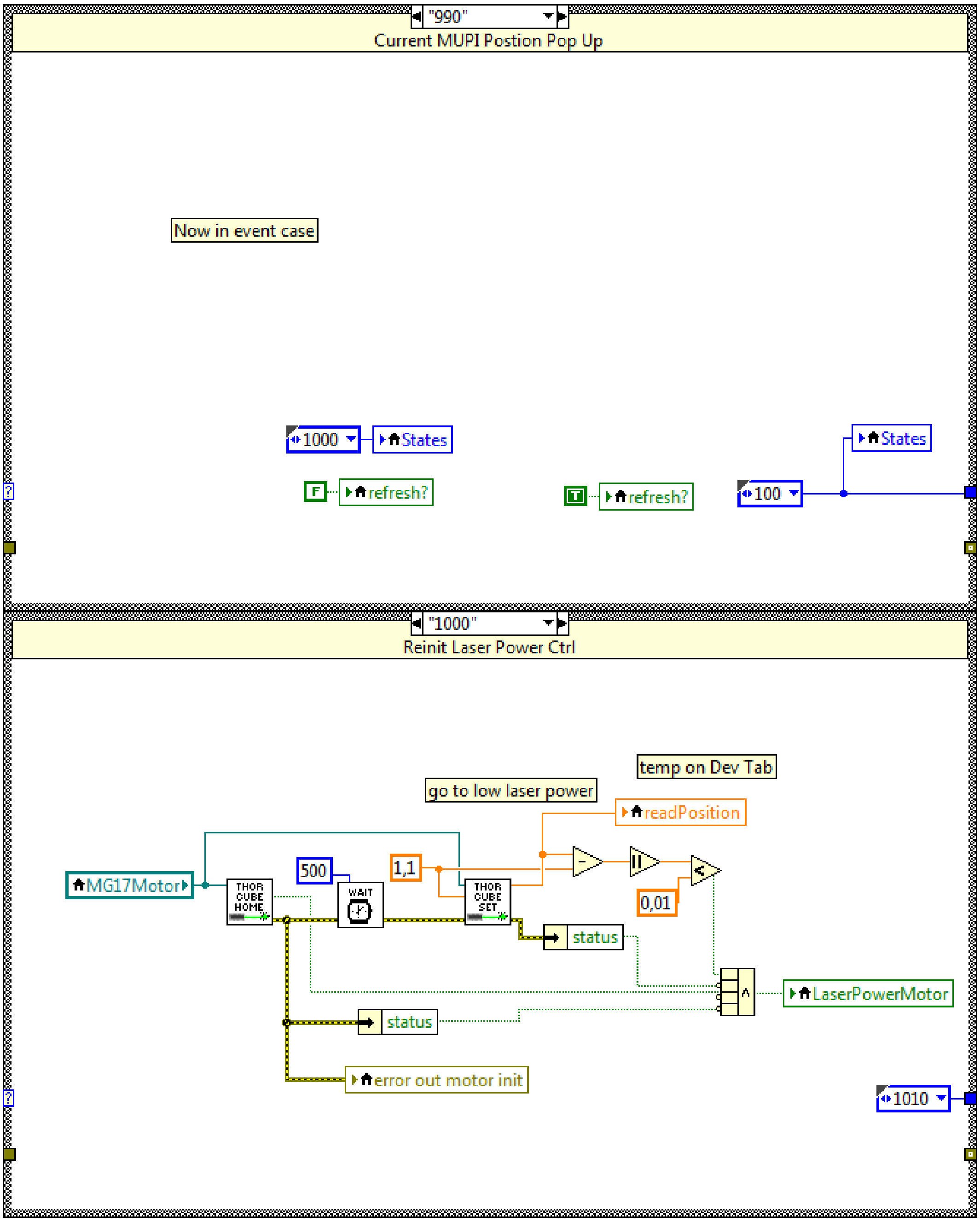

"990"
Current MUPI Postion Pop Up
Now in event case
1000
States
F
refresh?
T
refresh?
100
States
"1000"
Reinit Laser Power Ctrl
temp on Dev Tab
go to low laser power
readPosition
MG17Motor
THOR CUBE HOME
500
WAIT
1,1
THOR CUBE SET
0,01
status
LaserPowerMotor
status
error out motor init
1010

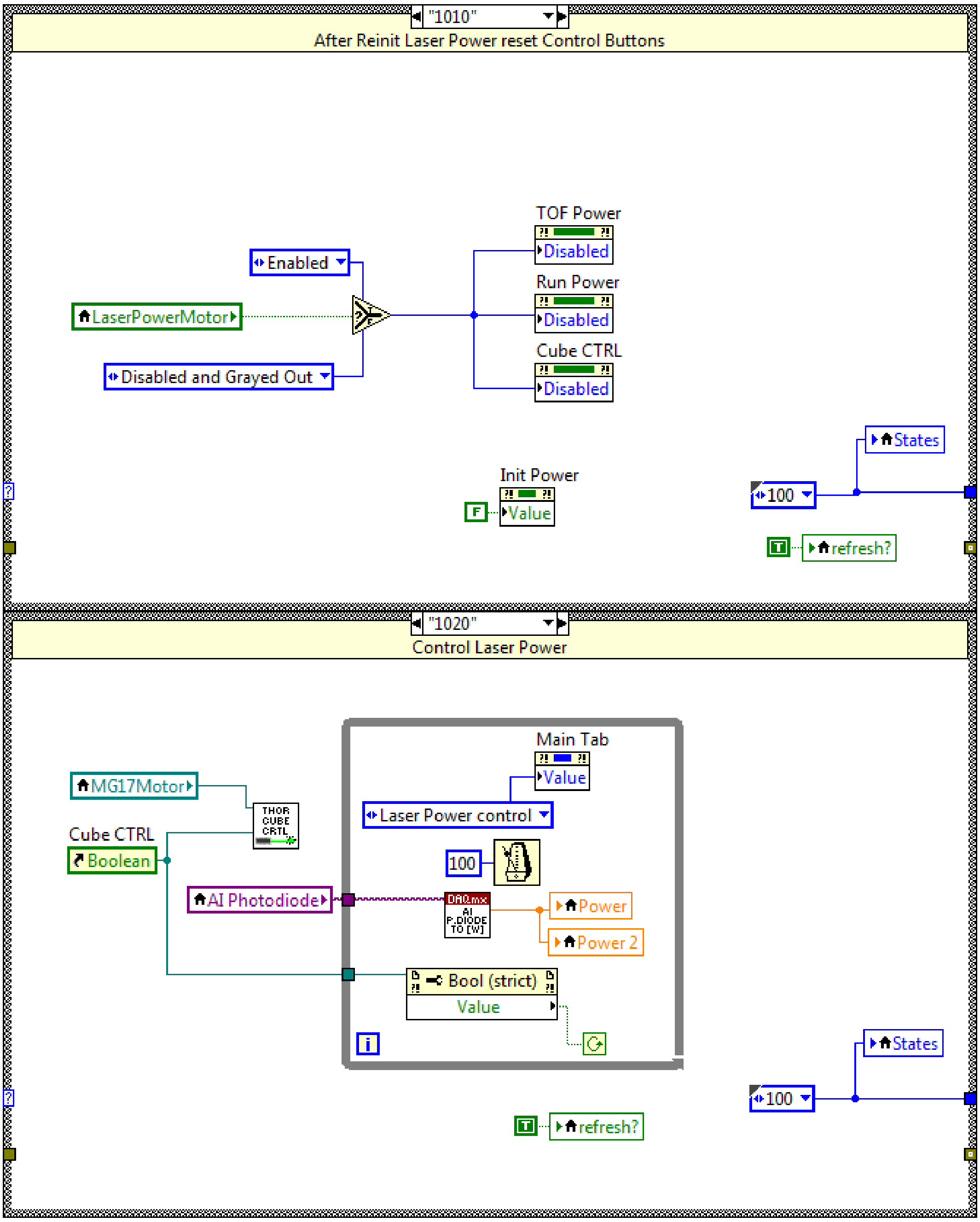
"1010"
After Reinit Laser Power reset Control Buttons
TOF Power
Disabled
Enabled
Run Power
LaserPowerMotor
Disabled
Cube CTRL
Disabled and Grayed Out
Disabled
States
Init Power
100
F
Value
T
refresh?
"1020"
Control Laser Power
Main Tab
Value
MG17Motor
Laser Power control
THOR CUBE CRTL
Cube CTRL
Boolean
100
AI Photodiode
DAQmx
AI P.DIODE TO [W]
Power
Power 2
Bool (strict)
Value
i
States
100
T
refresh?

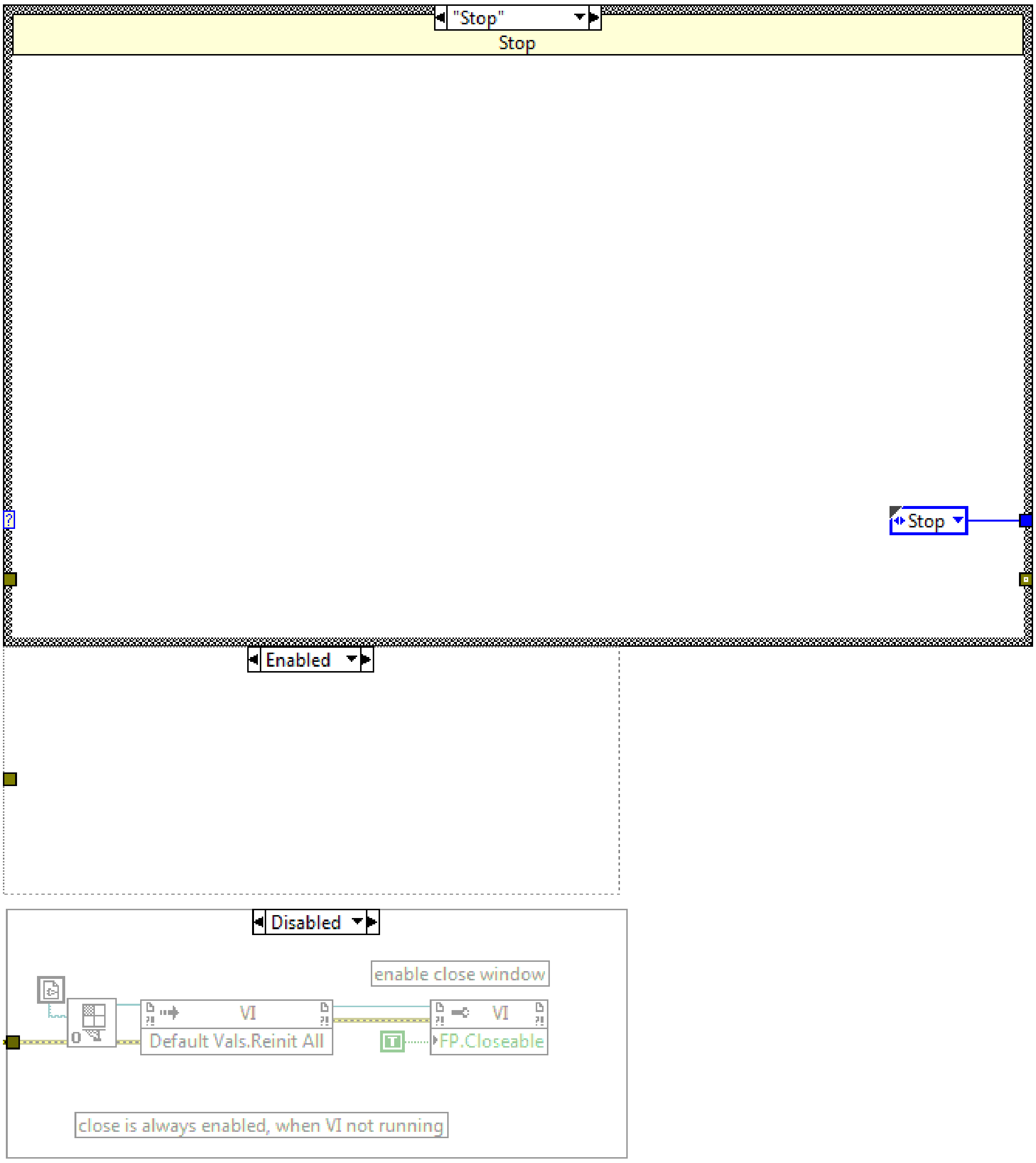
"Stop"
Stop
Stop
Enabled
Disabled
enable close window
VI
Default Vals.Reinit All
VI
FP.Closeable
close is always enabled, when VI not running

2 – List of SubVIs

AnalogIn-AccFFT.vi
The DAQ example has been adjusted. The sample clock.vi creates the time resolution. The sample rate is set on the maximum with 100'000 per second. Therefore the numbers of samples is set by the integration time (1s to 10s). The elapsed time is only used for benchmarking purposes.
The PS/PSD vi is build in from LabVIEW and performs a FFT on the data from the analogue input acquired before.
Afterwards the LabVIEW PeakDetector.vi returns all frequencies with a magnitude above 0.2.
Creating the FFT Array might be needed to save the result. However, it is time consuming and therefore not needed every time the vi is called.

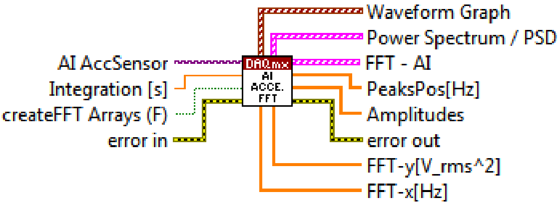

AnalogIN-Chopper.vi
example adapeted.

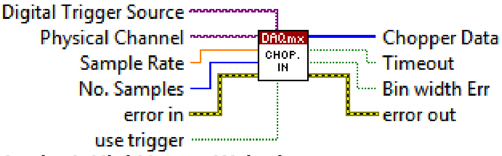

AnalogInHighVotage-Wait.vi
The analogue input from the power supply (read channel) is read until a given voltage is reached.
The power supply converts the 0V-5V linear to an 0kV to 20kV output and the other way round.
The Vi stops when the voltage +- the tolerance [V] or a timeout of 20s is reached.

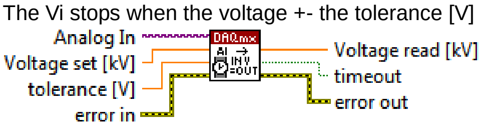

AnalogInLaserPower.vi
An analogue input from the photodiode is read to determine the power of the laser. A calibration is used and has to be changed within this vi:
calibration results 27.3.2015
linear Fit
3.72x-0.149
calibration results 27.07.2015
linear Fit
2.21 x +0
calibration results 06.10.2015
linear Fit
1.58 x +0
calibration results 19.11.2015
linear Fit
2,66 x +0

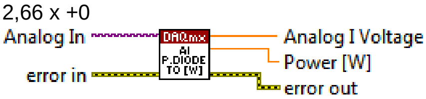

AnalogInMUPI.vi
Three analogue inputs from the MUPI are read (grating1, table, grating3). The calibration is copied from the previous LabVIEW programme, which converts the voltage form the gratings to a position. However, the calibration can be switched off and the voltage is displayed.

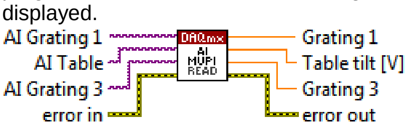

AnalogInVolt.vi
Reading analogue input [V] from the DAQ instrument. Adapted from the examples from LabVIEW.

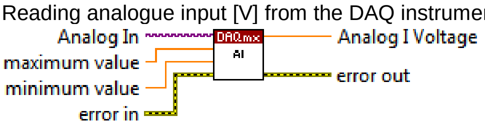

AnalogOutHighVoltage.vi
The power supply for the electrode converts the 0V-5V linear to an 0kV to 20kV output and the other way round.

Array-MotorPosCalib.vi

The VI converts the power values to motor positions according to calibration 06.10.2015:
p=-0.422*(-1.03+asin(0.11*(-9.34+x)));

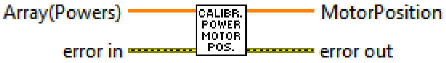

Array_tabletilt.vi

The VI is saving the table tilt from the MUPI over time. Every time the VI is called it adds the new voltage reading and a time stamp to the arrays, which can be displayed in a graph.
The VI must be first called in the reset mode. The reset clears all elements in the array.

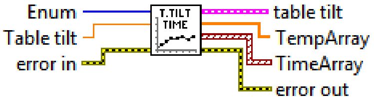

Array_Pressure.vi

The VI is saving the oven pressure reading over time.

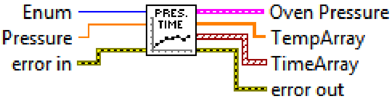

Array_Temperature.vi

The VI is saving the temperature reading over time.

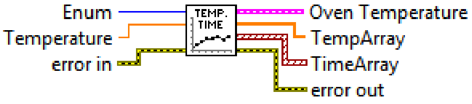

ArrayCreate-Measurement.vi

A start and an end value is needed. Using the amount of steps or the step size, the array is filled with the calculated values between the start and end. Afterwards the elements are shuffled in a second array.
If used for the Laser power, the motor position needs to be calibrated to the Laser power. That calibration can be included in this VI. Calibration is included (06.10.2015)

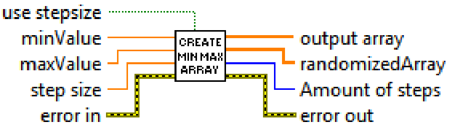

BeamProfil-Conversion.vi

The size of the pixel from the Thorlabs camera chip is used to convert the beam-array result into positions in µm.

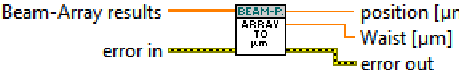

BeamProfil-makeGauss.vi

Creates an array to a Gaussian function determined by the given parameters. The horizontal array has a size of 1280 elements and the vertical 1024.
The 2D array contains the x and the y axis to plot the Gaussian function with the given parameter. The VI can either create the vertical or the horizontal Gaussian fit from the beam profile.
The Gaussian formula used here:
gauss [i] = Amp * exp(-((i+1)-mean)**2/(2 * (std**2))) + Off;

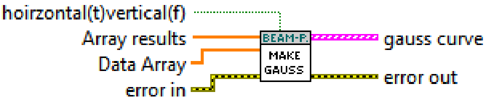

Calib_convertPiezoPos.vi

The VI converts the reading from the piezo jena system via GPIB and returns the position in nm, the calibration is used from the old LabVIEW code.

cluster_names.vi

Counter-usb6343.vi
I. Description:
This example demonstrates how to count digital events on a Counter Input Channel. The Initial Count, Count Direction, and Edge are all configurable.
Edges are counted on the counter's default input terminal (refer to section IV, I/O Connections Overview, below for more information), but could easily be modified to count edges on a PFI or RTSI line.
II. Instructions for Running:
1. Select the Physical Channel which corresponds to the counter you want to count edges on the DAQ device.
2. Enter the Initial Count, Count Direction, and measurement Edge to specify how you want the counter to count. Additionally, you can change the input terminal where events are counted using the channel property node.
Note: Use the Gen Dig Pulse Train-Continuous example to verify that you are counting correctly on the DAQ device.
III. Block Diagram Steps:
1. Create a Counter Input channel to Count Events. The Edge parameter is used to determine if the counter will increment on rising or falling edges.
2. Call the Start VI to arm the counter and begin counting. The counter will be preloaded with the Initial Count.
3. The counter will be continually polled until the Stop button is pressed on the front panel.
4. Call the Clear Task VI to clear the Task.
5. Use the popup dialog box to display an error if any.
IV. I/O Connections Overview:
The counter will count edges on the input terminal of the counter specified in the Physical Channel I/O control.
In this example the counter will count edges on the default input terminal on ctr0.
For more information on the default counter input and output terminals for your device, open the NI-DAQmx Help, and refer to Counter Signal Connections found under the Device Considerations book in the table of contents.

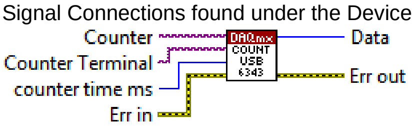

DAQ-get-USB6343.vi
The VI checks if the "USB-6343 (BNC)" is connected. If so, the device name is returned to create channels names with it.
The given name (e.g. "dev2") in the MAX is irrelevant. The VI searches for the Product Type in the list of all active DAQ devices.

Filename-a-b.vi
change string: a -> b -> ... -> ... until z using conversion ASCII to decimal
returns also if "z" received. Error is true if received sting is not "a" to "y" or if sting size is bigger than 1

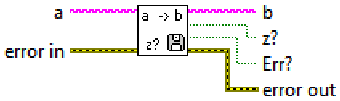

Filename-aaa-check.vi
VI checks if the string is only containing three small letters (zzz is ok). Returns false as ok for no error. Can be used for error handling.
TRUE means string is NOT ok.

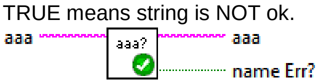

Filename-aa-check.vi

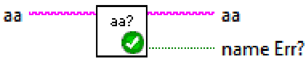

Filename-change-aa.vi

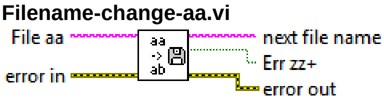

Filename-change-aaa.vi
VI takes the first three characters of the string and changes them: aaa -> aab ..... -> aaz -> aba -> ... until zzz
'Err zzz+' is true if received sting is zzz. However, does not indicate if the given string is not "aaa" to "zzy" (size test and Error from subVI not used)

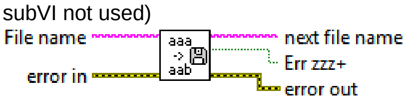

Filename-getnext_aaa.vi
The path, where the data is saved, needs to be changed in this VI !!!
"C:\Users\KDTLI -lab\Desktop\Daten\"

Creates Folder of the year and of the day (\Daten2015\0524\)
Complete path: ..\Daten\Daten2015\0417\aab
will check for any files named "aaa*" within the folder of the day and returns the complete path ending with the next file name (e.g. "aab").

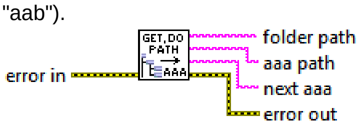

Filename-time-txt.vi
The VI creates a txt-file path from the aaa path with a string name and the current time, when the VI is called e.g.:
Z:\Work\Molekuele\Experimente\TLI_MQO2\Daten\Daten2015\0730\CountsVsTime_1610.txt
If the filename exists, a number will be added automatically to the end. VI will always return a non-existing filename.

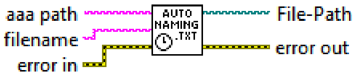

Files_moveFolderContent.vi

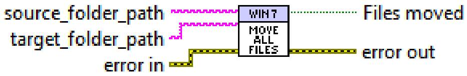

GPIB-2string-int-mean.vi
string form the GPIB after asking "rk"
expected answer: "rk,0,40000" will be converted into int 40000
also can take the mean between two strings from the GPIB
Error handling missing, here is not checked if string really looks like expected.

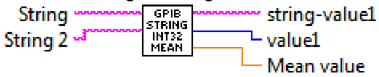

Header-addRow.vi
VI expects path of the header file, which must be created before. It adds a new line with a parameter name and value (. as decimal) or it adds a comment underneath depending on the value of boolean input.

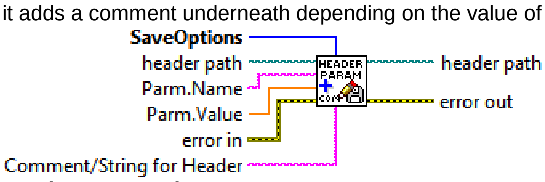

Header-create3.vi
The VI expects the path of the "aaa-file" as a string and creates a header. Taking the aaa-file path and name and adding "_header.txt". Afterwards the initial header lines are created.
Header, first lines e.g.:

Programme VI version 1.0
Filename aaa
Date 24.05.2015
Time 19:40
Molecule c60

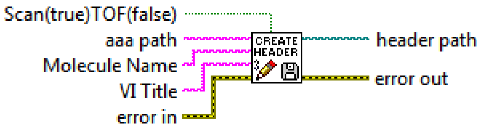

Logging-getnext-filepath.vi

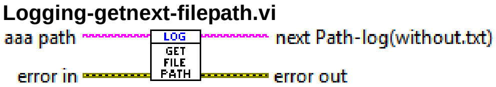

Matlab-BeamProfil.vi
The VI expects the 2D array resulting from a snapshot from the Thorlabs camera. A Matlab script is used to fit a horizontal and a vertical Gaussian.

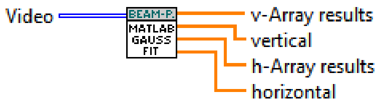

Matlab-lic-toolbox-check.vi
The VI checks if the license for the Matlab toolbox is available for this machine, because there are only a limited number of toolbox licenses available at the same time. Matlab must be completely closed to return a license to the server as available.

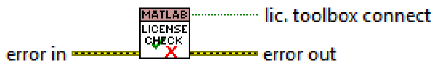

Matlab-sinfit.vi
The VI fits a sin function in the data from the interference scan. Matlab code for sin fit:

```
model         =  inline('c(1).*sin((2.*pi()./c(2)).*x + c(3)) + c(4)','c','x');
[beta,R,J,CovB] =  nlinfit(x0,y0,model,[mean(y0),266,0,0.5.*(max(y0)-min(y0))]);
sbeta        =  sqrt(diag(CovB));
```

dark counts are subtracted before

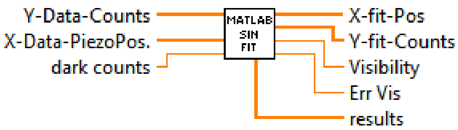

MCA3Cmd-new.vi
Execute a MCA3 command.

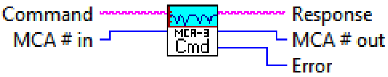

MCA3Dat-new.vi
Get a copy of the MCA-3 Data as [U32] array

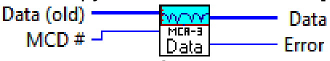

MCA3Par-new.vi
Gets the MCA-3 Settings

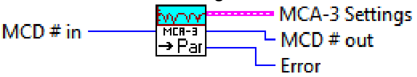

MCA3Run-1GO.vi

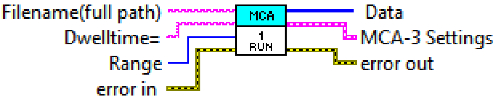

MCA3Set-check.vi

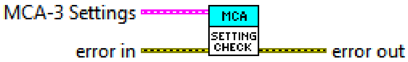

MeanCounts.vi
VI calculates the mean counts per second.

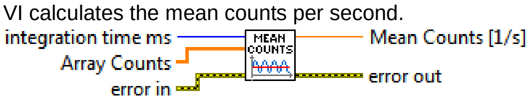

MeanLastArrayElems.vi

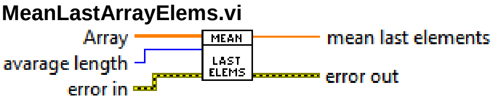

Piezo-GPIB-write.vi
Basically the communication example with GPIB write/read

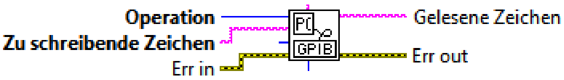

Piezo-Initialize.vi
VI structure is copied and adapted from previous LabVIEW programme. This communication used to be done before every scan. However, it puts the piezo in a undefended position and the next communication via GPIB needs to set the voltage of the piezo. This might be the reason, why every fist measurement point needed to be dropped from analysis.
check is GPIB connection status with the jena piezo system is working correctly.
command: cset,Channelnr,0 (Ch1,2,3)
enable port: command: ke
(manual: "switches on every activated channel")
This vi activates channel 0 and deactivates channels 1-3. GPIB address 8

Piezo-nextPos.vi

Piezo-readPos.vi
Uses the Calib_convertPiezoPos.vi

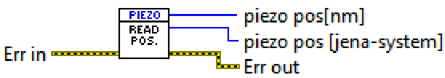

Piezo-read.vi

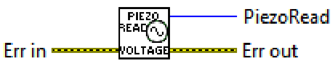

Piezo-setPos.vi

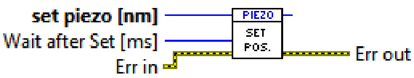

Piezo-set-read.vi
The VI sets the position of the jena piezo system (GPIB adress 8). The calibration (postion vs voltage) is copied from the previous LabVIEW programme: Start value times 0.818925, then add 180

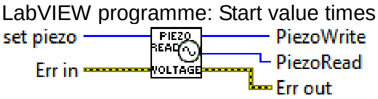

PopUp-AccSensor.vi
Pop up subVI opens front panel when called. The VI displays the FFT of the acceleration sensor for the chosen integration time. The x and y axis can be saved to a text file, but the save button has to be clicked before the run.

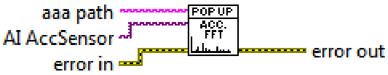

PopUp-BeamProfile-Cam.vi

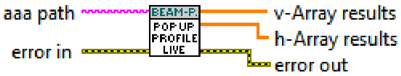

PopUp-Countdown.vi
The Pop up subVI opens the front panel when called. VI is used as an info box to the user. Text is expected by the VI and displayed. VI runs until user presses "OK".

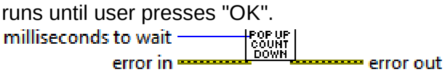

PopUp-Counter-Crl2.vi
The Pop up subVI opens the front panel when called. The user chooses the parameters and starts the process. Then the progression of the count rates is displayed. The mean is calculated and can be used as the dark count rate. Also, the count rate over time as displayed can be saved to a text file.
There is no clear or reset, it can just be recalled from the main programme after exit.

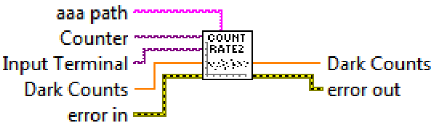

PopUp-Count-set.vi
The Pop up subVI opens the front panel when called. VI shows the old dark count rate and a new dark count rate can be set manually.

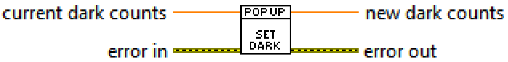

PopUp-getString.vi
The Pop up subVI opens the front panel when called. VI is used as an dialog box to the user. A text is supposed to be entered. VI runs until user presses "OK".

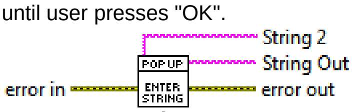

PopUp-MUPI2.vi
The Pop up subVI opens the front panel when called. When started and parameter are chosen, the VI displays the progression over time of the MUPI in the graphs. The displayed data can be saved to a text file.

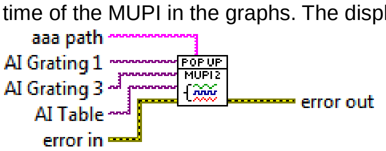

PopUp-OK.vi
The Pop up subVI opens the front panel when called. VI is used as an info box to the user. Text is expected by the VI and displayed. VI runs until user presses "OK".

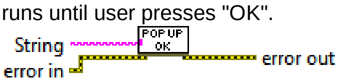

Pressure-read-com#-ch#.vi
The VI is mostly copied from the previous programme "pressure-record.vi". It can be used to read the pressure from the Leybold and from the Pfeiffer system. A channel has to be selected. The pressure DBL is extracted from a string, which comes from the VISA communication.

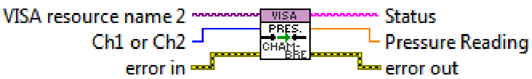

ScanDeflectometry_new.vi
Scan an interference pattern. Moving the 3rd grating with the piezo. which is controlled through a GPIB connection. Loop can be stopped by the calling VI through a reference stop.
Results from every loop are displayed live to the reference graph from the calling VI.

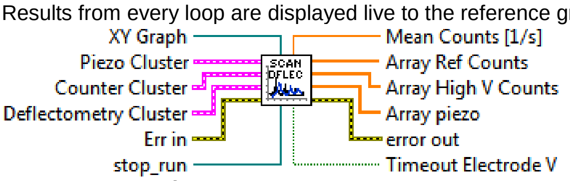

ScanIncrement.vi

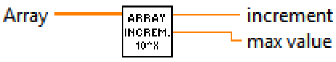

ScanInterference_new.vi

Scan an interference pattern. Moving the 3rd grating with the piezo. which is controlled through a GPIB connection. Loop can be stopped by the calling VI through a reference stop.
Results from every loop are displayed live to the reference graph from the calling VI.

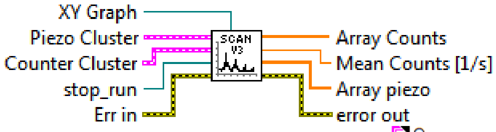

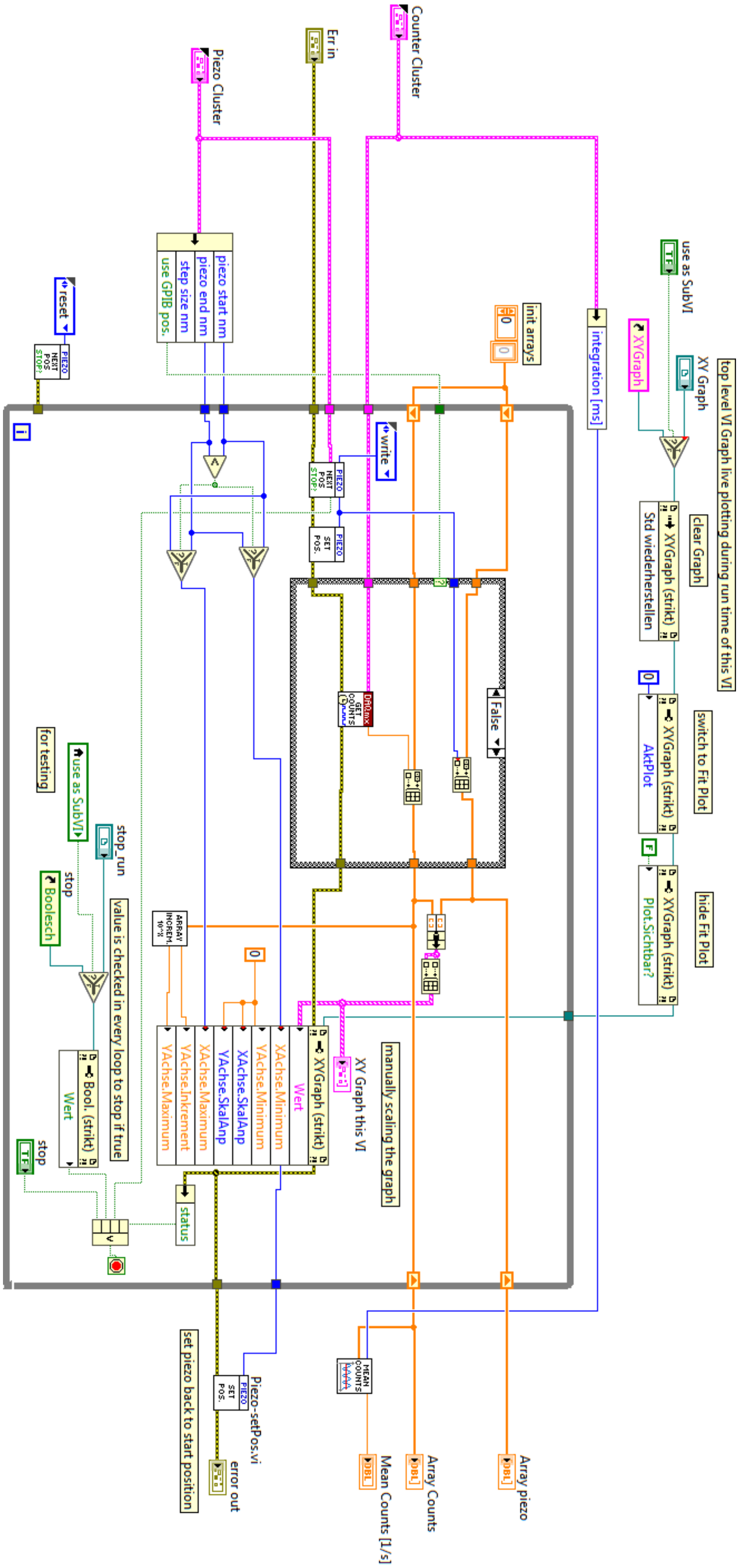

ScanMeasure1step.vi
In principle, this VI has the same functionality as the counter USB6343.
In addition it is reading the piezo position through the GPIB position. It reads out the position before and after getting the count rate. The average of those two values is returned as the piezo pos. GPIB. The VI is also waiting twice for 100ms for the piezo position to settle.
It was concluded, that the setting position of the piezo is more accurate than its own reading. It was shown that the reading value is fluctuating.

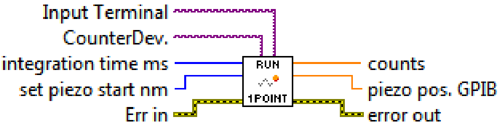

ScanMeasure1step_average.vi

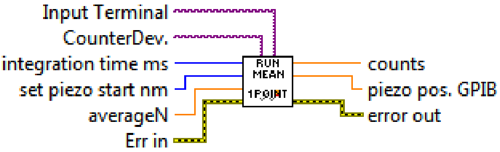

ScanMeasureCounts.vi

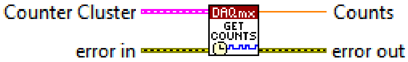

ScanMeasureCounts_Deflect.vi
Set ref. Voltage, wait unit set, get counts, set high voltage, wait until set, get counts

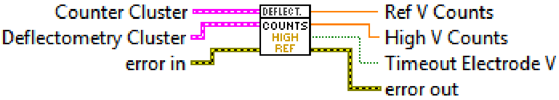

ShuffleArray.vi
The VI reorders the elements of an 1D array randomly and returns the new array.

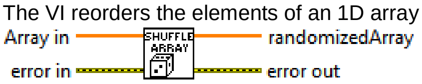

Telnet-makeArrays.vi
Communication to the Verdi laser GUI.

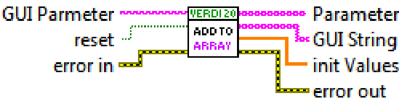

Telnet-makeString.vi
Building string to communicate with Verdi GUI via TCP/IP telnet connection.

Telnet-String2number.vi
String from Verdi GUI is converted into number.

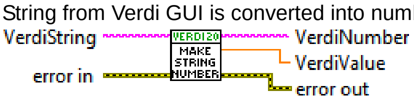

Telnet-Verdi20-getPara2.vi
The Telnet Line Client VI uses the Telnet VIs to simulate a simple Telnet Window (example). Developed into the VI getting list of parameters to read and returning the values and parameter names returning from GUI

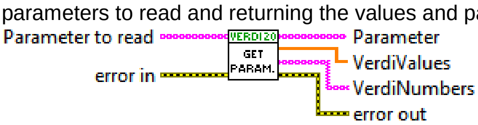

Telnet-Verdi20-shutter.vi
The Telnet Line Client VI is adopted and the shutter function from the Verdi laser can be controlled remotely.

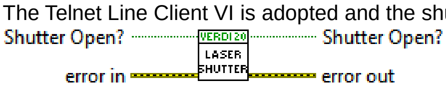

Telnet-Verdi20-init.vi
Checks if status is true to communicate.

ThorCam-init.vi
The order of the subVI is taken from the Thorlabs LabVIEW programme to control the camera. This VI checks if the camera is plugged in

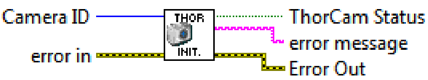

ThorCam-minExpT2.vi
This VI is taking one single snapshot with the smallest possible exposure time and returns the picture as a 2D array.
Every few runs a "transfer error" occurs. Therefore, wait functions have been include, which made the error less often. The error happens within the FreezeVideo.vi (replacing it with the snapshot.vi does not make a difference). Using the uc480Viewer software the frame rate has to be dropped and not set to automatic, otherwise frames are dropped. This might be the reason. However, try and error and connecting Thorlabs could not solve the problem yet.
If the error occurs, the subVI does not return a snapshot.

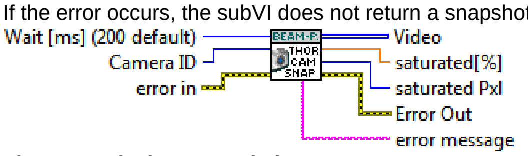

ThorCam-Pixel-saturated.vi
The VI checks if and how many pixel of the snapshot from the Thorlabs camera are saturated.

ThorCam-save.vi
The VI expects the path of the latest measurement (aaa path) without the file ending. It adds "_beamprofile.jpg" to the path. The snapshot form the camera will be saved as a jpg e.g.:
....\Daten\..\aaa_beamprofile.jpg

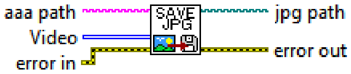

ThorCube-control.vi
The activeX control for the Thorlabs motor is called. The VI needs to me correctly stopped or the activeX control starts to get "bugy". It is stopped by a reference stop from the calling VI. The activeX control is also reacting live to the activeX control from the calling VI. (code was adapted from the Thorlabs LabVIEW documentation) GuideToLabVIEWandAPT.pdf

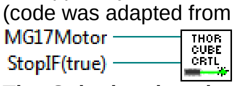

ThorCube-homing.vi
The VI is using the activeX control to use the homing function of the Thorlabs step motor control. Only when the motor is set to the home position, all further setPosition are calibrated and repeatable.
The home parameter can be saved and loaded from a file.

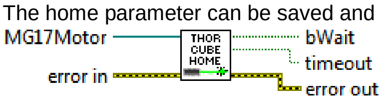

ThorCube-set-2power.vi
The VI changes the position of the motor until the power reading is with 0.5W of the desired power.
The VI uses the example from the Thorlabs LabVIEW documentation. It is adjusted and tested to set the motor to a given position, however the position read out feedback is arbitrary if the motor was moved manually for example. Homing the motor position should make the code work reliable.
REMARK:
the PRM1Z8 (rotational moving stage) is detected as a linear stage Z606(B)!!
That determines the range of the stage (0 to 6), which is not giving the full range of the rotational stage, which can have negative values and goes up to at least 18 (manually drive stage and read position in the LabVIEW activeX control, full range as not been tested)
Documentation:
C:\Program Files (x86)\Thorlabs\APT\APT Server\APT Server.chm
Programming Guide ->Motor Control -> Motor Control Methods

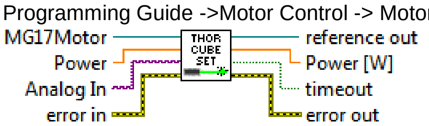

ThorCube-set-position.vi
This VI is similar to ThorCube-set-2power.vi, but it actually sets a position to the motor. However this position as no feedback. It depends on the homing and it could be changed manually without software knowing.

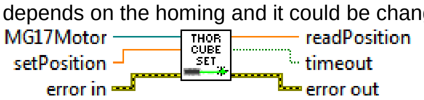

ThorCube-set-position-openRef.vi
This VI is like ThorCube-set-position, but the reference knot is not closed for the subVI to be called within a loop.

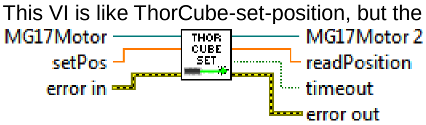

TOF-ChopperFreq.vi

VI calculates the chopper's frequency from an measured array from the photodiode and the bin width and ranged set before.

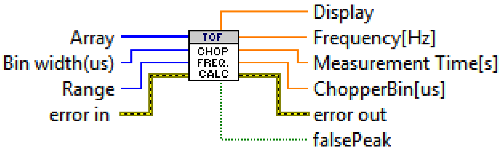

TOF-DwellT-calc.vi

This VI converts the bin width to the dwelltime expected by the fast card

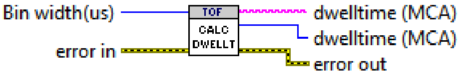

TOF-falseChopPeaks.vi

Making sure, that a peak in the photodiode data is not just two measurement points apart.

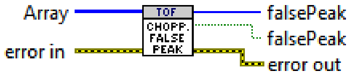

TOF-filepath.vi

Creating the file path to save the data from the photodiode and the MCA (fast card) from the aa TOF path.

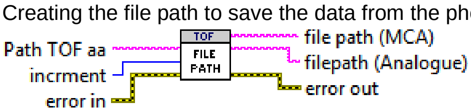

TOF-getnext-filepath.vi

Using the aaa path currently in use by the control software to create the next path for a TOF measurement, which is saved in a subfolder (...\Chopper\).

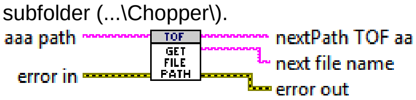

TOF-measure2.vi

Measuring a TOF with the Nr.ofRuns. Can be stopped by calling VI.

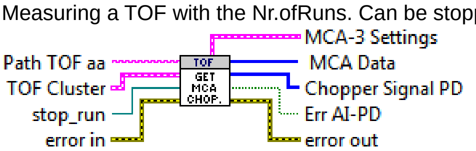

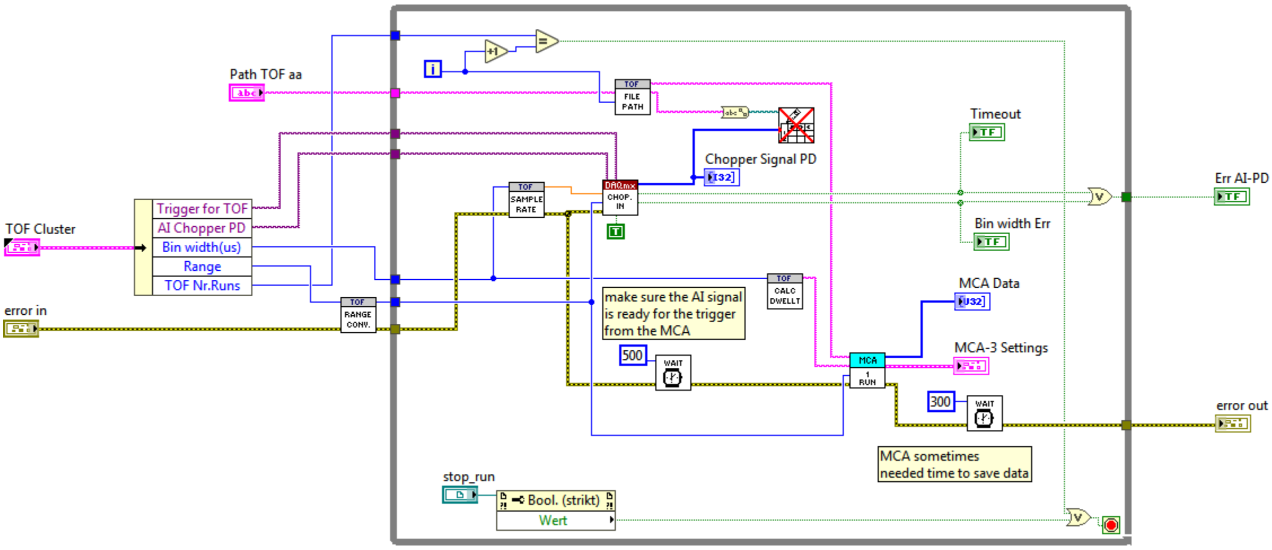

TOF-measure2Scan.vi
A TOF measurement, but without a loop.
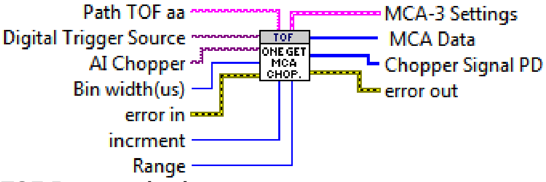

TOF-Range-calc.vi
The range can only be set in steps allowed by the MCA. The input is an enum and it returns a number.
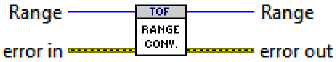

TOF-SampleRate-calc.vi
The MCA gets set with a bin width, but the NI card needs a sample rate. This VI converts it.
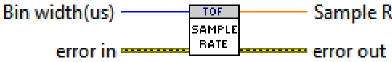

TXT-write-file-2D.vi
The VI saves two arrays to a file. The file path includes the file ending. The numbers from the arrays will be saved with 6 digits after the period.
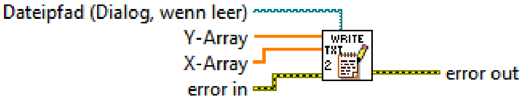

TXT-write-file-3D.vi
The VI is like the TXT-write-file-2D, but this VI can save three arrays (three columns) to a file.
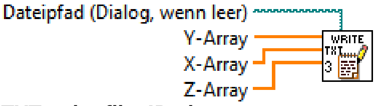

TXT-write-file-4D.vi
The VI is like the TXT-write-file-2D, but this VI can save fout arrays (4 columns) to a file.
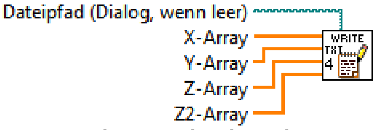

USBtc08Thermo-ChSelect.vi
The VI reads out one temperature value from one selected channel from the USB pico logger if the device is connected. The thermocouple must be from type K. The temperature is returned in Celsius [°C]. Does not crash if unplugged like the manufacture version, but only returns an error.
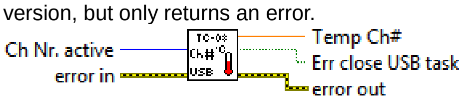

W7-ProgrX-open.vi
The VI uses the WindowsTasklist.vi to get a list with all open tasks. It searches the list for the Wavemeter Software and returns a true or false.


W7-ProgrX-start-.vi
The VI uses the cmd command to start the wlm_ws7.exe, which belongs to the Wavelength Meter software from HighFiness.
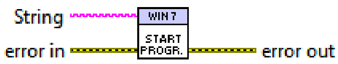

W7-Tasklist.vi
This VI returns Windows' currently running tasks in list of strings.
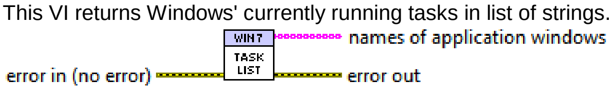

Wait.vi
This VI just uses the Wait in ms function. It is adjusted in a way that in can be used as a subVI. The waiting time in ms can be set from the calling VI.
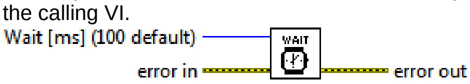

Wavemeter-get.vi
The VI calls the library "wlmData.dll". If the Wavelength software is running and set up correctly, the wavelength current wavelength will be returned as a double. The error handling is not used.
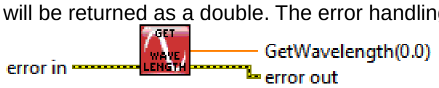

ZZ-clusterEmail.vi
Clusters all email addresses which can be handled from the control software for notifications.

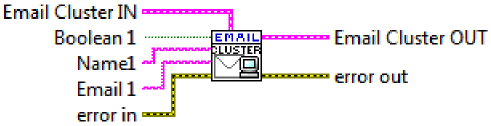

ZZ-emails.vi
List of the buttons and emails.

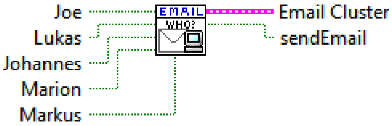

ZZ-get-wiki-par.vi
VI needs internet connection and returns the first paragraph of a random Wikipedia article every time it is called.

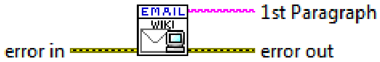

ZZ-gmail.vi
Sends an email to the recipient from the KDTLI gmail account.

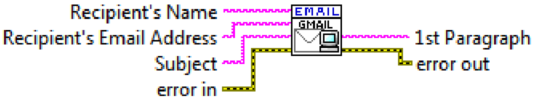

Type definitions:

Cluster_Counter.ctl
Cluster includes all parameters to use the counter from the DAQ card (Device Input, Counter Terminal, integration time and if the intergration time should be spilt into N interval over which an average, always return counts that respond to the integration time)

Cluster_Deflectometry.ctl
Delefectometry cluster includes all parameters for the electrode (Analog In and Out to set and read the Voltage from the power supply, the tolorance in Volts is needed to wait until the read has reached the set Voltage +- the tolerance).

Cluster_Piezo.ctl
The Piezo clusters contains the parameters start-, end-position and the step size in nm of the piezo (default and old parameter: start 50000nm, end 51064nm, step size 26nm).
If the use GPIB is true, it will be used to return the read out position in nm from the jena piezo instead of the set postion (the readout is fluctuating a lot).

Cluster_TOF.ctl
The TOF cluster contains the parameter for the trigger, the fast card and the input from the photodiode. The bin width in µs is the integration time and the range is the amount of bins. The range and bin parameter come from the fast card and its software. The number of runs is used to repeat the measurement.

Control_h_gauss_fit3.ctl
The control is adjusted to not show any labels or axis. It is placed next to the beamprofil to show the gaussian fit. The horizontal and vertical pixel/elements must fit the parameter of the camera and the fitted gaussian.
Info: check if axis is inverted and if the range is correct.

Control_v_gauss_fit2.ctl
The control is adjusted to not show any labels or axis. It is placed next to the beamprofil to show the gaussian fit. The horizontal and vertical pixel/elements must fit the parameter of the camera and the fitted gaussian.
Info: check if axis is inverted and if the range is correct.

MCA-Range.ctl
The enum type def is defined by all possible ranges the fast card can do.

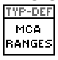

SaveOptions.ctl
The enum is used to pick what data type is saved in the next line in the header using the subVI "Header-addRow.vi"

StateMachine.ctl
This is a strict type definition. It includes all states that are usable in the state maschine. More possible states must be added here. Right now, there are 218 possible states (init, 1,...10,20...,1500, ErrorI..,stop and some more in between).

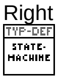

VarStates.ctl
The enum is used to selected between the states write, read and reset for individually programmed functional global variables (FGV) like "Array_Pressure.vi".